The Use of Mesoscale Oscillatory Baffled Reactors for Rapid Screening of Heterogeneously Catalysed Biodiesel Production Reactions

A thesis submitted to the Newcastle University for the Degree of Doctor of Philosophy

by

Valentine Chinaka Eze

School of Chemical Engineering and Advanced Materials
Newcastle University, United Kingdom

March 2014

[Abstract]

Abstract

Biodiesel is a renewable alternative to petro-diesel, derived from vegetable oils and animal fats. The use of biodiesel in place of petro-diesel leads to reduced emissions of greenhouse gases, especially CO_2, and ensures energy security. The most commonly used technology for biodiesel production is based on a homogeneously catalysed liquid phase reaction. The disadvantages of this process are the ongoing costs of catalyst replacement, the large number of downstream purification steps and production of low quality glycerol with consequently low market value. In principle, heterogeneous catalysts can solve these problems.

This research demonstrates that homogeneous alkali-catalysed biodiesel production was possible at an industrially acceptable level of conversion (> 96%) in ~ 5 min residence time, requiring a combination of high catalyst concentration and good mixing. Both the experimental and model simulations results clearly showed that rapid biodiesel production (reaction times below 2 min) at economically viable conversions can be achieved by increasing base catalyst and methanol concentrations without significant problems due to excess soap formation, even in the presence of water and free fatty acids.

A heterogeneous strontium zirconate based (SZB) catalyst showed substantial activity towards rapeseed oil transesterification, but there was significant loss in activity with or without the presence of water due to leaching of the active sites, $Sr(OH)_2$, into the methanol phase. The SZB catalyst cannot be re-used for triglyceride transesterification, as it acts in a similar manner to conventional homogeneous alkali catalysts.

A $PrSO_3H$-SBA-15 catalyst was active for carboxylic acids esterification with methanol, with the reaction rates increasing with reaction temperature and methanol molar ratio, but decreasing with water content and carboxylic acid chain length. Steric effects increased with carboxylic acid chain length, causing reductions in the esterification rates and turnover frequency. $PrSO_3H$-SBA-15 has very narrow pores (5.1nm) that are not large enough for significant triglyceride transport. Therefore, $PrSO_3H$-SBA-15 with expanded pore size, functionalised on a hydrophobic support would be required for simultaneous esterification of free fatty acids and triglyceride transesterification.

Finally, a mesoscale oscillatory baffled reactor (meso-OBR) was constructed and used to suspend and screen solid catalysts for transesterification and esterification reactions,

significantly reducing reagent required and waste generated due to the small volume (~10mL). This work is the first example of systematic screening of a solid-liquid-liquid reaction system in a meso-OBR. Continuous screening in the meso-OBR permits detailed kinetic studies, rapid optimisation of reaction conditions, and assessment of the reusability of the catalyst in a single experiment as opposed to multiple experiments in conventional batch reactor screening.

Dedication

Dedicated to

Rita, Chukwunaka and Chinyere

Acknowledgements

First and Foremost, I express my profound gratitude to God Almighty for giving me the strength and courage to complete this programme. Special thanks to my supervisors, Professor Adam P. Harvey and Dr. Anh N. Phan, for their keen supervision and insightful contributions to this research. Thanks for your mentorship, encouragement and sharp criticism. This research was made possible by your wealth of experience and vast scientific knowledge. I also express my appreciations to Rita, Chukwunaka and Chinyere for their patience and understanding, and to my siblings: Nduka, Chinwe and Chisom for their support and encouragement.

My acknowledgement will not be complete without appreciating the help and support I received from the following people in the course of this research:

- Dr. Jie Zhang of the School of Chemical Engineering & Advanced Materials, Newcastle University, for his assistance with the MATLAB modelling.
- Dr. Jose Renato de Oliveira Lima of the Institute of Chemistry, São Paulo State University, Brazil for supplying the strontium zirconate based catalyst.
- Dr. Karen Wilson and her team in Department of Chemistry, Cardiff University, for supplying the $PrSO_3H$-SBA-15 catalyst. Thanks for your assistance with the NH_3 and CO_2 pulse titration, surface area and porosity measurements through your team members Dr. Cyril Pirez and Dr. Jinesh Cherukkattu Manayil.
- CEAM technical and IT support: Stewart Latimer, Rob Dixon, Simon Daley, Julie Parker, Paul Sterling, Iain Ditchburn, Ian Strong, Brian Grover, Vincent Scott, and Daniel Padgett. Thanks for your excellent technical and IT support.
- ACMA Service: Pauline Carrick who performed the energy dispersive X-ray and Maggie White who carried out the X-ray diffraction analysis.
- CEAM members of the Process Intensification Group (PIG), administrative staff and office colleagues for their useful contributions.

This research was funded by the Petroleum Technology Development Fund (PTDF) of Nigerian Government.

[Table of Contents]

Table of Contents

[Table of Contents]

List of Publications

1. **Eze, V. C.,** Phan, A. N., Harvey, A. P. (2014). 'A more robust model of the biodiesel reaction, allowing identification of process conditions for significantly enhanced rate and water tolerance' *Bioresource Technology*, 156, pp. 222-231.

2. **Eze, V. C.,** Phan, A. N., Pirez, C., Harvey, A. P., Lee, A. F. and Wilson, K. (2013) 'Heterogeneous catalysis in an oscillatory baffled flow reactor', *Catalysis Science & Technology*, 3, (9), pp. 2373-2379.

3. Phan, A. N., Harvey, A. P. and **Eze, V**. (2012) 'Rapid Production of Biodiesel in Mesoscale Oscillatory Baffled Reactors', *Chemical Engineering & Technology*, 35, (7), pp. 1214-1220.

4. **Eze, V. C.,** Harvey, A. P. and Phan, A. N. (2012). 'Development of new designs of oscillatory baffled mesoreactor for continuous biodiesel production', *International Symposium for Chemical Reaction Engineering (ISCRE-22)*, Maastricht, Netherlands, 2^{nd} -5^{th} September, 2012.

5. **Eze, V. C.**, Phan, A. N, Harvey, A. P. and de Oliveira Lima, J.R. (i*n progress*). 'Screening a strontium zirconate-based heterogeneous catalyst for biodiesel production in a mesoscale oscillatory baffled reactor'.

6. **Eze, V. C.**, Harvey, A. P. and Phan, A. N. (*in progress*). 'Determination of the kinetics of biodiesel saponification in alcoholic hydroxide solutions'.

List of Figures

[List of Figures]

[List of Figures]

[List of Figures]

List of Tables

[List of Tables]

List of Abbreviations

ATR	attenuated total reflectance
BET	Brunauer-Emmett-Teller
BJH	Barret-Joyner-Halenda
CFPP	cold filter plugging point
CP	cloud point
CSTR	continuous stirred tank reactor
DG	diglyceride
EDX	Energy Dispersive X-ray
ER	Eley Rideal
FAME	fatty acid methyl ester
FFA	free fatty acid
FID	flame ionisation detector
FTIR	Fourier transform infrared
GC	gas chromatograph
GL	glycerol
IB	integral baffles reactor
JCPDS	Joint Committee for Powder Diffraction Standards
LHHW	Langmuir-Hinshelwood-Hougen-Watson
MA	methanol
ME	methyl ester (same as FAME)
Meso-OBR	mesoscale oscillatory baffled reactor
MG	monoglyceride
Mw	molecular mass
MW_A	molecular mass of species A
OBR	oscillatory baffle reactor
PHP	potassium hydrogen phosphate
QSSA	quasi-steady state approximation
rpm	revolutions per minute
RSO	rapeseed oil

RSO#	rapeseed oil or FAME
RTD	residence time distribution
SBA-15	Santa Barbara Amorphous type material no. 15 (mesoporous silica)
SE	sharp-edged helix with a central rod
SPC	smooth periodic constrictions
SZB	strontium zirconate based (a catalyst)
TCD	thermal conductivity detector
TG	triglyceride
TIS	tanks –in – series
TOF	turnover frequency of a catalyst ($time^{-1}$)
TON	turnover number
TPD	temperature programmed desorption
WW	wire wool packed reactor
XRD	X-ray diffraction

List of Nomenclature

λ	baffles spacing (m)
β	mole fraction of KOH available for saponification
ρ	density ($kg.m^{-3}$)
μ	dynamic viscosity (Pa.s)
ε_p	porosity of catalyst particle
$\sigma^2(t)$	variance (s^2)
$\sigma^2(\theta)$	normalised variance
$\gamma^3(t)$	skewness (s^3)
$\gamma^3(\theta)$	normalised skewness
θ	dimensionless time
θ_A	surface coverage of species A
θ_j	fraction of vacant catalytic active site
Φ	ratio of molar concentration
Φ_A	solvent association factor
ø	vacant catalyst active site
ψ	velocity ratio
ψ'	first constant for Taft equation
h	second constant for Taft equation
ν'	Van der Waals radii associated with substituent
ν	kinematics viscosity ($m^2.s^{-1}$)
ω	angular frequency of oscillation ($rad.s^{-1}$)
τ	residence time (s)

τ_i	residence time of tracer in i^{th} tank (s)
τ_p	tortuosity of catalysts pores
A_c	cross-sectional area of N_2 adsorbate (nm^2)
A_i	TCD peak area of exit pulse titration gas (mV.s)
A_s	GC peak area of methyl ester (mV.s)
A_{st}	TCD saturation peak area of exit pulse titration gas (mV.s)
A_{is}	GC peak area of internal standard (mV.s)
[A]	concentration of species A ($mol.L^{-1}$)
$[A]_o$	initial concentration of species A ($mol.L^{-1}$)
C_{is}	concentration of internal standard ($mg.L^{-1}$)
[Cat]	concentration of catalyst ($g.L^{-1}$ or $mol.L^{-1}$)
D	diameter of baffled reactor (m)
D_A	diffusion coefficient ($m^2.s^{-1}$)
D_e	effective diffusivity ($m^2.s^{-1}$)
D_o	baffle orifice diameter (m)
D_p	diameter of catalyst particles (nm)
E_a	Arrhenius activation energy ($J.mol^{-1}$)
E(t)	exit age distribution (s^{-1})
E(θ)	dimensionless exit age distribution
f_o	oscillatory frequency (Hz)
i	component
k	reaction rate constant ($L.mol^{-1}.s^{-1}$)
k'	apparent reaction rate constant ($L.mol^{-1}.s^{-1}$)

k_e	rate constant for esterification reaction ($L.mol^{-1}.s^{-1}$)
K_A	adsorption-desorption equilibrium constant for species A
$k_{ad(A)}$	rate constant for adsorption of species A (s^{-1})
$k_{d(A)}$	rate constant for desorption of species A (s^{-1})
K_{eq}	overall reaction equilibrium constant
k_o	pre-exponential factor for a second-order reaction ($L.mol^{-1}.s^{-1}$)
k_s	rate constant for forward surface reaction ($L.mol^{-1}.s^{-1}$)
k_{-s}	rate constant for reverse surface reaction ($L.mol^{-1}.s^{-1}$)
K_s	equilibrium constant for surface reaction
L	characteristic length of catalyst particle (m)
m	mass of sample (g)
n	moles of KOH required per mole of RSO or FAME (mol)
n_s	stoichiometric mole of active sites per mole pulse titration gas (mol/mol)
N	theoretical number of tanks-in-series
N_A	Avogadro's number, 6.022×10^{23} (mol^{-1})
P	pressure (Pa)
P_o	saturation pressure (Pa)
P/P_o	relative pressure
R	universal gas constant, 8.314 ($J.mol^{-1}.K^{-1}$)
R_f	relative response factor of methyl ester
$-r_A$	rate of reaction of species A ($L.mol^{-1}.s^{-1}$)
Re_n	net flow Reynolds number

Re_o	oscillatory Reynolds number
R_k	Kelvin pore radius (nm)
r_s	rate of surface reaction ($L.mol^{-1}.s^{-1}$)
S	slope of the BET plot (gram catalyst per gram N_2)
S_{BET}	Brunauer–Emmett–Teller surface area (m^2/g)
St	Strouhal number
t	time (s)
t_d	probe delay time
t_H	thickness of adsorbed N_2 film (nm)
Δt	time step in residence time acquisition (s)
T	temperature (K)
M_T	Thiele Modulus
u	fluid axial velocity ($m.s^{-1}$)
V	volume of injection loop in CO_2/NH_3 pulse titration (L)
V_{ad}	volume of N_2 adsorbate (L)
V_{bA}	molar volume of solute A at its boiling point ($L.mol^{-1}$)
V_{is}	volume of internal standard (L)
x_i	mass fraction (g/g) or mol fraction (mol/mol) of i^{th} component
x_o	centre-to –peak oscillatory amplitude (m)
X	fractional conversion

Chapter 1 Introduction

1.1 Background: Biofuels

Emissions of carbon dioxide to the atmosphere from the combustion of fossil fuels have become a global concern due to the associated climate change, which has adverse effects on human society. Moreover, fluctuations in fossil fuel supply resulting from various crises and political instability in exporting countries in Africa and Middle East (Asif and Muneer, 2007) have raised concerns for global energy security. A high degree of uncertainty in future global energy supply is anticipated, as finite fossil fuel deposits are depleted (Owen *et al.*, 2010). Therefore, increased renewable energy capacity that reduces emissions of greenhouse gases and dependence on fossil fuels is very important. This would ensure a cleaner environment and reduce the impact of any future energy crisis on fossil fuel-constrained economies (Lin *et al.*, 2011).

The quest for a cleaner environment and global energy security has caused a tremendous global increase in production and consumptions of biofuels in the last 10 years, especially as replacement for road transport fuels. However, fossil fuels remain the major source of transport fuels, and are responsible for substantial CO_2 emissions. For example, use of fossil fuels for road transport generated 28% of total USA CO_2 gas emissions in 2008 (Gately *et al.*, 2013). Similarly, in 2004, about 30% of total CO_2 emissions in the United Kingdom came from the transport sector (Hammond *et al.*, 2008). Globally, transport alone accounted for around 23% of energy-related CO_2 emissions in 2007 (IEA, 2009). Transport-related emissions of CO_2 continue to increase due to ever-increasing rates of road transport. Currently, the transport sector accounts for almost 60% of total world fossil energy demand, where approximately 50% of this was consumed in road transport (Berni, 2014). The demand for fuel in the transport sector is likely to increase further: the International Energy Agency (IEA) predicts that ownership of cars and trucks will increase from 700 million in 2005 to 2 billion in 2050 worldwide (IEA, 2009). Clearly, this represents a massive increase in emissions of greenhouse gases, especially CO_2. Therefore, it is imperative that a sustainable policy framework is developed, as well as efficient biofuel technologies that will meet our future energy needs from renewable sources. One of the liquid biofuels considered for this application is biodiesel.

1.2 Biodiesel

Biodiesel is the most commonly used liquid biofuels in the transport sector, representing about 82% of the biofuels production in the EU (Demirbas and Balat, 2006). It is the most attractive liquid biofuels in the transport sector due to its use as an alternative to petro-diesel. Other factors that makes biodiesel very attractive as a biofuel are the ease of production and environmental credentials: it is biodegradable and reduces pollutant emission (Cervero *et al.*, 2008).

Technically, the term "biodiesel" refers to mixtures of fatty acid alkyl esters produced by transesterification of vegetable oils and animal fats with alcohols or via esterification of free fatty acids (FFA) with alcohols. When methanol is used, the biodiesel produced consists mainly of mixtures of fatty acid methyl esters (FAME). Biodiesel can be used in conventional compression-ignition engines without any modifications, either in pure form or blended with petro-diesel. The direct application of biodiesel in diesel engines was due to the similarity in fuel properties between biodiesel and petrol-diesel (Ma and Hanna, 1999). Uses of biodiesel are associated with reductions in CO_2 emissions. Other benefits of biodiesel utilisation are: higher flash point, lower sulphur content, higher lubricity, smaller carbon footprint, and reduced particulate emissions (Yan, 2010; Di Serio *et al.*, 2008).

1.3 Catalysis of biodiesel production reactions

Biodiesel production occurs via either transesterification of vegetable oils and animal fats or esterification of FFA. These reactions use different primary alcohols such as methanol, ethanol, propanol and butanol (Zabeti *et al.*, 2009), particularly methanol, due to its low prices and availability (Xie and Yang, 2007). Biodiesel production reactions are usually catalysed. For instance, both acid and base catalysts can be used to catalyse vegetable oil transesterification reactions, but FFA esterification is catalysed only by acids. Transesterification is the most widely used process, as FFA esterification is only used for productions of biodiesel from feedstock that contains high levels of FFA. The transesterification process involves the reaction of triglycerides in the oleaginous feedstocks with alcohol (alcoholysis) to form fatty acid alkyl esters, through the interchange of alkoxy moieties (Schuchardt *et al.*, 1998).

Conventional biodiesel production uses base-catalysed homogeneous process, mainly alkali-metal hydroxides and methoxides (NaOH, KOH, $NaOCH_3$, $KOCH_3$), particularly sodium methoxide (Huber *et al.*, 2006). This necessitates various operating and capital costs downstream arising from the inability to recover the catalyst for further use, contamination of the glycerol by-product by soap from catalyst neutralisation, and the large amount of water and energy required for the washing and drying of the biodiesel (Figure 1.1).

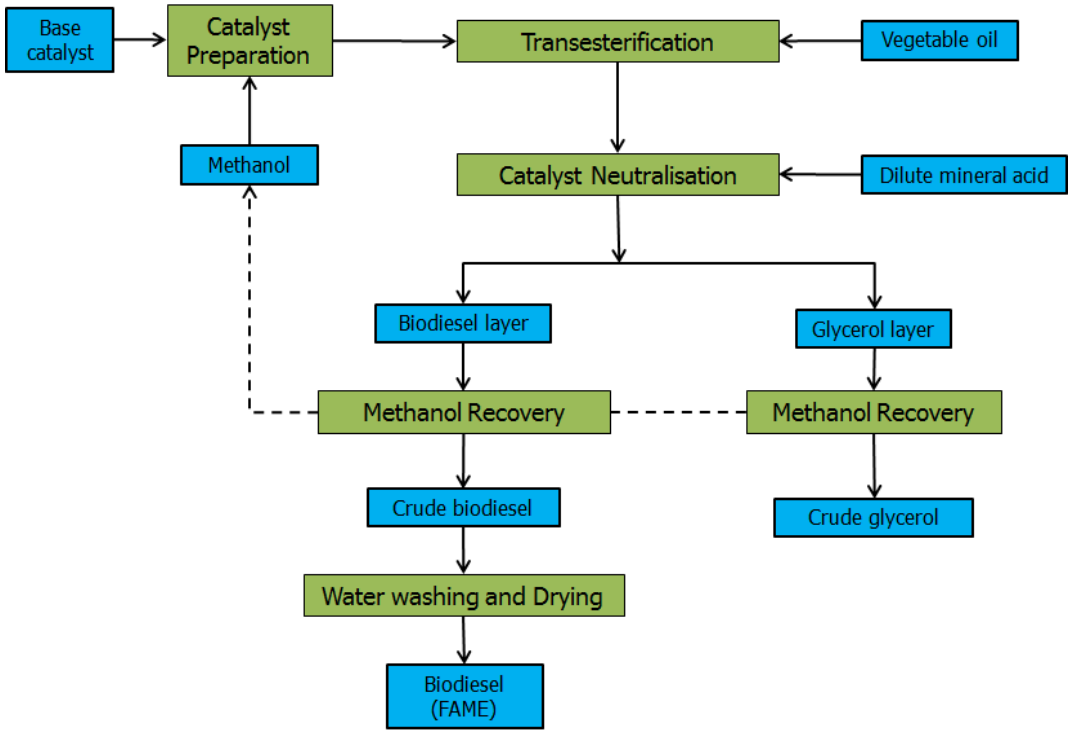

Figure 1.1: A typical homogeneous base-catalysed biodiesel process

The alkali catalysts, in particular, are sensitive to the presence of water and FFA, and take part in saponification side reactions, leading to reduced biodiesel yield. Saponification of triglycerides and FAME, and neutralisation of FFA in homogeneous base-catalysed transesterification leads to emulsification, making the products separation difficult (Demirbas, 2009; Demirbas, 2005). Process parameters in the homogeneous base-catalysed transesterification should be further investigated to find ways of accelerating the reaction and minimising the adverse effects of triglyceride and FAME saponification. Part of this study was devoted to both experimental and numerical investigations of the reaction kinetics and process parameters for base-catalysed homogeneous transesterification.

The added costs of downstream processing in the homogeneous process must be removed or reduced substantially to improve market competitiveness of biodiesel compared to the petro-diesel. To solve these problems, solid catalysts are required. Heterogeneous catalysts reduce the extra operating costs associated with catalyst neutralisation, water washing, continual replacement of catalysts, and produces higher purity biodiesel and glycerol (Figure 1.2). There is no requirement for catalyst neutralisation because the catalysts can be easily removed from the reaction mixture by simple filtration. Also, the glycerol produced via heterogeneous catalysis is not contaminated by salts; therefore, it would be able to command higher market prices than that produced by homogeneous process. When a truly heterogeneous catalyst is used, there will be no continual replacement of the catalysts, reducing further the operating costs.

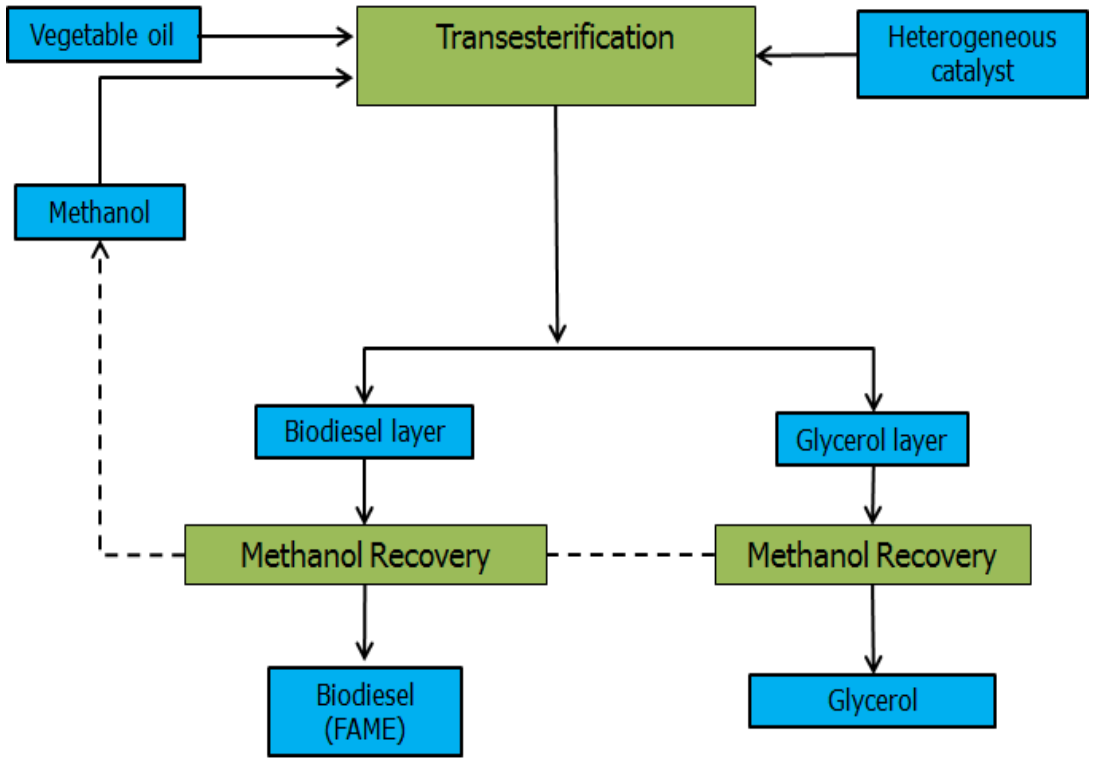

Figure 1.2: A typical heterogeneously-catalysed biodiesel process

A number of solid catalysts have been studied for application in catalysis of biodiesel production reactions (Helwani *et al.*, 2009; MacLeod *et al.*, 2008; Bournay *et al.*, 2005). Recently, supported SrO was reported to be catalytically active for vegetable oils transesterification and had improved reusability (Chen *et al.*, 2012a; Lima *et al.*, 2012; Yoosuk *et al.*, 2010). Silica supported SrO (SrO-SiO_2) had higher activity for FAME production than SrO, and was tolerant to water and FFA (Chen *et al.*, 2012a). FAME

yield >90% was achieved for olive oil transesterification at 6:1 methanol to oil molar ratio, 65˚C, and 5wt% SrO-SiO_2 catalyst in the presence of 3.23wt% water and 3.14wt% FFA. MgO-SrO also had substantial activity towards vegetable oil transesterification at 60˚C, even higher than that of SrO (Yoosuk *et al.*, 2010). However, slight leaching occurred on reuse of these catalysts (Chen *et al.*, 2012a; Yoosuk *et al.*, 2010).

Another investigation carried out using zirconia supported SrO (SrO-ZrO_2) showed that the catalyst had significant catalytic activity at reaction temperature of 60˚C (Lima *et al.*, 2012). FAME yield in excess of 98% was achieved after 3h for methanolysis of soybean oil at 12:1 methanol to soybean oil molar ratio using 3wt% of the SrO-ZrO_2. No study was carried out on the reusability of the SrO-ZrO_2 catalyst. Catalytic activity and reusability of the SrO-ZrO_2 catalyst was, therefore, investigated as part of this study.

As previously stated, base-catalysed transesterification processes are ineffective when processing triglyceride feedstock with high levels of FFA. Usually, a two-step process, acid-catalysed esterification of the FFA, followed by base-catalysed transesterification is recommended for feedstocks containing FFA $\geq$ 0.5wt% or water $\geq$ 0.3wt% (Moser, 2009; Canakci and Van Gerpen, 2003). As a part of this research, alkyl sulphonic acid functionalised mesoporous silica was investigated mainly for the FFA esterification step. Alkyl sulphonic acid functionalised mesoporous silica has been reported for FFA esterification and vegetable oil transesterification (Dacquin *et al.*, 2012; Karimi *et al.*, 2012; Dhainaut *et al.*, 2010; Melero *et al.*, 2008). Activity of the catalyst was investigated at reaction temperature of 60˚C by Dhainaut *et al*. (2010) and Dacquin *et al*. (2012). But, no catalyst stability test was reported by the authors. Melero *et al*. (2008) observed a decrease in sulphur content of the alkyl sulphonic acid functionalised mesoporous silica for transesterification of palm oil with methanol at 180˚C. The decrease in sulphur content was attributed to leaching. However, it was noted by Karimi *et al*. (2012) that deactivation of propyl sulphonic acid functionalised organosilicate in transesterification of canola oil with methanol at 150˚C could be due to either decomposition of sulphonic acid groups at the high reaction temperature or leaching into methanol.

Hence, further investigations are clearly necessary to screen the reusability of the alkyl sulphonic acid functionalised mesoporous silica. Stability of the catalyst was investigated in this study at reaction temperature of 60˚C, to avoid any possible thermal decomposition of the propyl sulphonic acid group.

1.4 Kinetics of transesterification reaction

Kinetics of vegetable oil transesterification in homogeneously catalysed process was first reported by Freedman *et al.* (1986). The investigation was carried out on transesterification of soybean oil with 1-butanol and methanol, using both acid (H_2SO_4) and base (NaOBu) catalysts. The authors proposed pseudo-first-order kinetics for the acid and base catalysed reactions at 30:1 alcohol to oil molar ratio. At 6:1 alcohol to oil molar ratio, second-order kinetics was proposed for both acid and base catalysed transesterification. Noureddini and Zhu (1997) also reported second-order kinetics in a transesterification of soybean oil at 6:1 methanol to oil molar ratio, using NaOH catalyst. The study showed that vegetable oil transesterification was initially mass transfer controlled, followed by kinetically controlled stage. However, other studies (Darnoko and Cheryan, 2000b; Mittelbach and Trathnigg, 1990) suggested that all the stages in transesterification reaction did not follow second-order.

The uncertainty in the reaction kinetics for the base-catalysed homogeneous transesterification of vegetable oils has persisted notwithstanding the amount of researches that have been carried out. Although most researchers agree that the reactions follow mainly second-order kinetics (Bambase *et al.*, 2007; Vicente *et al.*, 2005; Noureddini and Zhu, 1997), the reaction rate constants varied. The actual reaction rate constants for triglyceride transesterification remain unknown. This could be due to contributions from side reactions that were not considered by the conventional kinetic model, as well as the complexity in composition of vegetable oils. Vegetable oils used in transesterification reactions contain varying amounts of FFA and water which interferes with base-catalysed transesterification by neutralising the catalyst and causing hydrolysis and saponification. The conventional kinetic model assumes that transesterification reactions are kinetically controlled, with negligible side reactions (Bambase *et al.*, 2007; Vicente *et al.*, 2005). The model does not consider the effects of FFA neutralisation, saponification of triglyceride and FAME, and hydroxide-methoxide equilibrium of the alkali catalyst in methanol.

In this study, a new kinetic model for alkali-catalysed homogeneous transesterification of triglyceride (rapeseed oil) with methanol was developed by including the side reactions to the conventional kinetic model. The new kinetic model was expected to be more robust in predictions of effects of various process parameters that are not captured by the conventional kinetic model.

1.5 Oscillatory baffled reactors (OBRs)

Biodiesel production by transesterification of vegetable oil with methanol is initially a two-phase liquid-liquid reaction due to the immiscibility of oils and methanol. To enhance mass transport and accelerate the rate of the biodiesel production reactions, process intensification reactors that have biphasic liquid-liquid mixing capability are required. When solid catalysts are used, increased mass transfer limitations occur as the reaction is transformed from biphasic liquid-liquid reaction to three-phase solid-liquid-liquid reactions. This further necessitates the use of process intensification reactor that can be adapted for solid-catalysed liquid-liquid reactions. One of the reactors which can be used for such reactions are the OBRs.

OBRs are multiphase mixing reactors which use oscillatory flow in tubes containing equally spaced baffles to provide improved fluid mixing, enhancing heat and mass transport (Mackley and Ni, 1991; Mackley *et al.*, 1990). Because of the improved fluid radial mixing, plug flow can be achieved in the OBRs at moderate net flow Reynolds numbers (Mackley and Ni, 1991). The oscillatory flow mixing in OBR can also be used for suspension of solid particles of a wide range of sedimentation velocities (Reis *et al.*, 2005; Mackley *et al.*, 1993). Generally, OBRs are very attractive multiphase intensification reactors due to their ease of fabrication, capability for suspension of solid particles and simple scale up procedure. Fluid mixing in OBRs is decoupled from the net flow, which makes it possible to screen reactions with long residence times in OBR of reduced length-to-diameter ratio (Phan and Harvey, 2010; Harvey *et al.*, 2001).

In this study, mesoscale oscillatory baffled reactors (meso-OBRs) were used. The meso-OBRs have small volume “millilitre” which allows for the use of small amounts of reagents, and reduces the wastes generated. The improved multiphase fluid mixing of the OBRs was applied in screening of liquid-liquid reactions in homogeneously catalysed rapeseed oil transesterification with methanol. The capability of the OBRs to uniformly suspend solid particles was applied for suspension and screening of the solid catalysts used in the transesterification and esterification reactions.

1.6 Aims and Objectives

The aim of this study was to evaluate the use of meso-OBRs as laboratory-scale screening platform for two-phase (liquid-liquid) and three-phase (solid-liquid-liquid)

systems. The systems studied were homogenous and heterogeneous catalysed biodiesel production reactions. Biodiesel production reactions were investigated because of the importance of biodiesel as a renewable transport fuel.

The following objectives were defined:

1. To use meso-OBR platform to rapidly screen, both in batch and continuous mode, the catalytic activity and optimal conditions of heterogeneous acid and base catalysts, using suspended catalyst particles for rapeseed oil transesterification and FFA esterification with methanol.

2. To use meso-OBR platform to rapidly screen process parameters in alkali-catalysed homogeneous transesterification of rapeseed oil with methanol using various alkali catalysts - KOH, NaOH and $NaOCH_3$.

3. To study the alkali-catalysed homogeneous transesterification of rapeseed oil with methanol using both experimental investigations and numerical modelling, to find optimal conditions and explain drop in FAME yields.

4. To evaluate the steady state performance of the meso-OBRs in alkali-catalysed homogeneous transesterification of rapeseed oil with methanol, as proof-of-concept for liquid-liquid reactions.

5. To characterise various meso-OBR designs by evaluations of their residence time distributions as a function of net flow Reynolds number, oscillatory Reynolds number and velocity ratio. The meso-OBR designs were: integral baffles, sharp-edged helical baffles with a central rod and wire wool packing.

6. To investigate the kinetics of rapeseed oil and FAME saponification in methanol-KOH solutions.

Chapter 2 Literature Review

2.1 Biodiesel production and consumption – a global outlook

Globally, biofuels production has increased significantly since 2000, mainly due to contributions from USA, Brazil, the European Union (EU), Malaysia and India (IEA, 2010). Most of these biofuels are bio-ethanol and biodiesel, which are used as liquid fuels for automobiles. Bio-ethanol is produced commercially at an industrial scale for use either on pure form or blended with gasoline for liquid transport fuel. Brazil currently has the most comprehensive supply, domestic consumption and export of bio-ethanol worldwide, initially driven by the oil shocks of 1970's (Berni, 2014). The substantial bio-ethanol program in Brazil was due to the availability of raw materials from sugarcane and molasses from sugar industry.

Biodiesel, an alternative to petro-diesel derived from renewable sources such as vegetable oils and animal fats, is the most commonly used biofuel. It is by far the biggest biofuel consumed in the EU, representing about 82% of the biofuels production (Demirbas and Balat, 2006). There has been a tremendous growth in biodiesel production and consumption worldwide in the last 10 years, driven by energy security and environmental concerns. These issues have prompted regional bodies to come up with legislation mandating the use of biofuels, especially biodiesel. For instance, the total biodiesel production in the Europe Union (EU) member states grew from 3,184 million metric tonnes in 2005 to 21,904 million metric tonnes in 2010 (EBB, 2013), approximately a 590% increase. By 2012, biodiesel production in the EU had increased to 23,538 million metric tonnes, with Germany continuing as the largest producer at ~30% of the total biodiesel produced. Biodiesel production in United Kingdom remained at ~1.5% of the total biodiesel produced in the EU from 2005 – 2010, and increased to 2.4% in 2012.

The rapid growth in biodiesel consumption in the EU was due to favourable policies and the European Biofuels Directives. Biofuels consumption of about 5.75% by volume was proposed for all fossil fuels used in transport by European Biofuels Directive (2003/30/EC). Though the Directive was not met by most EU states, it bolstered the growth of biodiesel market in the Europe. Thus, the Biofuels Directive was replaced with the Renewable Energy Directive (2009/28/EC), which took effect in 2011,

mandating the use of renewable energy in the transport sector among the EU states. In the UK, the Renewable Transport Fuel Obligation was implemented by the Department for Transport to reduce CO_2 emissions. It is mandatory from 2013-2014, that all road transport fuels sold in the UK must contain 5.0% by volume of renewable (Department for Transport, 2011). The European Renewable Energy Directive projects 10% renewable energy for all transport fuels used in the Europe by 2020 (Department for Transport, 2011). These directives are targeted at enhancing the EU's energy security, economic growth and mitigating global warming.

Notwithstanding this rapid development in biodiesel capability worldwide, this technology remains in its infancy in most countries in Africa, including Nigeria. While Europe contributes about 55% of world biodiesel production, 29% from USA, 9% from Asia and Oceania, the total biodiesel production in Africa remained the lowest at about 0.06% (IEA, 2010).

Biodiesel utilisation has the capacity to reduce emissions of CO_2, thereby reducing climate change, create a market for agricultural products such as vegetable oils, and open a new frontier for economic empowerment of the rural poor. However, there are some concerns about possible food shortages and damage to ecosystems. Careful consideration must be given to any uses of edible oil for biodiesel production to avoid global food crisis. There should be a balance between the use of vegetable oils for food and biodiesel, through regional legislations. Government policies should also provide a rational option for land use to ensure that arable land meant for food production will not be used for biofuels. It is expected that biodiesel production in the future will be mainly dependent on excess edible oils from rapeseed oil, sunflower oils, soybean oil, palm oil, restaurant waste oils and animal fats, and non-edible oils from algae and *Jatropha* (Wang *et al.*, 2007).

2.2 Rapeseed oil as a feedstock for biodiesel production

Biodiesel is produced from renewable sources of triglyceride. These sources include edible oilseeds, algae, animal fats and low-value materials, such as waste cooking oil and greases (Moser, 2009). Other alternative feedstocks have also been considered for biodiesel production, mainly non-edible oils, including *Jatropha curcas, Sterculia foetida and Ceiba pentandra* (Ong *et al.*, 2013; Kalbande *et al.*, 2008), which grow in tropical climates. Choice of triglyceride feedstock is a very important decision in

biodiesel production. This was due to the strict requirement that biodiesels used in diesel engines must meet fuel properties prescribed in regional standards to ensure engine safety. The two major biodiesel fuel standards are ASTM D6751 (ASTM, 2008) in the USA and Canada, and EN 14214 in the EU developed by the European Committee for Standardization (CEN, 2003). For any biodiesel component to be used either in pure form or blended in petro-diesel, it must meet these quality standards (Moser, 2009). Therefore, suitable technologies and feedstocks must be used to ensure compliance of the biodiesel produced with the relevant standards. The choice of feedstock for biodiesel production varies with climate and availability. Rapeseed oil (RSO) and sunflower oil are the predominant feedstocks used in the Europe, soybean and animal fats in USA, and palm oil in tropical regions (Demirbas, 2006). Oilseeds accounted for 81% of the biodiesel produced in 2007 worldwide, with 48% from RSO, 22% from soybean oil and 11% from palm oil (International Grain Council, 2008). The dominance of RSO among vegetable oils used for biodiesel production in the Europe, including the UK, was due to its availability, low price and superior fuel properties of the alky esters derivatives (Mittelbach, 2006).

Rapeseed (*Brassica napus* L.ssp. *oleifera*), is a bright yellow flowering member of the mustard plant family (*Brassicaceae*). The wide cultivar of rapeseed has limited application due to the high content of erucic acid (~54%) which causes damage to cardiac muscles, and has a bitter taste from its glycosinolate content (O'Brien, 2008). Before the genetic modification of the wide rapeseed in the 1960 – 1970 by Canadian researchers (Canola Council of Canada, 2011), RSO was mainly used as raw material for paint production, soap making and lamp oil. The genetic modification lead to the development of a new species of RSO commonly known as canola oil, with low levels of erucic acid and glycosinolate (Mittelbach, 2006).

The wide applications of oil from the modified rapeseed (*Brassica napus)* have led to a sharp rise in RSO production globally in the last 10 years, rising from 13,372 million metric tonnes in 2000 to 23,516 million metric tonnes in 2010, and currently at 25,273 million metric tonnes (USDA, 2013). European Union states play a dominant role in the worldwide RSO production (Figure 2.1), accounting for nearly 40% of global RSO production (USDA, 2013). Rapeseed typically has about 40 – 45% oil content (Mittelbach, 2006; Matthaus and Bruhl, 2001), which can be increased further by 40%, through genetic modifications (Vigeolas *et al.*, 2007).

Biodiesel produced from RSO has excellent fuel properties due to the high content of oleic acid in RSO, typically about 52 – 65 wt%, which has been identified as a suitable fatty acid for enrichment in fatty acid profile (Knothe, 2008). This was due to the improved fuel properties of methyl oleate compared with methyl esters of other fatty acids (Kinney and Clemente, 2005). FAME produced from RSO have low cloud point (CP) and low cold filter plugging point (CFPP) (Knothe, 2008), evidencing good flow property of biodiesel from RSO. CP is the temperature at which the biodiesel becomes cloudy as a result of formations of small FAME wax crystals, indicating an onset of crystallisation. The CFPP refers to the lowest temperature at which a diesel fuel can still pass through standard filter at specified time. At temperatures below the CFPP, massive formation of waxy FAME precipitate occurs, plugging the diesel engine filter. Biodiesel produced from RSO has CFPP typically in the range of – 6˚C to – 8˚C, which is lower than that of palm oil, soybean oil, sunflower oil and coconut oil (Knothe, 2008).

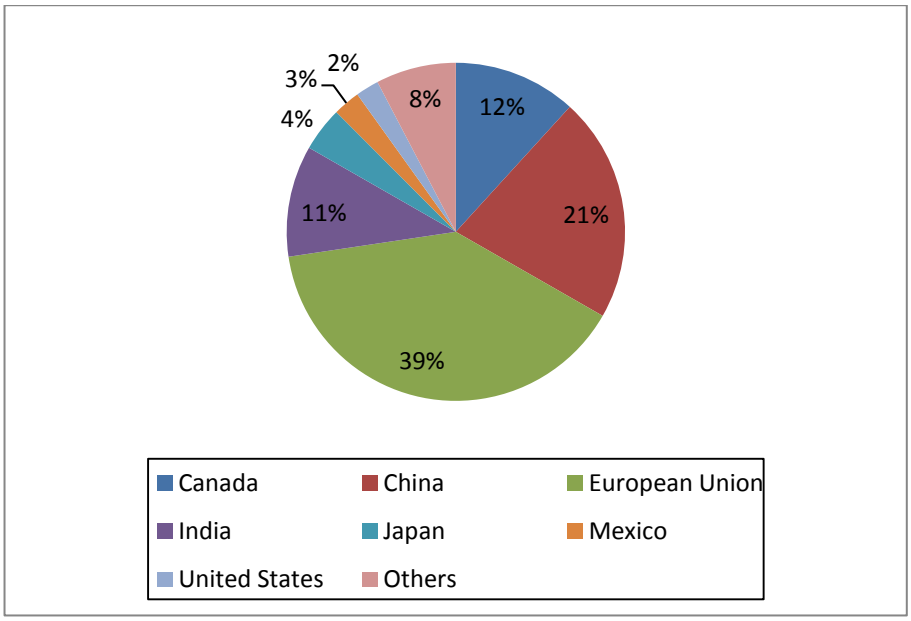

Figure 2.1: Distribution of world RSO production in 2010 (USDA, 2013) (pie chats plotted from the reported data).

2.3 Biofuels productions from vegetable oils

Biofuels for diesel engine application can be formulated by blending in petro-diesel, micro-emulsion in alcohol, cracking, and transesterification of vegetable oils (Hou *et al.*, 2007). Pure vegetable oils can also be used as biofuels for diesel engine. For instance, peanut oil was used as diesel engine fuel in 1893, when Rudolf Diesel ran his prototype diesel engine in Augsburg, Germany (Ramadhas *et al.*, 2004). Though, peanut oil was

successfully used by Rudolf Diesel, direct application of vegetable oils is not recommended for diesel engines because of their high viscosity, which ranges from 10 to 20 times greater than that of petro-diesel (Keera *et al.*, 2011). Due to high viscosity of vegetable oils, poor atomization of the oil occurs in combustion chamber, resulting in major engine problems like nozzle coking and blockage by deposits (Srivastava and Prasad, 2000). Other problems associated with the direct use of vegetable oils are their high CP, high surface tension, low cetane number, presence of phosphatides impurities, and susceptibility to the formation of sludge and coke on combustion (Haas, 2005). In cold climates, high CP of vegetable oils causes lots of technical setbacks during operations.

In order to circumvent these problems, direct blending of vegetable oil in petro-diesel, micro-emulsion in alcohol, cracking (pyrolysis) and transesterification of the oils with alcohols were used. Direct blending of vegetable oil in petrol-diesel and micro-emulsions in simple alcohols are not viable options due to engine fouling. Technical problems such as engine coking, gumming and sticking of piston rings equally persists in these methods (Di Serio *et al.*, 2008; Ramadhas *et al.*, 2004). The only improvement obtained by the use of direct blending and micro-emulsion is the improved spray characteristics and combustion of the fuel. Therefore, productions of renewable alternatives to petro-diesel have been largely concentrated on pyrolysis and transesterification of vegetable oils.

Pyrolysis is a catalytic or thermal process where heavy molecules are split into smaller units in the absence air (Maki-Arvela *et al.*, 2007; Snare *et al.*, 2007). In vegetable oil pyrolysis, triglycerides are cracked into smaller molecules by a combination of catalyst and heating (Fortes and Baugh, 2004). It can also be carried out by cracking of sodium salt (soaps) of fatty acids, which gives even higher yield than cracking of triglycerides (Demirbas, 2002). Vegetable oils pyrolysis occurs at temperatures of about 300 – 500˚C in the presence of catalysts such as SiO_2/Al_2O_3 and SO_4^{2-}/ZrO_2 (Eterigho *et al.*, 2011; Lima *et al.*, 2004), producing mainly of alkane compounds, which are similar to those in petro-diesel. This helps to overcome problems such as high viscosity, coking and gumming associated with pure vegetable oil and its blends. However, biofuels obtained through cracking contains an amount of total acid value above the standard value of $0.50 mg.KOH.g^{-1}$ for pure biodiesel (EN 14214 and ASTM D6751). Therefore, downstream processing is required, adding to the cost of production.

Technically, pyrolysis is not a method for producing biodiesel. The biofuels produced by cracking of vegetable oil consists mainly of alkane compounds, unlike biodiesel which is chemically a mixture of fatty acid alkyl esters. The term "biodiesel" specifically refers to fatty acid alkyl esters produced by transesterification of vegetable oils with alcohols or via esterification of FFA with alcohol. For any biofuels to be used as biodiesel, it must meet the EN 14214 and ASTM D6751 biodiesel standards. The biodiesel production reactions – transesterification and esterification were reviewed in details.

2.4 Biodiesel production reactions

2.4.1 Transesterification of triglycerides

Transesterification process involves the reaction of triglycerides (main components of vegetable oils or animal fats) with short chain primary alcohols (methanol) to produce FAME and by-product glycerol via three stepwise reversible removals of the fatty acid moieties from the triglyceride (Issariyakul and Dalai, 2012; Bambase *et al.*, 2007; Darnoko and Cheryan, 2000b). These reaction steps are shown in Figure 2.2. The most commonly used transesterification method is the conventional process that uses alkali-catalysed homogeneous transesterification reaction (Balat and Balat, 2010). Over 60% of the world biodiesel was produced through this method, especially with sodium methoxide (Huber *et al.*, 2006).

The rate of each step in the transesterification reaction is a function of reaction temperature, methanol to oil molar ratio, type of catalyst and its concentration. Conventional transesterification process is usually carried out at temperatures in the range of 25˚C – 65˚C, with the rate of biodiesel yield increasing with temperatures (Bambase *et al.*, 2007; Vicente *et al.*, 2005). For instance, FAME yields of approximately 25% at 25˚C, 84% at 40˚C and 92% at 60˚C were reported after 20min reaction time for transesterification using 6:1 methanol to sunflower oil molar ratio and 0.5wt% NaOH based on the oil (Bambase *et al*., 2007).

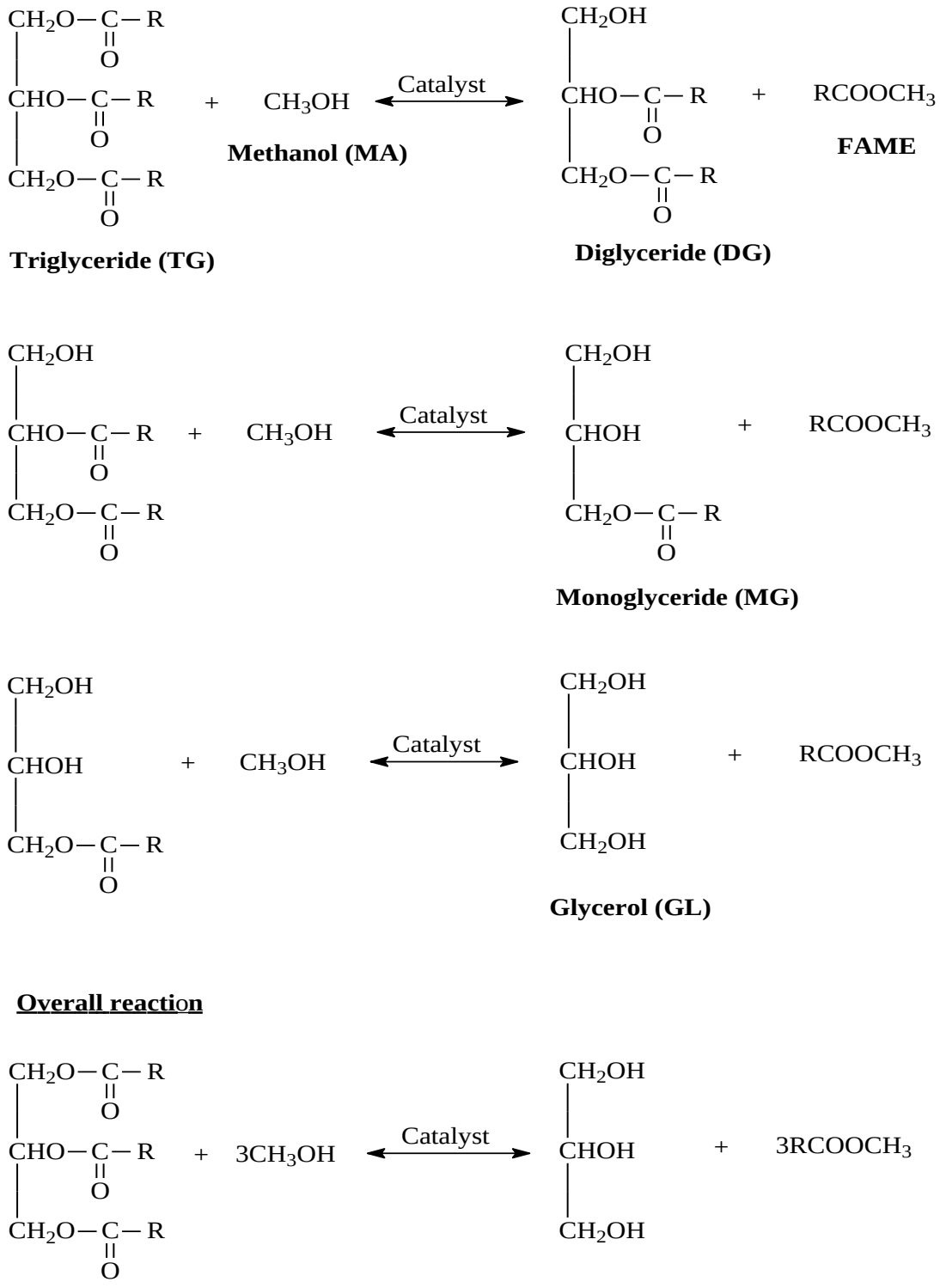

Figure 2.2: Step-wise transesterification reactions

Reaction temperatures used in conventional transesterification processes are usually below the boiling point of methanol to prevent the formation of bubbles which inhibits mass transfer on the phases' interface (Liu *et al.*, 2007). Due to the reversible reactions in transesterification, excess methanol is required to shift the equilibrium towards production of FAME, according to Le Chatelier's principles. Therefore, a molar ratio of

methanol to oil above the stoichiometric requirement (3:1) is required. The methanol to oil molar ratio of 6:1 was reported as the optimal condition for base-catalysed transesterification (Keera *et al.*, 2011; Rashid and Anwar, 2008; Freedman *et al.*, 1984). It was reported that solubilisation of methanol and glycerol phases occurred at methanol to oil molar ratios above 6:1, resulting in FAME loss (Rashid and Anwar, 2008). However, some studies have shown that methanol to oil molar ratio above 6:1 can be used to achieve high FAME yield, i.e 99% FAME yield was achieved for transesterification at 9:1 methanol to soybean oil molar ratio, 56˚C and 1.2wt% KOH, using zigzag micro-reactor (Wen *et al.*, 2009).

Transesterification reaction is mass-transfer controlled at the initial stage followed by kinetically controlled stage (Klofutar *et al.*, 2010; Stamenković *et al.*, 2008; Freedman *et al.*, 1984). To enhance mass transfer and miscibility of oil and methanol, effective multiphase mixing reactors were used (Mazubert *et al.*, 2013). Co-solvents such as tetrahydrofuran and n-hexane have also been used to enhance miscibility of oil in methanol (Doell *et al.*, 2008; Kim *et al.*, 2004; Gryglewicz, 1999; Boocock *et al.*, 1998). During transesterification reaction, formations of diglyceride, monoglyceride and FAME improves the mass transfer, as these species serve as surfactants by transforming the biphasic reaction into a single phase. As the reaction proceeds, the monophasic reaction mixture returns to two phases of FAME and glycerol. A separation occurs if mixing is not sufficient, decreasing the rate of the reaction because most catalysts reside in the glycerol phase.

2.4.2 Esterification of carboxylic acids

Esterification is a reversible reaction of carboxylic acids with alcohol (e.g. methanol) to produce alky esters and water in the presence of acid catalysts (Moser, 2009; Liu *et al.*, 2006c) as shown in Figure 2.3. Esterification of carboxylic acids has wide applications in the production of fine and speciality chemicals, including the manufacture of intermediates for fragrances, lubricants, fabrics and polymers (Hoydonckx *et al.*, 2004). It is a key step in biodiesel production to convert FFA to fatty acid alkyl esters (Wilson and Lee, 2012). FFAs are carboxylic acids with even-numbered hydrocarbon chains. The FFAs found in RSO have hydrocarbon chain lengths in the range of $C_{12} – C_{20}$, with degrees of saturation of 0 – 3 double bonds (Niczke *et al.*, 2007).

Fatty acid esterification becomes an important step in productions of biodiesel from feedstock containing high levels of FFA. If the feedstock contains more than 1% FFA, a two-step process: FFA esterification followed by alkali-catalysed transesterification is needed (Wang *et al.*, 2007; Wang *et al.*, 2005). Other studies suggest that acid-catalysed process should be used at FFA ≥ 0.5wt% (Canakci and Van Gerpen, 2003; Ma *et al.*, 1998).

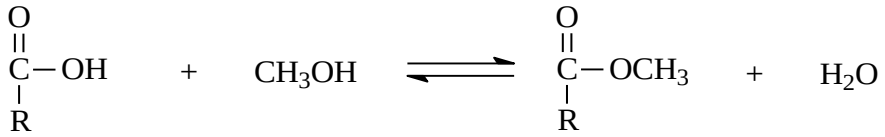

Figure 2.3: Carboxylic acid esterification

2.5 Catalysis of biodiesel production reactions

Biodiesel production reactions are carried out in the presence of catalysts, e.g. acid catalysts for esterification and either acid or base catalysts for transesterification. Some of the catalysts reported for the biodiesel production reactions are base catalysts (Mishra *et al.*, 2013; Balat and Balat, 2010; Bambase *et al.*, 2007; Huber *et al.*, 2006), acid catalysts (Wilson and Lee, 2012; Wang *et al.*, 2010; Moser, 2009; Liu *et al.*, 2006b; Hoydonckx *et al.*, 2004) and biocatalysts/enzymes (Lee *et al.*, 2013; Lam *et al.*, 2010; Jeong and Park, 2008). Biodiesel can also be produced by vegetable oil transesterification using a supercritical fluid process without catalysts (Lee and Ofori-Boateng, 2013; Glisic and Skala, 2009; Kusdiana and Saka, 2001).

Transesterification of vegetable oils via supercritical alcohol process and enzyme catalysis have not been used for commercial production of biodiesel due to the high operating costs. Supercritical methanolysis of oils is not cost-effective due to the high pressure (~8 MPa) and temperature (~ 350˚C) required for the reaction (Kusdiana and Saka, 2001). Enzyme-catalysed biodiesel synthesis remains too expensive to be used for any meaningful industrial application because of the high cost of enzymes, slow reaction rates, and deactivation of the enzymes (Lam *et al.*, 2010). Therefore, developments in biodiesel production catalysts have accordingly focused on acid and base catalysts, either in homogeneous or heterogeneous catalysis.

2.6 Homogeneous catalysis of biodiesel production reactions

2.6.1 Homogeneous base-catalysed biodiesel production process

The mechanism of base-catalysed transesterification process is summarised in Figure 2.4 (Lee *et al.*, 2009). The base catalyst (B) reacts reversibly with the alcohol to produce alkoxide ion which attacks on the carbonyl group of the triglyceride to form a tetrahedral intermediate, that decomposes to form fatty acid alky ester and a diglyceride ion. The base catalyst is regenerated when the diglyceride ion deprotonates the catalyst complex (BH^+) to form the diglyceride molecule. Similarly, the alkoxide ion reacts with the diglycerides to form monoglyceride and more alkyl esters, and subsequently with the monoglyceride to form glycerol and alkyl esters.

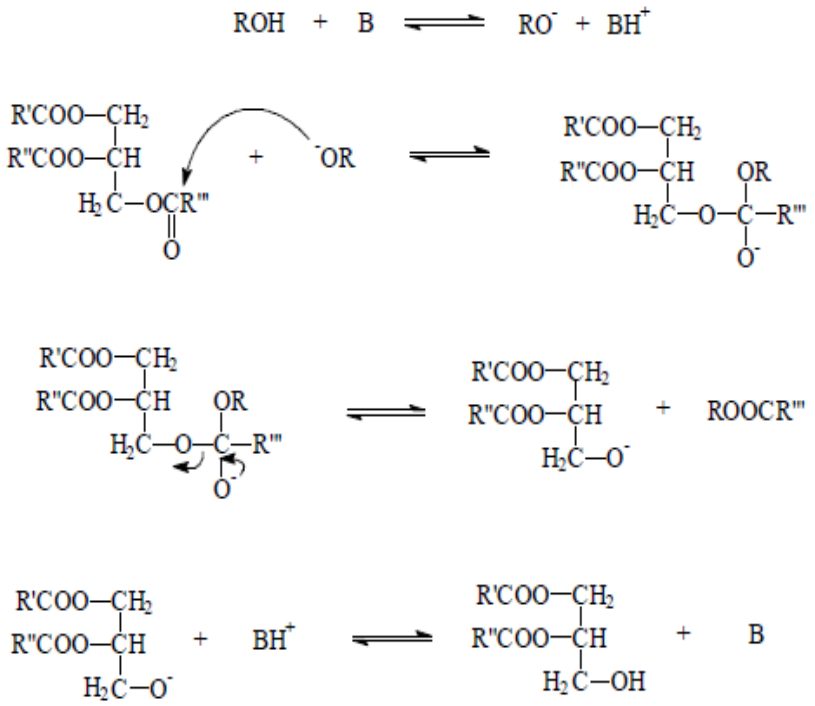

Figure 2.4: Mechanism of base-catalysed transesterification (Lee *et al.*, 2009)

Homogeneous base-catalysed transesterification are usually carried out at moderate temperatures (25 - 65˚C), methanol to oil molar ratio of 6:1 and mixing intensity of about 600rpm, using metal hydroxides and methoxides of sodium and potassium (Vicente *et al.*, 2004). For instance, the catalytic performance of NaOH, KOH, $NaOCH_3$ and $KOCH_3$ was investigated for methanolysis of sunflower oil at 6:1 methanol to oil molar ratio and 65˚C using a 100mL batch reactor at 600rpm mixing intensity and 1wt%

catalyst based on the oil (Vicente *et al.*, 2004). The FAME yield was 99.33% for $NaOCH_3$, 98.46% for $KOCH_3$, but only 86.71% for the NaOH, and 91.67% for the KOH after 4h reaction time. The lower FAME yields using the hydroxide catalysts was explained to be due to triglyceride saponification which led to increased FAME solubility in the glycerol phase, resulting in FAME losses. Triglyceride saponification (Figure 2.5) occurred in transesterification of waste frying oil using the homogeneous base catalysts (Leung and Guo, 2006). These studies did not investigate the kinetics of the triglyceride saponification.

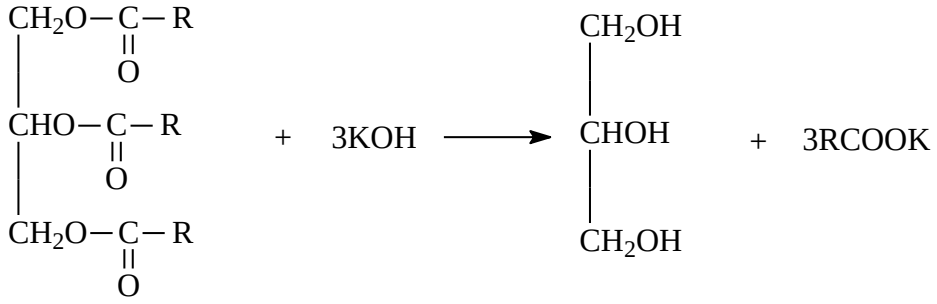

Figure 2.5: Triglyceride saponification in base-catalysed transesterification reaction.

Catalysis of citrulus colocynthis oil transesterification with methanol using NaOH, KOH, $NaOCH_3$ and $KOCH_3$ was studied (Elsheikh *et al.*, 2014). The reaction was performed in a 250mL batch reactor equipped with a stirrer at 600rpm at experimental conditions of 35 – 80˚C, 0.6 - 1.5wt% catalyst (based on oil) and methanol to oil molar ratio of 3:1 – 12:1. NaOH, KOH and $NaOCH_3$ catalysts achieved similar maximum FAME yield. The maximum FAME yield was achieved using 1.0wt% NaOH, 1.1wt% KOH, 1.2wt% $NaOCH_3$ and 1.3wt% $KOCH_3$ at 6:1 molar ratio, 60˚C and 100min reaction time. The FAME yields were 98% for NaOH, 95% for KOH, 94% for $NaOCH_3$ and 88% for $KOCH_3$. However, the amount of catalysts used was not indicative of the true performance due to the differences in their molecular weights. Considering the molar concentrations of the catalysts: 25mmol/g for NaOH, 17.9mmol/g for KOH, 18.5mmol/g for $NaOCH_3$, and 14.4mmol/g for $KOCH_3$, it is obvious that NaOH has the highest while $KOCH_3$ has the lowest concentration of active catalytic species which explains the trend in the FAME yields.

Effects of the catalyst type (NaOH, KOH, $NaOCH_3$ and $KOCH_3$), catalyst concentration, reaction temperature, methanol to safflower oil ratios and mixing intensity was investigated for transesterification of safflower oil using a 1L batch

reactor (Rashid and Anwar, 2008). The yield of FAME was in the order of catalyst $NaOCH_3$ > $KOCH_3$ > NaOH > KOH. Incomplete reaction of the safflower oil occurred at low methanol to oil molar ratios, e.g. 61% FAME yield was obtained at 3:1 compared to 98% at 6:1 after 120min reaction. The results clearly showed that more excess methanol was needed to drive the reaction towards higher FAME yield.

Other homogeneous base catalysts such as non-ionic bases like guanidines, amidines and triamino (imino)phosphoranes were used for transesterification (Schuchardt *et al.*, 1998). Around 90% FAME yield was obtained for RSO transesterification with methanol at 70˚C, 6:1 molar ratio of methanol to RSO and 1mol% of 1,5,7-triazabicyclo[4,4,0]dec-5-ene guanidine catalyst after 1h reaction time. Catalytic activity of the guanidine was comparable to that of conventional alkali catalysts. For instance, 98.7% FAME yield was obtained at 70˚C, 6:1 molar ratio of methanol to RSO and 1mol% NaOH after 1h reaction time. More research has to be carried out to evaluate the overall costs of the guanidine-catalysed process and the availability of such catalyst for large scale biodiesel production. Similar to conventional alkaline catalysts, guanidine cannot be used for transesterification of feedstock containing FFA.

In summary, homogeneous base-catalysed reactions are widely used for biodiesel production. The reactions occur at high rates due to the high basicity of the base catalysts. However, this process is not recommended in processing of feedstock containing ≥ 0.5wt%. In the presence of FFAs (≥ 0.5%) or water (≥ 0.3%), the alkali catalysts become ineffective due to soap formation and catalyst deactivation (Leung and Guo, 2006; Canakci and Van Gerpen, 2003; Ma *et al.*, 1998; Freedman *et al.*, 1984). Base catalysts react with FFA to form soap, causing difficulty in separation of biodiesel and glycerol. Water had more effect on alkali-catalysed transesterification due to increased soap formation and emulsification (Demirbas, 2009).

2.6.2 Homogenous acid-catalysed biodiesel production process

A two-step process, acid-catalysed esterification of the FFA, followed by base-catalysed transesterification, or acid-catalysed transesterification is recommended for feedstocks containing high levels of FFAs (≥ 0.5wt%) or water (≥ 0.3wt%). The most commonly used acids for homogeneous biodiesel reactions are sulphuric, phosphoric, hydrochloric and organic sulphonic acids (Balat and Balat, 2010; Cardoso *et al.*, 2009; Lotero *et al.*, 2005; Schuchardt *et al.*, 1998). Among these, the most frequently used catalyst is

sulphuric acid because of its higher activity, cheap price and availability (Naik et al., 2008; Bondioli, 2004). The mechanism of acid-catalysed transesterification is described in Figure 2.6. The acid-catalysed transesterification proceeds through the protonation of the triglyceride carbonyl group to form a carbocation. This exposes the triglyceride carbonyl group to nucleophilic attack by alcohol to form a tetrahedral intermediate as shown in the step 2 (Schuchardt et al., 1998). The intermediate decomposes to form diglyceride and fatty acid alkyl ester, and regenerates the catalyst. These reaction steps are repeated to convert diglyceride to monoglycerides, and finally monoglyceride to fatty acid alkyl ester and glycerol.

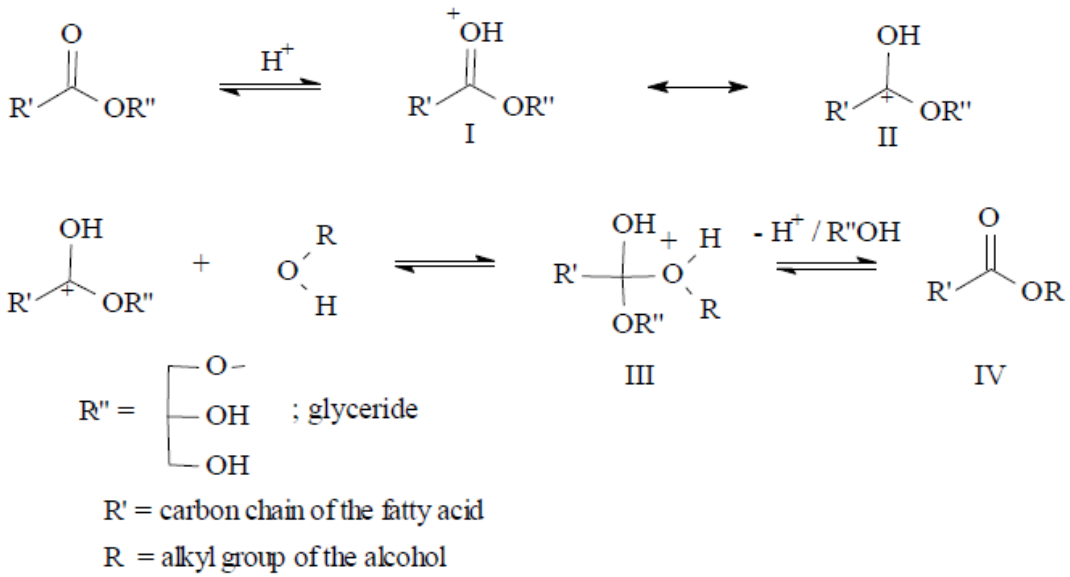

Figure 2.6: Reaction mechanism for acid-catalysed transesterification (Schuchardt *et al.*, 1998)

Mechanistic steps for the acid-catalysed esterification of carboxylic acids (FFA) are shown in Figure 2.7. The protonation of the organic acid carbonyl oxygen by the catalyst leads to the formation of a carbocation, exposing the organic acid carbonyl carbon to nucleophilic attack by alcohol. A tetrahedral intermediate formed decomposed to yield an alkyl ester and water. This reaction is reversible since protonation of the produced alkyl esters followed by nucleophilic attack by water, regenerates the carboxylic acid and alcohol.

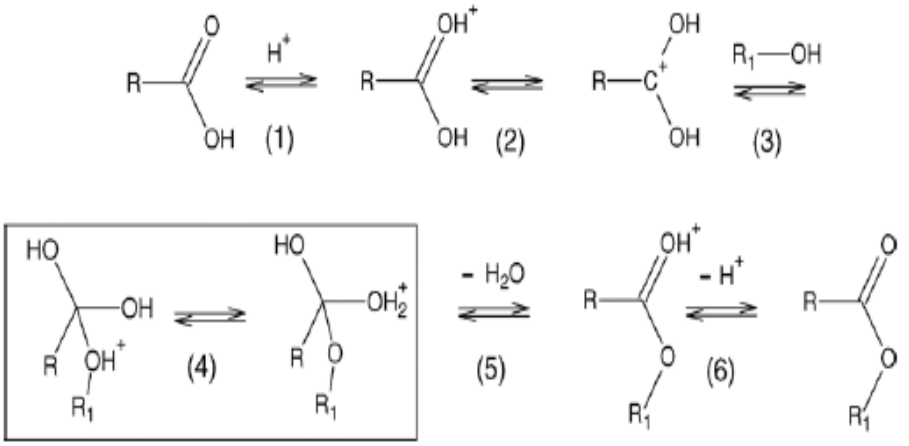

Figure 2.7: Reaction mechanism for carboxylic acid esterification (Liu *et al.*, 2006c)

Homogeneous acid-catalysed transesterification of soybean oil with methanol was investigated at 9:1 methanol to oil molar ratio, 1wt% catalyst and reaction temperatures of 100˚C and 120˚C using sulphuric, hydrochloric, formic, acetic, and nitric acids (Goff *et al.*, 2004). The reaction was carried out in 1mL sealed ampule glass tubes. After 20h reaction time, more than 99% FAME yield was reported for H_2SO_4 and less than 0.7% for other acids at 120˚C. Freedman *et al*. (1986) also studied transesterification of soybean oil with 1-butanol using sulphuric acid catalyst at 30:1 1-butanol to soybean oil molar ratio, 1mol% H_2SO_4, and reaction temperatures in the range of 77 – 117˚C. The rate of soybean oil transesterification was strongly dependent on temperature, e.g. more than 99% alkyl esters yield was achieved at 77˚C temperature after 20h reaction time, but only 3h reaction time was required to obtain similar yield at 117˚C temperature (Freedman *et al.*, 1986).

Simultaneous esterification and transesterification of vegetable oils with high FFA using H_2SO_4 catalyst was also investigated (Prošková *et al.*, 2013; Zabeti *et al.*, 2009). 95% FAME yield was achieved after 7h reaction time for transesterification at a molar ratio of 10:1 methanol to animal waste fats containing 23.63wt% FFA, using 2wt% H_2SO_4 and 95˚C, compared to 53% FAME yield at 20:1 molar ratio, 8wt% NaOH and 80˚C after similar reaction time (Prošková *et al.*, 2013). Notwithstanding this advantage, acid-catalysed biodiesel production is less favoured than the base-catalysed process because of the slow reaction rate of acid catalysed transesterification (Cervero *et al.*, 2008; Freedman *et al.*, 1984). The rate of acid-catalysed transesterification is about 4000 times slower than that of a alkali-catalysed process (Cervero *et al.*, 2008).

Therefore, a two-stage process, with H_2SO_4 acid-catalysed esterification in a pre-treatment step followed by base-catalysed transesterification is preferred. Another disadvantage of the acid-catalysed homogeneous biodiesel process is that all the equipment has to withstand the corrosive effect of the acids. The cost of corrosion resistant vessels contributes to the cost of acid-catalysed process.

In summary, homogeneously alkali-catalysed biodiesel production process is commonly used in the industry. Homogenous base-catalysed transesterification reactions have fast reaction rates and occur at moderate temperatures (25 – 65˚C). However, use of homogeneous catalysts for biodiesel production has a technical setback associated with downstream purifications of the products. This adds to the operating costs due to the following operations:

a) Downstream purification of the biodiesel produced

b) Treatment of the waste water from biodiesel washing steps

c) Continual replacement of the catalyst

Glycerol produced in the homogeneous biodiesel process has low market value because of its low quality due to contamination by the salts formed during neutralisation. Homogeneous biodiesel process also generates huge amount of waste water that must be treated to reduce the pH to an acceptable level before discharging into the environment. Therefore, replacement of the homogeneous catalysts with solid catalysts would reduce the cost of downstream purification and waste water treatment. Heterogeneous catalysis also produces glycerol of higher purity which commands higher market price and adds value to the commercial biodiesel productions. To effectively reduce the overall cost of biodiesel production, the solid catalysts must be able to catalyse the biodiesel production reactions at moderate temperatures similar to homogenous catalysts. A suitable heterogeneous catalyst for biodiesel reaction will be reusable, such that the spent solid catalysts could be economically regenerated for further use. This will save the cost for continual replacement of catalysts.

2.7 Heterogeneous catalysis of biodiesel production reactions

The demand for efficient technology for biodiesel processing has led to huge research interest in heterogeneous catalysis of biodiesel production reactions. Use of heterogeneous catalyst may eliminate downstream processing steps and produce high quality of by-product glycerol. Several solid catalysts have been investigated for catalysis of biodiesel production reactions. These catalysts can be broadly classified into solid bases and acids. Most of the catalysts reported in these categories are solid base catalysts such as supported alkali metals and alkaline earth metal catalysts, and solid acid catalysts such as sulphated zirconia, mixed metal oxides, sulphonic acid functionalised porous silica.

2.7.1 Supported alkali metal catalysts

Base-catalysed biodiesel productions using heterogenised alkali metals and their compounds were investigated (Noiroj *et al.*, 2009; Liu *et al.*, 2008; MacLeod *et al.*, 2008; Kim *et al.*, 2004) as shown in Table 2.1. Kim *et al*. (2004) reported that 94% FAME yield was obtained after 2h reaction time, for batch transesterification of soybean oil at 60˚C, using 50mL of oil, 18.3mL methanol, 10mL n-hexane co-solvent and 1g of Na/NaOH/Al_2O_3 catalyst doped with 20wt% Na and 20wt% NaOH. There was no investigation of the catalyst stability. Alkali metal salts ($LiNO_3$, $NaNO_3$ and KNO_3) supported on calcium oxide were screened for biodiesel production by RSO transesterification (MacLeod *et al.*, 2008). More than 99% FAME yield was achieved after 3h reaction time for transesterification at 6:1 methanol to RSO molar ratio and 60˚C, using 5wt% of either catalyst. Leaching of the catalysts occurred, however, the catalysts were used for up to 5 cycles without substantial loss of catalytic activity (MacLeod *et al.*, 2008).

Leaching was also reported for palm oil transesterification at 15:1 methanol to oil molar ratio using KOH/Al_2O_3 and KOH/NaY (Noiroj *et al.*, 2009). About 51% loss of KOH from KOH/Al_2O_3 and 3% from KOH/NaY occurred in palm oil transesterification at 15:1 methanol to oil molar ratio, 60˚C, 6wt% catalyst and 3h reaction time. As shown in Table 2.1, the supported alkali metals catalysts leached into the reaction mixture (Noiroj *et al.*, 2009; Liu *et al.*, 2008; MacLeod *et al.*, 2008). This indicates that, these catalysts behave similar to homogeneous alkali catalysts, in that the supported alkali metal catalysts resided in the reaction medium. Removal of the leached catalysts from the

products requires substantial downstream purification. Therefore, such catalysts cannot be used as suitable heterogeneous catalysts for biodiesel production.

Table 2.1: Supported alkali metal based catalysts used for transesterification

Nature of catalyst	Reaction conditions (Feed ratio in mol: mol)	%FAME Yield	Stability of Catalyst	References
Al_2O_3 doped with: Na = 20 wt% NaOH = 20 wt% (Na/NaOH/Al_2O_3)	CH_3OH: Soybean oil = 9:1 co-solvent: n-heptane Catalyst: 1g T = 60˚C; t = 2h	~94%	Not reported	(Kim *et al.*, 2004)
CaO doped with 5wt% salts: $LiNO_3$/CaO $NaNO_3$/CaO KNO_3/CaO	CH_3OH: RSO = 6:1 Catalyst: 5wt% of the oil T = 60˚C; t = 3h	≥ 99%	Leached	(MacLeod *et al.*, 2008)
SBA-15 doped with 20wt% KOH (KOH/SBA-15)	CH_3OH: palm oil = 11.6:1 Catalyst: 3.91wt% of oil T = 70˚C; t = 5h	87.3%	Not reported	(Abdullah *et al.*, 2009)
Al_2O_3 doped with 35wt% KNO_3 (KNO_3/Al_2O_3)	CH_3OH:soybean oil = 15:1 Catalyst = 6.5wt% of oil T = reflux (~65˚C), t = 7h	87%	Not reported	(Xie *et al.*, 2006)
Al_2O_3 & NaY zeolite doped with KOH: 25wt% KOH/Al_2O_3 10wt% KOH/NaY	CH_3OH: palm oil = 15:1 Catalyst: 6wt% of the oil T = 60˚C, t = 3h	91.1%	Leached	(Noiroj *et al.*, 2009)
Al_2O_3 doped with K_2CO_3 & KF: K_2CO_3/Al_2O_3 KF/Al_2O_3	CH_3OH: soybean oil = 6:1 Catalyst: 8wt% of the oil T = 70˚C, t = 1.5h	~80%	Leached	(Liu *et al.*, 2008)

2.7.2 Alkaline earth metal catalysts

Alkaline earth metal oxides and hydroxides have been used to catalyse vegetable oil transesterification in biodiesel productions, as shown in Table 2.2. Gotch *et al*. (2009) investigated the catalytic activity of alkaline earth metal oxides: MgO, CaO, SrO and BaO for transesterification of canola oil with methanol. The authors noted that the catalytic activities of these oxides were in the order of their basic strength: MgO ≤ CaO << SrO ≤ BaO, in methanolysis of canola oil at 6:1 molar ratio and 50˚C, using 1mol% catalyst. The FAME yields achieved for the alkaline earth metal oxides were >95% for BaO and SrO, and <10% for MgO and CaO (Gotch *et al.*, 2009). Chen *et al*. (2012a) reported that no reaction occurred when using MgO catalyst, and that only 15.1% FAME yield was achieved after 3h reaction time for transesterification of olive oil with methanol at 6:1 molar ratio and 65˚C using 5wt% CaO catalyst. The FAME yield obtained using CaO was much lower than 80% FAME yield obtained after 15min reaction time when using SrO catalyst at same operating conditions (Chen *et al.*, 2012a).

However, other studies suggest that CaO can be used as catalyst to achieve high FAME yield in biodiesel production. For instance, 98% FAME yield was achieved after 3h in methanolysis of chicken oil at 13.8:1 molar ratio and 65˚using 4.9wt% CaO obtained from crab and cockle shells (Boey *et al.*, 2011). Transesterification of palm oil with methanol at 12:1 molar ratio and 60˚C, using 10wt% of CaO synthesised from shells of eggs, golden apples, snails and meretrix venus was also used to achieve 90% FAME yield after 2h reaction time (Viriya-empikul *et al.*, 2012). Another study equally showed that more than 99% FAME yield was achieved after 2h reaction time for transesterification of canola oil at 9:1 molar ratio and 65˚C, using 3wt% nanocrystalline CaO (Zhao *et al.*, 2013). The poor catalytic activity reported for CaO by Gotch *et al.* (2009) and Chen *et al*. (2012a) may have to do with their method of CaO catalyst preparation. Loss of catalytic activity via the formation of $CaCO_3$ and $Ca(OH)_2$ on reaction with atmospheric CO_2 and H_2O, respectively, has been reported for CaO catalyst used in transesterification reaction (Zhao *et al.*, 2013).

MgO was consistently reported to have negligible activity in catalysis of vegetable oil transesterification (Chen *et al.*, 2012a; Gotch *et al.*, 2009; Gryglewicz, 1999). Even when used in triacetin transesterification with methanol at 6:1 molar ratio, 60˚C, and 2wt% MgO, only 18% methyl esters yield was obtained after 8h reaction time (López *et al.*, 2005). Higher rate of methyl ester formation was expected for triacetin due to the

small molecular size. Triacetin is a small molecular triglyceride formed from glycerol and three acetic acid moieties.

Table 2.2: Alkaline earth metal catalysts used for transesterification

Nature of catalyst	Reaction conditions (Feed ratio in mol: mol)	% FAME Yield	Stability of Catalyst	References
$Ba(OH)_2$ $Ca(OCH_3)_2$ CaO $Ca(OH)_2$ MgO	CH_3OH:RSO = 4.5:1 Catalyst: 15mol% of the oil T = 70˚C (methanol reflux) t = 2.5h	97% 95% 95% 0% 0%	Not reported	(Gryglewicz, 1999)
MgO	CH_3OH: triacetin = 6:1 Catalyst: 2wt% of triacetin T= 60˚C, t = 8h	18%	Not reported	(López *et al.*, 2005)
Nanocrystalline CaO	CH_3OH: soybean oil = 27:1 Catalyst: 0.25g T = room temperature, t = 24h	>99%	Leached74 % yield on 5 cycles.	(Reddy *et al.*, 2006)
MgO CaO SrO BaO	CH_3OH: Canola oil = 6:1 Catalyst: 1mol% of the oil T = 50˚C, t = 2h	< 10% < 10% > 95% >95%	Leached 38% yield on reuse for SrO	(Gotch *et al.*, 2009)
Magnesia supported SrO: SrO-MgO	CH_3OH: palm olein = 9:1 Catalyst: 5wt% of the oil T = 60˚C, t = 2h	97.3%	Leached 70% on 5^{th} cycle	(Yoosuk *et al.*, 2010)
CaO from shells	CH_3OH:chicken oil = 13.8:1 Catalyst: 4.9wt% of the oil T = 65˚C, t = 3h	98%	Not reported	(Boey *et al.*, 2011)
CaO from shells	CH_3OH:chicken oil = 13.8:1 Catalyst: 4.9wt% of the oil T = 65˚C, t = 3h	98%	Not reported	(Boey *et al.*, 2011)
CaO from shells	CH_3OH: palm oil = 12:1 Catalyst: 10wt% of the oil T = 60˚C, t = 2h	>90%	Not reported	(Viriya-empikul *et al.*, 2012)

Table 2.2 (contd): Alkaline earth metal catalysts used for transesterification

Nature of catalyst	Reaction conditions (Feed ratio in mol: mol)	% FAME Yield	Stability of Catalyst	References
MgO CaO SrO SrO/CaO SrO/SiO_2	t = 3h t = 3h t = 15min t = 20min t = 10min <u>Reaction conditions:</u> CH_3OH: olive oil = 6:1 Catalyst: 5wt% of the oil T = 65˚C.	0% 15.1% 80% 95% 95%	Leached: SrO/SiO_2 80% on 4th cycle	(Chen *et al.*, 2012a)
$SrO\text{-}ZrO_2$	CH_3OH: soybean oil = 12:1 Catalyst: 3wt% of the oil T = 60˚C, t = 3h	98%	Not reported	(Lima *et al.*, 2012)
Nanocrystalline CaO	CH_3OH: canola oil = 9:1 Catalyst: 3wt% of the oil T = 65˚C, t = 2h	>99%	Leached Aggregated	(Zhao *et al.*, 2013)

As shown in Table 2.2, the major setback with the use of alkaline earth metal oxides for biodiesel production reaction was the stability of the oxides. The catalysts were shown to be gradually leaching into the reaction mixture (Zhao *et al.*, 2013; Chen *et al.*, 2012a; Gotch *et al.*, 2009; Reddy *et al.*, 2006). This contaminates the reaction products and complicates the downstream purification. CaO leaching was reported for soybean oil methanolysis at 27:1 molar ratio, using 0.25g of CaO catalyst at room temperature, eading to a reduction in the FAME yield, e.g. 99% for fresh CaO after 24h reaction time but only 74% on the 5th cycle (Reddy *et al.*, 2006). Leaching of SrO was also noted in transesterification of canola oil with methanol at 6:1 molar ratio, 50˚C and 1 mol% SrO, in which the FAME yield dropped from >95% for fresh catalyst to 38% for reused catalyst (Gotch *et al.*, 2009).

Structural modification of SrO to improve its reusability was investigated using magnesia, silica and zirconia as catalyst supports (Chen *et al.*, 2012a; Lima *et al.*, 2012; Yoosuk *et al.*, 2010). Magnesia modified SrO was used to catalyse transesterification of palm olein with methanol at 9:1 molar ratio, 5wt% catalyst, and 60˚C with the FAME

yield of 97.3% after 2h reaction time (Yoosuk *et al.*, 2010). The SrO-MgO catalyst was more active than either SrO or MgO due to new strong basic sites from the SrO-MgO interaction. However, the SrO-MgO was prone to leaching, as only about 70% FAME yield was achieved on the 5th cycle compared with 97.3% for the fresh catalyst. Another study also reported that 95% FAME yield was achieved after 10min reaction time for SrO/SiO_2 compared to 80% FAME yield for SrO after 15min reaction time, in methanolysis of olive oil at 6:1 molar ratio, 65˚C, and 5wt% catalyst (Chen *et al.*, 2012a) The maximum FAME yield obtained at a shorter reaction time for SrO/SiO_2 than for SrO was attributed to the higher Brønsted basicity in SrO/SiO_2. The SrO/SiO_2 had water and FFA tolerance, as FAME yield >90% was achieved using olive oil containing 3.23wt% water and 3.14wt% FFA (Chen *et al.*, 2012a). However, there was a slight leaching of the SrO/SiO_2 catalyst, as the FAME yield dropped to about 80% on 4^{th} cycle. Generally, there was an improvement in the catalytic stability of the supported SrO catalysts when compared with un-supported SrO reported by Gotch et al. (2009).

Recently, a zirconia supported SrO ($SrO\text{-}ZrO_2$) catalyst was studied for soybean oil transesterification with methanol (Lima *et al.*, 2012). 98% FAME yield was achieved after 3h using the $SrO\text{-}ZrO_2$ catalyst in a transesterification of soybean oil at 12:1 methanol to soybean oil molar ratio, 60˚C, and 3wt% catalyst. The ZrO_2 was expected to enhance the stability of SrO, and prevent any loss of SrO to leaching. However, stability of the catalyst to leaching was not investigated. Therefore, further studies are required to evaluate the reusability of the $SrO\text{-}ZrO_2$ catalyst for heterogeneous transesterification reactions.

2.7.3 Sulphated zirconia catalysts

Solid acids were investigated mainly for application in processing of vegetable oils that contain high levels of FFA. Among the solid acids that have been studied, sulphated zirconia (SO_4^{2-}/ZrO_2) is the most commonly used acid for heterogeneously catalysed biodiesel production (Deshmane and Adewuyi, 2013a; Garcia *et al.*, 2008; Suwannakarn *et al.*, 2008; Jitputti *et al.*, 2006). These studies indicated that sulphated zirconia has catalytic activity that was comparable to that of sulphuric acid (Table 2.3). For instance, FAME yields of 96.8% for soybean oil transesterification and 96% for the oleic acid esterification were reported after 1h reaction time for reactions at 20:1 methanol to soybean (oleic acid) molar ratio, using 5wt% sulphated zirconia (Garcia *et*

al., 2008). Similarly, Jitputti *et al*. (2006) obtained 95.8% FAME yield after 1h reaction time for methanolysis of palm kernel oil at 6:1 molar ratio and 200˚C, using 3wt% sulphated zirconia catalyst. Sulphated zirconia has substantial catalytic activity for vegetable oil transesterification even at moderate temperature (60˚C). About 85% FAME yield was achieved after 80min reaction time in transesterification at 9:1 methanol to soybean oil and 60˚C, using 2wt% of nanocrystalline sulphated zirconia of the type,$ClSO_3^{2-}/ZrO_2$ (Deshmane and Adewuyi, 2013a).

Table 2.3: Sulphated zirconia catalysts used in biodiesel production reactions

Nature of catalyst	Reaction conditions (Feed ratio in mol: mol)	%FAME Yield	Stability of Catalyst	References
SO_4^{2-}/ZrO_2	CH_3OH:Palm kernel oil = 6:1 Catalyst: 3wt% of the oil T = 200˚C, t = 1h	95.8%	Leached. 27.7% on reuse	(Jitputti *et al.*, 2006)
SO_4^{2-}/ZrO_2	CH_3OH:Tricaprylin = 12:1 Catalyst: 10wt% of the oil T = 120˚C, t = 2h	84%	Leached. 85% activity loss on reuse	(Suwannakarn *et al.*, 2008)
SO_4^{2-}/ZrO_2	CH_3OH:Soybean oil = 20:1 CH_3OH: Oleic acid = 20:1 Catalyst: 5wt% of oil or acid T = 120˚C, t = 1h	96.8% 96%	Leached ~20% on 4th cycle	(Garcia *et al.*, 2008)
$ClSO_3^{2-}/ZrO_2$ Nano crystals	CH_3OH:Soybean oil = 9:1 Catalyst: 2wt% T = 60˚C, t = 80 min (10 wt% FFA in oil)	85%	No leaching reported	(Deshmane and Adewuyi, 2013a)

However, severe leaching was reported when using sulphated zirconia catalysts, e.g. the FAME yields dropped from 95% to 20% on the 4th cycle for the soybean oil transesterification with the evidence of sulphate ions in the reaction mixture (Garcia *et al.*, 2008). When reused the catalyst, FAME yield for the palm kernel oil transesterification decreased drastically from 95.8% to 27.7% (Jitputti *et al.*, 2006). About 85% loss on catalytic activity was reported by Suwannakarn *et al.* (2008) for methanolysis of tricarprylin at 12:1 molar ratio and 120˚C, using 10wt% sulphated

zirconia catalyst. The catalytic activity loss was due to the leaching of sulphate ions (SO_4^{2-}) from the zirconia (ZrO_2) matrix. These findings clearly indicated that the sulphated zirconia catalysts are not suitable heterogeneous catalysts for biodiesel production reactions.

2.7.4 Mixed metal oxide catalysts

Mixed metal oxides such as $WO_3.ZrO_2.Al_2O_3$, $Al_2O_3.SnO$, $Al_2O_3.ZnO$, $WO_3.ZrO_2$, $TiO_2.ZrO_2$, and $Al_2O_3.ZrO_2$ were investigated for catalysis of biodiesel production reactions (Furuta *et al.*, 2006; Macedo *et al.*, 2006; Bournay *et al.*, 2005; Furuta *et al.*, 2004). Catalytic activity of these catalysts was due to the presence of Lewis acid sites which is higher than that of the individual oxides (Furuta *et al.*, 2006; Furuta *et al.*, 2004).

$WO_3.ZrO_2.Al_2O_3$ was used to catalyse soybean oil transesterification and esterification of n-octanoic acid (Furuta *et al.*, 2004). The reactions were carried out in a fixed bed reactor of 4g $WO_3.ZrO_2.Al_2O_3$ at atmospheric pressure. 90% FAME yield was achieved after 20h residence time, for continuous soybean oil transesterification at 40:1 methanol to oil molar ratio and 250˚C, and 100% yield of methyl octanoate for continuous esterification of n-octanoic acid at 4.5:1 methanol to acid molar ratio and 200˚C (Furuta *et al.*, 2004). There were no reductions in the activity of the catalyst after 100h on stream (5 cycles), indicating catalytic stability. Soybean oil transesterification with methanol was investigated in a stirred tank batch reactor using 10g of oil, 1.5g of methanol and 0.5g, 60˚C and 0.5g of $Al_2O_3.SnO$ ($Al_2O_3.ZnO$) catalysts, where 80% FAME yield was achieved after 4h reaction time for each catalyst with no catalyst deactivation after 4 cycles (Macedo *et al.*, 2006). Furuta *et al*. (2006) also showed that mixed oxides of $TiO_2.ZrO_2$ and $Al_2O3.ZrO_2$ can catalyse biodiesel production reactions. FAME yields of 84% for $TiO_2.ZrO_2$ and 80% for $Al_2O_3.ZrO_2$ were reported after 20h reaction time for continuous transesterification of soybean oil with methanol in a fixed bed of 4g $TiO_2.ZrO_2$ or $Al_2O_3.ZrO_2$ catalyst using 40:1 methanol to oil molar ratio and 250˚C. No catalyst deactivation occurred after 5 cycles.

The studies above suggest that mixed metal oxides such as $WO_3.ZrO_2.Al_2O_3$, $Al_2O_3.SnO$ and $Al_2O_3.ZnO$, $WO_3.ZrO_2$, $TiO_2.ZrO_2$, and $Al_2O_3.ZrO_2$, can be used as heterogeneous catalysts for biodiesel production reactions. The Lewis acidity of these mixed metal oxide catalysts allow for simultaneous catalysis of both esterification and

transesterification reactions. This will allow for processing of waste oils that normally contains high levels of FFA. Some of these mixed metal oxides catalysts have been applied for commercial productions of biodiesel. For instance, an Al_2O_3.ZnO spinel catalyst was commercialised as Esterfip-H^{TM} technology by the French Institute of Petroleum, producing 160,000 tonnes of biodiesel per annum from rapeseed oil (Bournay *et al.*, 2005). The Esterfip-H^{TM} process operated at pressures of 40-60 bar, 180 – 220˚C and excess methanol, achieving FAME and glycerol yields in excess of 98% (Mazubert *et al.*, 2013).

The disadvantages of the mixed oxide catalyst are the high operating temperatures and use of large excess of methanol. When large excess of methanol is used, additional operating cost will be incurred for the methanol recovery. Heterogeneous catalysts for biodiesel production that operates at moderate temperatures would also be more economical in reductions of the costs of heating. Biodiesel production reactions using the mixed metal oxides occur at very slow rate, e.g., 20h reaction time was required to achieve 90% FAME yield (Furuta *et al.*, 2004), compared to about 1h for conventional base-catalysed transesterification process.

2.7.5 Sulphonic acid functionalised porous silica catalysts

Porous silica materials are used as catalyst supports due to their large surface area and porosity which allows for increased number of active sites of the supported catalyst. Applications of the porous silica as a supporting material for alkyl sulphonic acids were investigated (Dacquin *et al.*, 2012; Karimi *et al.*, 2012; Dhainaut *et al.*, 2010; Melero *et al.*, 2008). Propyl sulphonic acid functionalised on mesoporous silica (9nm pore size) was used to achieve 95% FAME yield after 2h reaction time in transesterification of palm oil at 10:1 molar ratio and 180˚C and 6wt% of the catalyst (Melero *et al.*, 2008). The spent catalyst had 13.2wt% less sulphur than the fresh catalyst, which was attributed to leaching. Another study also investigated the use of propyl sulphonic acid functionalised pore-expanded mesoporous silica (pore size of 4 – 14nm) for catalysis of triolein transesterification and palmitic acid esterification at 30:1 methanol to triolein (palmitic acid) molar ratio and 60˚C, using 0.05g of the catalyst (Dacquin *et al.*, 2012). About 0.1 – 0.3% FAME yield was achieved after 6h reaction time for the triolein methanolysis, and 23 – 34% for the palmitic acid esterification. A much lower FAME yield obtained (Dacquin *et al.*, 2012) compared to Melero *et al*.(2008) was due to the

use of lower reaction temperature and less catalyst loading. In addition, the catalyst used in Melero *et al.* (2008) had H^+ active site concentration of 0.8mmol/g compared to 0.45mmol/g reported by Dacquin *et al*. (2012).

Transesterification of glyceryl trioctanoate and palmitic acid esterification were catalysed using alkyl sulphonic acid functionalised mesoporous silica (Dhainaut *et al.*, 2010). The FAME yields after 6h reaction time at 60˚C were 2.5% for transesterification at 30:1 methanol to glyceryl trioctanoate molar ratio using 1wt% of the catalyst, and 55.4% for palmitic acid esterification at 30:1 methanol to palmitic acid molar ratio with 2wt% of the catalyst. The authors did not investigate the stability of the catalyst. An investigation by Karimi *et al.* (2012) showed that 98% FAME yield was achieved after 4hr reaction time in transesterification of canola oil at 100:1 methanol to oil molar ratio and 150˚C, using 6wt% propyl sulphonic acid functionalised ethyl-periodic mesoporous organosilicate. The catalyst was not stable as the FAME yield dropped to 70% after 4 cycles. The FAME reduction was explained as due to either decomposition of sulphonic acid groups at the high reaction temperature or leaching into methanol. The actual cause of the catalyst deactivation was not determined.

Generally, the alky sulphonic acid supported on porous silica had slow rates for catalysis of transesterification reactions, unless when used at elevated temperature (Karimi *et al.*, 2012; Melero *et al.*, 2008). These catalysts may be prone to leaching as decrease in catalytic activity was reported (Karimi *et al.*, 2012; Melero *et al.*, 2008). However, leaching was not clearly established for the alkyl sulphonic acid supported on silica. It was not clear what caused the catalyst deactivation reported because thermal decomposition was suspected to be responsible for the catalyst deactivation at 150˚C (Karimi *et al.*, 2012). Therefore, the 13.2wt% loss in sulphur content of spent catalyst at 180˚C (Melero *et al.*, 2008) could also be due to thermal degradation. More studies are required to screen the catalytic activity and stability of the alkyl sulphonic acid supported on porous silica at lower reaction temperatures.

2.8 Process intensification reactors for multiphase reactions

Process intensification in chemical engineering is defined as a "substantially smaller, cleaner, and more energy efficient technology" (Stankiewicz and Moulijn, 2000). Small scale but more energy efficient reactors are generally classified as process intensification reactors. They are invaluable devices in multiphase reactions because of

their capacity for effective mixing and enhanced mass and heat transfer, leading to a great reduction in reaction time. The use of intensification reactors is more imperative in screening of heterogeneously catalysed liquid-liquid reactions due to the additional mass transfer limitations that arise from the transformation of the biphasic liquid-liquid reaction to solid – liquid – liquid reaction.

2.8.1 Micro-reactors

These are micro-structured reactors with well defined structure of channels that have internal diameters of about 10 – 500μm (Dessimoz *et al.*, 2008). Due to their small internal diameters, these reactors have micro-channels of large surface area to volume ratio, specifically in the range of 10, 000–50, 000m^2 per m^3 (Jähnisch *et al.*, 2004). The fluid mixing in micro-reactors arises mainly from convective transport arising from the recirculation zones and/or diffusion between the two immiscible phases (Mazubert *et al.*, 2013; Jovanović *et al.*, 2011; Dessimoz *et al.*, 2008). Diffusion is enhanced by the large interfacial areas between the immiscible liquid phases which reduce the length of the diffusion path.

The intensity of fluid mixing in the micro-reactors is a function of the flow regime and droplet size, which are governed by the physical properties of the fluid and reactor geometry (Dessimoz *et al.*, 2008; Kockmann, 2008). Due to the laminar flow in micro-reactors, the flow regimes for immiscible liquids are typically in either slug-flow or parallel flow (Dessimoz *et al.*, 2008). As shown in Figure 2.8, the mechanism for mass transport in slug flow involves both convective transport and diffusion. Hence, the intensity of mixing in slug flow could be enhanced by increased recirculation and large interfacial areas for diffusion. Use of micro-reactors with zigzag channels greatly enhances formation of vortices and recirculation (Wen *et al.*, 2009).

In parallel flow regime, no recirculation zone occurs. Therefore, the extent of mixing depends only on molecular diffusion across the interfacial areas of the immiscible phases. In general, whereas mass transport in the parallel flow pattern depends on the micro-reactor geometry only, that of slug flow depends on both micro-reactor geometry and intensity of recirculation which changes with fluid flow rates (Mazubert *et al.*, 2013).

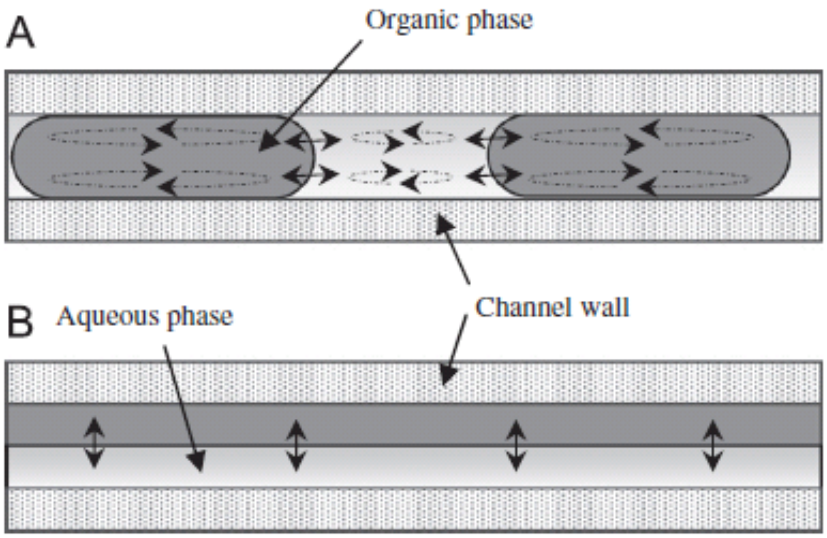

Figure 2.8: Two-phase liquid–liquid flow patterns in glass micro-reactors: (A) slug flow; (B) parallel flow (Dessimoz *et al.*, 2008)

Micro-reactor technology has been used for intensification of biodiesel production reactions (Kalu *et al.*, 2011; Wen *et al.*, 2009; Sun *et al.*, 2008). Sun *et al.* (2008) reported a continuous transesterification of cottonseed oil with methanol in capillary micro-reactor of 0.25mm internal diameter, where 99% FAME yield was achieved after 5.89min reaction time for transesterification at 6:1 methanol to cottonseed to oil molar ratio, 60˚C and 1wt% KOH catalyst. 100% FAME yield was obtained after 1.5min for continuous KOH-catalysed soybean oil transesterification with methanol using a slit-channel micro-reactors at 60˚C and 3.32wt% KOH catalyst (Kalu *et al.*, 2011). The reaction time was greatly reduced in the micro-reactors compared to conventional processes carried out on stirred tank reactors which require about 1h reaction time.

A more rapid intensification of the biodiesel reaction was reported for transesterification of soybean oil using 0.25mm internal diameter zigzag micro-channels reactor (Wen *et al.*, 2009). Only 28s was required to achieve over 99% FAME yield for the transesterification at 9:1 methanol to soybean oil molar ratio, 56˚C and 1.2wt% NaOH catalyst. The zigzag micro-reactor was more effective than the capillary channels micro-reactors in intensification of the biodiesel reaction due to the formation of smaller droplets (Mazubert *et al.*, 2013; Wen *et al.*, 2009). The formation of smaller droplets leads to an increased interfacial area of the reactants and enhanced reaction rates.

In summary, biodiesel productions reactions can be intensified using micro-reactors, by significantly reducing the reaction time. However, these reactors are not suitable for

screening of solid catalyst particles due to potentials for clogging and blockage of the narrow channels. Solid catalysts can only be screened in the micro-reactor by coating the walls of the flow channels with the catalytic materials. This procedure is costly and time consuming.

2.8.2 Spinning reactors

Spinning reactors are shear reactors that operate by using high centrifugal forces generated by rotation of a disk or tube upon which liquid is dispersed in a thin film. The reactors generate very thin film of the reactant fluid which reduces the diffusion path and accelerate mass and heat transfer. The most commonly used spinning reactor was the spinning disc reactor which was used mainly for polymerisation and synthesis of nanoparticles (de Caprariis *et al.*, 2012; Pask *et al.*, 2012).

Recently, spinning reactors were applied for intensification of continuous biodiesel production reactions (Qiu *et al.*, 2012; Qiu *et al.*, 2010). More than 98% FAME yield was achieved after 40s using a spinning tube reactor in transesterification of canola oil with methanol at 40 – 60˚C and NaOH catalyst (Qiu *et al.*, 2010). A spinning disc reactor was also used to obtain about 80% FAME yield in few seconds, for continuous transesterification of canola oil with methanol at 6:1 molar ratio, 40˚C, 1000rpm disc rotation speed and 1wt% NaOH catalyst (Qiu *et al.*, 2012). These indicated that a high degree of micro-mixing and enhanced mass transport generated by the spinning reactors was very effective in accelerating two-phase liquid-liquid reactions. The problem associated with the spinning reactors was that solid catalyst particles are very difficult to handle using this technology. Heterogeneous biodiesel catalysts can only be screened by coating them on the spinning disc or tube.

2.8.3 Acoustic reactors

Acoustic reactors, also called ultrasonic reactors, are type of intensification reactors that use acoustic energy to generate cavitation phenomena necessary for multiphase mixing in liquid-liquid reactions. Acoustic reactors use ultrasounds in the range of 20–50 kHz to induce the formation and cessation of bubble cavities due to pressure variations, which is called cavitation (Gole and Gogate, 2012). Ultrasounds induce the formation of bubble cavities when the local pressure is less that the saturation pressure. This leads to

a release of large magnitude of energy over small locations that result in high temperature and pressures, leading to local turbulence and internal circulation (Mazubert *et al.*, 2013; Gole and Gogate, 2012; Gogate, 2008). Fine emulsions are generated during cavitation which increase the interfacial areas between the immiscible liquid phases and enhances the reaction rates through improved heat and mass transport.

The ultrasonic reactor has been applied for intensification of homogeneous (Kumar *et al.*, 2010; Thanh *et al.*, 2010; Colucci *et al.*, 2005) and heterogeneous (Deshmane and Adewuyi, 2013b; Chen *et al.*, 2012b; Gryglewicz, 1999) transesterification reactions. These studies were all carried out at 20 – 25 kHz frequency. Colucci *et al.* (2005) used ultrasonic reactor to achieve 99.4% FAME yield after 15min reaction time for batch transesterification at 6:1 methanol to soybean oil molar ratio, 40˚C and 1.5wt% KOH. Another study by Kumar *et al.* (2010) showed that ultrasounds can be used to intensify transesterification of vegetable oils, where 98% FAME yield was obtained after 7min for transesterification at 6:1 methanol to coconut oil molar ratio, 0.75wt% KOH, and autogenous (38 – 50˚C) temperature. The ultrasounds reactor was also used to achieve 99% FAME yield after 50min reaction time for transesterification at 5:1 methanol to canola oil molar ratio and 0.7wt% KOH catalyst at room temperature (Thanh *et al.*, 2010). A long reaction time in Than *et al.* (2010) could be explained by the lower reaction temperature, methanol molar ratio and catalyst loading.

For the heterogeneous catalysis, 95% FAME yield was achieved in 2.5h using an ultrasonic reactor for transesterification of soybean oil with methanol at 4.5:1 methanol to oil molar ratio, 65˚C and 15mol% CaO catalyst (Gryglewicz, 1999). When CaO doped with alkali metal salt (KF/CaO) was used, 97% FAME yield was obtained after 1h for soybean oil transesterification at 12:1 methanol to oil molar ratio, 65˚C, and 3wt% of the catalyst (Chen *et al.*, 2012b). The more rapid reaction using the KF/CaO was due to the large methanol to oil molar ratio (12:1) used and probably as a result of leaching of the alkali metal salt. Recently, transesterification of soybean oil with methanol using an acoustic reactor was investigated where 90% FAME yield was achieved after 1.5h reaction for reactions at 9:1 methanol to soybean oil molar ratio, 65˚C and 1wt% $Ca(OCH_3)_2$ (Deshmane and Adewuyi, 2013b).

In summary, ultrasonic reactors can be applied in intensification of both homogenously and heterogeneously catalysed biodiesel production reactions. FAME yield >98% was achieved in the ultrasonic reactor at 7min reaction time compared to 1h for conventional

homogeneous transesterification in stirred tank batch reactors. However, the reaction time was not as much reduced as that reported in the micro-reactors (28s) and spinning reactors (40s). Another method for intensification of multiphase reactions such as triglyceride transesterification was by the use of oscillatory flow mixing in baffled reactors.

2.9 Process intensification using OBR technology

OBRs are multiphase mixing reactors which use oscillatory flow in tubes containing equally spaced baffles to provide improved fluid mixing, enhancing heat and mass transport (Mackley and Ni, 1991; Mackley *et al.*, 1990; Brunold *et al.*, 1989). Because of the improved fluid mixing, plug flow can be achieved in oscillatory flow mixing reactors at moderate net flow Reynolds numbers (Mackley and Ni, 1991). The oscillatory flow mixing in OBR also has the capability for suspension of particles of a wide range of sedimentation velocities (Reis *et al.*, 2005; Mackley *et al.*, 1993). The ability of these reactors to suspend solid particles can be harnessed for suspension and screening of solid catalysts. Fluid mixing in OBRs is decoupled from the net flow, which makes it possible to screen reactions with long residence times in OBR of reduced size (Phan and Harvey, 2010; Harvey *et al.*, 2001). A typical conventional OBR is shown in Figure 2.9.

Figure 2.9: A conventional OBR (Zheng *et al.*, 2007)

The reactor is made of baffled tube of internal diameter D, with equally spaced annular sharp-edged baffles inserted along the inner wall of the tube. The conventional OBR has optimal baffle spacing of 1.5D and baffle orifice diameters of 0.5D (Zheng *et al.*, 2007).

When fluid oscillation is imposed upon these equally spaced baffles along the length of the tube, vigorous eddy mixing occurs. The eddies formed at the edges of the baffles enhance the radial mixing, with radial velocities which is proportional to the axial velocities in the tube (Mackley and Ni, 1991). Due to the enhanced radial mixing, sharp residence time distributions occur in the OBRs, leading to a near plug flow behaviour.

2.9.1 Novel mesoscale designs of OBRs

Mesoscale oscillatory baffled reactors, meso-OBRs, are novel screening reactor based on the oscillatory mixing technology (Reis *et al.*, 2005; Harvey *et al.*, 2003a). Meso-OBR combines the multiphase fluid mixing, particle suspension capability and near plug flow behaviour in the conventional OBR, with small scale for screening and production of specialist chemicals (Zheng *et al.*, 2007; Reis *et al.*, 2006b; Reis *et al.*, 2004). The small volume (millilitres) of meso-OBR allows for the use of small volumes of costly chemicals in screening of reactions and productions of expensive chemicals.

Meso-OBRs were originally made of tubes with smooth periodic constrictions (SPC), as shown in Figure 2.10. The SPC meso-OBR was made of glass tube of 4.4mm internal diameter, with smooth periodic constrictions spaced at 13.0mm intervals. The constricted orifice has 6.4mm length and 1.6mm diameters. Recently, meso-OBRs with different baffle designs such as central baffles (Figure 2.11(a)), helical baffles (Figure 2.11(b)) and integral baffles (Figure 2.11(c)) were developed (Phan *et al.*, 2011a; Phan and Harvey, 2010). These meso-OBRs were made of glass tubes of 340mm length and 5mm internal diameter. In the integral and central baffle designs, the tubes contained baffles of about 2.5mm orifice, equally spaced at 7.5mm along the length of the tube. The helical baffles contained a helix coiled periodically at 7.5mm pitch along the length of the tube.

When meso-OBRs are operated at above certain minimum net flow Reynolds number, the mixing and residence time distribution of the flow becomes independent of the net flow. Generally, the meso-OBRs achieve fluid mixing at lower flow rates than the conventional OBRs which requires $Re_n \geq 50$ (Stonestreet and Van Der Veeken, 1999). For instance, net flow Reynolds number ≥10 provided optimal fluid mixing in SPC meso-OBR (Harvey *et al.*, 2003a). But, other studies do suggest that plug flow can be achieved in meso-OBRs (integral, helical and central baffles) over a wide range of

oscillatory conditions at net flow Reynolds numbers below 10 (Phan *et al.*, 2011a; Phan and Harvey, 2010).

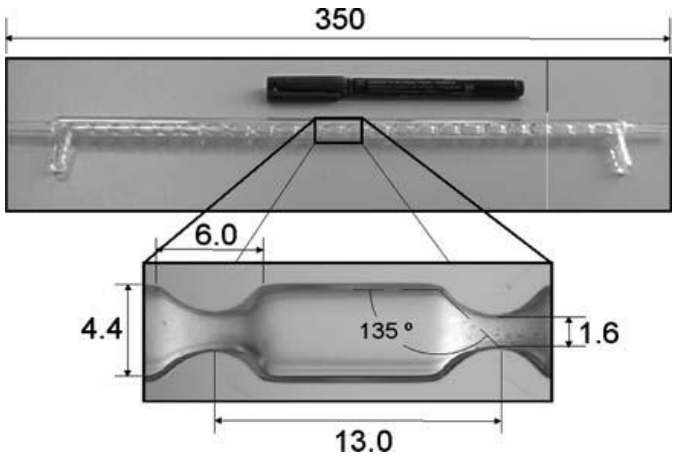

Figure 2.10: Smooth periodic constrictions meso tube (Reis *et al.*, 2006a)

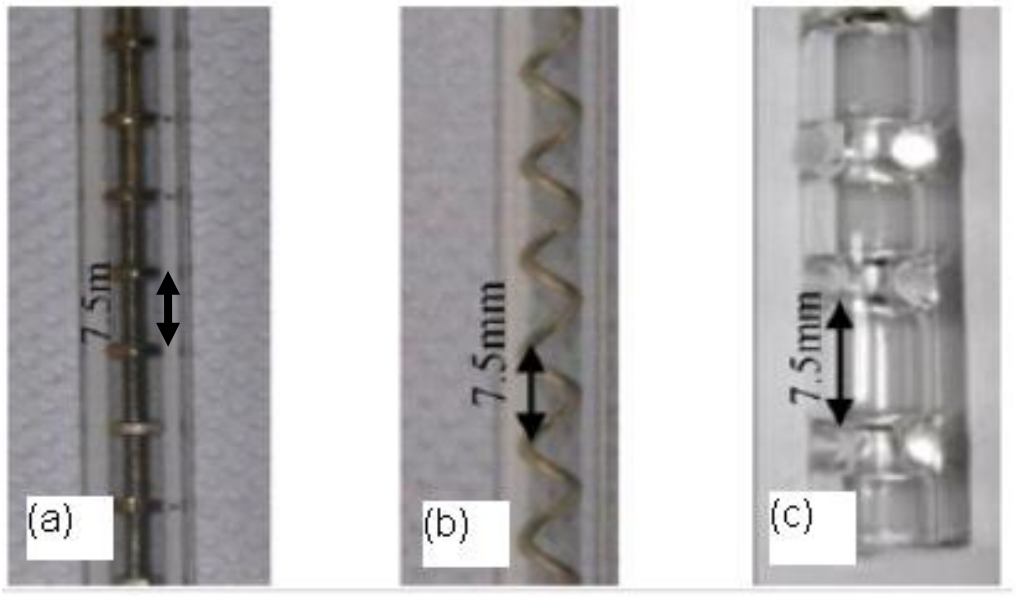

Figure 2.11: Other designs of meso-OBR: (a) central baffles, (b) helical baffles and (c) integral baffles (Phan and Harvey, 2010)

2.9.2 Fluid mixing in OBRs

Fluid mixing is achieved in OBRs through periodic formation and destruction of eddies in the baffled tubes (Ni *et al.*, 2002; Howes *et al.*, 1991; Brunold *et al.*, 1989). As shown in Figure 2.12, fluid separation occurs as the flow passes through the baffle constriction, leading to formation of eddies downstream of the baffle constriction. Initial

eddies formed due to fluid separation are pushed into the bulk fluid flow as the fluid decelerates. This periodic formation and destruction of eddies causes fluid mixing, enhancing mass and heat transport.

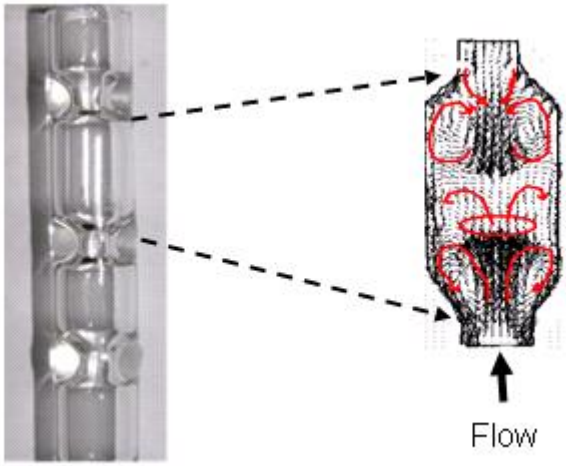

Figure 2.12: Fluid mixing in OBRs

The extent of the continuous eddies formation and dissipation increases with the number of baffles in the OBR (Brunold *et al.*, 1989). In effect, each of the cavities in the OBR acts like a continuous stirred tank reactor, approximating the flow pattern in entire length of the OBR to stirred tanks in series. The fluid mixing in OBRs is decoupled from the net flow, and can be controlled by the oscillatory frequency and amplitude (Harvey *et al.*, 2001). This allows for independent control of the mixing intensity and the net flow in the OBRs, allowing reactions of long residence times to be performed in OBRs of reduced length-to-diameter ratio.

The effectiveness of fluid mixing and radial transport in OBRs is controlled by the net and oscillatory flow conditions, as well as the geometry of the tube (Phan and Harvey, 2010; Reis *et al.*, 2005; Harvey *et al.*, 2003a; Harvey *et al.*, 2003b). These factors are usually expressed in terms of dimensionless parameters as shown in equations (2.1) – (2.4) (Harvey *et al.*, 2003b): net flow Reynolds number (Re_n), oscillatory Reynolds number (Re_o), velocity ratio (ψ) and Strouhal number (St). Re_n is a measure of the rate of net fluid flow into the reactor which is dependent on the superficial fluid velocity corresponding to the throughput. In conventional OBRs, $Re_n \geq 50$ is required to achieve flow separation (Stonestreet and Van Der Veeken, 1999). For meso-OBRs, minimum Re_n reported to ensure flow separation was 10 for SP meso-OBR (Reis *et al.*, 2005) and as low as $Re_n = 1.25$ for central baffles design (Phan *et al.*, 2011a).

$$Re_n = \frac{\rho UD}{\mu} \quad (2.\ 1)$$

$$Re_o = \frac{\omega x_0 \rho D}{\mu} = \frac{2\pi f_o x_0 \rho D}{\mu} \quad (2.\ 2)$$

$$Str = \frac{D}{4\pi x_0} \quad (2.\ 3)$$

$$\psi = \frac{Re_o}{Re_n} \quad (2.\ 4)$$

Where:

P: density of the fluid ($kg.m^{-3}$); U: superficial net flow velocity ($m.s^{-1}$)

ω: angular oscillation frequency ($rad.s^{-1}$); μ: dynamic viscosity of the fluid (Pa.s).

D: internal diameter of the tube (m); f_o: oscillatory frequency (Hz)

x_o: centre-to-peak amplitude of oscillation (m)

The intensity of fluid mixing in the OBRs is governed by Re_o, which is controlled by the amplitude (centre-to-peak) and frequency of the oscillation. Oscillatory flow in OBRs is provided by means of diaphragms, bellows or pistons, at one or both ends of the tube; or by moving a set of baffles up and down from the top of the tube (Ni *et al.*, 2002). When conventional OBRs are used, Re_o ~ 100 was required to achieve flow separation (Stonestreet and Van Der Veeken, 1999), and Re_o ~50 for SPC meso-OBR (Reis *et al.*, 2005). In other meso-OBR designs, such as integral and central baffles, Re_o ~ 30 – 50 was required to achieve flow separation (Phan *et al.*, 2011a). Therefore, there are specific regions of oscillation conditions required to operate OBRs in plug flow. For instance, Re_o in the ranges of 100–300 are the optimal values required to generate symmetrical vortex rings within the cavities of the SPC meso-OBR (Reis *et al.*, 2005). The mixing in the SPC meso-OBR was reported to be more chaotic when Re_o greater than 300 was used, as the flow resembles that of a single continuous stirred tank reactor (CSTR) rather than an interconnected series of CSTRs.

A range of Re_o and Re_n ratio exits for optimal plug flow performance of OBRs. These values of Re_o and Re_n are related through ψ, which measures the dominance of the oscillatory mixing. The Re_o is required to dominate the Re_n to ensure that the flow is fully reversing, i.e. ψ must be greater than unity (Harvey *et al.*, 2003a; Stonestreet and Van Der Veeken, 1999). ψ in the range of $2 \leq \psi \leq 6$ was required for optimal plug flow

behaviour in conventional OBR (Stonestreet and Van Der Veeken, 1999). The highest degree of plug flow was also achieved at $4 \leq \psi \leq 8$ for central baffles meso-OBR and $5 \leq \psi \leq 10$ for integral baffles meso-OBR at Re_n = 4.3 - 34 (Phan and Harvey, 2010). Another study showed that the range of ψ required for optimal plug flow was $39 \leq \psi \leq 40$ at Re_n = 1.27 for central baffles meso-OBR (Phan *et al.*, 2011a). These studies clearly indicate that the ψ for plug flow behaviour was strongly dependent on net flow conditions. Therefore, plug flow may be achieved even at higher ψ when lower Re_n was used.

Another dimensionless parameter used in characterisation of oscillatory flow mixing in OBRs is the Strouhal number. This parameter measures the extent of eddy propagation and axial dispersion in the OBR. Axial mixing in OBRs is controlled mainly by the amplitude of oscillation (Reis *et al.*, 2005; Ni and Pereira, 2000). The effectiveness of this eddy propagation measured by St is strongly dependent on the diameter of the OBR and the amplitude of oscillation.

Apart from the net flow and oscillation conditions, the effectiveness of fluid mixing in the OBRs equally depends on some geometric parameters of the reactor, such as the internal diameter of the tube, D, baffle spacing (λ) and baffle orifice diameter (D_o). These factors have been investigated extensively and optimised at λ= 1.5D and D_o = 0.5D (Phan *et al.*, 2011a; Stonestreet and Van Der Veeken, 1999; Baird and Stonestreet, 1995).

2.9.3 Residence time distributions of OBRs.

Residence time distribution (RTD) is a tool widely used in reactor engineering for characterisations of flow patterns in continuous flow reactors. It is a probability distribution function that describes the amount time a given segment of fluid spends inside a chemical reactor (Danckwerts, 1995). This function determines the extent of axial dispersion in continuous flow reactors, i.e., the extent of fluid dispersion along the axis or length of the reactor. Hence, RTD data could be used to measure the flow characteristics or flow patterns of the OBR in comparison with the flow behaviour of ideal flow reactors: plug flow or CSTR. Ideally, a plug flow reactor has zero axial dispersion, while an ideal CSTR has infinite axial dispersion (Levenspiel, 1999). RTDs of various OBR designs have been widely investigated using a pulse tracer injection technique (Phan *et al.*, 2011a; Phan and Harvey, 2011; Phan and Harvey, 2010;

Stonestreet and Van Der Veeken, 1999; Howes and Mackley, 1990). The RTDs data were usually analysed using statistical moment approach: mean residence times, exit age distribution curve (E-curve), variance and skewness (Fogler, 2005; Levenspiel, 1999).

Experimental residence time: $$\tau = \frac{\sum_i (t_i C_i \Delta t_i)}{\sum_i (C_i \Delta t_i)} \quad (2.5)$$

Distribution curve: $$E(t) = \frac{C_i}{\sum_i (C_i \Delta t_i)} \quad (2.6)$$

Variance: $$\sigma(t)^2 = \sum_i [(t_i - \tau)^2 . E(t) \Delta t_i] \quad (2.7)$$

Skewness: $$\gamma(t)^3 = \sum_i [(t_i - \tau)^3 . E(t) \Delta t_i] \quad (2.8)$$

Where:

C_i: concentration of the tracer at time t_i (mol.dm^{-3})

t_i: time spent by ith segment of tracer in the reactor (s)

$\Delta t_{i:}$ time intervals in the data acquisitions (1s)

The statistical moments in the equations (2.5) – (2.8) are usually converted to the dimensionless and normalised forms in (2.9) – (2.12) to enable for more accurate comparison of experimental results from different process parameters.

Dimensionless time: $$\theta = \frac{t_i}{\tau} \quad (2.9)$$

Distribution curve: $$E(\theta) = \tau E(t) = \tau \frac{C_i}{\sum_i (C_i \Delta t_i)} \quad (2.10)$$

Normalised variance: $$\sigma(\theta)^2 = \frac{\sigma(t)^2}{\tau^2} = \sum_i [(\theta_i - 1)^2 . E(\theta) \Delta \theta_i] \quad (2.11)$$

Skewnes: $$\gamma(\theta)^3 = \sum_i [(\theta_i - 1)^3 . E(\theta) \Delta \theta_i] \quad (2.12)$$

Two models that are widely used to characterise flow reactors are the tanks-in-series (TIS) model and axial dispersion model, of which the TIS is the most commonly used model for quantitative assessment of the RTDs of OBRs (Phan *et al.*, 2011a; Phan and Harvey, 2011; Stonestreet and Van Der Veeken, 1999). The TIS model treats the baffled

reactors as a combination of equally sized CSTRs in series, where the mixing in each baffle cavity resembles that of a single CSTR. The main parameter of practical importance in the TIS model is the theoretical number of tanks-in-series, N, used for quantitative assessment of the RTDs of the baffles reactors. For N number of tanks in series, the exit age distribution under pulsed injection is determined as follows (Fogler, 2005; Levenspiel, 1999).

$$E(t) = \frac{C(t)}{\int_0^\infty C(t)dt} = \frac{t^{(N-1)}}{(N-1)!\tau_i^N} e^{-(t/\tau_i)} \quad (2.\ 13)$$

$$\tau = \frac{\int_0^\infty tC(t)dt}{\int_0^\infty C(t)dt} = N\tau_i \quad (2.\ 14)$$

(τ_i is the residence time of the tracer in the each tank)

The statistical moments used for the estimations of the theoretical number of tanks in series can be expressed in dimensionless forms:

Dimensionless time: $$\theta = \frac{t}{\tau} = \frac{t}{N\tau_i} \quad (2.\ 15)$$

$$E(\theta) = \tau E(t) = \frac{N(N\theta)^{N-1}}{(N-1)!} e^{-N\theta} \quad (2.\ 16)$$

$$\sigma(\theta)^2 = \frac{\sigma(t)^2}{\tau^2} = \int_0^\infty (\theta - 1)^2 . E(\theta) d\theta = \frac{1}{N} \quad (2.\ 17)$$

$$\therefore N = \frac{1}{\sigma(\theta)^2} \quad (2.\ 18)$$

Numbers of tanks in series for the OBRs were estimated from the normalised variance shown in equation (2.17). The initial estimate of N was obtained from the experimental RTD data by combining of equation (2.11) and (2.17). Estimated initial value of N was substituted into the exit age curve from equation (2.16) and compared to the E-curve from equation (2.10). The value of N was changed to compare the two E-curves in terms of shape, spread and height of the tracer exit age distribution, until the best correspondence was achieved (Phan and Harvey, 2011). Plug flow behaviour is achieved when the exit age distribution, $E(\theta)$, of the RTD is normal and Gaussian in shape (N≥10) as shown in Figure 2.13.

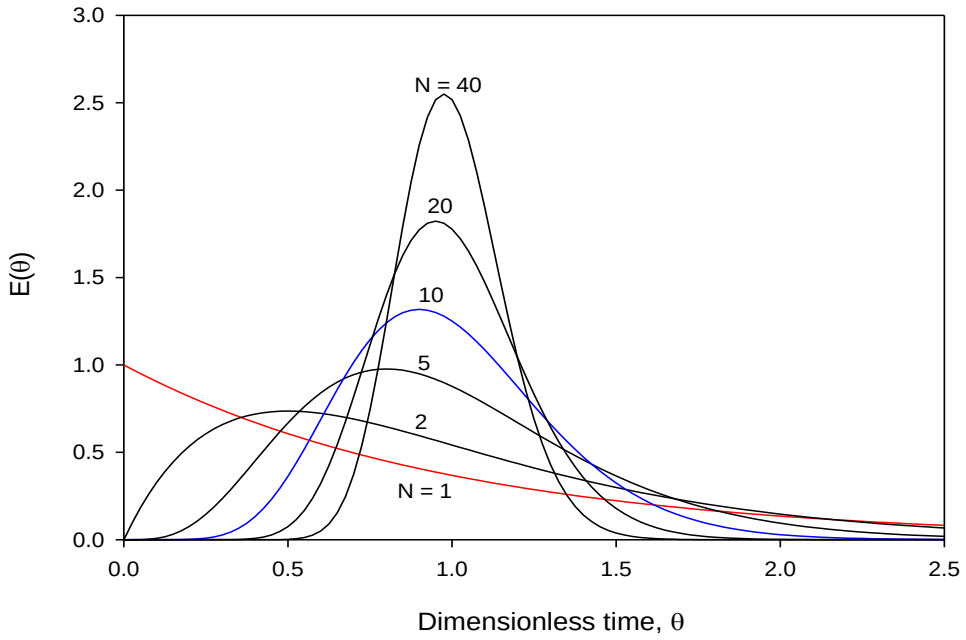

Figure 2.13: RTDs for the tanks-in-series model

Near plug flow behaviour was reported in various OBR designs at specified oscillation (amplitude and frequency) and net flow conditions (Phan *et al.*, 2011a; Phan and Harvey, 2010; Reis *et al.*, 2010; Mackley and Ni, 1991). The studies demonstrated that radial mixing dominates at the right net flow and oscillation conditions. This approximates the whole length of the OBR to CSTRs in series, resulting in plug flow behaviour achieved in OBRs. At N < 10, the E-curve becomes increasingly skewed to the right as the values of N decreases (Levenspiel, 1999). That was an indication that axial dispersion has become a predominant mechanism of mixing at these conditions.

2.10 Applications of OBRs

2.10.1 Multiphase mixing for intensification of homogeneous transesterification

Applications of OBRs for multiphase fluid mixing in intensification of biodiesel production reactions were investigated in various OBR designs (Phan *et al.*, 2011b; Zheng *et al.*, 2007; Harvey *et al.*, 2003b). Continuous transesterification of RSO was carried out in a 1.56dm^3 conventional OBR at 5:1 methanol to oil molar ratio, temperatures of 20 – 70˚C, residence time of 10 – 30 min and about 0.9wt% NaOH catalyst, using oscillation conditions Re_o = 700 and ψ = 18 (Harvey *et al.*, 2003b). The

OBR used was a conventional design with 25mm internal diameter, 37.5mm baffle spacing and 12.5mm baffle orifice diameter. It was reported that biodiesel that meets ASTM standards (FAME > 96%) was produced at 10 – 15 min residence time.

Intensification of biodiesel production was also investigated in an SPC meso-OBR of 5mm internal diameter, containing periodic constrictions of 1.6mm orifice spaced equally at 15.2mm (Zheng *et al.*, 2007). The small volume (millilitre) of the reactor reduced the amount of reagents used and the waste generated. Zheng *et al.* (2007) reported that biodiesel that meets the EN 14214 standards for biodiesel (FAME >96%) was obtained after 35 min reaction for batch and 30 – 40min for a continuous flow, in a transesterification of refined vegetable oil at 6:1 methanol to oil molar ratio and 60˚C, using 4.2wt% $NaOCH_3$ based on methanol. The reaction was performed in batch using an SPC meso-OBR of 20cm length and 4.8mL total volume. For the continuous transesterification, 8 interconnected SPC meso-OBRs of 103mL total volume were used. The oscillation conditions used to achieve the above FAME yields were 10Hz frequency and 2mm centre-to-peak amplitude (Re_o = 134, St = 0.2). Net flow condition for the continuous screening was at Re_n = 1.9 (ψ =70).

Another study investigated the steady states and dynamic screening of biodiesel reactions via transesterification of RSO with methanol in a meso-OBR with a sharp-edged helical baffles with a central rod design (Phan *et al.*, 2011b). The screening was carried out by transesterification of RSO at 9:1 methanol to oil molar ratio, using 4 interconnected baffled glass tubes of 5mm internal diameter. Each glass tube (340mm length) contained sharp-edged helix of 1.2mm flat wire coiled at 7.5mm pitch and 1.2mm round central rod. The sharp-edged helix with a central rod was effective in mixing of methanol and RSO, as ~90% FAME yield was achieved at 10min residence time when the reaction was carried out at 50˚C, 1wt% KOH and oscillation condition, Re_o = 316 and St = 0.1 (Phan *et al.*, 2011b).

The above studies showed that there was a significant reduction in reaction time for the biodiesel production using the OBRs. For instance, Harvey *et al.* (2003b) reported about 80% reduction in reaction time compared with 1h for conventional base-catalysed homogeneous transesterification in stirred tank batch reactors. Reaction time was also reduced for the transesterification using the sharp-edged helical baffles with a central rod meso-OBR, considering the lower reaction temperature (50˚C) used (Phan *et al.*, 2011b). The longer reaction time of ~35min reported by Zheng *et al.* (2007) could be

due to the use of lower oscillation mixing intensity, Re_o = 134. Homogeneous transesterification of vegetable oil is a two-phase liquid-liquid reaction. Hence, increased oscillatory mixing increases mass transport and accelerates the reactions.

2.10.2 Suspension of solid particles

Suspension of solid particles of varying sedimentation velocities have been studied using both conventional and meso-OBR designs (Reis *et al.*, 2005; Mackley *et al.*, 1993). The capability of the conventional and meso - OBRs for particle suspension was due to the enhanced fluid mixing and mass transport in the baffled tubes. Mackley et al. (1993) investigated the suspensions of solid particles in a conventional OBR of 140mm length and 23mm internal diameter, with baffles of 0.5D orifice diameter equally spaced at 1.5D along the tube. $Re_o \geq 150$ were reported to be sufficient to suspend particles of resin beads of terminal velocity of 45mm/s in water. The distribution of the suspended particles within each baffle cavity was nearly uniform at oscillatory velocities many times higher than the terminal velocity of the particles (Mackley *et al.*, 1993). At this condition, the ratio of the concentrations of the suspended particles between adjacent cavities remained constant, indicating uniform particle suspension.

Another investigations of particle suspension by oscillatory mixing was carried out using SPC meso-OBR (Reis *et al.*, 2005). Particles of ion exchange resin of 150 - 180µm diameter with 23.0cm/s sedimentation velocity, polyamine of 40 - 75µm diameter with 1.5cm/s sedimentation velocity, and silica resin of 40 - 75µm diameter with 2.5cm/s sedimentation velocity were suspended in water at various oscillation conditions and SPC orientations. The oscillation frequency and tube orientation had effect on the ability of the tube to suspend particles. For instance, more particles were suspended at high frequency and low amplitude, and when the tube was in a horizontal orientation (Reis *et al.*, 2005). The energy required to keep the particles suspended depended on the frequency. When the SPC was inclined vertically, there was an increase in static pressure, such that more energy was needed to counteract gravity and keep the particles suspended (Reis *et al.*, 2005).

These studies clearly demonstrated that solid particles can be effectively suspended using the oscillatory flow in OBRs. The ability of the OBRs to suspend solid particles can be applied in suspension and screening of heterogeneous catalysts for biodiesel production. This allows the OBRs to be adapted for both homogeneously catalysed

liquid-liquid reactions and heterogeneously catalysed solid-liquid-liquid reactions. The capability of the OBRs for fluid mixing in two-phase liquid-liquid reactions and suspensions of solid particles were applied in this study. Process development using the OBR also has an advantage of simple scale-up procedure.

2.11 Kinetics of triglyceride transesterification

Kinetics of homogeneously catalysed transesterification of vegetable oil was first reported by Freedman *et al.* (1986). The investigation was carried out on transesterification of soybean oil with 1-butanol and methanol, using both acid (H_2SO_4) and base (NaOBu) catalysts. The authors proposed pseudo-first-order kinetics for the acid and base catalysed reactions at 30:1 alcohol to oil molar ratio. At 6:1 alcohol to oil molar ratio, second-order kinetics was proposed for both acid and base catalysed transesterification. Noureddini and Zhu (1997) also reported second-order kinetics in a transesterification of soybean oil at 6:1 methanol to oil molar ratio, using NaOH catalyst. The study showed that vegetable oil transesterification was initially mass transfer controlled, followed by kinetically controlled stage.

Other studies (Darnoko and Cheryan, 2000b; Mittelbach and Trathnigg, 1990) reported that all the stages in transesterification reaction did not follow second-order. The uncertainty in the reaction kinetics was further demonstrated in another study, which showed that the kinetic model that best fits the experimental data for KOH catalysed methanolysis of palm oil at 6:1 methanol to oil molar ratio was pseudo-second-order initially, followed by first-order or zero-order kinetics (Darnoko and Cheryan, 2000b). However, most researchers agree that triglyceride transesterification occurs via three consecutive step-wise reactions (section 2.4.1). These reactions are presented in equation (2. 19).

$$\begin{aligned} &TG + MA \underset{k_2}{\overset{k_1}{\rightleftharpoons}} FAME + DG \\ &DG + MA \underset{k_4}{\overset{k_3}{\rightleftharpoons}} FAME + MG \\ &MG + MA \underset{k_6}{\overset{k_5}{\rightleftharpoons}} FAME + GL \end{aligned} \tag{2.19}$$

Overall reaction:

$$TG + 3MA \underset{k_{-t}}{\overset{k_t}{\rightleftharpoons}} 3FAME + GL$$

(MA: methanol; TG: triglyceride; DG: diglyceride; MG: monoglyceride; GL: glycerol)

2.11.1 Kinetic models for homogeneous transesterification

Homogeneous catalysis of transesterification reaction uses catalysts that are in the same phase as either one or both reactants. Conventional kinetic model for the base-catalysed transesterification reaction was based on assumptions that the reactions are kinetically controlled, and that negligible side reactions (FFA neutralisation and saponification) occur (Vicente *et al.*, 2005).

$$r_{TG} = \frac{d[TG]}{dt} = -k_1[TG][MA] + k_2[DG][FAME] \tag{2. 20}$$

$$r_{DG} = k_1[TG][MA] + k_4[MG][FAME] - k_2[DG][FAME] - k_3[DG][MA] \tag{2. 21}$$

$$r_{MG} = k_3[DG][MA] + k_6[GL][FAME] - k_4[MG][FAME] - k_5[MG][MA] \tag{2. 22}$$

$$\begin{aligned} r_{FAME} = \frac{d[FAME]}{dt} &= k_1[TG][MA] + k_3[DG][MA] + k_5[MG][MA] \ldots \\ &- k_2[DG][FAME] - k_4[MG][FAME] - k_6[GL][FAME] \end{aligned} \tag{2. 23}$$

$$r_{GL} = \frac{d[GL]}{dt} = k_5[MG][MA] - k_6[GL][FAME] \tag{2. 24}$$

$$r_{MA} = \frac{d[MA]}{dt} = -\frac{d[FAME]}{dt} \tag{2. 25}$$

Where:

$r_{A:}$ rates of formation of species A ($mol.L^{-1}.time^{-1}$)

[A]: concentration of species A ($mol.L^{-1}$)

k_i: rate constants of the individual transesterification reactions ($L.mol^{-1}.time^{-1}$).

The homogeneous kinetic model was developed using a set of differential rate equations of the second-order kinetic reactions of the various chemical species involved in TG transesterification as shown in equations (2.20) - (2.25) (Bambase *et al.*, 2007; Vicente *et al.*, 2005). These equations were solved with MATLAB using ODE45 solver (Runge-Kutta method) to obtain the reaction rate constants. At the moderate excess alcohol molar ratio (e.g. 6:1) second-order reaction was used and the rates of reverse reactions were negligible initially (Bambase *et al.*, 2007; Vicente *et al.*, 2005; Darnoko and Cheryan, 2000b; Noureddini and Zhu, 1997). Hence, only the rate constants for the forward reactions (k_1, k_3, k_5) determine the initial kinetics. The rate determining step for transesterification was TG → DG reaction due to the molecular size of the TG, compared to the smaller sizes of DG and MG (Bambase *et al.*, 2007; Darnoko and Cheryan, 2000b; Noureddini and Zhu, 1997). Therefore, steric effect may be a contributing factor to the lower reaction rate of the TG. Other studies suggested that the rate determining step for the transesterification could be DG → MG reaction (Karmee *et al.*, 2006) or MG → GL reaction (Vicente *et al.*, 2005). The variation in the rate determining step was due to the differences in composition of fatty acids in feedstock.

In summary, the actual reaction kinetics and rate constants in transesterification remain unknown. Although there was an agreement on the rate determining steps among researchers (Bambase *et al.*, 2007; Darnoko and Cheryan, 2000b; Noureddini and Zhu, 1997), the reaction rate constants varied. This could be due to saponification side reactions and the complexity in composition of vegetable oils: FFA and water which interferes with base-catalysed transesterification by neutralising the catalyst and causing hydrolysis and saponification. Integration of the reaction kinetics for the side reactions into the conventional kinetic model will improve the robustness and accuracy of the kinetic model for the homogeneous base-catalysed transesterification.

2.11.2 Kinetic model for heterogeneous transesterification

Heterogeneous catalysis transforms the hitherto biphasic liquid-liquid vegetable oil transesterification reaction in into solid-liquid-liquid three-phase reaction. Hence, the reaction kinetics is complicated by diffusion, adsorptions and desorption of the reacting species and products considering the reaction steps shown below (Belfiore, 2003; Yadav and Mehta, 1994):

i. Diffusion of the reactant molecules from bulk liquid phase to the external surface of the solid catalyst

ii. Diffusion of the reactants molecules from the surface of the solid catalyst into the pore network for porous catalysts.

iii. Chemisorptions of the reactants on the catalytic active sites

iv. Reactions of the chemisorbed reactant molecules to form activated complex

v. Decomposition of the activated complex to form products adsorbed on the catalytic active sites

vi. Desorption of the reaction products from the interior catalyst active sites to the external surface.

vii. Diffusion of the reaction products from the catalyst pores to the bulk liquid phase.

The rate determining steps commonly reported for heterogeneously catalysed transesterification are surface reactions (Xiao *et al.*, 2010; Dossin *et al.*, 2006; Hattori *et al.*, 2000) and methanol adsorption (Dossin *et al.*, 2006; Hattori *et al.*, 2000). These reactions generally proceed by either Eley-Rideal (ER) or Langmuir-Hinshelwood-Hougen-Watson mechanism (LHHW) mechanism. Kinetics of heterogeneously catalysed transesterification follows LHHW model when using solid catalysts containing Lewis acid/base sites (Xiao *et al.*, 2010), while ER mechanism was followed by solid base catalysts (Dossin *et al.*, 2006; Hattori *et al.*, 2000). A solid catalyst that leached substantially into the reaction media cannot be considered heterogeneous as the reaction mechanism of such catalysts followed kinetic mechanisms similar to that of homogeneous transesterification (Di Serio *et al.*, 2008).

2.11.3 ER kinetic mechanism for transesterification

ER mechanism for transesterification reaction assumes that the reactions proceed via chemisorptions of one of the reactants and subsequent reaction of the adsorbed species with another reactant in the bulk liquid phase. In transesterification reaction that was catalysed by solid base, the adsorbed species is the methanol (Dossin *et al.*, 2006). The reaction produces FAME and a molecule of DG which is adsorbed on the catalyst surface. Lastly, the DG desorbs and diffuses into the bulk liquid phase. DG and MG react similar to the TG, following the ER reaction scheme shown in equation (2.26).

1.	$\mathrm{MA} + ø \leftrightarrow \mathrm{MA}ø$	(adsorption of methanol)	
2.	$\mathrm{MA}ø + \mathrm{TG} \leftrightarrow \mathrm{FAME} + \mathrm{DG}ø$	(surface reaction)	(2. 26)
3.	$\mathrm{DG}ø \leftrightarrow \mathrm{DG} + ø$	(desorption of product)	

(ø: vacant catalyst site)

The ER kinetic models for TG transesterification can be written with rate determining steps based on surface reaction (Xiao *et al.*, 2010; Dossin *et al.*, 2006; Hattori *et al.*, 2000) as shown in equation (2.27).

$$-r_{TG} = r_s = k_s[TG]\theta_{MA} - k_{-s}[FAME]\theta_{DG} \qquad (2.\ 27)$$

θ is fractional surface coverage of the adsorbed species; k_s and k_{-s} are the rate constants for the forward and reverse surface reactions, respectively; [X] is the bulk concentration of species X. The rates of adsorption-desorption of the MA and DG are given in equations (2.28) and (2.29). The equilibrium constants for adsorption-desorption of the MA and DG is shown in equation (2.30).

$$r_{ad(MA)} = k_{a(MA)}[MA]\theta_j - k_{d(MA)}\theta_{MA} \qquad (2.\ 28)$$

$$r_{ad(DG)} = k_{a(DG)}[DG]\theta_j - k_{d(DG)}\theta_{DG} \qquad (2.\ 29)$$

$$K_{MA} = \frac{k_{a(MA)}}{k_{d(MA)}}; \qquad K_{DG} = \frac{k_{a(DG)}}{k_{d(DG)}} \qquad (2.\ 30)$$

k_a and k_d represent the rate constants for adsorption and desorption, respectively, while θ_j is the fraction of the catalytic sites that remains unoccupied. It is expected that reacting molecules that have hydroxyl group similar to MA could adsorb on the catalyst surface. Therefore, the total surface coverage of the catalyst was written to include adsorption of MA, DG, MG and GL, as in equation (2.31).

$$\theta_j = 1 - \theta_{MA} - \theta_{DG} - \theta_{MG} - \theta_{GL} \quad (2.31)$$

Surface coverage of these reacting species were obtained using equilibrium state approximation, i.e., the rates of adsorption and desorption are equal, and net rate of adsorption-desorption equals zero at equilibrium. Therefore, the surface coverage of MA, DG, MG and GL are shown in equation (2.32).

$$\theta_{MA} = K_{MA}[MA]\theta_j$$

$$\theta_{DG} = K_{DG}[DG]\theta_j$$

$$\theta_{MG} = K_{MG}[MG]\theta_j$$

$$\theta_{GL} = K_{GL}[GL]\theta_j \quad (2.32)$$

The surface reaction determined ER model was re-written as shown in equation (2.33).

$$r_s = k_s K_{MA}[TG][MA]\theta_j - k_{-s}K_{DG}[FAME][DG]\theta_j \quad (2.33)$$

$$\theta_j = K_{MA}[MA]\theta_j - K_{DG}[DG]\theta_j - K_{MG}[MG]\theta_j - K_{GL}[GL]\theta_j \quad (2.34)$$

The rate equation for the surface reaction in equation (2.36) was obtained by combining equations (2.27) and the Langmuir adsorption isotherm for the reaction scheme in equation (2.35).

$$\theta_i = \frac{K_i[i]}{(1+\sum K_i[i]} \quad (2.35)$$

(Where, i = MA, DG, MG, GL)

$$r_s = \frac{k_s K_{MA}[TG][MA] - k_{-s} K_{DG}[FAME][DG]}{(1 + K_{MA}[MA] + K_{DG}[DG] + K_{MG}[MG] + K_{GL}[GL])} \quad (2.\ 36)$$

Equation (2.36) was simplified further to give equation (2.40), considering the equilibrium constant for the surface reaction (K_s). At equilibrium, the forward and reverse surface reactions are equal such that the net rate of the surface reaction becomes zero. The rate constant for the reverse surface reaction was replaced with equation (2.39).

$$r_s = \frac{k_s K_{MA}[TG][MA] - k_{-s} K_{DG}[FAME][DG]}{(1 + K_{MA}[MA] + K_{DG}[DG] + K_{MG}[MG] + K_{GL}[GL])} = 0 \quad (2.\ 37)$$

$$K_s = \frac{k_s}{k_{-s}} = \frac{K_{DG}}{K_{MA}} . \left(\frac{[FAME][DG]}{[TG][MA]}\right) = \frac{K_{DG}}{K_{MA}} . K_{eq} \quad (2.\ 38)$$

$$k_{-s} = \frac{k_s K_{MA}}{K_{DG} K_{eq}} \quad (2.\ 39)$$

$$r_s = \frac{k_s K_{MA}\left([TG][MA] - \frac{K_{DG}}{K_{eq}}[FAME][DG]\right)}{(1 + K_{MA}[MA] + K_{DG}[DG] + K_{MG}[MG] + K_{GL}[GL])} \quad (2.\ 40)$$

The ER model in equation (2.40) is more complex than the ER kinetic model developed by Dossin *et al.* (2006a) for transesterification of ethyl acetate with methanol. This was due to the complexity of TG transesterification. Competitive adsorption of DG, MG and GL on the catalyst sites was expected for the TG transesterification. For a simple transesterification reaction, such as methanolysis of ethyl acetate, the ER mechanism involves only adsorption of MA and the ethanol by-product. Therefore, the ER kinetic model in equation (2.40) simplifies to equation (2.41), similar to that reported (Dossin *et al.*, 2006).

$$r_s = \frac{k_s K_{MA}}{(1 + K_{MA}[MA] + K_D[D])} \left([MA][B] - \frac{K_D}{K_{eq}}[C][D]\right) \quad (2.\ 41)$$

Where: B is ethyl acetate; C is methyl acetate; D is ethanol.

On the other hand, when methanol adsorption is assumed to be the rate determining step, an overall reaction equation for TG transesterification is given by equation (2.42). The rates of adsorption-desorption of the DG, MG, GL and the surface reactions of the chemisorbed reactants MA and TG are assumed to be in equilibrium.

$$r_{ad(MA)} = k_{a(MA)}[MA]\theta_j - k_{d(MA)}\theta_{MA} = k_{a(MA)}.\frac{\theta_{MA}}{K_{MA}} - k_{d(MA)}\theta_{MA} \quad (2.\ 42)$$

$$r_{ad(MA)} = \frac{k_{a(MA)}[MA] - k_{d(MA)}K_{MA}[MA]}{1+K_{MA}[MA]+K_{DG}[DG]+K_{MG}[MG]+K_{GL}[GL]} \quad (2.\ 43)$$

Recall that:

$$\theta_{MA} = K_{MA}[MA]\theta_j \ ; \quad [MA] = \frac{[FAME][DG]}{K_{eq}[TG]}$$

$$\theta_{MA} = \frac{K_{MA}[MA]}{1+K_{MA}[MA]+K_{DG}[DG]+K_{MG}[MG]+K_{GL}[GL]} \quad (2.\ 44)$$

Therefore,

$$r_{ad(MA)} = \frac{k_{a(MA)}\left([MA]-\frac{[FAME][DG]}{K_{eq}[TG]}\right)}{(1+\frac{K_{MA}\,[FAME][DG]}{K_{eq}[TG]}+K_{DG}[DG]+K_{MG}[MG]+K_{GL}[GL])} \quad (2.\ 45)$$

Again, for transesterification of simple esters such as ethyl acetate, equation (2.45) can be reduced to equation (2.46), which is similar to that developed by Dossin *et al*. (2006a) for methanolysis of ethyl acetate when adsorption of methanol is the rate the rate determining step.

$$r_s = \frac{k_s K_{MA}}{\left(1+\frac{K_{MA}\,[C][D]}{K_{eq}[B]}+K_D[D]\right)}\left([MA]-\frac{K_D}{K_{eq}}\frac{[C][D]}{[B]}\right) \quad (2.\ 46)$$

Generally, the ER model can be written for the overall TG transesterification reaction based on the fractional surface coverage of the reactants. These rate equations are shown in equation (2.47), are similar to ER kinetic mechanism developed for vegetable oil transesterification (Yussof, 2012). The elementary reactions were based on the established consecutive three-step reaction mechanism in transesterification (Bambase *et al.*, 2007; Vicente *et al.*, 2005).

$$r_{TG} = -k_1[TG]\theta_{MA} + k_2[FAME]\theta_{DG}$$

$$r_{DG} = k_1[TG]\theta_{MA} + k_4[FAME]\theta_{MG} - k_2[FAME]\theta_{DG} - k_3[DG]\theta_{MA}$$

$$r_{MG} = k_3[DG]\theta_{MA} + k_6[FAME]\theta_{GL} - k_4[FAME]\theta_{MG} - k_5[MG]\theta_{MA}$$

$$r_{FAME} = k_1[TG]\theta_{MA} + k_3[DG]\theta_{MA} + k_5[MG]\theta_{MA} - k_2[FAME]\theta_{DG} \ldots$$
$$-k_4[FAME]\theta_{MG} - k_6[FAME]\theta_{GL}$$

$$r_{GL} = k_5[MG]\theta_{MA} - k_6[FAME]\theta_{GL}$$

$$r_{MA} = \frac{d[MA]}{dt} = -\frac{d[FAME]}{dt} \qquad (2.47)$$

2.11.4 LHHW kinetic mechanism for transesterification

The LHHW kinetic mechanism assumes that all the reacting species are adsorbed on the catalyst surface. Therefore, heterogeneous transesterification proceeds via adsorption-desorption equilibriums of all the reactants and products to the vacant active sites of the catalysts, followed by surface reactions of the adsorbed species (Endalew *et al.*, 2011). Surface reactions between chemisorbed reactant molecules produce an activated complex which decomposes to form products that are also adsorbed on the catalyst sites. The reaction products diffuse from the catalyst sites into the bulk liquid phase. In vegetable oil transesterification, TG and MA adsorbed on adjacent active sites (dual sites) of the catalyst react to form DG and FAME. The surface reactions follow the established three consecutive stepwise reactions for TG transesterification. Therefore, the DG formed reacts similarly to form MG, which also reacts to form GL.

Generally, considering the first reversible reaction in TG transesterification: $TG + \mathrm{MA} \leftrightarrow \mathrm{DG} + \mathrm{FAME}$, a LHHW reaction scheme in equation (2.48) can be written.

1	$\mathrm{TG} + ø \leftrightarrow \mathrm{TG}ø$	(adsorption of TG)	
2.	$\mathrm{MA} + ø \leftrightarrow \mathrm{MA}ø$	(adsorption of MA)	
3	$\mathrm{TG}ø + \mathrm{MA}ø \leftrightarrow \mathrm{DG}ø + \mathrm{FAME}ø$	(surface reaction)	(2. 48)
4.	$\mathrm{DG}ø \leftrightarrow \mathrm{DG} + ø$	(desorption of DG)	
5.	$\mathrm{FAME}ø \leftrightarrow \mathrm{FAME} + ø$	(desorption of FAME)	

Two cases of LHHW models previously developed (Hayes and Mmbaga, 2012; Dossin *et al.*, 2006) were described in this review. These models based the rate determining step on either the surface reaction or adsorption of methanol. In the first case of LHHW model, mass transport and diffusion are very fast compared to the surface reaction of the chemisorbed species such that the surface reaction becomes the rate-determining step. The overall reaction kinetics equation for the transesterification is given by equation (2.49).

$$-r_{TG} = r_s = k_s\theta_{MA}\theta_{TG} - k_{-s}\theta_{DG}\theta_{FAME} \quad (2.\ 49)$$

The rate of adsorption-desorption for the reacting species is given by equation (2.50), with the equilibrium constant (K_i) for adsorption-desorption. Recall that adsorption-desorption of all the reacting these species occurs: i = TG, MA, DG, MG, GL, and FAME.

$$r_{ad(i)} = k_{a(i)}[i]\theta_j - k_{d(i)}\theta_i \quad (2.\ 50)$$

$$K_i = \frac{k_{a(i)}}{k_{d(i)}}$$

Using an equilibrium state approximation, the fractional surface coverage of the reacting species was solved. Therefore, rate of the surface reaction was written as equations (2.51).

$$\mathrm{r_s} = \mathrm{k_s K_{MA}[MA] K_{TG}[TG]\theta_j^2} - \mathrm{k_{-s} K_{DG}[DG] K_{FAME}[FAME]\theta_j^2} \quad (2.\ 51)$$

A generalised Langmuir adsorption isotherm for the reaction species is shown in equation (2.52).

$$\theta_i = \frac{K_i[i]}{(1+\sum K_i[i]} \quad (2.\ 52)$$

Where, i = MA, TG, DG, MG, GL and FAME

$$\theta_{MA} = K_{MA}[MA]\theta_j; \theta_{TG} = K_{TG}[TG]\theta_j$$

$$\theta_{DG} = K_{DG}[DG]\theta_j$$

$$\theta_{MG} = K_{MG}[MG]\theta_j$$

$$\theta_{GL} = K_{GL}[GL]\theta_j$$

$$\theta_{FAME} = K_{FAME}[FAME]\theta_j \quad (2.53)$$

$$\theta_j = 1 - \theta_{MA} - \theta_{TG} - \theta_{DG} - \theta_{MG} - \theta_{GL} - \theta_{FAME}$$

The overall kinetic rate equation in (2.54) was obtained by combining equations (2.49) and (2.52). Equation (2.54) was simplified further, considering the equilibrium constant (K_s) for the surface reaction to obtain equation (2.55).

$$r_s = \frac{k_s K_{MA} K_{TG}[TG][MA] - k_{-s} K_{DG} K_{FAME}[DG][FAME]}{(1+K_{MA}[MA]+K_{TG}[TG]+K_{DG}[DG]+K_{MG}[MG]+K_{GL}[GL]+K_{FAME}[FAME])^2} \quad (2.54)$$

$$r_s = \frac{k_s K_{MA} K_{TG}\left([TG][MA] - \frac{[DG][FAME]}{K_{eq}}\right)}{(1+K_{MA}[MA]+K_{TG}[TG]+K_{DG}[DG]+K_{MG}[MG]+K_{GL}[GL]+K_{FAME}[FAME])^2} \quad (2.55)$$

Recall that:

$$K_s = \frac{k_s}{k_{-s}} = \frac{K_{DG}K_{FAME}}{k_s K_{MA} K_{TG}} . \left(\frac{[DG][FAME]}{[TG][MA]}\right) = \frac{K_{DG}K_{FAME}}{k_s K_{MA} K_{TG}} . K_{eq} \; ; \quad k_{-s} = \frac{k_s K_{MA} K_{TG}}{K_{eq} K_{DG} K_{FAME}}$$

Similarly, for simple reaction such as: M$A + B \leftrightarrow C + D$, the LHHW kinetic model in equation (2.55) was written as equation (2.56). This is identical with what was reported for such reactions (Hayes and Mmbaga, 2012; Dossin *et al.*, 2006).

$$r_s = \frac{k_s K_{MA} K_B}{(1+K_A[MA]+K_B[B]+K_C[C]+K_D[D])^2}\left([MA][B] - \frac{[C][D]}{K_{eq}}\right) \quad (2.56)$$

$$r_{ad(MA)} = k_{a(MA)}[MA]\theta_j - k_{d(MA)}\theta_{MA} = k_{a(MA)} . \frac{\theta_{MA}}{K_{MA}} - k_{d(MA)}\theta_{MA} \quad (2.57)$$

Secondly, when MA adsorption is the rate determining step, the LHHW kinetic model assumes that adsorption-desorption of the species TG, DG, MG, GL and FAME, and the

surface reactions of the chemisorbed reactants TG and DG are in equilibrium. Hence, the overall reaction rate equation is given by equation (2.57). The overall reaction in equation in (2.58) was obtained considering the equilibrium conditions for the surface reactions and methanol adsorption.

$$r_{ad(MA)} = \frac{k_{a(MA)}\left([MA] - \frac{[DG][FAME]}{K_{eq}[TG]}\right)}{(1+\frac{K_{MA}[DG][FAME]}{K_{eq}[TG]}+K_{TG}[TG]+K_{DG}[DG]+K_{MG}[MG]+K_{GL}[GL]+K_{FAME}[FAME])} \qquad (2.58)$$

For a simple reaction of the type: $MA + B \leftrightarrow C + D$, LHHW kinetic model in equation (2.58) was simplified to equation (2.59). LHHW kinetic model in equation (2.59) was similar to that developed by Hayes and Mmbaga (2012) and Dossin *et al*. (2006a) for such reactions when MA adsorption was the rate determining step.

$$r_{ad(MA)} = \frac{k_{a(MA)}}{(1+\frac{K_{MA}[C][D]}{K_{eq}[B]}+K_B[B]+K_C[C]+K_D[D])}\left([MA] - \frac{[C][D]}{K_{eq}[B]}\right) \qquad (2.59)$$

Finally, when the overall three consecutive reaction steps involved in TG transesterification are considered, a LHHW kinetic model of the type in equation (2.60) could be written. The LHHW kinetic model was based on the fractional surface coverage of the all the reacting species for TG transesterification.

$$\begin{aligned}
r_{TG} &= -k_1\theta_{TG}\theta_{MA} + k_2\theta_{DG}\theta_{FAME} \\
r_{DG} &= k_1\theta_{TG}\theta_{MA} + k_4\theta_{MG}\theta_{FAME} - k_2\theta_{DG}\theta_{FAME} - k_3\theta_{DG}\theta_{MA} \\
r_{MG} &= k_3\theta_{DG}\theta_{MA} + k_6\theta_{GL}\theta_{FAME} - k_4\theta_{MG}\theta_{FAME} - k_5\theta_{MG}\theta_{MA} \\
r_{FAME} &= k_1\theta_{TG}\theta_{MA} + k_3\theta_{DG}\theta_{MA} + k_5\theta_{MG}\theta_{MA} - k_2\theta_{DG}\theta_{FAME} \ldots \\
&\quad -k_4\theta_{MG}\theta_{FAME} - k_6\theta_{GL}\theta_{FAME} \\
r_{GL} &= \frac{d[GL]}{dt} = k_5\theta_{MG}\theta_{MA} - k_6\theta_{GL}\theta_{FAME} \qquad (2.60) \\
r_{MA} &= -r_{FAME}
\end{aligned}$$

2.12 Kinetics of esterification reactions

Kinetic mechanism for carboxylic acid esterification involves the protonation of the organic acid carbonyl oxygen by the catalyst, followed by nucleophilic attack by alcohol (Liu *et al.*, 2006c). This process involves a simple reversible reaction in equation (2.61), following a second-order reaction with first-order for each reagent in homogeneously catalysed reactions (Liu *et al.*, 2006a).

$$\mathrm{MA} + \mathrm{A} \leftrightarrow \mathrm{E} + \mathrm{W} \qquad (2.\ 61)$$

(A: carboxylic acid; MA: methanol; E: ester; W: water).

A homogeneous kinetic model can be written for the carboxylic acid esterification as shown below in equation (2.62). Where k_1 and k_{-1} are the forward and reverse esterification rate constants, respectively.

$$-r_A = -k_1[A][MA] - k_{-1}[E][W] \qquad (2.\ 62)$$

$$(-r_A = -r_{MA} = r_E = r_W)$$

However, the kinetic mechanism for esterification reaction is complicated when heterogeneous catalysts are used. The rate determining step in carboxylic acid esterification can be any of the elementary reaction steps, including external mass transport in the bulk liquid, adsorption, desorption, and surface reactions. Therefore, heterogeneous kinetic models based on LHHW and ER mechanism was applied for the esterification process.

As shown in equation (2.61), the LHHW kinetic model for carboxylic acid is similar mechanism to that of simple reactions: $MA + B \leftrightarrow C + D$ as described in section 2.11.4. The LHHW mechanism for heterogeneous esterification follows equation (2.56) when surface reaction is the rate limiting step and equation (2.59) when methanol adsorption is the rate limiting step.

But, studies (Kirumakki *et al.*, 2006; Liu *et al.*, 2006b; Liu *et al.*, 2006a) suggest that heterogeneous catalysis of organic acids esterification follows mainly ER mechanism. The process occurs through a single-site mechanism where the rate determining step is the reaction between adsorbed carboxylic acid and alcohol in the liquid phase

(Kirumakki *et al.*, 2006). However, the ER kinetic model for the carboxylic acid esterification deviates from the conventional ER kinetics due to competitive adsorption of methanol on the catalyst surface and poor adsorption of the non-polar alkyl esters (Liu *et al.*, 2006b; Liu *et al.*, 2006a). A modified ER kinetic model developed by Liu *et al.* (2006a) was described below. The model assumes that the rate limiting step is the surface reactions of the adsorbed carboxylic acid with MA in the bulk liquid phase.

1.	$A + ø \leftrightarrow Aø$	(adsorption of carboxylic acid)	
2.	$MA + ø \leftrightarrow MAø$	(adsorption of methanol)	
3.	$Aø + MA \leftrightarrow Eø + W$	(surface reaction)	(2. 63)
4.	$Eø \leftrightarrow E + ø$	(desorption of the ester)	
5.	$W + ø \leftrightarrow Wø$	(adsorption of water)	

The overall rate kinetics in equation (2.64) was written based on the reaction scheme in equation (2.63). The surface reaction in equation (2.65) was derived using the ER kinetics and simplified as shown in equation (2.66).

$$r_s = k_s[MA]\theta_A - k_{-s}[W]\theta_E = k_s K_A[MA][A]\theta_j - k_{-s}K_E[W][E]\theta_j \quad (2.\ 64)$$

$$r_s = \frac{k_s K_A[A][MA] - k_{-s}K_E[E][W]}{(1 + K_A[A] + K_{MA}[MA] + K_E[E] + K_W[W])} \quad (2.\ 65)$$

$$r_s = \frac{k_s K_A}{(1 + K_A[A] + K_{MA}[MA] + K_E[E] + K_W[W])}\left([A][MA] - \frac{[E][W]}{K_{eq}}\right) \quad (2.\ 66)$$

Recall that:

$$\theta_j = K_A[A]\theta_j - K_{MA}[MA]\theta_j - K_E[E]\theta_j - K_W[W]\theta_j$$

$$\theta_i = \frac{K_i[i]}{(1 + \sum K_i[i])}; \qquad i = \text{A, MA, E, W}$$

And the equilibrium conditions:

$$K_s = \frac{k_s}{k_{-s}} = \frac{K_E}{K_A}.\left(\frac{[E][W]}{[A][MA]}\right) = \frac{K_E}{K_A}.K_{eq}\ ;\ k_{-s} = \frac{k_s K_A}{K_E K_{eq}}$$

Considering the poor adsorption of the non-polar esters molecules, the ER model in equation (2.66) could be reduced to equation (2.67), which was similar to that previously reported for liquid phase carboxylic esterification over a sulphonic acid functionalised solid catalyst (SAC-13) (Liu *et al.*, 2006a).

$$r_s = \frac{k_s K_A}{(1+K_A[A]+ K_{MA}[MA]+K_W[W])}\left([A][MA] - \frac{[E][W]}{K_{eq}}\right) \quad (2.67)$$

In summary, LHHW and ER kinetic models can be applied for heterogeneous catalysed biodiesel production reactions to predict the reaction mechanisms. However, it is important to consider the interactions of the reacting species with the catalyst sites. The modified ER model was reported to give better fit than LHHW and conventional ER models for carboxylic acid esterification (Liu *et al.*, 2006a).

2.13 Diffusion limitations in heterogeneous catalysis

In heterogeneous catalysed biodiesel production reactions, the diffusion of the reacting species in bulk liquid phase, intra-particle diffusions in pore sites and surface reactions determine the overall rate of the reaction (Belfiore, 2003; Yadav and Mehta, 1994). Mass transport of the reacting species in the bulk liquid phase is expected to be negligible when an effective mixing is applied (e.g. using OBR). At these conditions, the catalysts pores may be filled with the reactants, but low diffusivity of the liquid may limit the reaction. This is particularly important for transesterification because of the large molecular size of the TG. When large excess of methanol is used, the reaction is reduced to a first-order reaction.

Effects of the internal mass transfer on the heterogeneously catalysed reaction process can be evaluated using the physical parameters of the catalyst, such as particle size, porosity, tortuosity and the observed reaction rate. Thiele modulus (M_T) was used to measure the effectiveness of the internal diffusion by calculations based on these physical parameters and the observed reaction rate constant as shown in equation (2.68). M_T is defined as a ratio of the rate of diffusion of a limiting reactant (e.g. TG or FFA) into the catalyst pores, to the rate of the surface reaction. When the rate of internal diffusion is high, the overall rate of the reaction is limited by the surface reaction and M_T tends to zero.

$$M_T = L\sqrt{\frac{k_1}{D_e}} \quad (2.\ 68)$$

$$D_e = \frac{D_A \epsilon_p}{\tau_p}$$

Where:

k_1: pseudo-first-order rate constant for the reaction (s^{-1})

D_e: effective diffusivity of the limiting reactant into the pores of the catalysts ($cm^2.s^{-1}$)

L: characteristic length of the catalyst particles (cm)

D_A: molecular diffusion coefficient of the limiting reactant ($cm^2.s^{-1}$)

ϵ_p: porosity of the catalyst particles

τ_p: tortuosity of the catalyst pores

For different materials, ϵ_p are usually in the range of 0.3 – 0.8, and the τ_p from 1.4–12 (Veljkovic *et al.*, 2009). D_A can be calculated from the Wilke-Chang equation (Wilke and Chang, 1955) shown in equation (2.69). The molar volume of the limiting reactant at its boiling point (V_{bA}) are estimated using a correlation between molar and critical volumes (Sastri *et al.*, 1997).

$$D_A = \frac{7.4*10^{-8}}{T(V_{bA})^{0.6}}(\Phi_A M_W)^{0.5} \quad (2.\ 69)$$

Where:

Φ_A: association factor

M_w: molar mass of the solvent (excess reactant)

T: reaction temperature (K)

μ: viscosity of the reaction mixture (mPa.s)

V_{bA}: molar volume of the solute (limiting reactant) at the boiling point ($cm^3.mol^{-1}$)

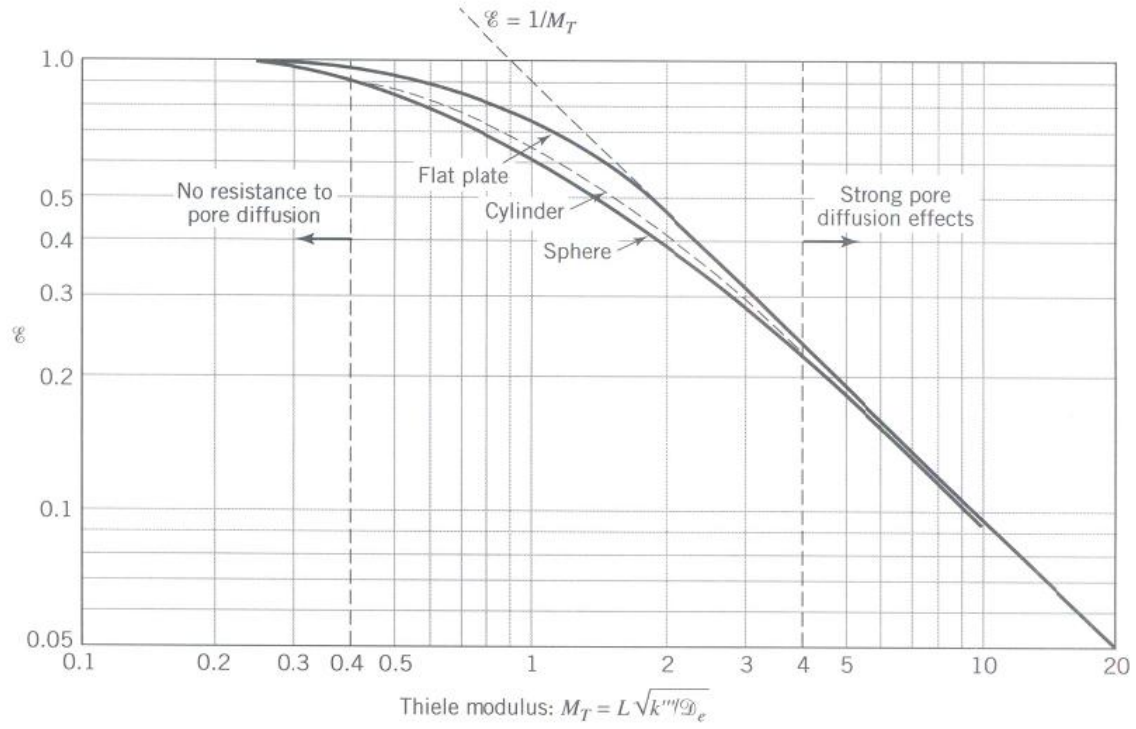

Figure 2.14: Effectiveness factor versus Thiele modulus for porous particles (Levenspiel, 1999).

As shown in Figure 2.14, heterogeneous catalysts have an internal effectiveness factor (ε) in the range of 0 – 1. The effectiveness of the catalyst increases with a decrease in the M_T or small catalyst particles. At this condition, more catalyst surface area is available, which increases the rate of reaction. At $M_T < 0.4$, the effectiveness factor for the internal diffusion is assumed to be unity, since the concentrations of the reactants remain nearly same at the bulk liquid phase and catalyst pores (Veljkovic *et al.*, 2009; Levenspiel, 1999). But, at $M_T > 4$, the centre of the particles is starved of reactants, thus unused for catalysis. To increase the effectiveness of a solid catalyst for biodiesel production reaction, small particles sizes are required. However, when fine catalysts particles are used, removal of the spent catalyst from the reaction mixture becomes difficult.

Chapter 3 Materials and Methods

3.1 Introduction

This section describes the chemicals, reactors, laboratory equipment and other accessories used in the experiments. The catalysts screened in the work were also described here. Three meso-OBRs, the integrally baffled, sharp-edged helically baffled with a central rod, and the stainless steel wire wool packing were evaluated by characterisation of the flow patterns using RTD study and steady state performance in alkali-catalysed (KOH) homogeneous transesterification of RSO with methanol. The RTD test was carried out by injecting pulses of KCl as a tracer. The integrally baffled meso-OBR was used for screening solid catalysts based on its steady state performance and FAME conversion.

Homogeneously catalysed transesterification of RSO was further studied in integral baffled meso-OBR and stirred tank batch reactor, using various alkaline catalysts – NaOH, KOH, $NaOCH_3$. The kinetics of FAME and RSO saponification were also investigated using methanol-KOH solution. This study was used to obtain the kinetic data used in modelling of the base-catalysed homogeneous transesterification reactions.

The solid catalysts investigated in this work were strontium zirconate based (SZB) catalyst and propyl sulphonic acid functionalised mesoporous silica ($PrSO_3H$-SBA-15). These catalysts were characterised and screened for their activity in esterification and transesterification reactions. The SZB catalyst was obtained from São Paulo State University – UNESP, Brazil, and the $PrSO_3H$-SBA-15 from Cardiff University, UK.

All the sample analysis for the related biodiesel production reactions - esterification and transesterification, was performed using a gas chromatograph (GC).

3.2 Materials

3.2.1 Chemicals

Chemicals used in the study were broadly classified into triglycerides, carboxylic acids, methanol and analytical standards. The source of triglyceride used was RSO. RSO consist mainly of triglyceride molecules with even-numbered fatty acids, mostly in the range of palmitic acid (C_{16}) to eicosenoic acid (C_{20}) chain lengths (Table 3.1).

Table 3.1: Fatty acid profile of the rapeseed oil

Type of Fatty acid	Molecular formula	Mw. (g/mol)	Fatty acids (wt %)
Palmitic ($C_{16:0}$)	$C_{15}H_{31}COOH$	256.4	5.3
Stearic ($C_{18:0}$)	$C_{17}H_{35}COOH$	284.5	1.7
Oleic ($C_{18:1}$)	$C_{17}H_{33}COOH$	282.5	63.2
Linoleic ($C_{18:2}$)	$C_{17}H_{31}COOH$	280.5	19.8
Linolenic ($C_{18:3}$)	$C_{17}H_{29}COOH$	278.4	8.6
Icosenoic ($C_{20:1}$)	$C_{19}H_{37}COOH$	310.5	1.4

Table 3.2: Properties of the reactant chemicals

Reactants	%Assay	Mw. (g/mol)	Bp (˚C)	*Density (kg/m^3)	%water
RSO	98.7	881.4	-	918	0.03
Methanol	99.8	32.04	64.7	791	-
Propanoic acid	99.5	74.08	141	993	≤0.25
Hexanoic acid	99	116.16	203	927	NS
Lauric acid	98	200.32	296.1[b]	883	NS
Palmitic acid	98	256.42	351.5[b]	852	NS

*Density at 25˚C; NS: not specified; Mw: molecular mass; [b]Data from ChemNet

Various carboxylic acids used were, propanoic, hexanoic, lauric and palmitic acids. The esterification and transesterification reactions were carried out using methanol. Table 3.2 contains the physico-chemical properties of all the reactants used. The RSO was obtained from Henry Colbeck (UK) while anhydrous methanol and the carboxylic acids were purchased from Sigma-Aldrich, UK.

3.2.2 Catalysts

The homogeneous catalysts used were potassium hydroxide (KOH), sodium hydroxide (NaOH) and sodium methoxide ($NaOCH_3$). The physico-chemical properties of the KOH and NaOH (Sigma-Aldrich) and $NaOCH_3$ (Alfa Aesar) are shown in Table 3.3. Potassium hydrogen phthalate (PHP) and HCl were obtained from Sigma-Aldrich with 99.5% purity and 37%, respectively. PHP was used as a primary standard for the standardisation of the alkali (KOH, NaOH and $NaOCH_3$) solutions.

Table 3.3: Physico-chemical properties of the homogeneous alkali catalysts

Catalysts	% Assay	Mw (g/mol)	Form	Density (kg/m^3)	Active ions content (mmol/g)[b]
KOH	90	56.11	flakes	2040	16.04
NaOH	97	40.0	pellets	2130	24.25
$NaOCH_3$	30[a]	54.02	Liquid	967.8	5.55
HCl	37	36.46	Liquid	1200	10.15
PHP	99.5	204.22	crystals	-	-

[a]Weight percent in methanol; [b]Active ions in terms of H^+, OH^- or CH_3O^-

Table 3.4: Physico-chemical properties of the heterogeneous catalysts

Catalysts	Physical form	S_{BET} (m^2/g)	Pore size BJH (nm)	Active sites (mmol/g)
SZB	Power (~8µm)	16.4	3.9	1.42
$PrSO_3H$-SBA-15	Power (~0.6µm)	705	5.1	0.43

The heterogeneous catalysts were SZB catalyst of the type $SrZrO_3.xSr(OH)_2.yH_2O$ and $PrSO_3H$-SBA-15. The $PrSO_3H$-SBA-15 catalyst supplied by Cardiff University, UK was synthesised by grafting mercaptopropyl trimethoxysilane to preformed SBA-15, followed by oxidation with 30% H_2O_2 (Dacquin *et al.*, 2012; Pirez *et al.*, 2012). The SZB catalyst obtained from São Paulo State University – UNESP, Brazil was synthesised via a citrate route, using 0.5M aqueous solutions of zirconium oxynitrate and strontium nitrate and 1.5M citric acid, and calcined at 900˚C for 1hr (Lima *et al.*, 2012). Table 3.4 summarises the properties of the heterogeneous catalysts.

3.2.3 Analytical standards

A range of analytical standards were used in the study including methyl hexanoate, methyl octanoate, methyl laurate, methyl palmitate and methyl heptadecanoate (C_{17}). They were used as the GC internal standards for the identifications and quantification of methyl ester yields in the transesterification and esterification reactions. The analytical standards were prepared using either heptane or methanol as solvent. All the analytical standards and heptane were obtained from Sigma-Aldrich, UK and have properties as shown in Table 3.5.

Table 3.5: Properties of the analytical standards

Analytical Standards	% purity	Mw. (g/mol)	Bp (˚C)	Density (kg/m^3)
Heptane	99.5	100.20	98	684
Methyl propanoate	99	88.11	79	915
Methyl hexanoate	99	130.18	151	885
Methyl octanoate	99	158.24	194.5	877
Methyl laurate	99.5	214.34	262	870
Methyl palmitate	99	270.45	332.1[a]	852
Methyl heptadecanaote	99	284.48	337.1[a]	874[a]
Methyl oleate	99	296.49	351.4[a]	874

[a]ChemNet.

3.3 Reactors and laboratory equipment

3.3.1 Batch reactor

The experiments were carried out using various types of reactors. These included a 100mL jacketed three-neck batch reactor (Figure 3.1). The reactor was a glass vessel with an internal diameter of about 7cm and three necks that allowed for connections with a condenser, a sampling unit and a thermocouple. Heating was provided by circulation of hot water inside the outer jacket.

Figure 3.1: Jacketed 3-neck stirred tank batch reactor

3.3.2 Meso-OBR designs used in the study

Three meso-OBRs (i) integral baffles, (ii) wire wool packing, (iii) sharp-edged helix with a central rod were evaluated in this study. The integral baffled meso-OBR (Figure 3.2(a)) was a glass tube of 340mm length and 5mm internal diameter. The tube contained orifice baffles of about 3mm length and 2.5mm diameter equally spaced at 7.5mm along the length of the tube. The integral baffled meso-OBR had about 25% open cross-sectional area. The sharp-edged helical baffle with a central rod design shown in the Figure 3.2(b) was also a glass tube of 340mm length and 5mm internal diameter. The tube was inserted with 1mm sharp-edged helix and a 1.2mm central rod. The helix was coiled periodically along the length of the tube at 7.5mm pitch with the sharp-edge towards the direction of the flow. The open cross-sectional area of the helical baffled meso-OBR was approximately 25%, similar to that of the integral baffled meso-OBR. The integral baffles and sharp-edged helix with a central rod meso-OBRs designs were selected based on their ease of fabrication and excellent multiphase mixing performance (Phan *et al.*, 2011b).

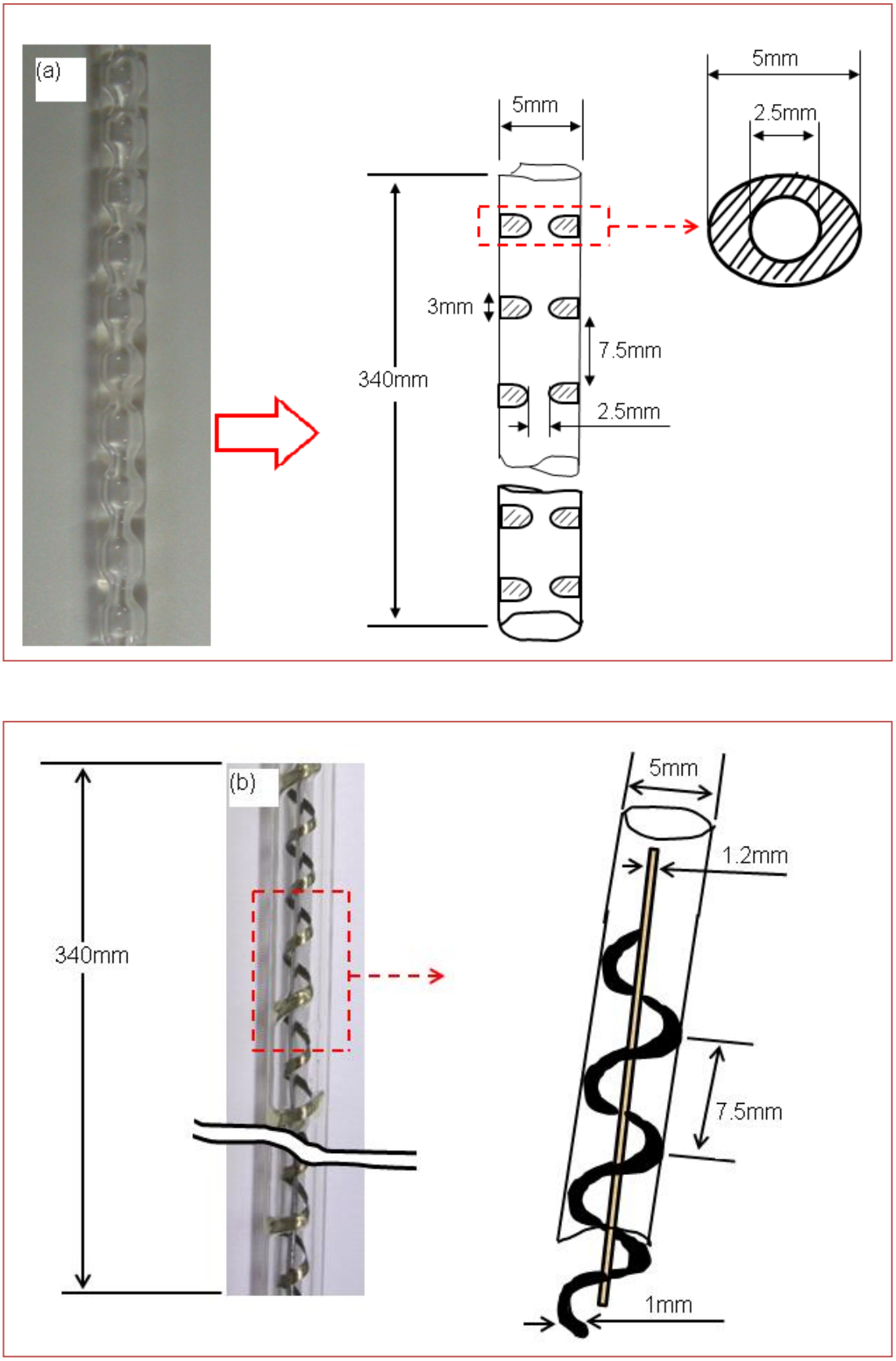

Figure 3.2: Meso-OBRs and their schematics (a) Integral baffles, (b) sharp-edged helix with a central rod

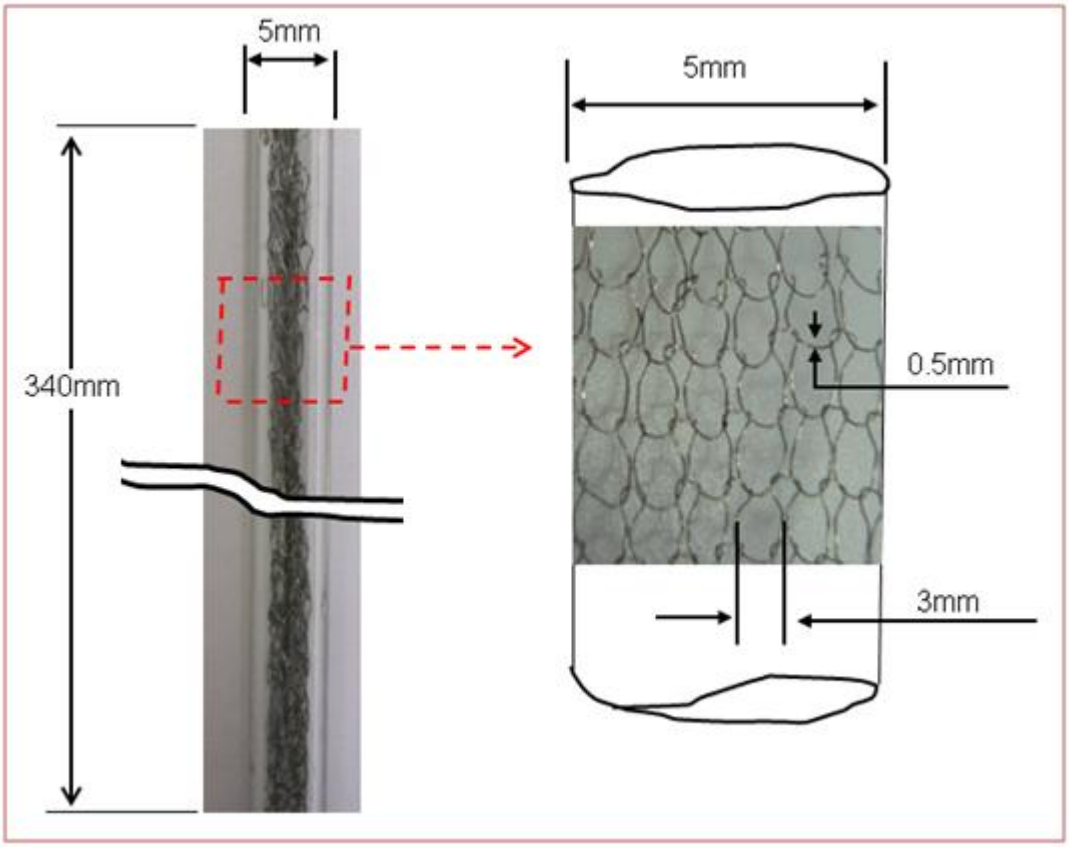

Figure 3.3: Wire wool packed reactor and the schematic

Figure 3.3 shows the wire wool packed reactor. The reactor was a glass tube of 340mm length and 5mm internal diameter which was packed with a knitted 0.5mm wire diameter stainless-steel wire mesh (KnitMesh Technologies). The wire wool (~3mm aperture) was loosely packed inside the glass tube with a volume of the wire wool around 22% of that of the tube. The open cross-sectional areas of these meso-OBRs were within the range of 20 – 40% commonly used for conventional OBRs (Stonestreet and Harvey, 2002). These values were higher than 13% reported for SPC meso-OBR (Reis *et al.*, 2005), leading to lower frictional losses. Frictional losses increase as the open cross-sectional area of the meso-OBR decreases. The wire wool packed tube was selected to evaluate the RTD and effectiveness of oscillatory packed reactors in liquid-liquid multiphase reactions.

3.3.3 Laboratory equipment and accessories

Laboratory equipment used and their errors are shown in the Table 3.6. Furthermore, other laboratory accessories were also used as listed below.

i. Syringe pumps: Confluent PVM syringe pumps (Eurodyne Ltd.) for providing the oscillations and net flows, and NE-300 syringe pumps for net flows.

ii. A Clifton 16101 magnetic stirrer used to provide the mixing (±1.8rpm) in the reactions using the stirred tank batch reactor

iii. A temperature controlled water bath (Ecoline, LUADA E100) for heating (±0.05°C)

iv. A Fuke 51 (K/J) thermocouple with K-probe for the temperature measurement (±0.05°C) in the reaction system.

v. A Memmert Beschickung-loading oven (model 100-800) used for the drying (±0.25°C) of the samples drying

vi. Electronic weighing balance: Delta Range mettler PM4800 weighing balance (±1mg) and A&D HR-200 weighing balance (±5mg).

vii. BioCold Laboratory Freezer operated at -20°C for storage of samples.

Table 3.6: Laboratory equipment used in the studies

Laboratory equipment	Quantities Measured	Error (± %)
Quantachrome ChemBET-3000 TPR/TPD	NH_3/CO_2 pulse titration	0.04 – 0.1
Quantachrome surface area and pore size analyser (NOVA 2000e)	Surface area and pore sizes	0.1 – 0.2
Varian 800 FTIR spectrometer	Functional groups	-
Hitachi S2400 SEM fitted with an Oxford Instruments Isis 200 ultra-thin window EDX detector	Micro-structures Elemental composition with EDX detector	0.08 – 0.1 (EDX)
PANalytical X-ray diffractometer (X'pert PRO)	XRD analysis of crystallinity	-
Hach-Lange conductivity meter (CDM210) with E61M014 cell.	Conductivity for RTD study	0.4 – 2.2
Malvern Bohlin visco 88 viscometer	Viscosity	0.5
5890 Hewlett Packard Series II GC	Analysis of samples	-

3.4 Experimental methods

3.4.1 Characterisations of the heterogeneous catalysts

The solid catalysts were subjected to several physical and chemical characterisations using various techniques, such as elemental analysis by energy dispersive X-ray (EDX), quantification of the catalyst active sites by CO_2 pulse (SZB) and NH_3 pulse ($PrSO_3H$-SBA-15) titrations. Fourier transform infrared (FTIR) spectroscopy was used to identify the functional group of the catalysts, by the FTIR spectra collected using a Pike Technologies diamond crystal plate attenuated total reflectance (ATR) in a transmission mode. Finally, surface area, porosity and crystallinity of the catalysts were determined. The SZB and $PrSO_3H$-SBA-15 catalysts were used as received.

3.4.2 Determinations of the active sites concentration of the catalysts.

Active sites of the SZB catalyst and $PrSO_3H$-SBA-15 catalysts were quantified by pulse titration using a ChemBET-3000 TPR/TPD (Quantachrome Instruments). The instrument was equipped with a thermal conductivity detector (TCD) and controlled by TPRWin software. CO_2 pulse titration was used for the SZB, and NH_3 pulse titration for the $PrSO_3H$-SBA-15.

For the SZB catalyst, about 98.0mg catalyst was placed in a U-shaped quartz tube which was then fitted into the ChemBET instrument. The sample was outgassed for 2hr at 120˚C and 20mL/min helium gas to remove moisture and any impurities of the catalyst. The temperature of the sample was then reduced to 40˚C at the constant helium flow of 20mL/min before the CO_2 titration was started. Pulses of CO_2 at 295K and 2atm were injected onto the sample at 5min interval using a 50µL loop until there were no further chemisorptions of the CO_2, as shown by the TCD. This was indicated as the CO_2 peaks in the exit gas remained constant.

Similarly, the active sites density of the $PrSO_3H$-SBA-15 catalyst was quantified. Approximately 50mg catalyst was placed in a U-shaped quartz tube and the tube fitted to the ChemBET-3000 instrument before the sample was outgassed at 150˚C at 20mL/min helium for 2hr. The NH_3 chemisorptions was performed at 100˚C to prevent any physisorption of NH_3 on the silica surface (Pirez *et al.*, 2012). Pulses of NH_3 were injected into the sample using a 500µL gas syringe until the NH_3 signal reached plateau.

Pulse titrations of the active sites were stopped after the catalytic sites were saturated indicated by the exit stream of the CO_2 or NH_3 (Figure 3.4). The amount of CO_2 or NH_3 chemisorbed on the catalyst was calculated. This is the active sites content. When the catalytic active sites are saturated, the peak area of the exit pulse titration gas was equivalent to the concentration in the injection loop.

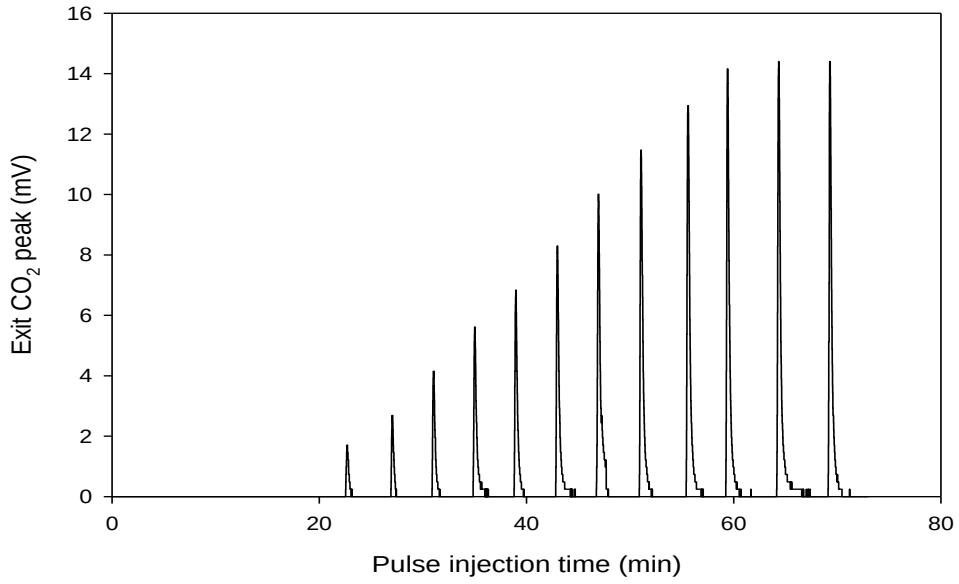

Figure 3.4: TCD peaks for CO_2 pulse titration for the SZB catalyst

The active site densities of the catalysts were calculated using equation (3.1). The calculations were based on the stoichiometry of the reactions.

$$Active\ site\ density\ (mmol.g^{-1}) = (1000)\left(\frac{PV}{RT}\ \frac{n_s}{m}\right)\sum_{i=1}^{n}\left(1-\frac{A_i}{A_{st}}\right) \qquad (3.1)$$

Where:

P: pressure of the pulse gas (atm); T: temperature of the pulse gas (K)

V: volume of the pulse injection loop (L); m: mass of the catalyst used (g)

R: universal gas constant (0.082 L.atm.mol^{-1}.K^{-1}); n: total number of pulse injections

A_i: peak area of exit CO_2 or NH_3 gas in ith pulse injection (mV.s)

A_{st}: saturation peak area of exit CO_2 or NH_3 (mV.s)

n_s: stoichiometric moles of active sites to the pulse gas (n_s = 1 for NH_3; n_s = 2 for CO_2)

The chemical reactions that occurred in the CO_2 or NH_3 pulse titrations are shown below:

i. CO_2 pulse titration of strontium zirconate based catalyst (SZB)

$$SrZrO_3.xSr(OH)_2.yH_2O + CO_2 \longrightarrow SrZrO_3.xSrCO_3.(y+1)H_2O$$

(2 mole of OH^- active site per 1 mole CO_2: $n_s = 2$)

ii. NH_3 pulse titration of propyl sulphonic acid in $PrSO_3H$-SBA-15

$$PrSO_3H\text{-}SBA\text{-}15 + NH_3 \longrightarrow PrSO_3NH_4\text{-}SBA\text{-}15$$

(1 mole of H^+ active site per 1 mole NH_3: $n_s = 1$)

3.4.3 Functional group identification by FTIR spectroscopy

FTIR analysis was performed on two catalysts: $PrSO_3H$-SBA-15 and SZB using a Varian 800 FT-IR spectrometer, to determine the relevant functional groups in the samples. The FTIR spectra were collected at the range of 600 to 4000cm^{-1} and 2cm^{-1} resolution using a Pike Technologies diamond crystal plate ATR in a transmission mode.

3.4.4 Surface area and pore size analysis

Surface areas and pore sizes of the catalysts were measured using a Quantachrome multi-station surface area and pore size analyser (NOVA 2000e) controlled via NOVAWin software. The samples were degassed overnight at 120˚C to remove moisture and any other volatile impurities. N_2 adsorption/desorption isotherms of the samples were recorded at relative pressures of 0 – 1.0 (Figure 3.5). Brunauer-Emmett-Teller (BET) surface area of the catalyst was calculated using the N_2 adsorption isotherm data at the relative pressures of 0 – 0.2 (Brunauer *et al.*, 1938). The pore size of the catalyst was determined from the N_2 desorption isotherm using Barrett-Joyner-Halenda (BJH) method (Barrett *et al.*, 1951). Calculations of the BET surface area and BJH pore size of the catalysts are shown in Appendix A.

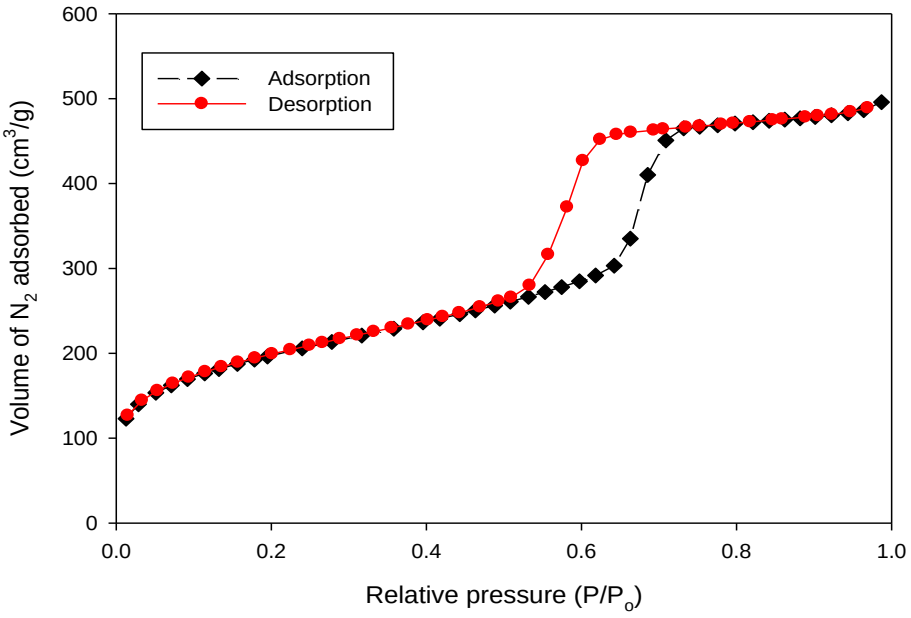

Figure 3.5: N_2 adsorption and desorption isotherm of the $PrSO_3H$-SBA-15

3.4.5 Determinations of elemental compositions of the catalysts by EDX

Elemental compositions of the SZB and $PrSO_3H$-SBA-15 catalysts were determined using EDX. The samples were mounted on aluminium stubs and analysed in a low vacuum mode at 2kV, using an Environmental Scanning Electron Microscope (Hitachi S2400) equipped with Field Emission Gun (FEI X30 ESEM-FEG). The elemental composition was determined using EDX analysis based on Rontec Quantax software.

3.4.6 X-ray diffraction analysis of the catalysts

X-ray diffraction (XRD) analysis of the catalysts was performed on the $PrSO_3H$-SBA-15 and SZB catalysts to investigate the crystallinity of the samples. The analysis was carried out using a PANalytical diffractometer (X'pert PRO, PW 3064) with a goniometer PW 3050/60 (theta to theta) equipped with a copper anode (Kα1 = 1.540598Å, Kα2 = 1.544426Å) at operating conditions of 40 kV and 40mA. The XRD data was collected over the 2θ range of 5 – 100° and a scan step size of 0.03°. The diffractograms were analysed using the diffraction standard patterns in Joint Committee for Powder Diffraction Standard (JCPDS) files.

3.5 Fatty acid profile and molecular masses of glycerides and FAME

The fatty acid composition of RSO was obtained by converting the RSO into FAME via transesterification with methanol and analysed using the BS EN 14103:2003 standard (BSI, 2003). The reaction was carried out in a 100ml three-neck jacketed batch reactor connecting to a condenser, a sampling unit and a thermocouple for monitoring reaction temperatures, as shown in Figure 3.6. The reactor was assisted with a magnetic stirrer (Clifton 16101) to provide mixing. About 57.6mL (≈ 52.9g) RSO was placed in the reactor and heated to a temperature of 60˚C through the circulation of hot water inside the jacket. This was followed by adding 14.4mL (11.4g) pre-heated anhydrous methanol containing 0.53g KOH into the reactor and mixing vigorously at 600rpm using the magnetic stirrer. These corresponded to methanol to RSO molar ratio of 6:1 and 1.0wt% KOH (based on RSO), which are normally used for alkali-catalysed biodiesel production (Keera *et al.*, 2011; Rashid *et al.*, 2009).

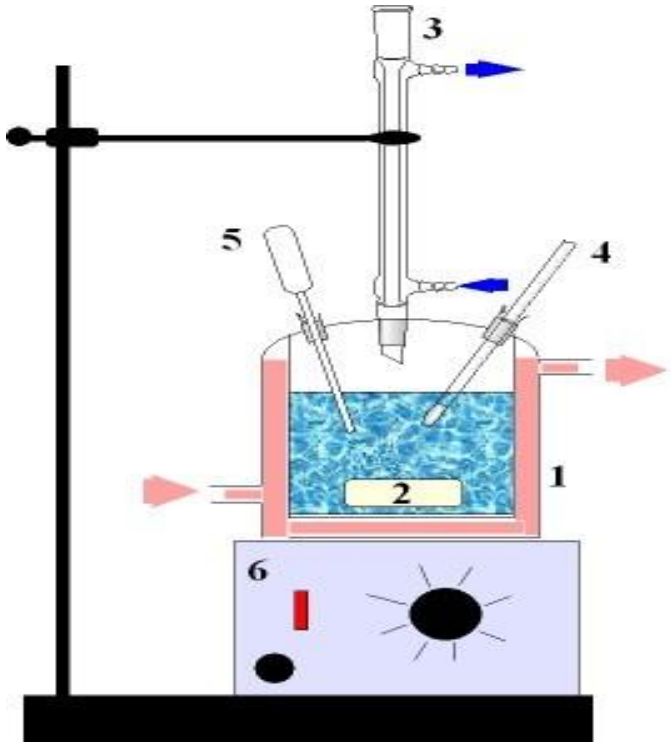

Figure 3.6: Experimental set-up for batch transesterification**,** reactor (1), magnetic bar (2), condenser (3), thermocouple (4), sampling port (5) and magnetic stirrer (6)

The reaction was run for 3hr. After 1hr reaction time, 1mL of the reaction mixture was collected at every 30min and analysed for FAME content. This was continued until there was no further increase in FAME content. The sample mixture was allowed to separate into two layers, mainly of FAME in the upper layer and by-product glycerol in

the bottom layer. The sample was analysed for FAME using a GC. FAME profiles of RSO and the molecular masses of the triglyceride, diglyceride, monoglyceride and FAME from the RSO were calculated as shown in equations (3.2) - (3.6).

Fatty acid composition: $$\%FA_i = \frac{A_i}{\sum_{i=1}^{n} A_i} x\ 100 \quad (3.2)$$

Triglyceride: $$MW_{RSO} = 3\left(\sum_i x_i . MW_{FA_i}\right) + 38 \quad (3.3)$$

Diglyceride: $$MW_{DG} = 2\left(\sum_i x_i . MW_{FA_i}\right) + 56 \quad (3.4)$$

Monoglyceride: $$MW_{MG} = \left(\sum_i x_i . MW_{FA_i}\right) + 74 \quad (3.5)$$

FAME: $$MW_{FAME} = \left(\sum_i x_i . MW_{FA_i}\right) + 14 \quad (3.6)$$

Where:

$\%FA_i$: percentage composition of i^{th} fatty acid; A_i: the percentage peak area of i^{th} fatty acid; MW_i: molecular mass of the i^{th} compound ($g.mol^{-1}$); x_i: mass fraction of the i^{th} fatty acid.

3.6 Measurements of viscosities of the reactants and the reaction mixtures.

Viscosity of RSO, methanol, carboxylic acids (propanoic, hexanoic, lauric, and palmitic acids) and the reaction mixtures without were determined. This was carried out at various temperatures (40, 50 and 60˚C) using a Bohlin visco 88 viscometer. About 12mL sample was placed in a 12mL coaxial cup placed inside a heated water bath. The viscometer was started as soon as the sample was heated to a desired temperature (40, 50 and 60˚C). Viscosities of the samples were recorded continuously until the mixture was homogenised and the viscosity remained constant (See Appendix B).

3.7 Characterisation of flow patterns inside the meso-OBRs

The experimental set-up for characterising the flow patterns of the meso-OBR is shown in Figure 3.7. The system comprised of a 340mm length and 5mm internal diameter baffled (wire wool packed) glass tube. The base of the meso-OBR was connected to three Confluent PVM syringe pumps through Swagelok fittings, while the top was

connected to a 4mm diameter and 103mm length E61M014 conductivity probe. The conductivity probe was connected to a CDM210 conductivity meter. The tip of the probe was positioned in the centre of the glass tube (without touching the wall) at the exit baffle cavity before the tracer left the system to minimise any disturbances to the flow inside the reactor. The syringe pumps were used to provide net flow, oscillate the fluid, and inject the aqueous KCl. The set-up was used to investigate the RTDs of the meso-OBRs, namely, integral baffles, wire wool packed tube and sharp-edged helix with a central rod baffles.

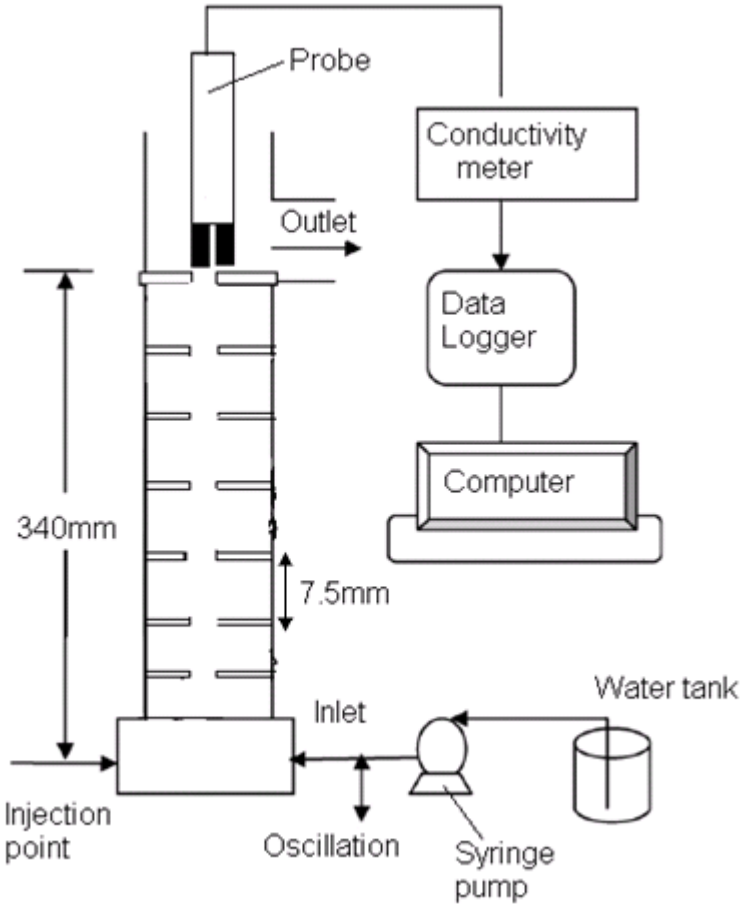

Figure 3.7: Schematic of the experimental set-up for determination of RTDs of the meso-OBRs. Adapted from (Phan *et al.*, 2011a)

3.7.1 Acquisitions and analysis of the RTD data

A E61M014 conductivity probe was calibrated prior to RTD experiments using several aqueous solutions of KCl at concentrations of 0, 0.05M, 0.10M, 0.15M, 0.20M, 0.25M, corresponding to 0g/L, 3.73g/L, 7.46g/L, 11.18g/L, 14.92g/L and 18.64g/L, respectively. There was a linear relationship between concentration and its corresponding

conductivity with R^2 of 0.998 (Figure 3.8(a)). Concentration (density) of the KCl tracer had no effect on the RTD profiles of meso-OBRs at 0.1M (7.46g/L) – 3M (223.65g/L) and injection volume of about 100µL as shown in Figure 3.8(b) (Phan *et al.*, 2011a). The RTD profiles in Figure 3.8(b) also indicate that KCl injection technique was reproducible.

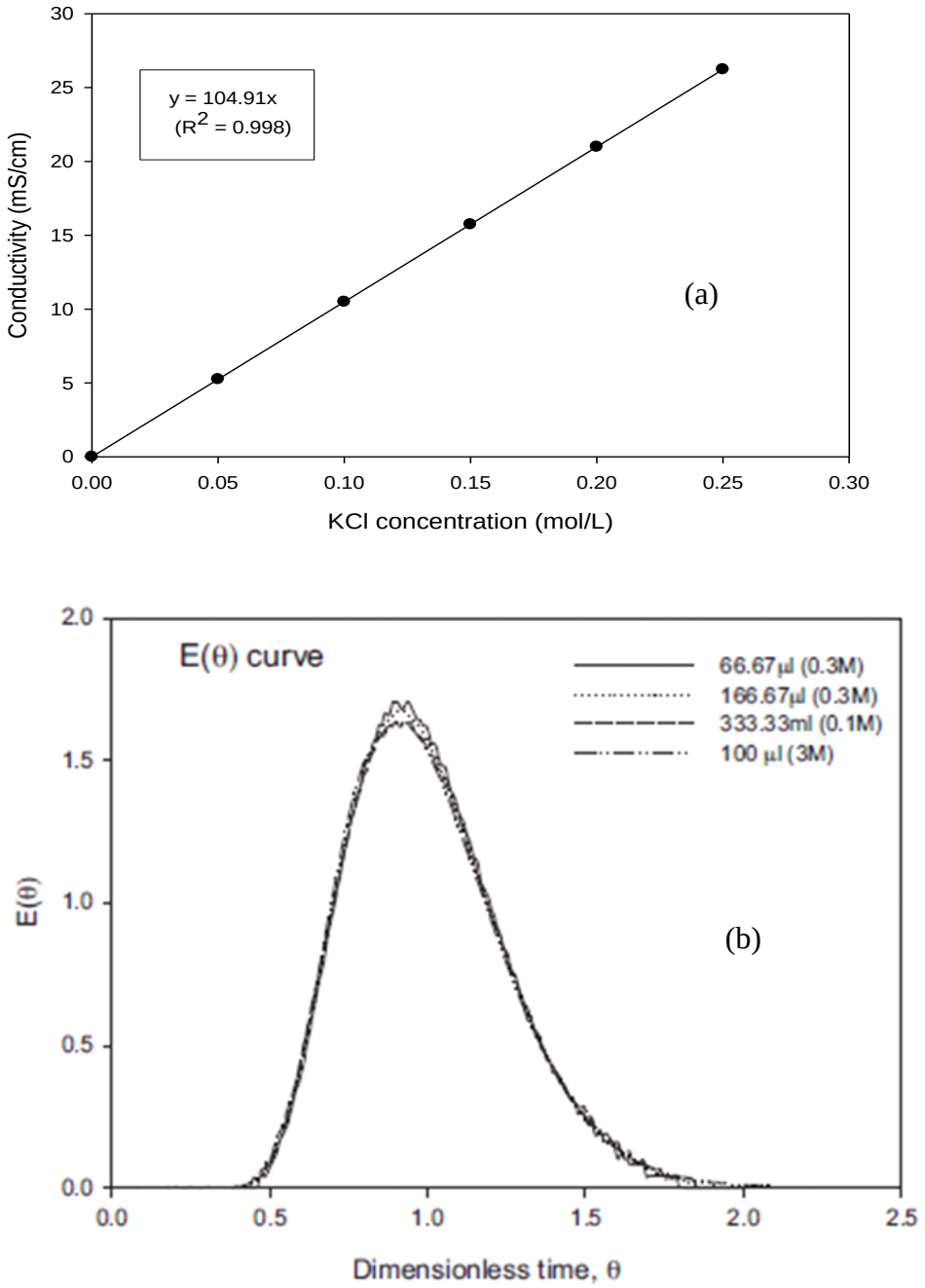

Figure 3.8: (a) KCl calibration curve used for the RTD analysis, (b) RTD of meso-OBR at various KCl tracer concentrations and injection volume (Phan *et al.*, 2011a)

The RTD experiments were carried out at room temperature (24-25˚C) using distilled water as continuous fluid at residence times of 2.5min to 60min. This corresponds to net flows of 0.17ml/min to 4.0ml/min (Re_n = 0.72 – 17) and oscillatory mixings in a range of 2 – 4.5Hz frequency and 1 – 8mm amplitude (Re_o = 60 – 1130). The pump commands for the PVM syringe pumps are shown in Appendix C.

Each RTD experiment began after the system had been filled with distilled water and oscillated for at least 2min at the desired oscillation frequency and amplitude and net flow rate of water to expel air bubbles and stabilise the system. A known amount of the tracer (100µl of 0.25M KCl) was rapidly injected into the base of the reactor (opposite the entry port of the net flow) to produce a near pulse injection (Phan *et al.*, 2011a), and the data was immediately recorded. At the exit of the reactor, the 4mm diameter E61M014 conductivity probe (~2.30s delay time) connecting to CDM210 conductivity meter (Hach-Lange Ltd) was used to acquire the conductivity-time data at 1s interval and logged into the computer through a DaqPro 5300 data logger controlled by a Picolog software. The data acquisition was continued until the conductivity of the fluid returned to the initial value (before the tracer injection).

Flow patterns of the meso-OBRs were characterised using the dimensionless and normalised forms of the statistical moments: mean residence time, exit age distribution curve (E-curve), variance and skewness (Fogler, 2005; Levenspiel, 1999). This was to allow for comparison of experimental results from the various process parameters.

Dimensionless time: $$\theta = \frac{t_i - t_d}{\tau} \quad (3.\ 7)$$

Distribution curve: $$E(\theta) = \tau E(t) = \tau \frac{C_i}{\sum_i (C_i \Delta t_i)} \quad (3.\ 8)$$

Normalised variance: $$\sigma(\theta)^2 = \frac{\sigma(t)^2}{\tau^2} = \sum_i [(\theta_i - 1)^2 . E(\theta) \Delta\theta_i] \quad (3.\ 9)$$

Skewness: $$\gamma(\theta)^3 = \sum_i [(\theta_i - 1)^3 . E(\theta) \Delta\theta_i] \quad (3.\ 10)$$

Where:

C_i: concentration of the KCl tracer at time t_i ($mol.L^{-1}$)

t_i: time that i^{th} segment of the tracer spent in the reactor (s)

Δt_i: time intervals in the data acquisitions (1s)

t_d: delay time of the probe (2.30s)

3.7.2 Evaluations of the RTD data using the TIS model

TIS model was used for quantitative assessment of RTDs of the meso-OBRs. This model treats the meso-OBRs as a combination of equally sized CSTRs in series, where the mixing in each baffle cavity resembles that of a CSTR. RTD data from the meso-OBRs were analysed using the TIS model as reported in Phan *et al.* (2011), based on equations (3.11) – (3.14).

Dimensionless time: $$\theta = \frac{t_i - t_d}{\tau} = \frac{t_i - t_d}{N\tau_i} \quad (3.11)$$

Dimensionless E-Curve: $$E(\theta) = \tau E(t) = \frac{N(N\theta)^{N-1}}{(N-1)!} e^{-N\theta} \quad (3.12)$$

Normalised variance: $$\sigma(\theta)^2 = \frac{\sigma(t)^2}{\tau^2} = \int_0^\infty (\theta - 1)^2 . E(\theta) d\theta = \frac{1}{N} \quad (3.13)$$

Theoretical number of tanks in series: $$N = \frac{1}{\sigma(\theta)^2} \quad (3.14)$$

An initial estimate of N was obtained from the experimental RTD data by combining equation (3.9) and (3.13). The estimated value of N was substituted into the exit age curve from equation (3.12) and compared to the E-curve from equation (3.8). The value of N was changed to compare the two E-curves in terms of shape, spread and height (Phan and Harvey, 2011), until the value of N that minimised the sum of squared residuals/errors was achieved (least squares method). The delay time (2.30s) of the probe in the aqueous KCl solution had no effect on the RTD profile of the meso-OBRs, as the RTDs were similar with or without considerations of the delay time even at the shortest residence time used in the study (Figure 3.9(a)). This was due to the relatively short delay time of the probe compared to the range of residence times (2.5min – 60min) investigated. The RTDs of the meso-OBRs measured by conductivity method using aqueous KCl injection was reproducible as shown in Figure 3.9(b). This was consistent with the reports of Phan *et al*. (2011a) shown in Figure 3.7.

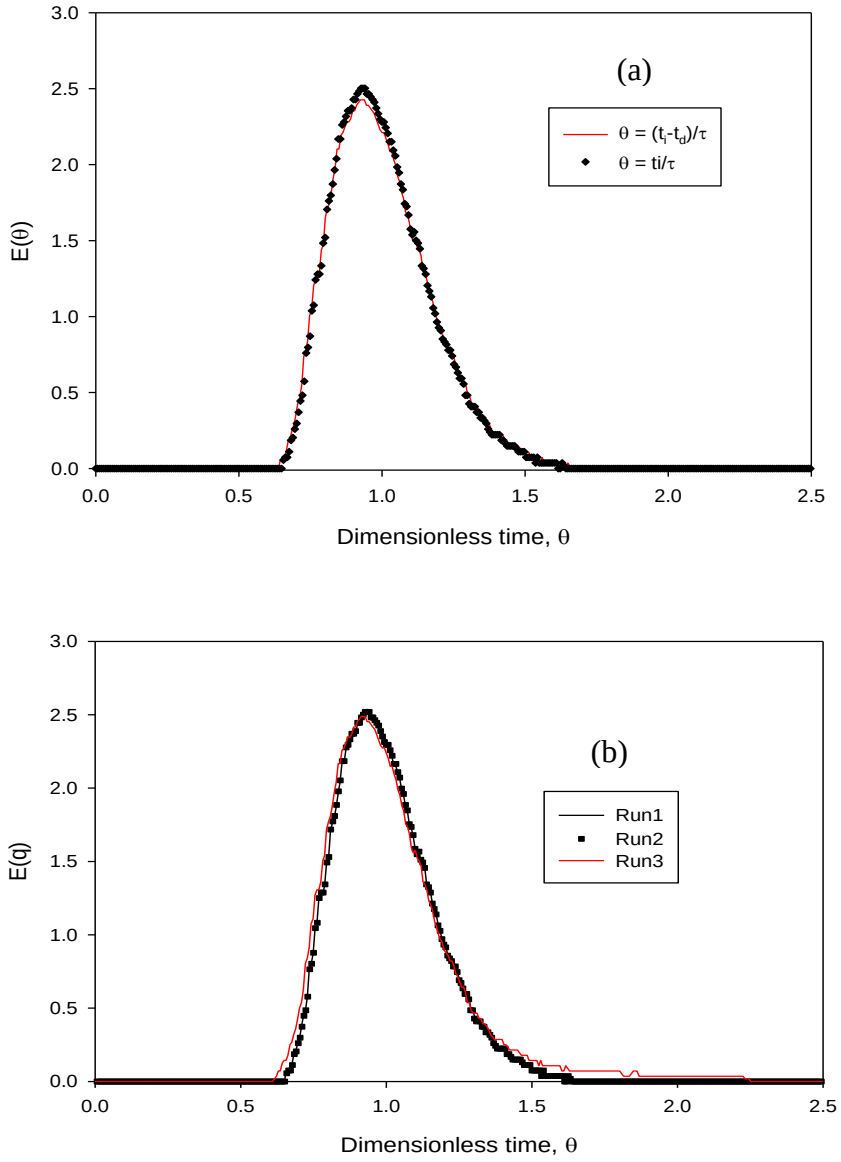

Figure 3.9: RTDs of the integral baffles meso-OBR at 2.5min residence time (Re_n = 17) (a) effects of probe delay time, (b) reproducibility of the KCl tracer injection method

3.8 Homogeneous alkali-catalysed transesterification.

Alkali-catalysed transesterification of RSO with methanol was carried out using the integral baffles, wire wool packed reactor and a sharp-edged helix a with central rod baffles to select a suitable meso-OBR for screening of catalysts. Transesterification was also carried out in a 100mL stirred tank batch reactor to provide data for the numerical modelling.

3.8.1 Continuous alkali-catalysed transesterification in the meso-OBRs

The experimental set-up for steady state performances for continuous alkali-catalysed biodiesel production from RSO is shown in Figure 3.10. Four 340mm height and 5mm diameter baffled tubes were connected together using Swagelok fittings and placed vertically in a LUADA E100 water bath set at a temperature of 60˚C. This provided a total volume of approximately 29 mL for the integral baffles, 30mL for wire wool packed reactor and 35mL for the sharp-edged helix with a central rod. The second and fourth baffled tubes were connected to valves for releasing gas bubbles trapped in the system. The third vertical baffled tube was connected to a K-probe thermocouple (Fuke 51 (K/J)) to measure the reaction temperature.

The RSO was heated up to 60˚C in a 500mL reservoir placed in the heated water bath while 2M solution of KOH was maintained at 40˚C in a 500mL reservoir using a Clifton, 16101 magnetic stirrer. Anhydrous methanol at room temperature (24-25˚C) and the 2M KOH were pumped continuously through a pre-heating line of 60˚C before entering the first tube. Two Confluent PVM syringe pumps were used to pump in RSO and 2M KOH while the anhydrous methanol was dispensed by an NE-300 syringe pump. Another Confluent PVM syringe pump was used to provide the oscillatory mixing by setting the frequency and centre-to-peak amplitude of the oscillation. The flow rates of the reactants were set to correspond to 6:1 methanol to RSO molar ratio and 1.5wt% KOH (based on oil). Steady-state screening was performed at a fixed residence time (τ) of 10min (Re_n of 1.74) and Re_o of 36 – 160 for the three meso-OBRs as shown in Table 3.7. The densities and viscosities parameters used for the calculations of the Re_n and Re_o are shown in Appendix B.

Table 3.7: Flow conditions used in the experiments

Re_o	(ψ)	St	x_o (mm)	f_o (Hz)
160	92	0.05	8	4.5
107	61	0.1	4	6
71	41	0.1	4	4
36	20	0.2	2	4

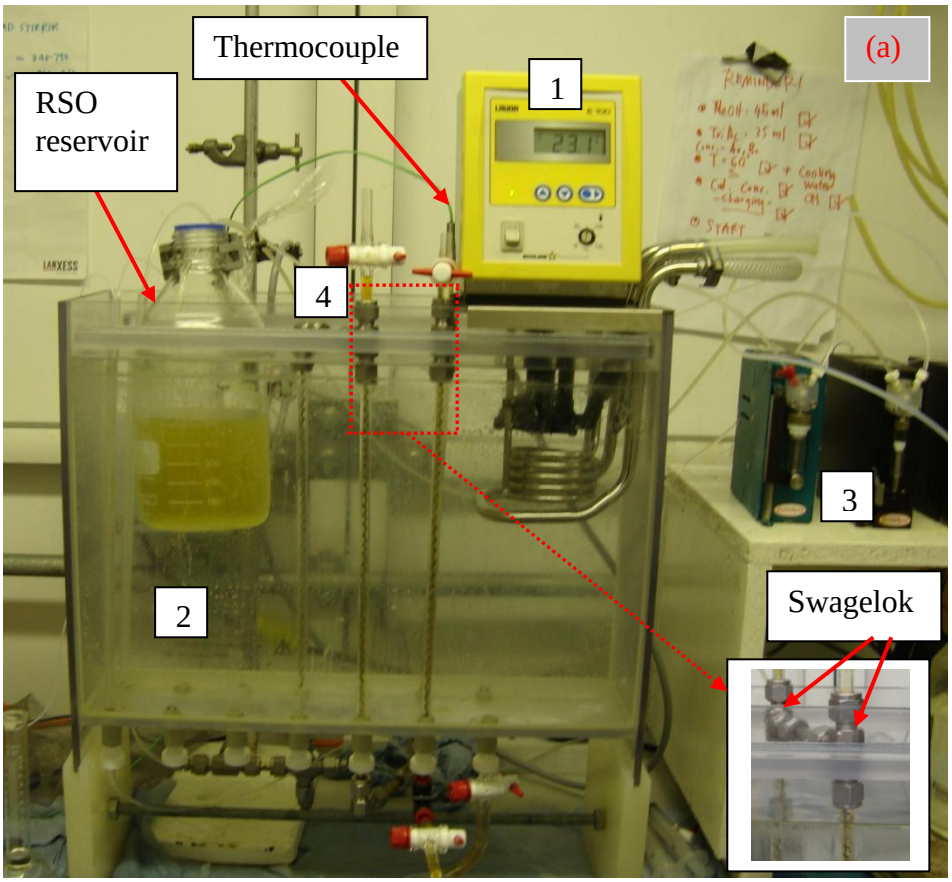

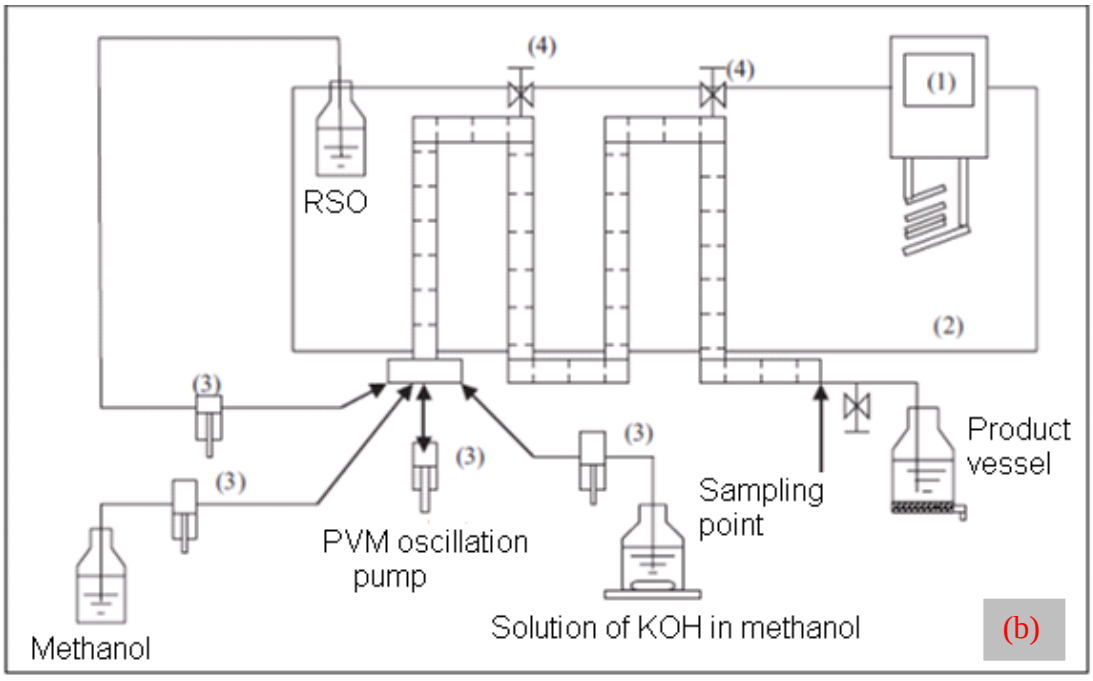

Figure 3.10: (a) Experimental set-up (b) schematics for continuous alkali-catalysed methanolysis of RSO: (1) Temperature controller, (2) water bath, (3) syringe pumps, (4) valves

The effects of residence time, type and concentration of catalysts on FAME yield were investigated using the integral baffled design. The experimental conditions were 60˚C reaction temperature, 6:1 methanol to RSO molar ratio, Re_o of 160, τ in the range of 2.5 – 20min and catalyst (KOH, NaOH and $NaOCH_3$) loadings of 0.75 – 1.5wt% (based on RSO). After one residence time (1τ), approximately 1mL of the reaction mixture was collected at 5min interval for 60min (6τ). The samples were quenched immediately using 0.1mL HCl of 0.1M and stored in a freezer at -20˚C for GC analysis.

3.8.2 Alkali-catalysed transesterification of RSO in batch reactor

Alkali-catalysed transesterification of RSO with methanol was investigated in a stirred tank batch reactor using the set-up described in section 3.5 (Figure 3.6). The reactor was a 100ml three-neck jacketed glass batch reactor equipped with a condenser, a thermocouple and a magnetic stirrer operating at 600rpm. This mixing speed was chosen because the reaction was mixing independent at higher mixing velocities ≥ 600rpm (Figure 3.11).

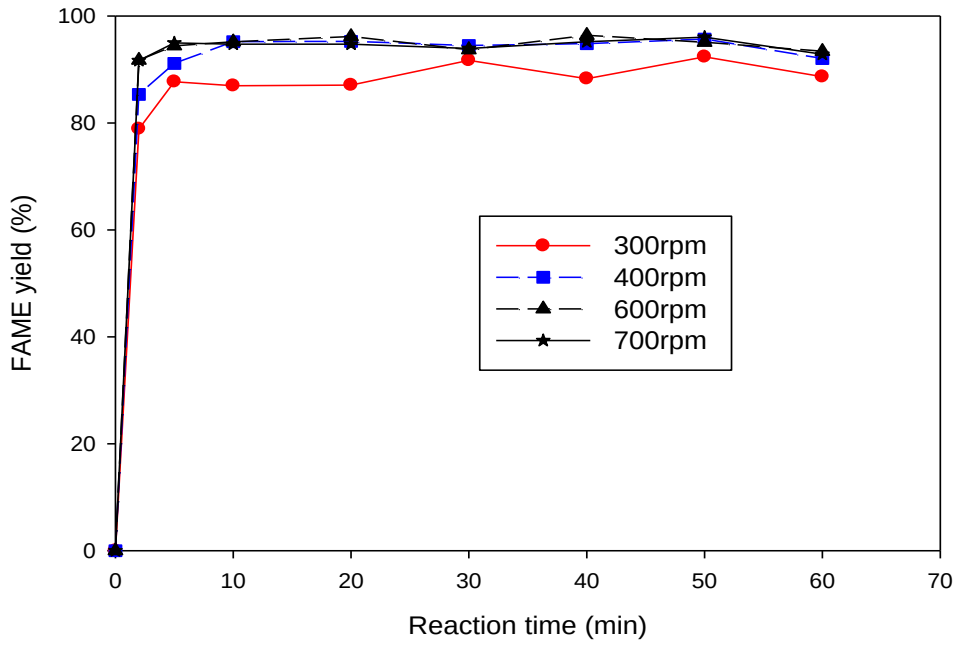

Figure 3.11: The effects of mixing speed on FAME yields for the stirred tank batch reactor for transesterification at 6:1 methanol to RSO molar ratio, 60˚C and 1.5wt% KOH (based on RSO)

The reaction was tested at the following conditions: (i) reaction temperatures of 40 - 60˚C, (ii) methanol to RSO molar ratios of 3:1 – 300:1 and (iii) 0.5 – 1.5wt% of KOH catalyst. RSO was heated in the reactor to a temperature of 40, 50 or 60˚C through the circulation of hot water inside the jacket. As soon as the desired temperature was reached, a required amount of pre-heated methanol was added into the reactor. Approximately 0.5ml reaction mixture was taken at various times, usually 1, 2, 5, 8, 10, 15, 20, 30, 40, 50 and 60mins, and transferred into a 2ml pre-weighed vial containing 0.05ml HCl 0.1M to quench the reaction. These samples were stored at -20˚C in a freezer for GC analysis.

3.8.3 RSO saponification in methanol-hydroxide solution

RSO saponification was carried out in a 0.5M KOH in methanol solution at a temperature of 40, 50 or 60˚C using the set-up shown in Figure 3.6. Approximately 75mL of the 0.5M KOH-methanol solution was heated in a 100mL jacketed reactor to a desired temperature through the circulation of hot water inside the jacket. About 6g of pre-heated RSO was transferred into the reactor and mixed vigorously at 600rpm using a magnetic stirrer. The amounts of RSO, methanol and KOH in the mixture correspond to 300:1 methanol to RSO molar ratio and 35wt% KOH (based on RSO), which were similar to a procedure reported for the saponification of fats and oils in ethanol-hydroxide solution (AOCS, 1998).

10mL of the reaction mixture was taken at various interval times for 60min using a 10mL pipette and transferred into a 100mL conical flask containing 10mL HCl 0.5M. The excess HCl was then determined by titration with 0.5M methanol-KOH to quantify the amount of RSO that was saponified. Potassium hydrogen phthalate was used to standardise the methanol-KOH solution, which was then used to standardise the HCl solution. 0.5mL reaction samples were also collected using a 1000µL micropipette at various times up to 60min, quenched immediately with 0.5mL of 0.5M HCl, and stored in a freezer at -20˚C for GC analysis.

3.8.4 FAME saponification in methanol-hydroxide solution

FAME saponification was also studied using the experimental set-up in Figure 3.6 and the procedure described in section 3.8.3. The FAME was obtained via a

transesterification process at a molar ratio of methanol to RSO of 6:1, reaction temperature of 60˚C and reaction time of 10min (Phan *et al.*, 2012). The FAME (97.85%) was dried in the oven for 12hr at 105˚C to remove all water and then saponified with 0.5M NaOH and 0.5M KOH in methanol solution at a temperature range of 40 - 60˚C. The effect of water on FAME saponification was examined by performing the FAME saponification with methanol containing 0 – 12.5 vol% water.

About 0.5mL reaction sample was collected using a 1000µL micropipette at various interval times for 60min and transferred into a pre-weighed 2mL vial containing 0.5mL of 0.5M HCl, to quench the reaction immediately. All the samples were stored in a freezer at -20˚C for GC analysis.

3.9 Transesterification of RSO with methanol using the SZB catalyst

The catalytic activity of SZB catalyst for transesterification of RSO with anhydrous methanol was screened using the set-up shown in Figure 3.12.

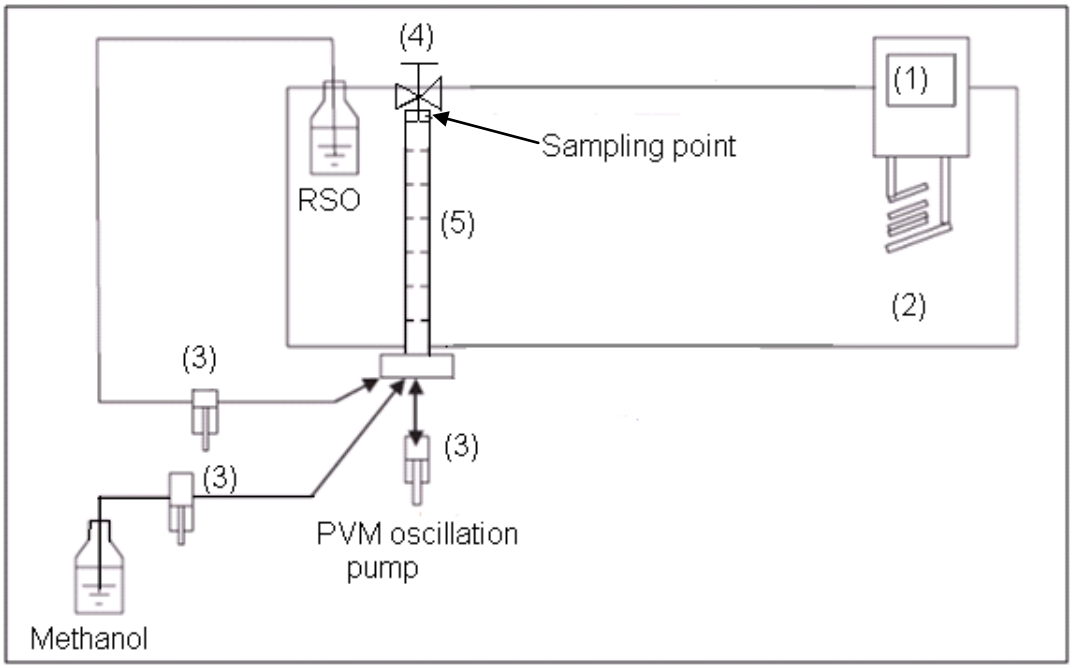

Figure 3.12: Experimental set-up for the suspension and screening of the catalyst: (1) water bath, (2) temperature controller, (3) syringe pumps, (4) output valve and (5) integral baffled meso-OBR

The reactor used in the Figure 3.12 was a 340mm length and 5mm inner diameter integral baffled meso-OBR was placed vertically inside a water bath, giving a total reactor volume of 10mL. The inlet of the reactor was connected to three Confluent

PVM syringe pumps to provide net flows of RSO and methanol and to oscillate the reaction mixture. A valve was fitted at the top of the reactor where samples were collected.

3.9.1 Suspension and screening of the SZB catalyst

Batch transesterification reactions were studied at 12:1 methanol to RSO molar ratio, 60˚C and 3%wt of SZB catalyst and various oscillation conditions, e.g. 2Hz and 4mm (Re_o = 49), 4.5Hz and 4mm (Re_o = 112), 4Hz and 6mm (Re_o = 148), and 4.5Hz and 8mm (Re_o = 223) using the set-up shown in Figure 3.12. The reaction was shown to be mass-transfer independent at $Re_o \geq 148$ (see section 4.6.1).

3.9.2 Influence of methanol-to-RSO molar ratios and reaction temperature

Batch transesterification of RSO were studied at 24:1, 12:1 and 6:1 methanol to RSO molar ratios, 60˚C and 3.0wt% catalyst (based on RSO) and oscillation condition Re_o of 223. The amounts of the SZB catalyst shown in Table 3.8 were suspended in the proportionate amount of RSO at 60˚C. The required amounts of methanol were pumped into the reactor from a reservoir maintained at 60˚C.

Table 3.8: Flow conditions used in the investigations

Methanol: RSO molar ratio	RSO (g)	Methanol (g)	SZB Catalyst (mg)
6:1	7.3	1.6	219.8
12:1	6.1	2.7	183.2
24:1	4.6	4.0	136.9

3.9.3 Effect of the SZB catalyst loading and water content on transesterification

Effect of the SZB catalyst loading was investigated for batch transesterification of RSO at 12:1 methanol to RSO molar ratio, 60˚C and catalyst loading of 1.5 – 4.5wt% (based on RSO) using the procedure in section 3.9.2. A required amount of the catalyst was suspended in 6.1g (6.6mL) RSO heated at 60˚C, and followed by adding 2.7g (3.4mL) methanol heated at 60˚C into the reactor. Water tolerance of SZB catalyst was studied by transesterification of RSO at 60˚C, 12:1 methanol to RSO molar ratio and 3wt%

catalyst loading in the presence of 0 – 2vol% water. The catalyst suspension and fluid mixing in the reactor was provided by oscillatory mixing at Re_o of 223.

3.9.4 Leaching and reusability of the SZB catalyst

The SZB catalyst was soaked in fresh methanol to examine its stability and resistance to leaching. About 276mg SZB catalyst was suspended in 10mL anhydrous methanol inside the integral baffled meso-OBR shown in Figure 3.12, at 60˚C for 60min under an oscillatory mixing at 4.5Hz and 8mm (Re_o = 2430). The mixture was then filtered through a 0.45µm syringe filter. The residue was washed twice with fresh methanol and dried in an oven at 105˚C for 8hr. The filtrate and residue were used to catalyse RSO transesterification at 24:1 methanol to RSO molar ratio and 60˚C. 5.0mL methanol filtrate was reacted with 5.0mL RSO without any addition of fresh catalyst. 5.0mL of fresh methanol was also reacted with 5.0mL of RSO using 3wt% of the SZB catalyst residue.

3.9.5 Continuous transesterification of RSO with the SZB catalyst

Continuous SZB-catalysed transesterification of RSO with methanol was examined at 12:1 methanol to RSO molar ratio, 60˚C and 3.0wt% catalyst (based on RSO). The reaction conditions used were similar to that reported for the catalytic activity test on the SZB catalyst in a batch reactor (Lima *et al.*, 2012). About 183mg SZB catalyst was suspended in the integral baffled meso-OBR reactor (Figure 3.12) containing 10mL methanol heated at 60˚C and mixing condition Re_o of 233 and followed by continuous flows of RSO and methanol from preheated reservoirs at 60˚C. The total flow rate of RSO and methanol was 0.50mL/min (Re_n of 0.42), corresponding to a 20min residence time. The top of the reactor was fitted with a 0.45µm syringe filter to prevent any loss of the charged catalyst in the continuous transesterification.

3.9.6 Sample Collections

Approximately 0.2mL of sample was collected at 5, 10, 30, 60, 90, and 120 min using 1.0mL syringes fitted with a 0.45µm syringe filters. The samples were immediately stored in a freezer at -20˚C to prevent any further reaction which might occur as a result of any leaching of catalytically active species.

3.10 Esterification of carboxylic acids using the $PrSO_3H$-SBA-15 catalyst

The $PrSO_3H$-SBA-15 was investigated for catalytic activity in RSO and transesterification esterification of carboxylic acids with methanol. The catalyst was suspended and screened using the integral baffled meso-OBR as shown in Figure 3.12. The valve at the sampling point was fitted with a 0.45μm syringe filter, whilst the base of the reactor was connected to three Confluent PVM syringe pumps to provide the oscillation for efficient fluid mixing and particle suspension, and net flow of the reactants.

3.10.1 Batch esterification of various carboxylic acids

The reactor was operated in a batch mode for screening the esterification of propanoic, hexanoic, lauric and palmitic acids. When the reactor was operated in batch mode, the oscillatory mixing was induced without net flow into the reactor. The oscillatory mixing (4.5Hz & 8mm), which corresponds to Re_o of 2300 – 2400, was used for the organic acids esterification at 60˚C and 30:1 methanol to acid molar ratio. The high value of Re_o in the process was due to low viscosities (0.35 – 0.37mPa.s) of the reaction mixtures at a 30:1 methanol to acid molar ratio. Conversion of the acids to methyl esters was independent of the mixing intensity at $Re_o \geq 676$. The oscillatory mixing was sufficient to uniformly suspend the $PrSO_3H$-SBA-15 catalyst particles, as shown in Figure 3.13.

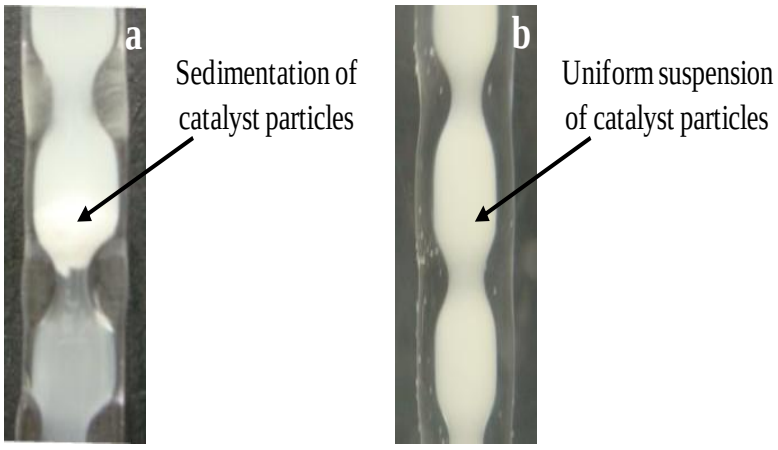

Figure 3.13: $PrSO_3H$-SBA-15 catalyst suspension in an OBR (a) without oscillation; and (b) with oscillation of 8mm amplitude and 4.5Hz frequency (Re_o = 2400)

The carboxylic acids esterification was carried out using about 5wt% $PrSO_3H$-SBA-15 (based on the acids) which was suspended in a proportionate amount of methanol. The reactor was pre-heated to 60˚C before the required amount of acid was added in from a reservoir heated at 60˚C (or 63-65˚C for palmitic acid). The experimental conditions for the reactions are shown in Table 3.9.

Table 3.9: Experimental conditions for the carboxylic acids esterification

Carboxylic acids	Acid (g)	Methanol (g)	Catalyst (mg)
Propanoic	0.56	7.1	28.0
Hexanoic	0.82	6.7	41.0
Lauric	1.31	6.3	65.5
Palmitic	1.62	6.0	81.1

3.10.2 Effects of temperature, catalyst loading, feed ratios and water levels

The effects of temperature, catalyst loading, feed ratios and water levels on heterogeneous $PrSO_3H$-SBA-15 catalysed esterification were investigated in batch mode using the integrally baffled meso-OBR set-up in Figure 3.12. Hexanoic acid was used as a representative carboxylic acid. The hexanoic acid esterification was performed at reaction temperatures of 40 – 60˚C, catalyst loadings of 5 – 10wt%, methanol to hexanoic acid molar ratios of 1:1 – 30:1 and 0 - 5vol% water.

3.10.3 Reusability test for the $PrSO_3H$-SBA-15 catalyst

Spent $PrSO_3H$-SBA-15 catalyst obtained from the hexanoic acid esterification at 60˚C and 1:1 methanol to acid molar ratio was washed 3 times with methanol and dried in an oven set at 70˚C for 36hr. Esterification of hexanoic acid at 60˚C and 30:1 methanol to the acid molar ratio was performed in batch using 5wt% of the dried spent catalyst. The procedure used in the experiment was similar to that described in section 3.10.1.

3.10.4 Continuous esterification using the $PrSO_3H$-SBA-15 catalyst

Continuous esterification of hexanoic acid was investigated using the integral baffled meso-OBR set-up in Figure 3.12. The output valve was fitted with a 0.45µm syringe filter to prevent any loss of charged catalyst. 10wt% (82mg) of the $PrSO_3H$-SBA-15

catalyst was suspended in the reactor containing 10mL of methanol heated at 60˚C under Re_o of 2400. Hexanoic acid and methanol were dispensed continuously into the reactor from reservoirs held at 60˚C. The reaction was screened at 30:1 methanol to hexanoic acid molar ratio using ramped residence times of 30min and 60min, corresponding to feed net flow rates of 0.33mL/min (Re_n = 3.24) and 0.17mL/min (Re_n = 1.62). The reaction was run for a total of 255min: a running time of 105min at 30min residence time, followed by a rapid change in the residence time to 60min and another running time of 150min.

Effects of water on continuous esterification was investigated using hexanoic acid esterification at 60˚C, 30:1 methanol to hexanoic acid molar ratio, 10wt% $PrSO_3H$-SBA-15 catalyst and residence time of 60min (Re_n = 1.62). The system was spiked with 6mmol (0.1mL) of water at 150min running time ($t = 2.5\tau$), and the reaction continued for another 210min.

3.10.5 Sample collections

The carboxylic acid esterification reaction described in sections 3.10.1–3.10.4 was monitored by withdrawing about 0.2mL of the reaction mixture through 1.0mL syringe fitted with a 0.45μm VWR syringe filter at various interval times. All the collected samples were stored in a freezer at -20˚C for GC analysis.

3.11 GC analysis

Samples collected in the various experiments were analysed using a 5890 Hewlett Packard Series II GC. The GC conditions used are shown in Table 3.10. This analytical protocol was similar to that developed for analysis of FAME (Yussof, 2012).

Table 3.10: GC conditions used for the analyses

Column type	Varian CP Wax Capillary (BPX70)
Column length and internal diameter	30m and 0.32µm
Column film thickness	0.25mm
Split flow	18.75mL/min
Carrier gas (Helium) input pressure	7 psi
Column head pressure	4.5 psi
Air input pressure	32 psi
Hydrogen input pressure	22 psi
Injector temperature	250˚C
Oven temperature	Variable (230˚C max)
FID Detector temperature	250˚C
Injection volume	Variable (0.5 - 1µL)

3.11.1 GC calibration curve for determinations of methyl esters

GC calibration curves were prepared to quantify the methyl esters produced from the methanolysis of RSO, palmitic acid, lauric acid, hexanoic acid and propanoic acid in the experiments. C_{17} was used as the GC internal standard for quantification of FAME derived from RSO transesterification and esterification of palmitic and lauric acids. Methyl esters of hexanoic and propanoic acids were quantified using methyl octanoate and methyl hexanoate GC internal standards, respectively.

Mixtures of methyl oleate (99%), methyl palmitate (99%), methyl laurate (99.5%), methyl octanoate (99%) and methyl hexanoate (99%) prepared in various concentrations were used to determine the response factors for methyl esters. Methyl oleate was chosen as a representative for methyl esters produced from RSO because RSO used in the study had more than 63wt% oleic acid. The calibration curves were prepared by the correlations of the FID signal (mV.s) with the concentrations of the methyl esters in the mixture. Calibration mixtures used were prepared as shown in Table 3.11. Each of the methyl esters components was prepared in a stock of 250mg per millilitre of heptane (purity of 99.5%).

Table 3.11: Preparation of the calibration mixture for methyl esters

Components	Volume (µL)				
	Run (1)	**Run (2)**	**Run (3)**	**Run (4)**	**Run (5)**
Methyl Oleate	25	50	100	200	400
Methyl Palmitate	100	400	200	25	50
Methyl Laurate	400	200	50	100	25
Methyl Octanoate	200	25	400	50	100
Methyl Hexanoate	50	100	25	400	200

Various volumes of methyl esters in each run were measured from the stock solutions of 250mg/mL, and transferred into a 5mL vial. This was followed by the additions of 1mL of C_{17} internal standard. The C_{17} internal standard was prepared in stock solution of 10mg per millilitre of heptane. 0.5µL of the mixture of methyl esters and internal standard was manually injected into the GC using a 5µL GC syringe (SGE). Non-isothermal oven temperature protocol was used for the methyl esters separation. The initial oven temperature was set at 40˚C and held for 10min, then ramped at 20˚C/min to 120˚C and held for 5min, and finally ramped at 20˚C/min to 210˚C and held for 16.5min (40min run time). Each calibration mixture (run) was injected into the GC at least twice.

Data obtained from the GC measurements of the methyl esters in the calibration mixtures were used to calculate the relative response factor (R_f) of each of the methyl esters. The R_f was calculated from plots of the mass ratios of each methyl esters with respect to the C_{17} internal standard versus the peak area ratios using equation (3.15).

$$\left(\frac{m_s}{m_{is}}\right) = R_f . \left(\frac{A_s}{A_{is}}\right) \qquad (3.15)$$

Where:

R_f: response factor of the methyl ester response factor

m_s: mass of methyl ester (mg)

m_{is}: mass of internal standard (mg)

A_s: peak area (mV.s) of methyl ester

A_{is}: peak area (mV.s) of internal.

3.11.2 Sample preparations for quantification of the methyl esters

Internal standards for the analysis (C_{17} for FAME and methyl esters of palmitic and lauric acids, methyl octanoate (C_8) for hexanoic acid methyl ester and methyl hexanoate (C_6) for the propanoic acid methyl esters) were prepared in heptane at a concentration of 10mg/ml. Samples (50.0 – 80.0mg) were weighed in a 2mL vial using an A&D HR-200 weighing balance (error of ±1mg) followed by adding 1mL of the appropriate internal standard and shaking vigorously to obtain a homogeneous solution. About 0.5-1.0µL of the sample mixture was manually injected using the 5µL GC syringe. The oven temperature protocols used for the components separation are shown in Table 3.12.

Table 3.12: GC oven temperature programmes for the methyl esters separation

Reaction/ process[b]	IS[a]	Oven temperature programme
i. RSO ↔ FAME ii. $CH_3(CH_2)_{14}COOH$ iii. $CH_3(CH_2)_{10}COOH$	C_{17}	Isothermal temperature programme of 210˚C held for 30min
$CH_3(CH_2)_4COOH$	C_8	50˚C held for 3min, ramped at 30˚C/min to 180˚C and held for 2min, ramped at 30˚C/min to 210˚C and held for 10min
CH_3CH_2COOH	C_6	30˚C for 8min, ramped at 30˚C/min to 60˚C and held for 2min, ramped at 30˚C/min to 210˚C and held for 10min.

IS[a] : Internal Standard (10mg/mL); [b]reactions of the organic acids indicated.

3.11.3 Quantification of the methyl esters content in samples

The amounts of methyl esters in the samples were quantified based on the BS EN 14103:2003 (BSI, 2003) method in equation (3.16). R_f obtained from the methyl esters calibration in section 3.11.1 was used. Peak areas of the methyl esters in the sample (A_s) and that of the internal standard (A_{is}) were obtained from the relevant GC chromatogram. For the analysis of FAME from RSO transesterification, peak areas of all methyl esters in the FAME were integrated to give total peak area (ΣA_s).

$$\%Methyl\ esters\ \ content = R_f.\left(\frac{A_s}{A_{is}}\right).\left(\frac{V_{is}.C_{is}}{m_s}\right).(100) \qquad (3.16)$$

Where:

V_{is}: volume of the internal standard (1mL)

C_{is}: concentration of the internal standard solution (10mg/mL)

$m_{s:}$ mass of the sample (mg)

Figure 3.14 shows the chromatogram obtained for the GC analysis of FAME produced from RSO using isothermal temperature protocol at 210˚C. The first peak in the chromatogram is the collective peaks of solvent (heptane) and methanol. Six peaks corresponding to FAME from palmitic, stearic, oleic, linoleic, linolenic, and icosenoic were identified by standard FAME mixture and quantified using the C_{17} internal standard. Data from the GC analysis of the calibration mixtures in Table 3.11 were used to calculate the R_f of each methyl ester.

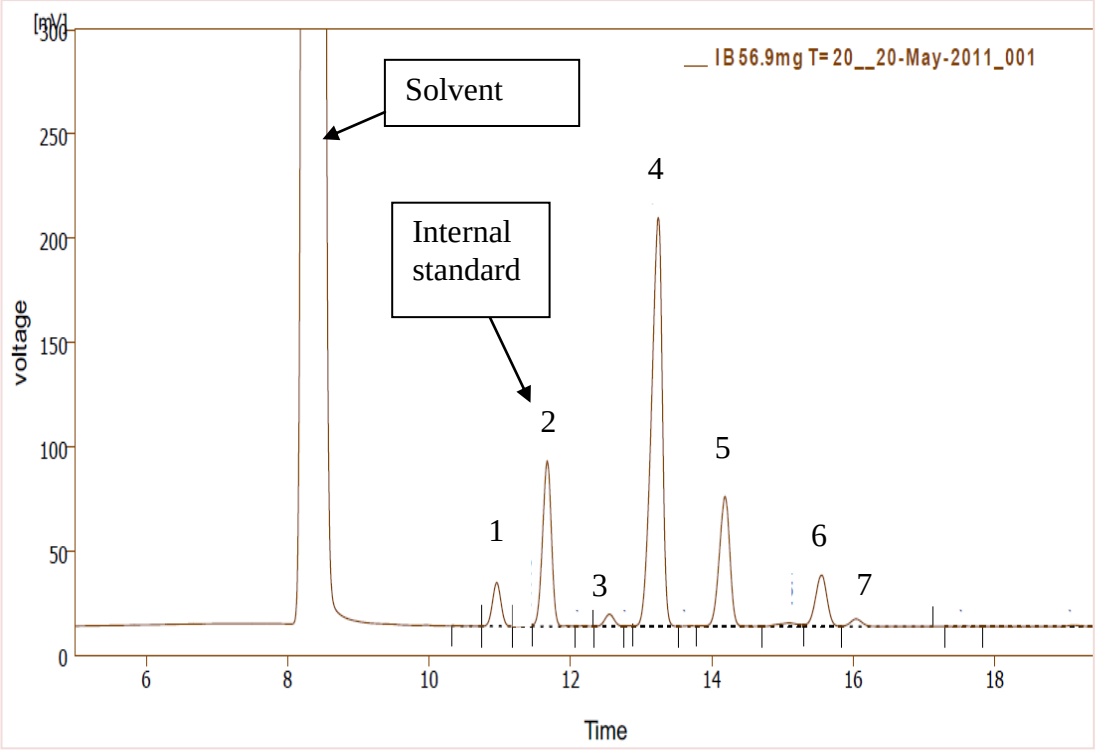

Figure 3.14: Chromatogram of fatty acid methyl esters from the RSO identified as: (1) palmitic, (3) stearic, (4) oleic, (5) linoleic, (6) linolenic, (7) icosenoic.

There was a linear relationship between peak area and mass ratios of the methyl esters and C_{17}, with correlation coefficient, $R^2 > 0.99$. Table 3.13 shows that the R_f of the methyl esters were approximately 1.10 for methyl hexanoate, 1.00 for methyl oleate, 1.01 for methyl octanoate, and 1.00 for methyl laurate. The calculated R_f values were consistent with Bannon *et al.* (1986). R_f from this study were slightly lower than reported by Singh *et al.* (2013) due to the use of higher molecular weight of methyl nanodecanoate ester (C_{19}) used as GC internal standard. Therefore, the assumption of unity for GC R_f is accurate in determination of FAME from fatty acids in the range of C_{12} - C_{20} chain length, using C_{17} internal standard. The propanoic acid methyl ester was quantified using methyl hexanoate as internal standard, whereas hexanoic acid methyl ester was quantified using methyl octanoate as internal standard. The choice of internal standard was such that the boiling points are different to ensure total separation, but not far apart to minimise the time required for components separation by GC.

Table 3.13: GC relative response factor for methyl esters

Methyl hexanoate	Methyl octanoate	Methyl laurate	Methyl oleate	References
1.10 $R^2 = 0.997$	1.01 $R^2 = 0.992$	1.00 $R^2 = 0.998$	1.00 $R^2 = 1.00$	This study
1.16	1.14	1.11	1.02	(Singh *et al.*, 2013)
-	-	-	0.996	(Bannon *et al.*, 1986)

Chapter 4 Results and Discussion

4.1 RTDs of the meso-OBRs

RTD profiles obtained from the experiments were fitted to the TIS models. The results are shown in Figure 4.1, for the three meso-OBRs (integral, wire wool and sharp-edged helix with a central rod designs) at a fixed residence time of 2.5min, approximately 4mL/min (Re_n = 17) and Re_o = 250 (2Hz frequency and 4mm amplitude).

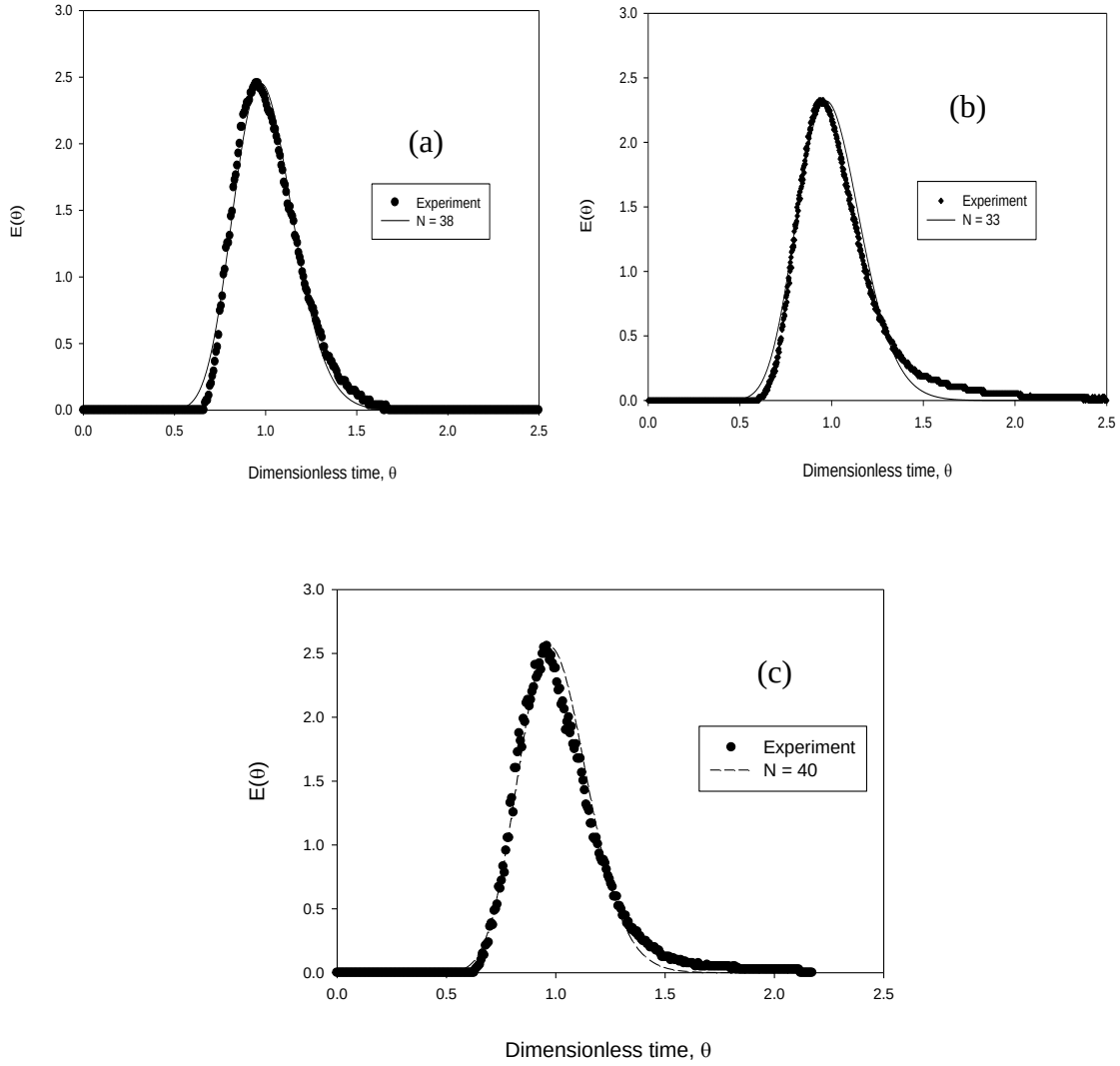

Figure 4.1: Experimental RTD profiles and TIS models at fixed residence time of 2.5min, Re_n ~ 17 (4.0mL/min) and oscillation at 2Hz frequency and 4mm amplitude (Re_o = 250), (a) integral baffles, (b) sharp-edged helix with a central rod, (c) wire wool

The RTD curves (Figure 4.1) fitted well with the TIS models in terms of height, shape and spread of the distribution. Due to the formation and dissipation of eddies in the meso-OBRs, relatively uniform radial mixing was obtained in these reactors. As a result, a high degree of plug flow was achieved at low net flow rates (Re_n ~17). For instance, N was above 30 for all the meso-OBRs (~340mm length) at the experimental conditions as shown in Figure 4.1. The values of N estimated for the integral baffles (Figure 4.1(a)) and wire wool packing (Figure 4.1(c)) meso-OBRs were slightly higher than that of the sharp-edged helix with a central rod (Figure 4.1(b)). This indicates that radial mixing may be more enhanced in the integral and wire wool meso-OBRs at the above flow conditions. The RTDs appears to be slightly tailed, suggesting small degree of axial dispersion in the flow.

The normalised variances calculated for the RTD profiles in Figure 4.1 were in the range 0.02 – 0.03. There was no significant difference between the average residence time of the KCl tracer and the hydraulic residence time for all the meso-OBRs. For instance, at the 2.5min hydraulic residence time which was used in the experiments, the mean residence times were 2.5±0.011min for integral baffles, 2.4±0.01min for sharp-edged helix with a central rod and 2.6±0.012min for the wire wool packing.

4.1.1 Effect of flow rates on the RTD of the meso-OBRs

Figure 4.2 shows the RTD profiles of the meso-OBRs at fixed residence times in the range of 2.5min – 60min for each meso-OBR, approximately net flow of 0.17 – 4.0mL/min (Re_n ~ 0.72 – 17). The RTD curves were narrower and more symmetrical at higher flow rates (shorter residence time), indicating that the degree of plug flow in the meso-OBRs increased with net flow rates at a fixed oscillation condition (Re_o = 250 and St=0.1). Consequently, N increased with the net flow rates for all the meso-OBR configurations as shown in Table 4.1. This was attributed to increase in axial dispersion of the KCl tracer at reduced net flows of the fluid into the reactor (longer residence time). Tracer diffusion had been reported as an important mechanism for mixing when an integral baffled meso-OBR was operated at low net flow rates (0.3 – 0.6mL/min), corresponding to Re_n ~1.25 – 2.5 (Phan *et al.*, 2011a).

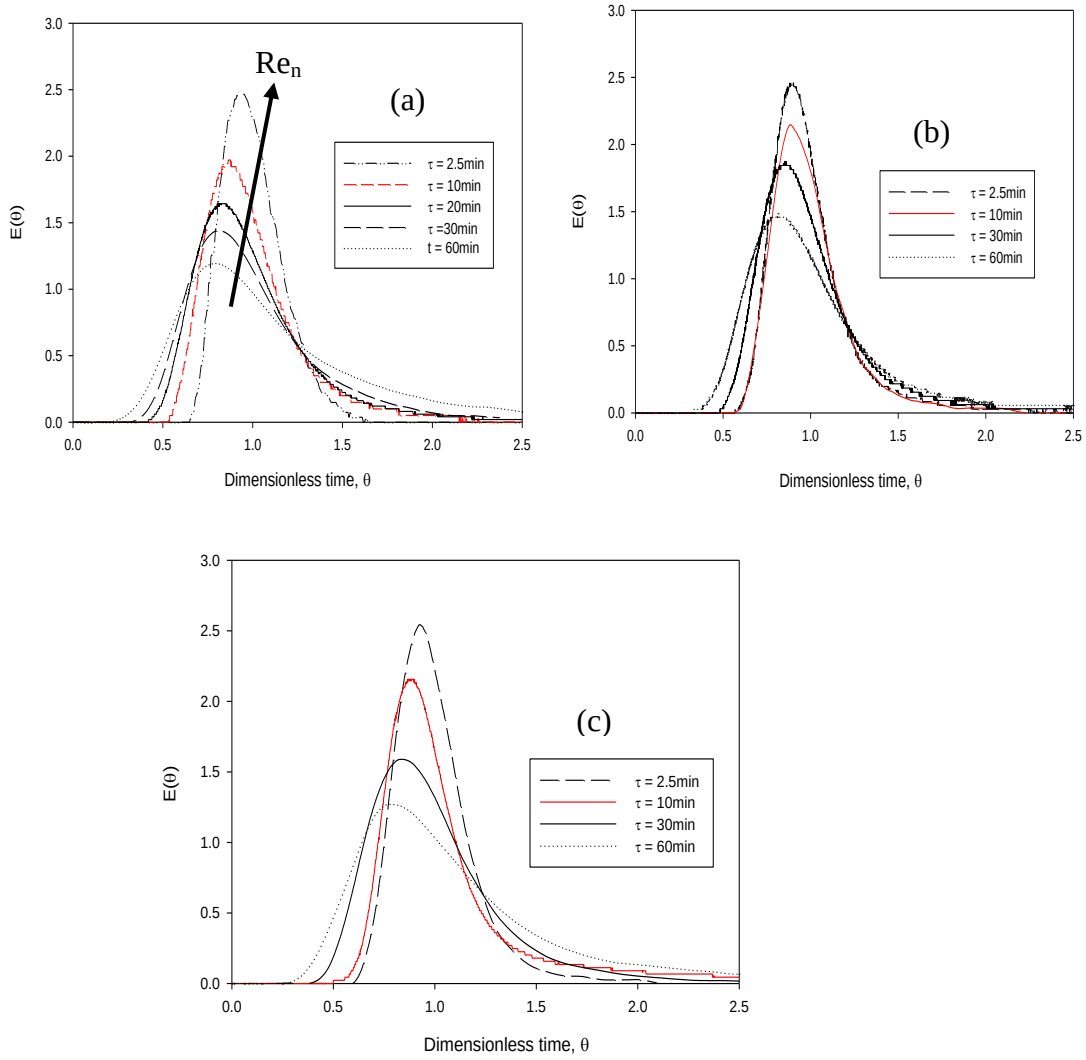

Figure 4.2: RTD profiles at oscillation conditions of 2Hz frequency and 4mm amplitude (Re_o = 250, St = 0.1) and fixed residence times of 2.5min – 60min for each meso-OBR, approximately net flow of 0.17mL/min – 4.0mL/min (Re_n ~ 0.72 – 17), (a) integral baffles, (b) sharp-edged helix with a central rod and (c) wire wool.

Table 4.1: Values of N for the meso-OBRs at various net flow rates

Residence time (min)	Net flow rates (mL/min)	Re_n	Integral baffles	Sharp-edged helix with a central rod	Wire wool packing	Velocity ratio, (ψ)[a]
2.5	4.0	17	38	37	40	15
10	0.5	4.25	23	28	30	59
30	0.33	1.40	12	17	18	178
60	0.17	0.72	10	13	13	347

[a] $\psi = Re_o/Re_n$

Table 4.1 clearly shows that N increased with net flow rates, i.e decrease in residence time. The maximum values of N were obtained at the shortest residence time of 2.5min (highest tested flow rates) for all the reactors. For instance, N = 38 for integral baffles, N = 33 for sharp-edged helix with a central rod and N = 40 for the wire wool packed reactor at τ = 2.5min (Re_n ~ 17). N decreased remarkably, from N ≥ 30 at 2.5min residence time to N ~ 10 at τ = 60min (Re_n ~ 0.72). The highest value of N was obtained at the lowest ψ for the three meso-OBRs because this represents the highest net flow rate (4.0mL/min). At lower net flow rates, substantial diffusion of the KCl tracer occurs which leads to increased axial mixing. As the residence time of the fluid increased (decreased net flow rates), there was a reduction in the degree of plug flow (N) of the meso-OBRs. Figure 4.2 also shows that right-tailing in the RTDs was more at lower fluid net flow rates. The flow patterns of the meso-OBRs tend towards that of a CSTR at lower fluid net flow due to the increased axial dispersion.

Table 4.2: Normalised variances for the meso-OBRs at various net flow rates

Net flow rates (Re_n)	Integral baffles	Sharp-edged helix with a central rod	Wire wool packing
17	0.03	0.03	0.02
4.25	0.07	0.06	0.04
1.40	0.12	0.11	0.11
0.72	0.14	0.13	0.13

As listed in Table 4.2, the normalised variances for the RTDs increased when decreasing net flow rates. This was due to increased tracer diffusion as the net flow rates of the fluid into the reactor decreases. However, N ≥ 10 for all the meso-OBRs: integrally, sharp-edged helix with a central rod, and wire wool packing. Therefore, these meso-OBRs can be operated in plug flow at 2.5min – 60min residence time, i.e approximately 0.17 – 4.0 mL/min (Re_n ~ 0.72 – 17) and Re_o of 250 (St = 0.1).

4.1.2 Effects of oscillation conditions on the RTDs of the meso-OBRs

Figure 4.3 shows the effect of oscillatory mixing intensity on the RTDs of the meso-OBRs at fixed residence time of 10min (Re_n ~ 4.25) and oscillation frequencies and amplitudes of 2Hz and 1mm (Re_o = 60, St = 0.4), 2Hz and 4mm (Re_o = 250, St = 0.1),

4.5Hz and 4mm (Re_o = 565, St = 0.1), and 4.5Hz and 8mm (Re_o = 1130, St = 0.05). The RTDs of the integral (Figure 4.3(a)) and sharp-edged helix with a central rod (Figure 4.3(b)) showed that there was an increase in N with the Re_o from 60 (St = 0.4) to 250 (St = 0.1). This indicates that at Re_o of 60, the vortex shedding was insufficient to fill the inter-baffles cavities in these reactors. Higher Re_o was required to ensure formation of eddies of appropriate length that would fill the cavities. However, an increase in Re_o above 250 led to a broadened and tailed RTDs for integral baffles (Figure 4.3(a)) and for sharp-edged helix with a central rod (Figure 4.3(b)). Broadening and tailing of the RTDs was particularly evident at higher amplitudes. For instance, the calculated values of N for the integral baffle design decreased from N = 23 at 4mm oscillation amplitude (Re_o = 250) to N = 5 at 8mm oscillation amplitude (Re_o = 1130). This broadly agrees with Reis *et al.* (2005) who observed that oscillation amplitude has more effect on axial dispersion, e.g. axisymmetry of the vortex rings in SPC meso-OBR was broken when Re_o increased from 12 (2.1Hz and 0.2mm) to 100 (1.1Hz and 3.8mm). Hence, the oscillation amplitude controls the length of the eddy propagation. If the eddy propagates too far, the tracer is moved into the next "tank" (baffle cavity), thereby increasing axial dispersion.

Figure 4.3(d) clearly showed that N for the integral and sharp-edged helix with a central rod reaches a maximum at a given optimal Re_o/Re_n ratio ($\psi \sim 60$), corresponding to Re_o ~250. The maximum values of N obtained were N = 23 for the integral baffle and N = 28 for the sharp-edged helix with a central rod. A further increase in Re_o above 250 resulted in a significant reduction in values of N. For the wire wool packing, $Re_o > 60$ did not improve the plug flow behaviour (Figure 4.3(c)), indicating that the reactor can be operated at even lower Re_o. Any increase in Re_o for the wire wool packing resulted in broadening and right-tailing of the RTD curves. The RTDs of the meso-OBRs were evidently more right-tailed at higher mixing intensities ($Re_o \geq 250$). That was an indication of chaotic mixing inside the reactors, leading to large axial dispersions and mixing of fluid elements of different age groups.

Interactions among Re_n, Re_o and N were evaluated in terms of velocity ratio ($\psi = Re_o/Re_n$) as shown in Figure 4.3(d). The ψ obtained from this study were considerably higher than reported for conventional (Stonestreet and Van Der Veeken, 1999) and central baffles meso-OBRs (Phan and Harvey, 2010). This study shows that the optimal ψ required to operate the meso-OBRs in plug flow at Re_n = 4.25 was $\psi \sim 60$ for the

integral baffles and sharp-edged helix with a central rod, and ψ ~ 11 for wire wool packed reactor. In conventional OBR, velocity ratio in the range of $2 \leq \psi \leq 4$ was optimal for plug flow operation at net flow conditions Re_n = 95 – 252 and St = 0.48 – 1.91 (Stonestreet and Van Der Veeken, 1999).

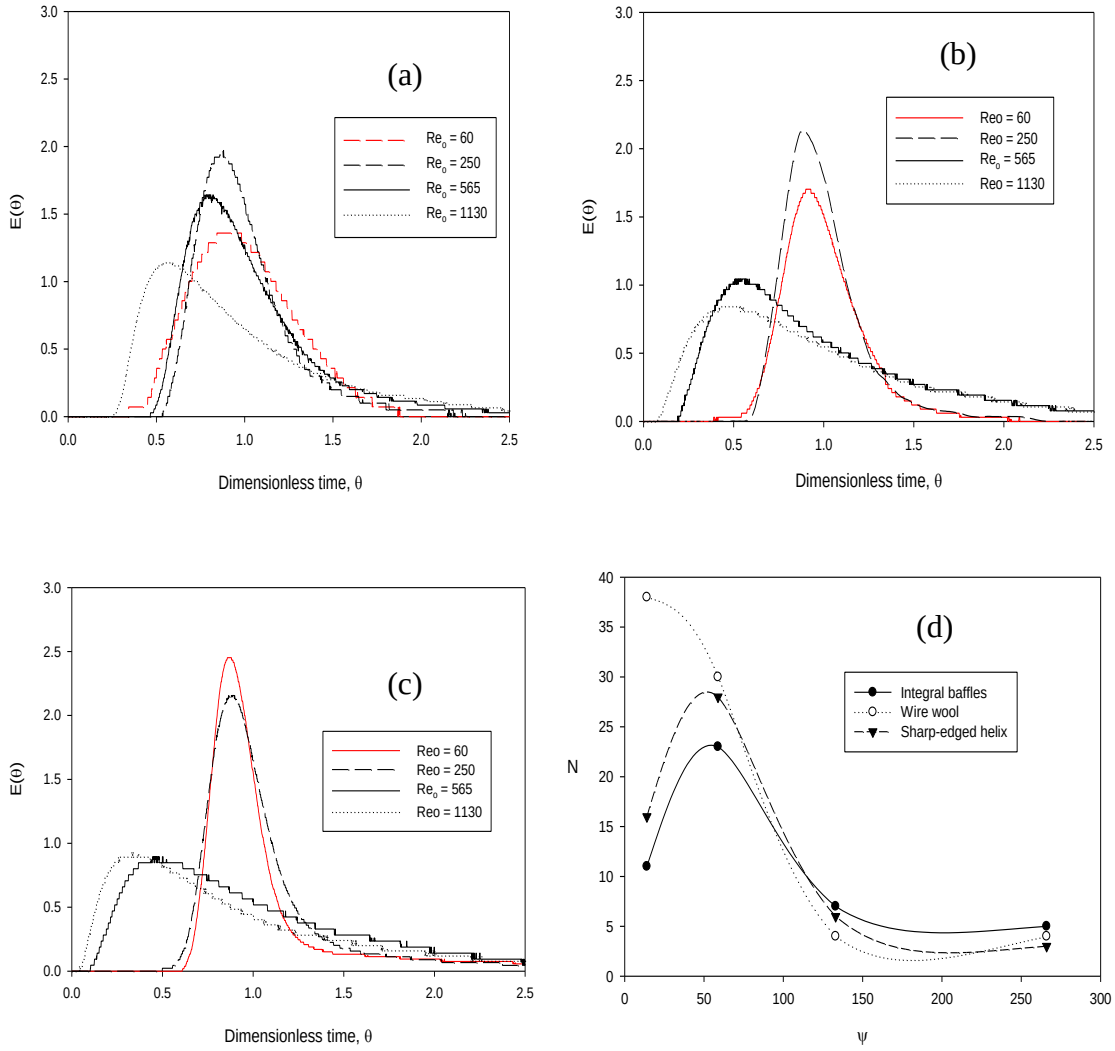

Figure 4.3: RTDs of the meso-OBRs at fixed residence time of 10min (Re_n ~ 4.25) and oscillation frequencies and amplitudes of 2Hz and 1mm (Re_o = 60, St = 0.4), 2Hz and 4mm (Re_o = 250, St = 0.1), 4.5Hz and 4mm (Re_o = 565, St = 0.1), and 4.5Hz and 8mm (Re_o = 1130, St = 0.05) for (a) integral, (b) sharp-edged helix with a central rod, (c) wire wool and (d) N versus ψ.

It was also reported that optimal plug flow performance at St = 0.4 – 0.8 was achieved in central baffles meso-OBR at ψ ~ 4 – 8 for Re_n = 17.1 – 34 (Phan and Harvey, 2010). The higher maximum ψ obtained in this study could be due to the use of low fluid net flow rates (Re_n = 4.25). This was supported by the work of Phan *et al.* (2011a), who observed that the highest degree of plug flow (N = 30 - 35) in an integral baffled meso-

OBR at low net flow rates (Re_n = 1.27) and $0.2 \leq St \leq 0.13$, was achieved at ψ in the range of $\psi \sim 39 - 40$. The studies at lower fluid flow rate suggest that near plug flow behaviour can be achieved at a various ψ range using low net flow rates. The net flow rates used in this study and in Phan *et al.* (2011a) were lower than $Re_n = 95 - 252$ reported by Stonestreet and Van Der Veeken (1999) and $Re_n = 17.1 - 34$ in by Phan and Harvey (2010). Flow energy of the fluid increases with the flow rate, such that less oscillatory mixing is required to achieve flow separation at higher net flow. For instance, fluid mixing can be achieved in static mixers at high fluid net flow even without oscillatory mixing.

In general, the RTD profiles of the meso-OBRs in Figure 4.3 indicate that these meso-OBRs can be operated in plug flow at $Re_o \sim 60$ and 4.25 Re_n. However, for optimal plug flow behaviour at the above net flow rate, $Re_o > 60$ will be required for the integral baffles and the sharp-edged helix with a central rod. For conventional OBRs, the onset of formation and cessation of eddies occurs at considerably more energetic mixing conditions, $Re_o \sim 100$ (Harvey *et al.*, 2003a). The Re_o required for fluid mixing is considerably lower for meso-OBRs. For instance, $Re_o \geq 50$ was required for effective fluid mixing in sharp-edged helical baffle with central rod at Ren of 7.2 (Phan and Harvey, 2011). It is clear that the onset of flow separation and eddy formation is strongly dependent on the baffle configuration and open cross-sectional area, which explains the flow behaviour of the integral baffles, wire wool packed reactor and sharp-edged helix with a central rod baffles in Figure 4.3. Integral baffles and sharp-edged helical baffles with a central rod have open cross-sectional areas of approximately 25% compared to the wire wool packed tube containing 22% wire wool by volume.

At the high oscillatory mixing conditions, Re_o = 565 (St = 0.1) and Re_o = 1130 (St = 0.05), broadened, tailed RTDs were observed (Figure 4.3). As a result, the normalised variance increased significantly from 0.17 to 0.32 for integral baffles, 0.25 to 0.39 for wire wool, and from 0.17 to 0.34 for sharp-edged helix with a central rod (Figure 4.4). At the mixing conditions using 8mm amplitude, the length of eddy propagation becomes considerably longer than the inter-baffles spacing/cavity (7.5mm for integral baffles and sharp-edged helix with a central rod and 3mm for the wire wool) leading to increased axial dispersion and more chaotic mixing inside the meso-OBRs. At the $Re_o \geq 565$, $N < 10$ was obtained for all the meso-OBRs, as shown in Figure 4.3(d). At these Re_o conditions, the TIS model does not give good fittings to the RTDs data due to the

large axial dispersions. Increase in oscillation mixing intensity, especially the oscillation amplitude, increased the eddy propagation length. For instance, as the amplitude of oscillatory mixing increased from 1mm (Re_o = 60) to 8mm (Re_o = 1130), the vortices generated travelled too far and interacted with adjacent baffles which resulted in increased axial dispersion. The meso-OBRs cannot be operated in plug flow at the 8mm oscillation and $Re_n \leq 4.25$; however, this condition could provide effective mixing when the meso-OBRs are operated in batch or as CSTR.

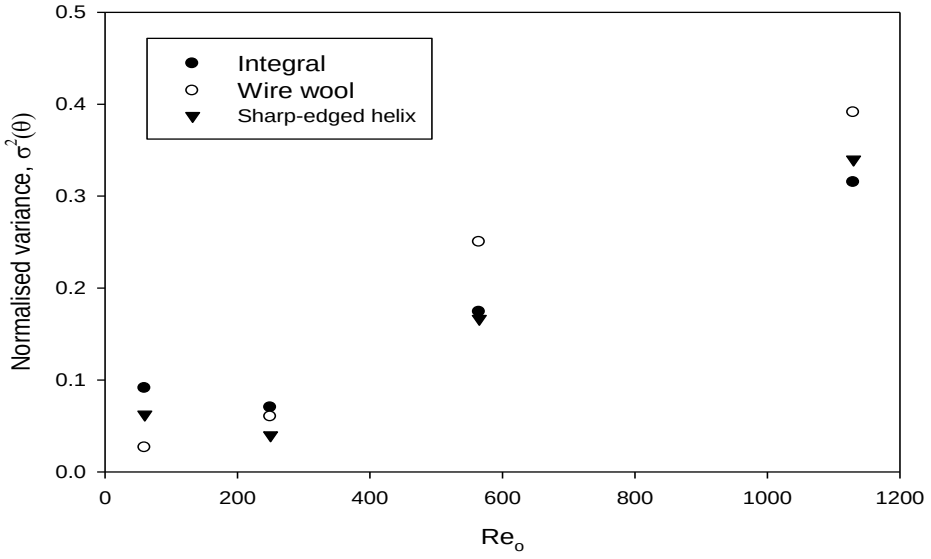

Figure 4.4: Normalised variance of the meso-OBRs at fixed residence time of 10min (Re_n ~ 4.25) and various oscillation mixing intensities at oscillation frequencies and amplitudes of 2Hz and 1mm (Re_o = 60, St = 0.4), 2Hz and 4mm (Re_o = 250, St = 0.1), 4.5Hz and 4mm (Re_o = 565, St = 0.1), and 4.5Hz and 8mm (Re_o = 1130, St = 0.05)

4.1.3 Summary

Three designs of meso- OBRs, namely integral baffles, wire wool and sharp-edged helical baffles with a central rod were characterised in terms of their RTDs. The investigation was carried out across a range of operating conditions: residence times of 2.5min – 60min, corresponding to net flow rates of 0.17mL/min – 4.0mL/min (Re_n ~ 0.72 – 17) and oscillation conditions of Re_o = 60 – 1130 (St = 0.05 – 0.4). This study investigated the RTDs of the meso-OBRs at much lower Re_n than reported in the literature. Wider Re_n and Re_o conditions were chosen to enable the evaluation of the steady state performance of the meso-OBRs in the RSO transesterification process and FFA esterification. A high degree of plug flow was obtained at ψ ~ 60 for both integral

and sharp-edged helix with a central rod baffles and ψ ~11 for the wire wool packed reactor.

4.2 Fatty acid profile and molar masses of the glycerides and FAME

Table 4.3 shows the fatty acids profile of the RSO. The methyl esters peaks obtained in the chromatogram shown in Figure 3.14 were used to quantify the fatty acids composition. Six major fatty acid methyl esters: palmitic, stearic, oleic, linoleic, linolenic, and icosenoic were quantified based on the known amount of C_{17} internal standard.

Table 4.3: Fatty acid profile of the RSO

Fatty acid[a]	Molecular formula	Mw. (g/mol)	% fatty acid	
			This study	(Niczke *et al.*, 2007)
Palmitic (C16:0)	$C_{15}H_{31}COOH$	256.4	5.3	4.3
Stearic (C18:0)	$C_{17}H_{35}COOH$	284.5	1.7	-
Oleic (C18:1)	$C_{17}H_{33}COOH$	282.5	63.2	64.7
Linoleic (C18:2)	$C_{17}H_{31}COOH$	280.5	19.8	16.5
Linolenic (C18:3)	$C_{17}H_{29}COOH$	278.4	8.6	9.4
Icosenoic (C20:1)	$C_{19}H_{37}COOH$	310.5	1.4	-

[a]saturated: 7.0%; monosaturated: 64.6%; and polysaturated: 28.4%

Table 4.4: Average molecular mass of glyceride and FAME from RSO

Chemical species	Average molecular mass (g/mol)
Triglyceride	881.4
Diglyceride	616.3
Monoglyceride	355.1
FAME	295.1

As shown in Table 4.4, RSO consists mainly of oleic acid, about 63wt% of total fatty acids. The fatty acid profile of the RSO used in this study was similar to that reported (Santos *et al.*, 2005). Average molecular mass of tri-, di-, mono-glycerides and FAME derived from RSO were 881.4g.mol^{-1} for triglyceride, 616.3g.mol^{-1} for diglyceride,

355.1g.mol^{-1} for monoglyceride and 295.1g.mol^{-1} for FAME (Table 4.4). These values agree with literature (Niczke *et al.*, 2007; Uosukainen *et al.*, 1998). For instance, an average molecular mass of 880g.mol^{-1} for triglyceride in RSO was reported by Uosukainen *et al.* (1998), whereas an average molecular mass of 296g.mol^{-1} was obtained for FAME derived from RSO (Niczke *et al.*, 2007).

4.3 Steady state performance of the meso-OBRs in continuous homogeneous transesterification

The effects of oscillation conditions on the steady state performances of the three meso-OBRs for continuous RSO transesterification at 60˚C, 6:1 methanol to RSO molar ratio and 1.5wt% KOH (based on RSO) are discussed in this section. The reactor was operated continuously for 60min running time for each mixing condition at a residence time (reaction time) of 10min. 1mL samples was taken at 5min intervals, starting from 10min (1τ), to study the effects of oscillation conditions on the induction time (time the FAME contents reached a steady state) and the consistency of the FAME contents. These two parameters are crucial and must be minimized to reduce the amount of waste generated during the start-up time.

4.3.1 Integral baffled meso-OBR

As shown in Figure 4.5, the FAME content was 10–30% at 10 min running time (1τ) at Re_o of 36, 71, and 107 and then increased to 70–80% at 2τ. However, no steady states were established as the FAME contents fluctuated in a range of 70–90 %. This was an indication of poor mixing inside the reactor. An average FAME contents were 74.8±13.2% at Re_o = 36, 81.7±5.6% at Re_o = 71 and 74.9±6.5% at Re_o = 107.

At higher oscillatory mixing, e.g. Re_o of 160, the FAME content was about 78% at 10min running time (t = 1τ), and quickly reached its steady state at t = 1.5τ with an average FAME content of 86.7±1.3%, indicating that Re_o >107 is required for biodiesel production in the integral baffled reactor at a net flow Re_n of 1.74. The findings in Figure 4.5 agreed with the trend in RTD profiles of the integral baffled meso-OBR discussed in section 4.1.2. A high degree of plug flow behaviour of the reactor was at Re_o = 250 (ψ ~ 60 and Re_n of 4.25). The integral baffles meso-OBR achieved the best steady state (highest FAME yield and lowest variance) at Re_o = 160 (ψ = 92 and Re_n =

1.74). At the Re_n = 1.74 used in the reaction, ψ above 60 was expected in line with the trend discussed in section 4.1.2. At Re_o = 36 – 107, the vortices produced were probably too small to fill the inter-baffles cavities in the integral baffled meso-OBR, resulting in insufficient mixing.

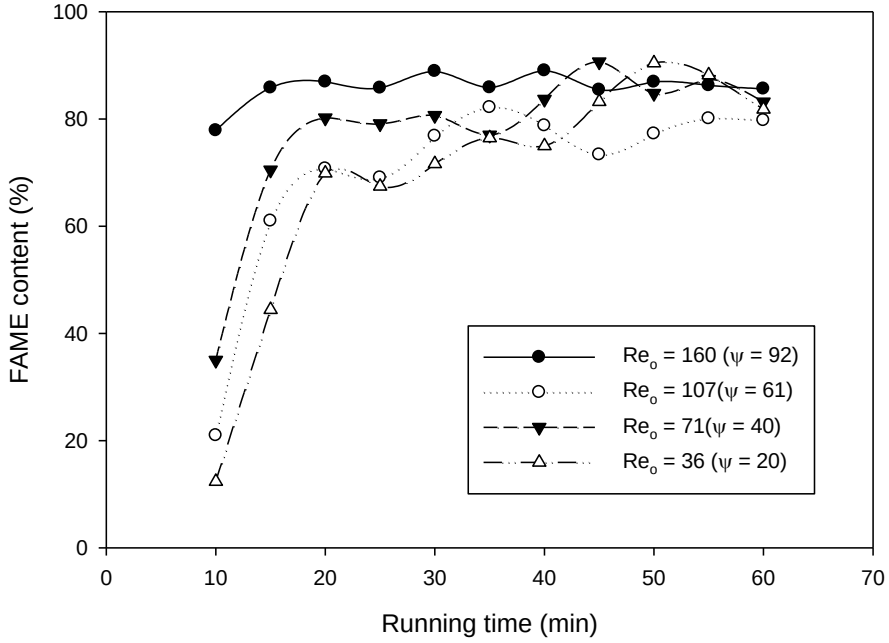

Figure 4.5: Effect of oscillation conditions on FAME content obtained from transesterification at 60˚C, 6:1 methanol to RSO molar ratio, flow rate Re_n = 1.74 and 1.5wt% KOH in the integral baffled meso-OBR

4.3.2 Helical baffled meso-OBR with a central rod

The FAME concentrations obtained using the helical baffled meso-OBR in Figure 4.6 showed that a steady state was achieved at approximately 25min running time ($t \sim 2.5\tau$) at Re_o = 160 (FAME content of 79.6±1.4%) and at $t \sim 3\tau$ for Re_o = 71 and 107 (average FAME contents of 74.1±1.8% and 74.2±1.0% and respectively). Significant instability in the FAME content was observed at Re_o = 36, as the FAME content varied from 68.4% to 80.7%. This was no doubt due to poor mixing as channelling and globular flow of methanol was observed at Re_o = 36 (see Figure 4.9), leading to a low degree of plug flow. Optimal plug flow behaviour of the helical baffled reactor was observed at a velocity ratio of $\psi \sim 60$ at a Re_n of 4.25. Similar to the integral baffled meso-OBR, $\psi >$ 60 will be required for optimal performance of the helical baffles at Re_n of 1.74.

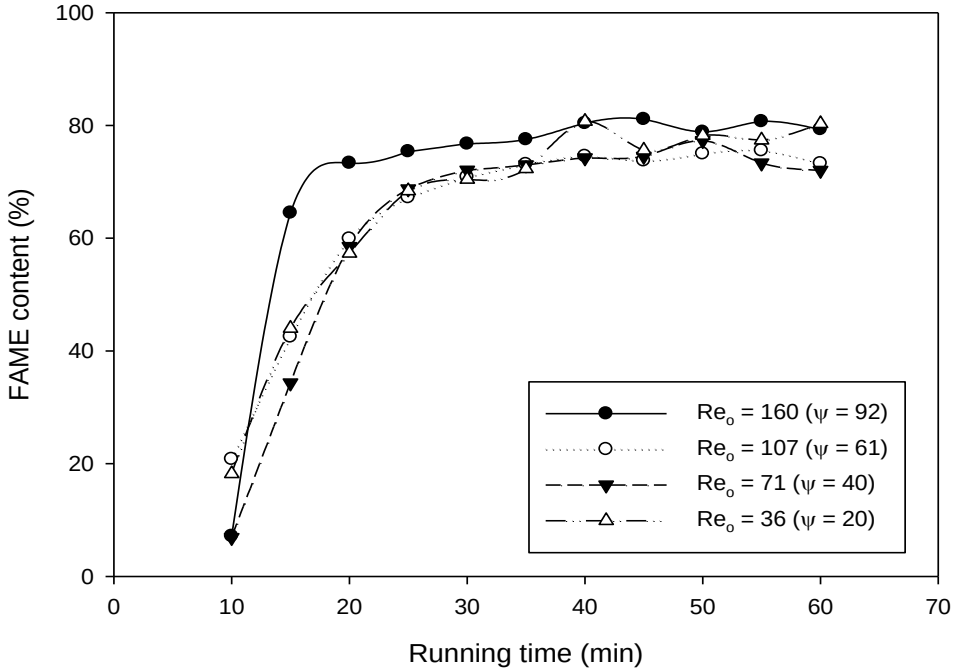

Figure 4.6: Effect of oscillation conditions on FAME content from transesterification at 60˚C, 6:1 methanol to RSO molar ratio, flow rate Re_n = 1.74 and 1.5wt% KOH using the helical baffled meso-OBR

The average FAME content was lower for the helical baffles than the integral baffles at Re_o = 160. This could be explained by the better radial mixing in integral baffles meso-OBR. For instance, it was observed that the values of N calculated from the RTD data of the integral baffles (N = 38) was slightly higher that of sharp-edged helix with a central rod (N = 33) at Re_o = 250 and Re_n = 17.

4.3.3 Wire wool packed reactor

The FAME contents obtained from transesterification using the wire wool packed reactor at Re_o = 36 – 160 are shown in Figure 4.7. At 10min running time (t = 1τ), the FAME content was approximately 10–30% for Re_o = 36, 71, and 106 and 45% for Re_o = 160. The wire wool packed reactor reached its steady state at 20min running time (t = 2τ), with the FAME content of 77.21±1.8% at Re_o = 107, 77.0±2.7% at Re_o=160, 75.7±3.6% at Re_o = 71 and 77.1±2.9% at Re_o = 36.

The results in Figure 4.7 indicated that Re_o had little effect on FAME contents using the wire wool packed reactor, as steady state was established at all tested Re_o. This indicates that the length of eddies produced at Re_o = 36 – 160 (ψ = 20 – 92) was sufficient to

encompass the ~3mm voids in the wire wool packed tube. The cavities (3mm) in the wire wool packed tube were considerably smaller than the baffle spacing of about 7.5mm for the integral baffles and 7.5mm helical pitch for the sharp-edged helix with a central rod. The trend in FAME contents in Figure 4.7 was supported by the RTD studies of wire wool packed tube (section 4.1.2), where high degree of plug flow was achieved at $Re_o < 60$ (ψ ~11).

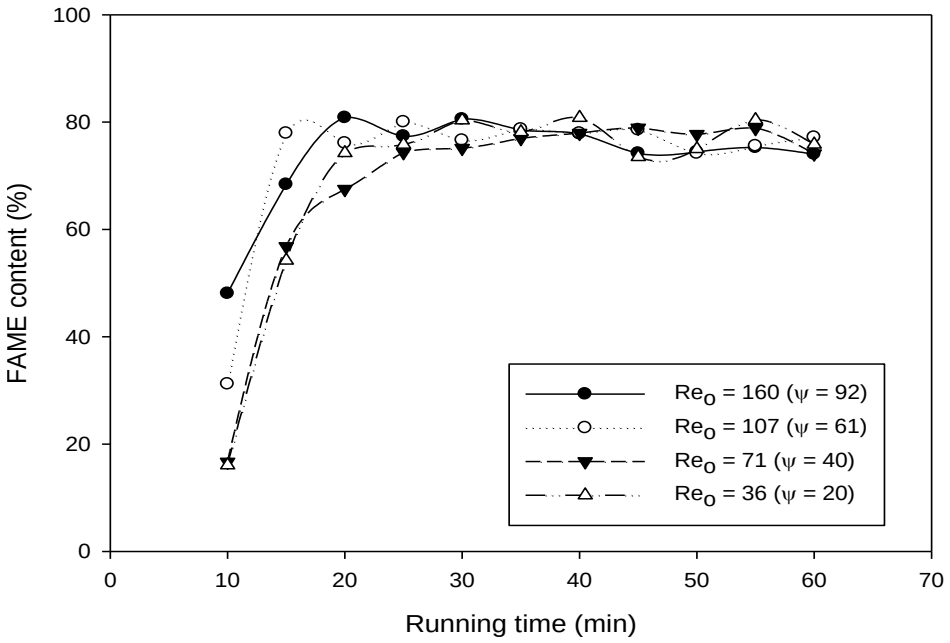

Figure 4.7: Effect of oscillation conditions on FAME content from transesterification at 60˚C, 6:1 methanol to RSO molar ratio, flow rate Re_n = 1.74 and 1.5wt% KOH using the wire wool packed reactor

In general, at Re_o = 160, the integral baffled meso-OBR produced steady state in FAME content in the shortest time (t = 1.5τ) compared to wire wool (2τ) and sharp-edged helical baffles (2.5τ). Furthermore, the highest FAME content (86.7±1.3%) was also achieved in the integral baffles compared to that obtained in the helical baffled meso-OBR (79.6±1.4%) and in the wire wool packed reactor (77.0±2.7%) as shown in Figure 4.8. The integral baffles meso-OBR was more effective for the homogeneous RSO transesterification with methanol. Based on the standard error for the FAME quantification which was ±1.3%, the errors in the FAME yields for the integral baffles and sharp-edged helix with a central rod were within the measurement error limit. However, higher error margin was calculated for the wire wool packing, which could be due to bypassing inside the reactor. The wire wool packed reactor achieved better steady states (less variance in FAME yield) at lower Re_o (Re_o = 36 - 107), but achieved ~9% lower FAME yield than the other two reactors.

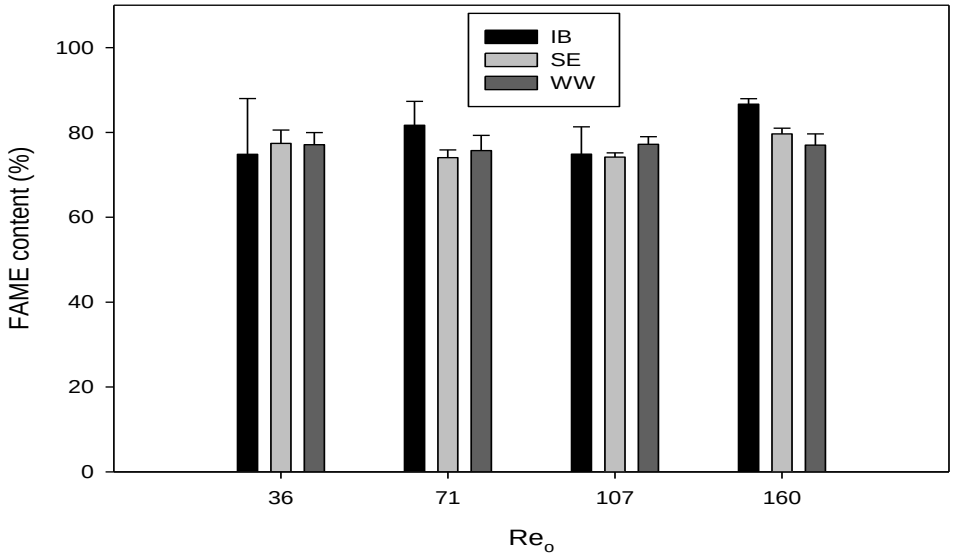

Figure 4.8: Average FAME content achieved by the meso-OBRs for continuous homogeneous transesterification at 60˚C, 6:1 methanol to RSO molar ratio, flow rate Re_n = 1.74 and 1.5wt% KOH: (IB) integral baffles, (SE) sharp-edged helical baffles with a central rod , (WW) wire wool packed tube

The three meso-OBRs screened in this study (integral baffles, sharp-edged helix with a central rod and wire wool packed reactor) had much shorter induction times than a CSTR, which required at least five volume replacements (5τ) to achieve a steady state for operations at 60min residence time (Darnoko and Cheryan, 2000a). The high variance in the FAME content at Re_o < 160 for the integral baffled meso-OBR was due to insufficient mixing, causing stratification of the glycerol phase and globular flow behaviour as shown in Figure 4.9.

Glycerol separation was particularly pronounced in the wire wool packed reactor at all tested mixing conditions. Because of the large surface area and rougher surface of the wire wool, glycerol was separated from the main stream and stuck onto the surface of the wire wool packing. This was responsible for the lower FAME content even when the wire wool baffled reactor was operated at Re_o = 160. Based on the superior performance of the integral baffles over the other meso-OBRs, the integral baffled meso-OBR was used for further investigation of alkali-catalysed RSO transesterification at the mixing condition, Re_o = 160 (4.5Hz frequency and 8mm amplitude).

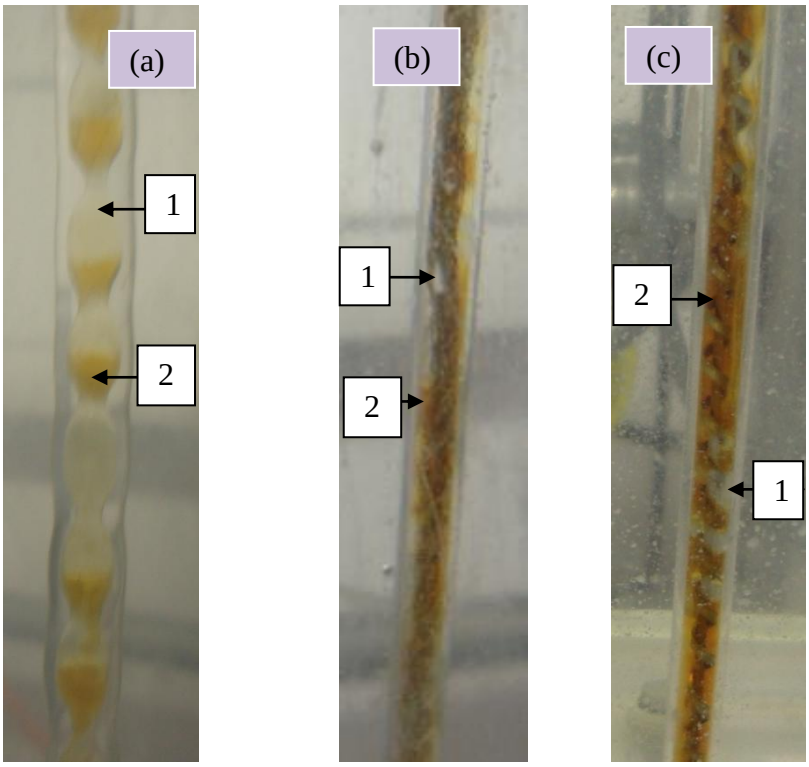

Figure 4.9: Photos showing (1) channelling/globular flow of methanol and (2) glycerol separation in continuous transesterification of RSO using the meso-OBRs at 60˚C and Re_o = 36 (a) integral baffles, (b) wire wool and, (c) helical baffles

4.3.4 Effect of residence time, catalyst type and concentration on FAME yield

FAME contents were obtained at residence times of 2.5 - 20min for RSO transesterification in the integral baffled meso-OBR at 6:1 methanol to RSO molar ratio, 60˚C, Re_o = 160, KOH (1wt% and 1.5wt%), NaOH (0.75wt% and 1.0wt%) and $NaOCH_3$ (1.5wt% and 1.0wt%) are shown in Figure 4.10. The FAME content was greatest at 5 min residence time (reaction time, τ) for 1.5wt% KOH, 10min residence time for 1.5wt% $NaOCH_3$ and 15min residence time for 1.0wt% NaOH. The FAME content decreased significantly with a further increase in residence time, i.e., from 96.2% at 5min to 76.6% at 15min for 1.5wt% KOH, 96.0% at 15min to 83.2% at 20min for 1.0wt% NaOH. For the $NaOCH_3$ catalyst, increasing the residence time from 5 to 10 min increased the FAME content slightly from 93.7% to the 95.6%. A further increase in residence times above 10 min caused about 6% reduction in the FAME content. It was also observed that the reaction mixture took longer to separate into two phases at residence times above 5 min for the 1.5wt% KOH and residence time above 20min for the 1.0wt% NaOH. The upper layer (FAME layer) obtained at long residence times was also cloudy, suggesting emulsification due to soap formation. This indicate that the

optimal residence times for the continuous transesterification at the above conditions was 2.5 - 5min for 1.5wt% KOH, 5 – 10min for 1.5wt% $NaOCH_3$ and 10 – 15 min for 1.0wt% NaOH.

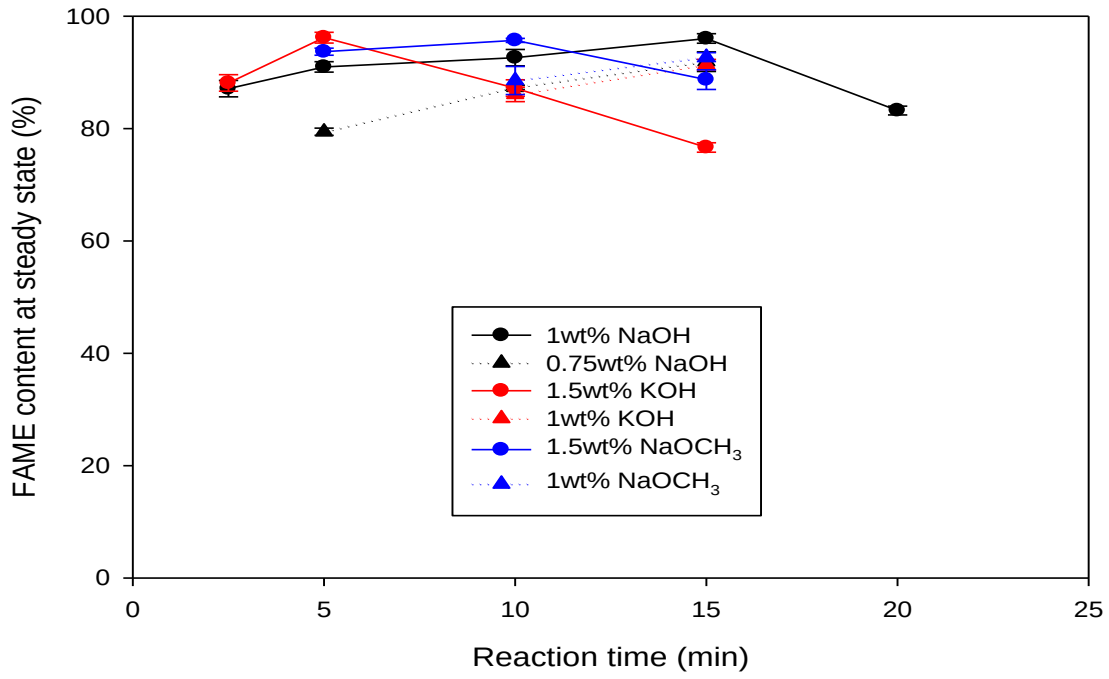

Figure 4.10: Effects of catalyst concentrations and residence times on FAME content in continuous transesterification of RSO at methanol 6:1 molar ratio, 60˚C and Re_o = 160 using the integral baffled meso-OBR

Optimal residence time of 60min was reported for transesterification of palm oil in a stirred-tank reactor operating at 6:1 methanol to oil molar ratio, temperature of 60˚C, and 1.0wt% of KOH (Darnoko and Cheryan, 2000a). The authors observed that the FAME content decreased from 85% to 78% when increasing the residence time from 60 min to 70 min. This phenomenon was explained as due to reverse reactions of FAME with glycerol to form glycerides, although the contents of free glycerol and monoglycerides were identical at both residence times. A more plausible mechanism for the reduction in FAME content with residence time is the saponification of the FAME product by base catalysts, as shown in equations (4.1) - (4.3). As indicated in equation (4.1), the equilibrium reaction is inevitable whether a methoxide or hydroxide catalyst is used, since a trace of water in the reagents (e.g. methanol and RSO) is enough to sustain the hydroxide/methoxide equilibrium.

$$CH_3OH + OH^- \leftrightarrow CH_3O^- + H_2O \quad (4.1)$$

$$TG + 3CH_3OH \leftrightarrow 3FAME + GL \quad (4.2)$$

$$FAME + OH^- \rightarrow Soap + CH_3OH \quad (4.3)$$

(Soap refers to the alkali-metal salt of the fatty acids)

An equilibrium concentration of 99.2 mol% ethoxide and 0.8mol% NaOH was reported for 0.1M NaOH that was prepared in anhydrous ethanol (Caldin and Long, 1954). But, when ethanol containing 1wt% water was used, the mole fraction of NaOH in the solution increased to 4.1mol%. The study indicated that some metal hydroxides may exist in alcohol/alkali catalyst solution used in homogeneous transesterification even when anhydrous alcohol was used. But, the concentration of alkoxide in such a solution is substantially higher than that of a metal hydroxide when anhydrous alcohols are used. Due to the existence of equilibrium OH^- and CH_3O^- in alcohol/alkali solution, transesterification and saponification reactions occur simultaneously. However, the rates of transesterification was much higher (~1500 times) than that of saponification due to the high concentration of alkoxide (Glass, 1971).

Initially, the rate of saponification of FAME (as in equation (4.3)) was negligible due to the low FAME concentration, but increased as the concentration of FAME increased. Experiments at low catalyst concentrations (0.75wt% for NaOH and 1.0wt% for KOH and $NaOCH_3$) demonstrated that FAME concentrations increased monotonically with residence times up to 10–15 min. In order to explain the experimental findings fully, modelling, taking into account the side reactions occurring in base-catalysed transesterification was developed and validated using experimental data. The modelling results were discussed in section 4.5.

4.3.5 Summary

Three oscillatory flow meso-OBRs (integral baffles, wire wool packing, and sharp-edged helical baffles with a central rod) were used for continuous alkali-catalysed homogeneous transesterification of RSO at a methanol: rapeseed oil molar ratio of 6:1, residence time of 10 min, and temperature of 60˚C, $Re_n < 2$ over a range of mixing conditions ($36 \leq Re_o \leq 160$). Steady states were achieved in all three designs in a short time, between 1.5 and 2.5 residence times. This allows rapid screening of process

conditions for two-phase liquid-liquid reactions, reducing significantly waste generated. This study demonstrated that biodiesel can be produced at an industrially acceptable level of conversion (> 96%) in ~ 5 min residence time, requiring a combination of high catalyst concentration and good mixing. The reaction time with the meso-OBRs is much lower than in commercial biodiesel processes (> 60min). Based on residence time reduction alone, the reactor could be replaced by a reactor of 1/24th the volume. In practice, the size reduction would be greater as in stirred tank reactors a substantial vapour space must be maintained. The results also demonstrate that FAME saponification occurs. This causes the FAME content to peak at a certain reaction time. This appears to only be an important feature at higher catalyst concentrations. To realise these high FAME concentrations at such short residence times, a reactor with good control of residence time, followed immediately by a catalyst quenching step would be required.

4.4 Saponification reactions in homogeneous alkali-catalysed transesterification

This section discusses investigations of the saponification side reactions in alkali-catalysed homogeneous transesterification of RSO using KOH as catalyst. The experiments were carried out in a 100mL jacketed batch reactor equipped with a magnetic stirrer operated at 600rpm.

4.4.1 Saponification of FAME and RSO in methanol-KOH solutions

FAME saponification was observed in the 0.5M methanol-KOH at all tested temperatures (40˚C to 60˚C) as in equation (4.3) (section 4.3.4). The rates of saponification of RSO and FAME increased with temperature as shown in Figure 4.11. The conversions of FAME to soap were 1.1 – 1.4 times higher than that of RSO. For instance, the conversions were 18%, 35% and 53% at 40˚C, 50˚C and 60˚C for RSO (Figure 4.11(a)), and 25%, 41% and 59% for FAME (Figure 4.11(c)) after 60min reaction time. The analysis of the reaction mixtures collected during the RSO saponification in 0.5M methanol-KOH at 60˚C (Figure 4.11(b)) indicated that the reaction proceeded via FAME formation.

There was a rapid conversion of RSO to FAME, which was then gradually saponified. The decrease in total alkali concentration obtained in the titration of samples from the

RSO saponification experiment was probably due to FAME saponification. Reactions of FAME with KOH to form soap caused a reduction in the KOH concentration. At a methanol-to-RSO molar ratio of 300:1, RSO transesterification was faster than saponification since the concentration of methoxide is about 110 times higher than that of KOH in the equilibrium (99.1mol % of the KOH existed as methoxide ions in the methanol-KOH solution).

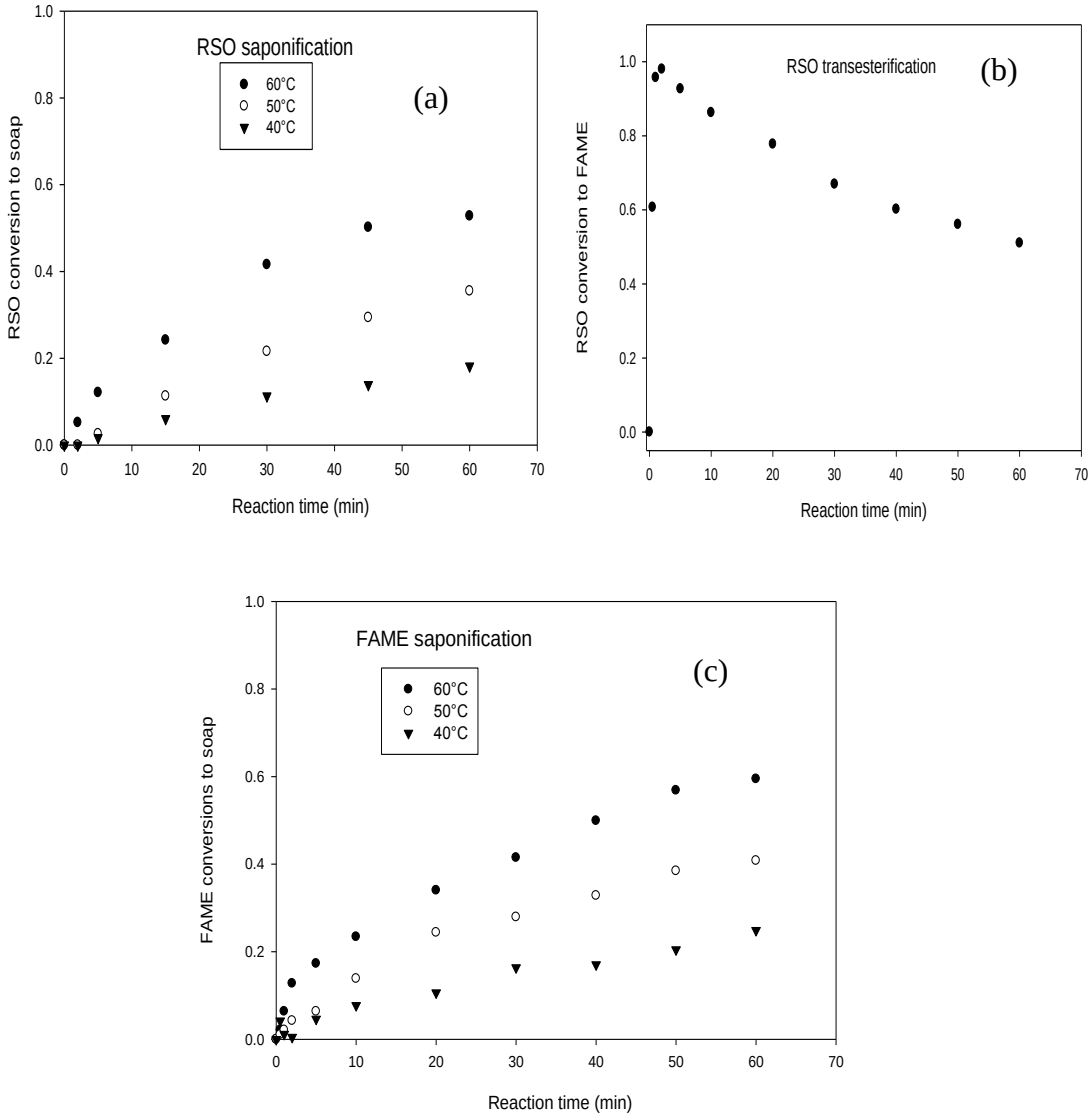

Figure 4.11: RSO and FAME saponification at mixing intensity of 600rpm over a temperature range of 40 – 60˚C: (a) and (b) 300:1 methanol to RSO molar ratio, 60˚C and 35wt% KOH and (c) 100:1 methanol to FAME molar ratio and 35wt% KOH

FAME saponification in methanol-KOH led to a reduction in the FAME content in Figure 4.11(b) and Figure 4.11(c), which was consistent with previous work discussed in section 4.3.4, of which there existed a maximum in the FAME yield versus reaction

time for alkali-catalysed transesterification. As shown in Figure 4.11(b), the maximum FAME content was obtained at 2min rather than 5min in the integral baffled meso-OBR for RSO transesterification at 6:1 molar ratio and 1.5wt% KOH, due to a higher catalyst concentration (35wt% KOH based on RSO) and methanol molar ratio (300:1) used.

This investigation provided more insight into the competitive reactions occurring in alkali-catalysed transesterification processes, and explained the experimental results observed in Figure 4.10 and in literature (Phan et al., 2012; Keera et al., 2011; Darnoko and Cheryan, 2000a). To prevent the unwanted competitive saponification reactions, the reaction must be quenched immediately as soon as the maximum FAME yield was achieved. This has not been reported in literature, despite the substantial amount of work conducted on base-catalysed transesterification of triglycerides.

4.4.2. Kinetics of the RSO and FAME saponification

Saponification of RSO and FAME in the 0.5M methanol-KOH solution was investigated in detail to provide a better understanding of the effect of these reactions on homogenous base-catalysed transesterification. The rate of saponification reactions were analysed by assuming a second-order reaction mechanism in which RSO and FAME were the limiting reactants as described in equation (4.4). The apparent rate constants (k') at various temperatures for the saponification reactions and the actual rate constants (k) were obtained from experimental data using equation (4.5), and listed in Table 4.5.

$$-\frac{d[RSO\#]}{dt} = k\beta[RSO\#]_0^2\,(1-X)(\Phi - nX) \tag{4.4}$$

$$\frac{1}{(\Phi-n)[RSO\#]_0}.\ ln\left[\frac{(\Phi-nX)}{\Phi(1-X)}\right] = k\beta t = k't \tag{4.5}$$

Where:

k': apparent saponification rate constant (L.mol^{-1}.min^{-1})

k: actual saponification rate constant (L.mol^{-1}.min^{-1})

[RSO#]: concentration of the RSO or FAME (mol/L)

$[RSO\#]_o$: initial concentration of the RSO or FAME (mol/L)

X: conversion of the RSO or FAME to soap.

Φ: ratio of the original concentrations of methanol-KOH solution to RSO or FAME

n: moles of KOH required for saponification of 1 mole of RSO or FAME

β: mole fraction of unreacted KOH in the KOH-methanol solution

Table 4.5: Rate constants for the RSO and FAME saponification

Temperature (˚C)	$k' * 10^{-3}$ (L.mol^{-1}.min^{-1})		k (L.mol^{-1}.min^{-1})	
	RSO	FAME	RSO	FAME
40	7.9	9.9	1.15	1.44
50	18.9	19.5	2.74	2.92
60	29.7	31.6	5.62	5.93
Activation energy (kJ.mol^{-1})	-	-	69.1	61.2

Table 4.6: Kinetic parameters for some saponification reactions

Substance and the saponification media	k (L.mol^{-1}.min^{-1})		Ea (kJ.mol^{-1})	References
	40˚C	50˚C		
Ethyl acetate and 0.05M NaOH in aqueous ethanol	3.88	8.07	61.5	(Smith and Levenson, 1939)[a]
Ethyl propanoate and 0.05M NaOH in aqueous ethanol	1.98	4.10	61.5	(Smith and Levenson, 1939) [a]
Ethyl laurate and 0.05M NaOH in aqueous ethanol	1.57 @ 45˚C	3.17 @ 55˚C	63.2	(Levenson and Smith, 1940) [a]
RSO and 0.5M methanol-KOH	1.27	2.74	69.1	This study
FAME and 0.5M methanol-KOH	1.44	2.92	61.2	This study

[a]Rate constants were calculated from the data reported by the authors

As shown in Table 4.5, saponification rate constants for the RSO and FAME increased with temperature. The rate constants increased from 1.15 L.mol^{-1}.min^{-1} to 5.62 L.mol^{-1}.min^{-1} for RSO and from 1.44.L.mol^{-1}.min^{-1} to 5.93 L.mol^{-1}.min^{-1} for FAME when the reaction temperatures increased from 40°C to 60˚C. In this temperature range the

FAME saponification rate constant ranged from 5 to 20% higher than that for RSO, probably due to larger size of the RSO molecule.

The activation energy for FAME saponification in this study was 61.2 kJ.mol^{-1}. This was similar to that for saponification of short chain carboxylic acid ethyl esters (Levenson and Smith, 1940; Smith and Levenson, 1939) as shown in Table 4.6. The actual rate constants for FAME saponification at 40˚C and 50˚C were similar to those for the ethyl laurate saponification at 45˚C and 55˚C. The similarity in the activation energies suggests that saponification occurs by the same mechanism regardless of the chain length of ester, as would be expected. The activation energy for the RSO saponification (69.1kJ.mol^{-1}) was close to that for the fatty acid alky esters, indicating that the RSO was saponified by the same mechanism as fatty acid alky esters.

4.4.3. Effect of water on FAME saponification

The effect of water on the saponification of FAME is shown in Figure 4.12 at 60˚C using 0.5M methanol-KOH solution containing 0 – 12.5 vol% water. The FAME concentration decreased over reaction time due to saponification. The rate of decrease in the FAME concentration was a function of the water content. For instance, at 10 min reaction time, the FAME concentrations decreased by 20, 43, 56 and 70% for 0 vol%, 2.5vol%, 5vol% and 12.5vol% water, respectively.

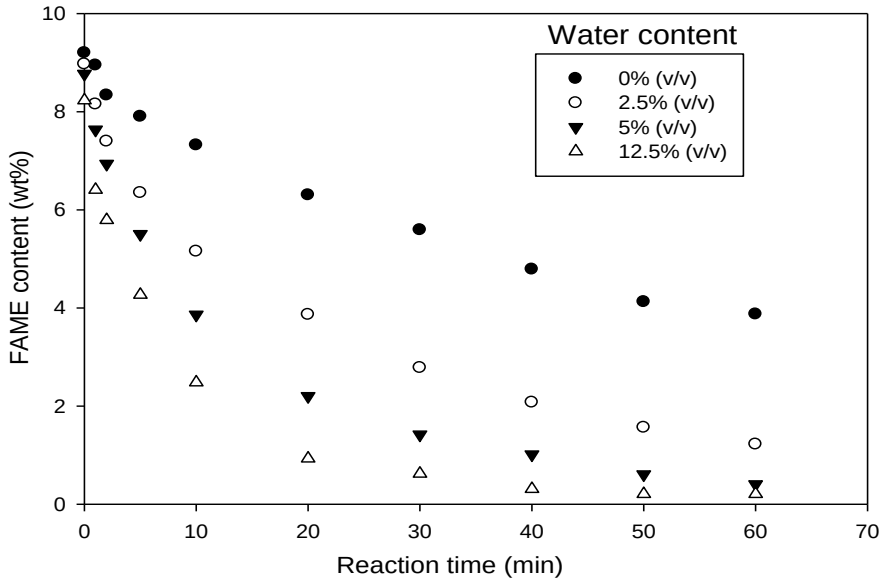

Figure 4.12: FAME saponification at 100:1 methanol to FAME molar ratio and 35wt% KOH, mixing intensity of 600rpm, 60˚C using methanol containing 0 – 12.5vol% water

The increase in FAME saponification rate due to the presence of water was because the hydroxide – methoxide equilibrium reaction (equation (4.6)), was pushed "backwards" to the formation of hydroxide ions side. As shown in Table 4.7, k' and the mole fractions of KOH increased significantly when increasing water content.

$$CH_3OH + OH^- \leftrightarrow CH_3O^- + H_2O \quad (4.6)$$

Table 4.7: Values of k' for FAME saponification at various water contents

Water in methanol (vol %)	k' (L.mol^{-1}.min^{-1})	Mole fraction (β) of KOH (%)	R^2
0	0.032[a]	0.69[a]	-
2.5	0.104	3.25	0.999
5.0	0.175	5.47	0.998
12.5	0.344	10.75	0.985

[a]Estimated based on KOH-methoxide equilibrium constant.

4.4.4 Summary

Saponification reactions of FAME and RSO in alkali-catalysed homogeneous transesterification were investigated. The rates of saponification of FAME increased with water content due to the hydroxide-methoxide equilibrium. Water reacts with methoxide ions to form more hydroxide species that accelerates saponification reactions. The findings suggest that FAME and RSO saponification side reactions could be substantial in homogeneous base-catalysed transesterification process and not negligible as assumed in conventional homogeneous kinetics model (Bambase *et al.*, 2007; Vicente *et al.*, 2005). Therefore, a new kinetic model including RSO and FAME saponification and the hydroxide-methoxide equilibrium is required to predict homogeneous base-catalysed transesterification process better than the conventional homogeneous model. The new kinetic model developed in this study by considering these side reactions were discussed in section 4.5.

4.5 Numerical modelling and validation for homogeneous alkali-catalysed transesterification

4.5.1. Conventional kinetic modelling and experimental validation

The conventional kinetic model for the base-catalysed homogeneous transesterification considers only the three stepwise transesterification reactions (Bambase *et al.*, 2007), giving the kinetic rate expressions summarised in equation (4.7).

$$r_{TG} = [CH_3O^-](-k_1[TG][MA] + k_2[DG][FAME])$$

$$r_{DG} = [CH_3O^-](k_1[TG][MA] + k_4[MG][FAME] - k_2[DG][FAME] - k_3[DG][MA])$$

$$r_{MG} = [CH_3O^-](k_3[DG][MA] + k_6[GL][FAME] - k_4[MG][FAME] - k_5[MG][MA])$$

$$r_{FAME} = [CH_3O^-](k_1[TG][MA] + k_3[DG][MA] + k_5[MG][MA] - k_2[DG][FAME] \ldots - k_4[MG][FAME] - k_6[GL][FAME])$$

$$r_{GL} = [CH_3O^-](k_5[MG][MA] - k_6[GL][FAME])$$

$$r_{MA} = -r_{FAME} \qquad (4.7)$$

The experimental data for validating the model were obtained from the RSO transesterification in a 100mL jacketed batch reactor. The kinetic parameters used in the conventional kinetic modelling of the alkali-catalysed homogeneous transesterification are shown in Table 4.8. The initial rate constants in Table 4.8 were derived from literature for (k_1 – k_6) (Bambase *et al.*, 2007). These rate constants were chosen because the trends of the predicted FAME concentration using them were consistent with the experimental data from this study. The rate constants reported for the homogeneous base-catalysed transesterification of vegetable oils with methanol vary widely (Bambase *et al.*, 2007; Vicente *et al.*, 2005; Darnoko and Cheryan, 2000b; Noureddini and Zhu, 1997). The initial values of k from Bambase *et al*. (2007) were adjusted to obtain the line of best fit (< 5% error) to the experimental data. Rate constants that fitted the experimental data were 1.75 times higher than those in literature, probably due to higher mixing intensity in the experiments. The kinetic model in equation (4.7) was solved using MATLAB by ODE45 solver (Runge-Kutta method).

Table 4.8: Rate constants used for the conventional kinetic model[#]

Rate constant (L. $mol^{-1}.min^{-1}$)	Reactions
$k_1 = 4.260\ x\ 10^9\ e^{-\frac{58,740}{RT}}$	TG ⟶ DG
$k_2 = 4.304\ x\ 10^6\ e^{-\frac{44,930}{RT}}$	DG ⟶ TG
$k_3 = 2.176\ x\ 10^{11}\ e^{-\frac{67,146}{RT}}$	DG ⟶ MG
$k_4 = 6.559\ x\ 10^9\ e^{-\frac{58,184}{RT}}$	MG ⟶ DG
$k_5 = 8.679\ x\ 10^5\ e^{-\frac{30,010}{RT}}$	MG ⟶ GL
$k_6 = 1.975\ x\ 10^7\ e^{-\frac{46,009}{RT}}$	GL ⟶ MG

[#]Modified rate constants from Bambase *et al.* (2007)

Figure 4.13 shows that at low catalyst concentrations (0.5wt% and 1wt%), the conventional kinetic model can be used to predict the alkali-catalysed homogeneous transesterification reactions. This was due to negligible saponification side reactions at low catalyst concentrations. For instance, in KOH-catalysed transesterification of RSO at operating conditions of 0.5wt% KOH (based on RSO), 3:1 methanol to RSO molar ratio and 60˚C reaction temperature, the FAME yields predicted by the model at 60min reaction time was 72.7% which agrees well with the experimental FAME yield of 74.3±1.1%. The model prediction in Figure 4.13 clearly indicated that the FAME yield increased from ~73% to 95% at 60min reaction time when a molar ratio of methanol to oil increased from 3:1 to 6:1. The predicted FAME yield was consistent with 94% achieved after 60min for transesterification at 6:1 methanol to RSO molar ratio and 60˚C.

However, the modelling results from the conventional kinetic model based in equation (4.7) cannot correctly predict the reactions in base-catalysed homogeneous transesterification at high catalyst concentration (35wt%). The conventional kinetic model predicts 99.9% FAME yield against an experimental value of 51%, for transesterification at 300:1 methanol to RSO molar ratio, 60˚C and reaction time of 60min. The poor prediction of the base-catalysed homogeneous transesterification at the

high catalyst concentration was due to the assumptions that side reactions are negligible. Derivations of the conventional kinetic model do not consider FFA neutralisation or saponification of RSO (triglyceride) and FAME. These assumptions do not hold at high alkali catalyst concentration due to substantial RSO and FAME saponification side reactions.

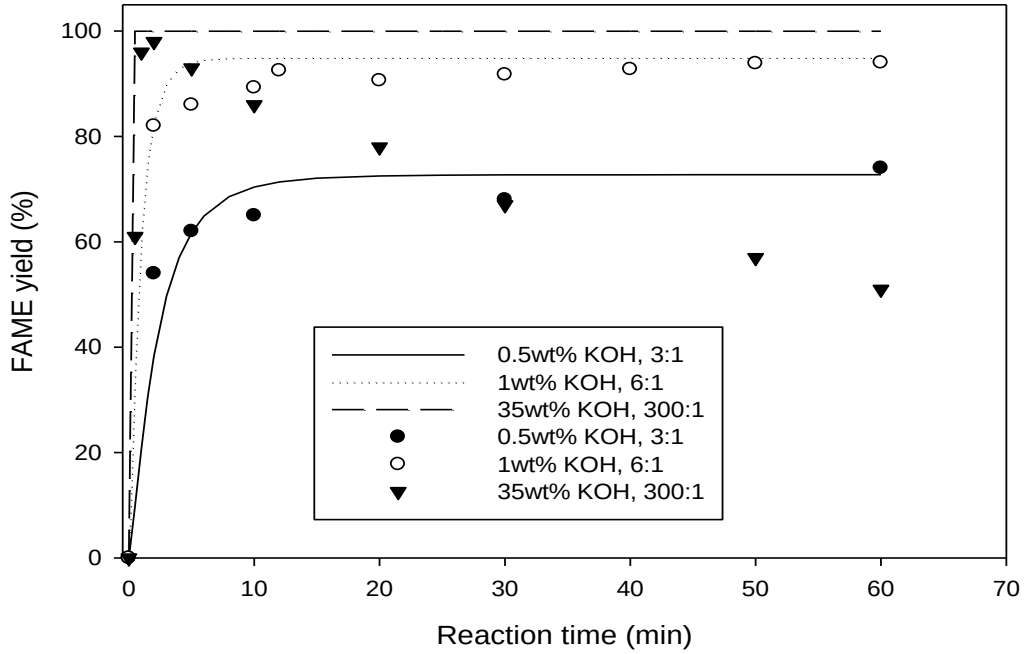

Figure 4.13: Homogeneous alkali-catalysed transesterification of RSO at 60˚C and mixing intensity of 600rpm: (i) 3:1 methanol to RSO molar ratio and 0.5wt% KOH; (ii) 6:1 methanol to RSO molar ratio and 1wt% KOH and (iii) 300:1 methanol to RSO molar ratio and 35wt% KOH. (dots: experimental data; lines: modelling results)

4.5.2. Development of a new kinetic model for alkali-catalysed transesterification

A new kinetic model was developed to improve the robustness of the conventional kinetic model. This would allow for predictions of more process parameters in the alkali-catalysed homogeneous transesterification. The new kinetic model was derived by integrating the kinetic parameters of the side reactions occurring in base-catalysed transesterification, such as RSO and FAME saponification in metal hydroxides (KOH) and hydroxide-methoxide equilibrium.

The rate expressions in equation (4.7) were modified by integrating the reaction kinetics TG and FAME saponification in metal hydroxides (KOH), FFA neutralisation and hydroxide-methoxide equilibrium in equations (4.8) – (4.11). The soap formations in equations (4.8) – (4.10) are assumed to be irreversible.

$$TG + 3OH^- \xrightarrow{k_7} 3Soap + GL \quad (4.8)$$

$$FAME + OH^- \xrightarrow{k_8} Soap + MA \quad (4.9)$$

$$FFA + OH^-(RO^-) \xrightarrow{k_9} Soap + H_2O\,(ROH) \quad (4.10)$$

$$CH_3OH + OH^- \underset{k_y}{\overset{k_x}{\rightleftharpoons}} CH_3O^- + H_2O \quad (4.11)$$

The combined reaction rate expressions for the new kinetic model developed for the base-catalysed homogeneous transesterification are summarised in equation (4.12).

$$r_{TG} = [CH_3O^-](-k_1[TG][MA] + k_2[DG][FAME]) - k_7[TG][OH^-]$$

$$r_{DG} = [CH_3O^-](k_1[TG][MA] + k_4[MG][FAME] - k_2[DG][FAME] - k_3[DG][MA])$$

$$r_{MG} = [CH_3O^-](k_3[DG][MA] + k_6[GL][FAME] - k_4[MG][FAME] - k_5[MG][MA])$$

$$r_{FAME} = [CH_3O^-](k_1[TG][MA] + k_3[DG][MA] + k_5[MG][MA] - k_2[DG][FAME] \ldots - k_4[MG][FAME] - k_6[GL][FAME]) - k_8[FAME][OH^-]$$

$$r_{MA} = [CH_3O^-](k_2[DG][FAME] + k_4[MG][FAME] + k_6[GL][FAME] - k_1[TG][MA] \ldots + k_y[H_2O] - k_3[DG][MA] - k_5[MG][MA]) + k_8[FAME][OH^-] - k_x[MA][OH^-]$$

$$r_{GL} = [CH_3O^-](k_5[MG][MA] - k_6[GL][FAME]) + k_7[TG][OH^-]$$

$$r_{OH^-} = k_y[H_2O][CH_3O^-] - k_x[MA][OH^-] - k_9[FFA][OH^-] - k_7[TG][OH^-] \ldots - k_8[FAME][OH^-]$$

$$r_{CH_3O^-} = k_x[MA][OH^-] - k_y[H_2O][CH_3O^-] - k_9[FFA][CH_3O^-]$$

$$r_{H_2O} = k_x[MA][OH^-] - k_y[H_2O][CH_3O^-] + k_9[FFA][OH^-]$$

$$r_{Soap} = [OH^-](k_7[TG] + k_8[FAME] + k_9[FFA])$$

$$r_{FFA} = -k_9([FFA][OH^-] + [FFA][CH_3O^-]) \quad (4.12)$$

4.5.3. Reaction scheme for the new kinetic model

The reaction scheme in Figure 4.14 was proposed for the overall reactions in the new kinetic model for the alkali-catalysed homogeneous transesterification of vegetable oils with methanol, based on the reactions summarised in equation (4.12). This is a particularly complex process. The reaction starts by the alkali-metal hydroxide (OH^-) reacting with methanol (CH_3OH) to form methoxide (CH_3O^-), the catalytic species, and water. The hydroxide-methoxide equilibrium favours formation of methoxide due to the higher acidity of methanol compared to water (Reeve *et al.*, 1979).

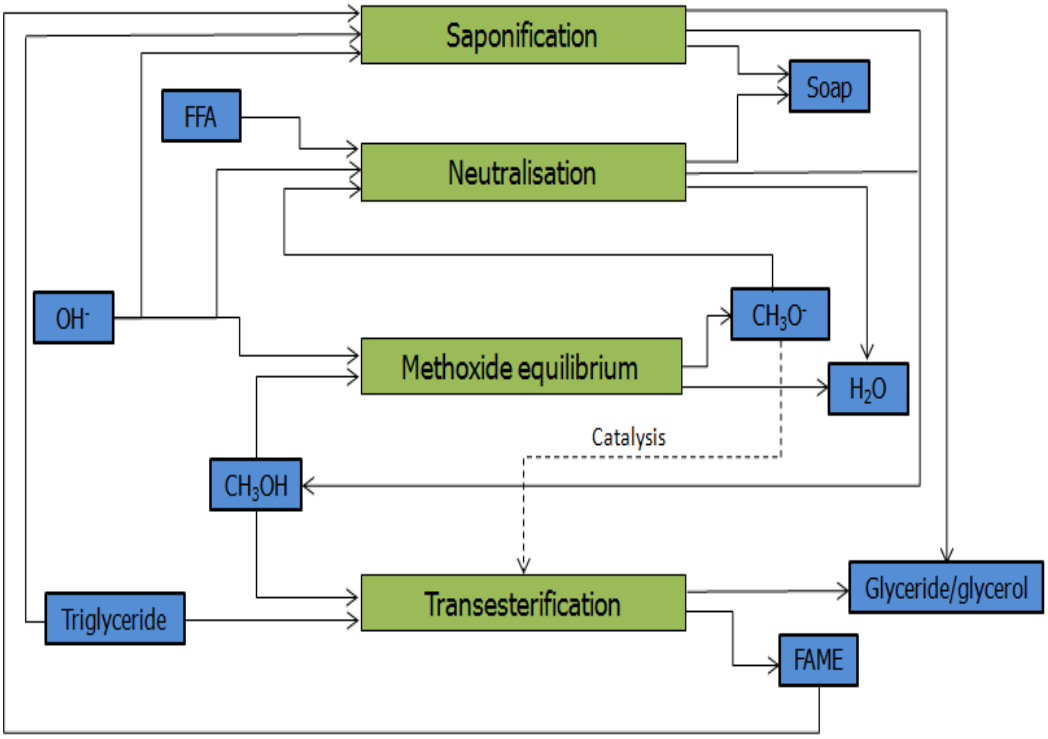

Figure 4.14: Proposed reaction scheme for alkali-catalysed homogeneous transesterification (OH^-/CH_3OH and transesterification are equilibrium reactions)

The OH^- and CH_3O^- ions in the solution participate in various reactions. CH_3O^- ions catalyse the reactions of triglyceride with methanol to form FAME and glycerol. Apart from glycerol, glycerides (diglyceride and monoglyceride) are also produced during triglyceride transesterification. The CH_3O^- ions consumed in the transesterification reaction are regenerated by the reactions of the glyceride ions with methanol. However, CH_3O^- that participates in the neutralisation of FFA to form soap and methanol cannot be regenerated. The loss in methoxide catalytic species due to neutralisation leads to decreased rate of FAME yield at high FFA contents.

The OH^- species participate in several reactions to form soap, such as saponification of triglyceride and FAME and FFA neutralisation. Reactions of OH^- ions with triglyceride and FAME lead to saponification and reduced FAME yield. Therefore, the concentration of OH^- must be minimised to achieve a high FAME yield. An addition of water into the alkali-catalysed transesterification process shifts the hydroxide-methoxide equilibrium towards formation of the metal hydroxide. Water also reacts with glyceride ions to form more OH^- in the system. These reactions lead to an increase in OH^- concentration which accelerates the saponification of triglyceride and FAME. This indicates that water has a negative effect on the alkali-catalysed homogeneous transesterification. It is important to note that even when metal alkoxides ($CH_3O^-M^+$) are used as catalysts, any water in the system would react with the $CH_3O^-M^+$ to form methanol and metal hydroxide, in accordance with the hydroxide-methoxide equilibrium.

Based on the proposed reaction scheme in Figure 4.14, triglyceride and FAME saponification must be minimised to achieve a high FAME yield. Saponification of triglyceride and FAME can be slowed down by using low catalyst loadings and anhydrous reagents to reduce OH^- regeneration. However, a reduction in the catalyst loadings also reduces the rates of the triglyceride transesterification. The reaction scheme indicates that a feasible condition for rapid biodiesel production is to use large excesses of methanol. This moves the hydroxide-methoxide equilibrium towards CH_3O^- formation, minimising OH^- concentration and reducing the OH^- regeneration whilst increasing the rate of triglyceride transesterification.

4.5.4. Experimental validation of the new kinetic model

The new kinetic model in equation (4.12) was solved using MATLAB by ODE45 solver (Runge-Kutta method). Kinetic data used for the modelling are shown Table 4.9. The initial rate constants for the transesterification ($k_1 – k_6$) were similar to that used for the conventional kinetic model in Table 4.8. Experimental validations of the modelling results from the new kinetic model developed in this study are shown in Figure 4.15. The results showed that the kinetic model based on equation (4.12) agreed well with the experimental data for all cases. This model was more robust than the conventional model in predictions of more process parameters due to the integration of kinetics of the possible side reactions into the new model.

Table 4.9: Rate constants used for the new kinetic model

Rate constant (L. $mol^{-1}.min^{-1}$)	Reactions	References
$k_1 = 4.260\ x\ 10^9\ e^{-\frac{58,740}{RT}}$	TG ⟶ DG	**
$k_2 = 4.304\ x\ 10^6\ e^{-\frac{44,930}{RT}}$	DG ⟶ TG	**
$k_3 = 2.176\ x\ 10^{11}\ e^{-\frac{67,146}{RT}}$	DG ⟶ MG	**
$k_4 = 6.559\ x\ 10^9\ e^{-\frac{58,184}{RT}}$	MG ⟶ DG	**
$k_5 = 8.679\ x\ 10^5\ e^{-\frac{30,010}{RT}}$	MG ⟶ GL	**
$k_6 = 1.975\ x\ 10^7\ e^{-\frac{46,009}{RT}}$	GL ⟶ MG	**
$k_7 = 1.269\ x\ 10^{11}\ e^{-\frac{69104}{RT}}$	RSO ⟶ Soap	This study
$k_8 = 1.962\ x\ 10^{10}\ e^{-\frac{61,160}{RT}}$	FAME ⟶ Soap	This study
$k_9 = 6.136\ x\ 10^5\ e^{-\frac{31,394}{RT}}$	FFA ⟶ Soap	(Morgunov *et al.*, 1977)
$K_{eq} = \frac{k_x}{k_y} = 3.2$ (79.5 (mol.L^{-1})	OH^- ⇌ CH_3O^-	(Reeve *et al.*, 1979; Caldin and Long, 1954)

**k_1 – k_6 are the modified rate constants from Bambase *et al.* (2007)

At low catalyst concentrations (0.5wt% and 1wt%), both the conventional and the new kinetic models can be used to predict the alkali-catalysed homogeneous transesterification reactions. That was due to negligible saponification side reactions at low catalyst concentrations. For instance, in transesterification of RSO at operating conditions of 0.5wt% KOH (based on RSO), 3:1 methanol to RSO molar ratio and 60˚C reaction temperature, the FAME yields predicted by the models at 60min reaction time were 72.7% for the conventional model and 72.2% for the new kinetic model. These values were close to 74.3±1.1% FAME yield from the experiment.

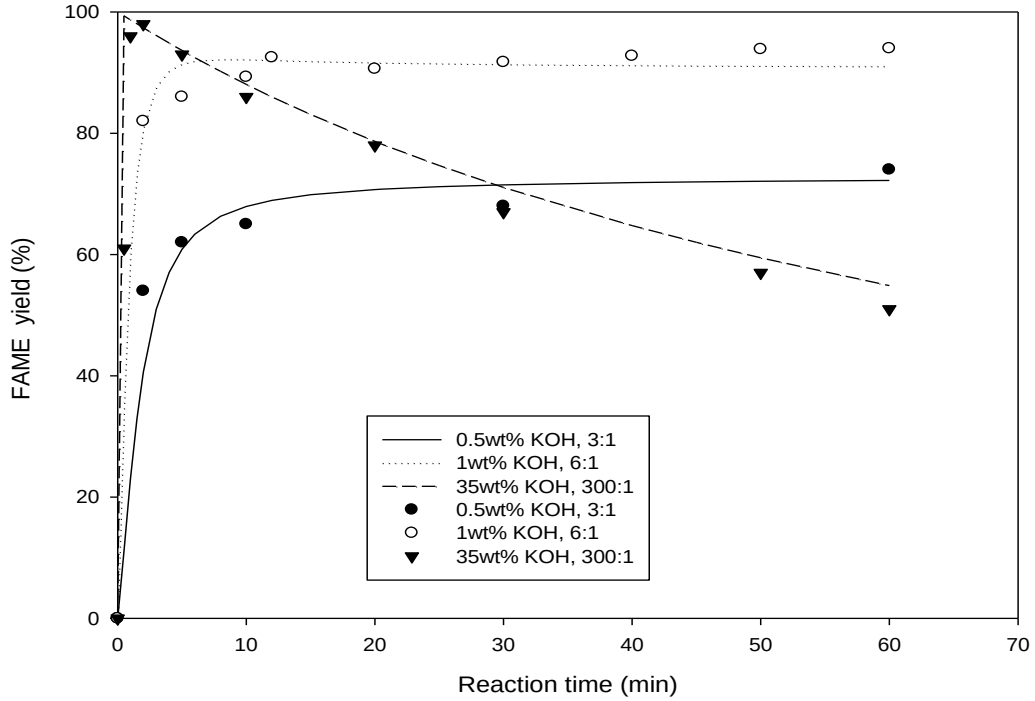

Figure 4.15: Homogeneous alkali-catalysed transesterification of RSO at 60˚C and mixing intensity of 600rpm: (i) 3:1 methanol to RSO molar ratio and 0.5wt% KOH; (ii) 6:1 methanol to RSO molar ratio and 1wt% KOH and (iii) 300:1 methanol to RSO molar ratio and 35wt% KOH. (dots: experimental data; lines: modelling results)

However, at high catalyst concentrations, only the new kinetic model can correctly predict process parameters for the alkali-catalysed transesterification of RSO. For instance, in the transesterification at 300:1 methanol to RSO molar ratio, 60˚C and 35wt% KOH, the FAME yields predicted by the models were 99.9% for the conventional model and 97.4% for the new kinetic model after 2min reaction time. The experimental FAME yield after 2min reaction time was 98% at these conditions. Deviations of the FAME yield predicted by the conventional kinetic model from the experimental results were substantial at longer reaction times (Figure 4.15). At 60min reaction time, the experimental FAME yield was 51%, compared to the predicted FAME yields of 99.9% for the conventional model and 54.9% for the new kinetic model, for the transesterification at 300:1 methanol to RSO molar ratio, 60˚C and 35wt% KOH. The decrease in FAME yield was due to FAME saponification which continued after the maximum FAME yield was achieved. The new kinetic model predicts more process parameters than the conventional model because rate kinetics of possible side reactions: RSO and FAME saponification, FFA neutralisation and methoxide-hydroxide equilibrium were integrated into the new kinetic model.

Both the experimental and new kinetic model results showed that increase in methanol and catalyst concentration greatly accelerates the rates of the transesterification reaction, as about 98% FAME yield was achieved in 2min reaction time. However, the downside side of operating at a high catalyst concentration (35wt%) and methanol molar ratio (300:1) is an increased cost of recovery of the large excess methanol. The use of huge amount of catalyst (35wt%) is also not cost-effective since the catalyst cannot be recovered. Lastly, rapid saponification of produced FAME occurs if the reaction was not quenched as soon as the maximum FAME yield was achieved. Based on the robustness of the new kinetic model developed in this study, more process parameters in alkali-catalysed homogeneous transesterification of RSO were investigated using the model.

4.5.5. Effect of reaction temperature on alkali-catalysed transesterification

Figure 4.16 below shows modelling and experimental results for RSO transesterification with methanol at reaction temperatures of 30-70˚C, 0.5wt% KOH and (a) 300:1 and (b) 6:1 methanol to RSO molar ratio. The FAME yield increased with temperature for both methanol molar ratios due to the dependence of reaction rate constants on temperature (Vicente *et al.*, 2004). At a 300:1 molar ratio in Figure 4.16(a), the predicted FAME yields at reaction temperatures of 30, 40, 50, 60 and 70˚C were 8.5%, 20.4%, 39.6%, 69.8% and 94.3%, respectively, after 5min reaction time. These were similar to the values obtained experimentally (23%, 41% and 67% at 40, 50 and 60˚C). At these conditions, the mole fractions of the available hydroxide ions are too small to cause noticeable levels of saponification; hence the reaction simply reaches its equilibrium.

At a 6:1 molar ratio (Figure 4.16(b)), the predicted FAME yield at the reaction temperatures of 30, 40, 50, 60 and 70 ˚C were 21.4%, 44.2%, 69.6%, 85.7% and 91.6% after 5min reaction time. The transesterification reaction and saponification of FAME and RSO were much faster at 6:1 than at 300:1 methanol to RSO molar ratio. A large excess of methanol (300:1) pushes the hydroxide-methoxide equilibrium towards methoxide formation, reducing the mole fraction of hydroxide ions and therefore preventing RSO and FAME saponification. As shown in Figure 4.16(a), the FAME yield was 99.9% at all tested temperatures after 60min reaction time at a 300:1 methanol to RSO molar ratio. The lower maximum FAME yield at the 6:1 molar ratio was due to the increased RSO and FAME saponification. At 30˚C, the FAME yields predicted by

the model were 90.6% for 6:1 molar ratio and 87.1% for 300:1 molar ratios at 60min reaction time. These results suggest that a reaction time >60min is required for transesterification at these molar ratios at 30˚C reaction temperature, which was in agreement with the findings in literature (Nakpong and Wootthikanokkhan, 2010).

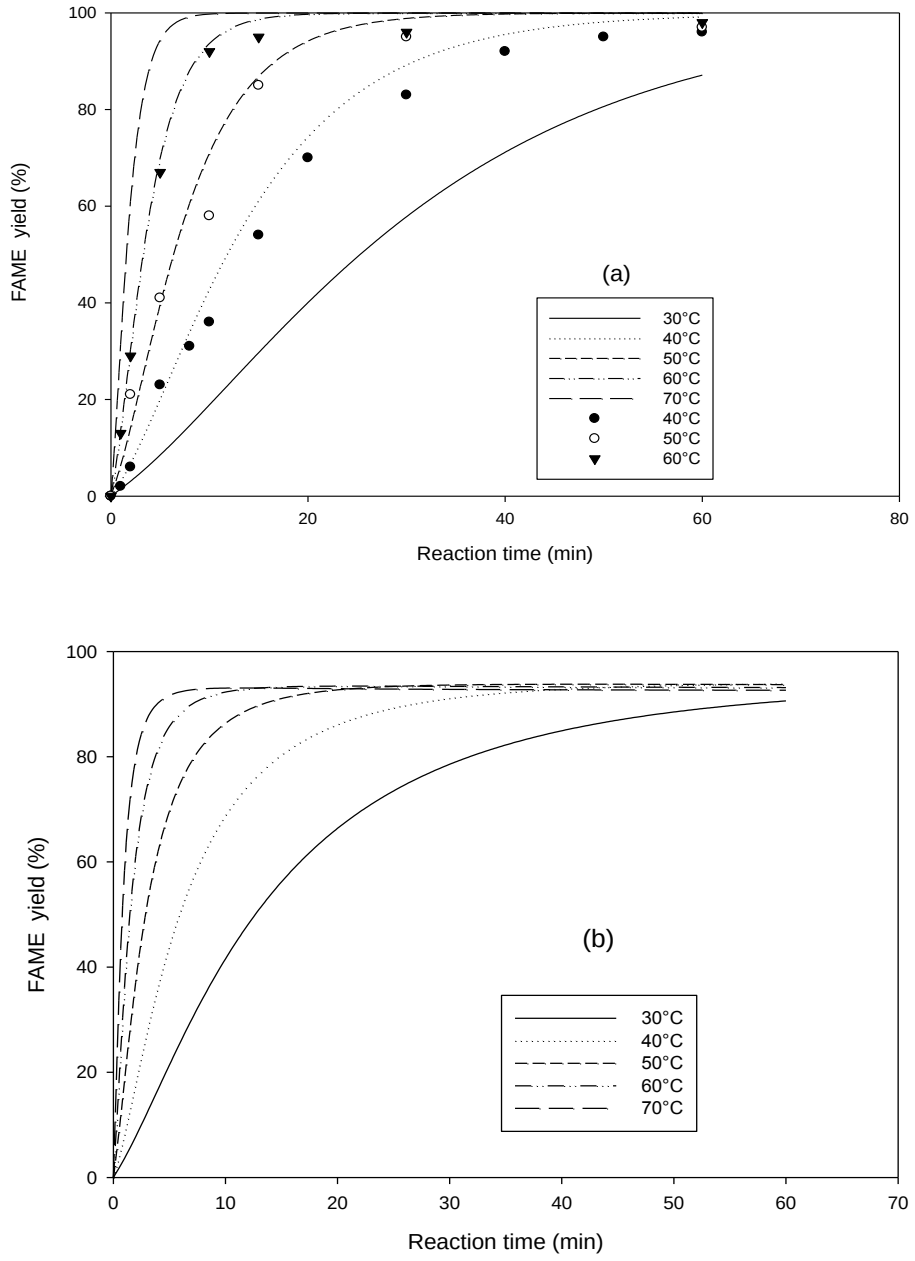

Figure 4.16: Homogeneous alkali-catalysed transesterification at 0.5wt% KOH, mixing at 600rpm, 30 – 70˚C temperatures and a molar ratio of methanol to RSO of (a) 300:1 and (b) 6:1 (dots: experimental data; lines: modelling results)

The rates of transesterification and saponification were highest at 70˚C, leading to the shortest time to achieve the maximum (93% FAME yield at 7min reaction time for a 6:1 molar ratio) and the highest rates of FAME saponification unless the reaction was

quenched. This prediction was in accordance with other findings (Dorado *et al.*, 2004), in which the FAME yield decreased when increasing temperature from 60 to 70˚C in alkali-catalysed methanolysis of used olive oil. However, the authors explained the results as being due to the acceleration of glyceride saponification at 70˚C. The findings in this study suggest that both glyceride and FAME saponification are accelerated when temperature increased from 60˚C to 70˚C.

4.5.6. Effect of methanol to oil molar ratios and hydroxide catalyst concentration.

The effect of molar ratio of methanol to RSO and hydroxide catalyst concentration on FAME yield in homogeneous KOH-catalysed transesterification of RSO at 60˚C and 0.5wt% catalyst is shown in Figure 4.17. The results in Figure 4.17(a) showed that FAME yield increased with increasing methanol molar ratios. Excess methanol in the reaction not only drives the transesterification equilibrium towards the product side and increases the rate of the reaction, but also shifts the hydroxide-methoxide equilibrium towards the formation of more methoxide ions, reducing FAME saponification. At low methanol molar ratios (e.g. 6:1), FAME saponification is evident after the maximum, e.g., the FAME yield decreased from 91% at 5min to 89% at 60min reaction time for 6:1 methanol to RSO molar ratio, 60˚C and 1.5wt% KOH.

A higher equilibrium FAME yield was obtained in continuous transesterification at 6:1 methanol to RSO molar ratio, 60˚C and 1.5wt% KOH, using the integral baffles meso-OBR (96.2%) than in a batch reactor (92.3 %). This was probably due to the enhanced mixing in the meso-OBR. Transesterification reaction passes from a mass transfer-controlled initial stage due to immiscibility of alcohol-oil mixture to kinetically-controlled stage (Bambase *et al.*, 2007; Vicente *et al.*, 2005; Darnoko and Cheryan, 2000b; Noureddini and Zhu, 1997). The reaction finally returns back to a mass transfer-controlled biphasic biodiesel – glycerol phases. This last stage of the triglyceride transesterification could be a bottle-neck for a base-catalysed homogeneous reaction, if the catalyst is lost to the glycerol phase due to poor mixing. A rapid decrease in the FAME yield in the integrally baffled meso-OBR after the equilibrium FAME yield reached was also observed, indicating that both transesterification and saponification reactions were intensified in the meso-OBR. At low catalyst concentration e.g. 0.5wt% KOH, there was a reduction in hydroxide ion concentration in the solution that reduced the rates of RSO and FAME saponification. This accounted for the increase in the

predicted equilibrium FAME yields. However, the rate of the RSO transesterification also decreased with decreasing catalyst concentration.

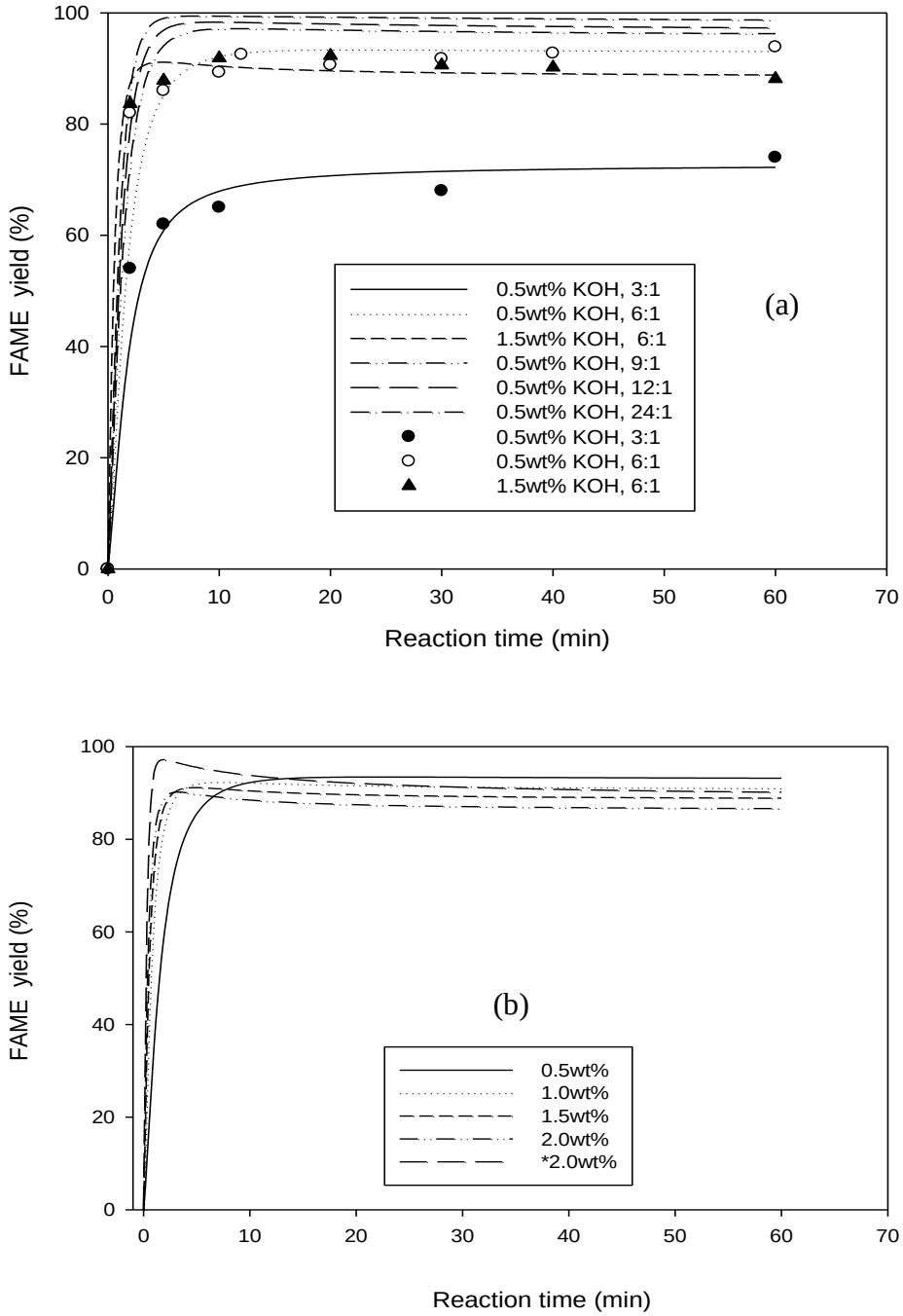

Figure 4.17: Homogeneous KOH-catalysed transesterification of RSO with methanol at 60˚C: (a) 0.5wt% and 1.5wt% KOH catalyst, 600rpm and 3:1 to 24:1 methanol to RSO molar ratios; (b) numerical results at 6:1 methanol to oil molar ratio (* molar ratio of methanol to oil of 12:1) over a range of KOH catalyst concentrations of 0.5 – 2.0wt% (dots: experimental data; lines: modelling results)

The effect of varying catalyst concentrations on the rates of FAME production in a homogenous alkali-catalysed transesterification was modelled as shown in Figure 4.17(b). The FAME yield increased with increasing catalyst concentration. As a result, the time to achieve the maximum FAME yield decreased with increasing catalyst concentrations, e.g. it decreased from 22min at 0.5wt% KOH to 3.5min at 2.0wt% KOH. The maximum FAME yield also decreased from 93% at 0.5wt% KOH to 90% at 2.0wt% KOH. At 60min reaction time, the predicted FAME yield decreased from 93% to 86.6% as the KOH catalyst concentration increased from 0.5wt% to 2.0wt% at 6:1 methanol to RSO and 60˚C. The trend here was similar to that observed in a continuous RSO transesterification using the integral baffled meso-OBR at 6:1 molar ratio,1.5wt% KOH and residence times of 2.5 – 15min (section 4.3.4), where the FAME content maximised between 2.5 – 5min and then decreased when residence time was above 5min.

Figure 4.17(b) indicates that the greater the catalyst concentration, the greater the rate of RSO and FAME saponification. However, this can be minimised by using higher methanol molar ratios, e.g. the predicted FAME yield was 97.1% at a 12:1 methanol to RSO molar ratio compared to 89.0% at a 6:1 methanol to RSO molar ratio at 60˚C, 2.0wt% KOH and 2min reaction time. The FAME yield of 97.1% at 2min decreased to 90.1% after 1h reaction time due to FAME saponification. Therefore, the reaction must be quenched as soon as the maximum FAME yield was reached to prevent any loss of the FAME product. This requires a reactor with tight control of residence time and a high degree of uniform mixing.

4.5.7 Effect of moisture and FFA on the alkali-catalysed transesterification

Figure 4.18 shows the effects of moisture and free fatty acids (FFA) on the alkali-catalysed transesterification at 60˚C, 1.0 wt% KOH catalyst and 6:1 methanol to RSO molar ratio, as predicted by the model. The water content was 0 – 1.0 wt% in the reaction mixture and FFA content was 0 – 1.0 wt% in RSO. Clearly, the FAME yield decreased when water was added. This was due to the backward shift in the hydroxide-methoxide equilibrium reaction, producing hydroxide ions which accelerate the rates of both triglyceride and FAME saponification. Therefore, more methanol was required to push the hydroxide-methoxide equilibrium forward to reduce the amount of hydroxide ions and to minimise saponification reactions. When the amount of FFA in RSO increased from 0wt% to 1.0wt%, the time to reach the maximum FAME yield of 92%

increased from for 7min 0wt% FFA to 12min at 1wt% FFA, as shown in Figure 4.18. This was attributed to the removal of methoxide ions from the reaction mixture by FFA neutralisation as noted in Figure 4.14.

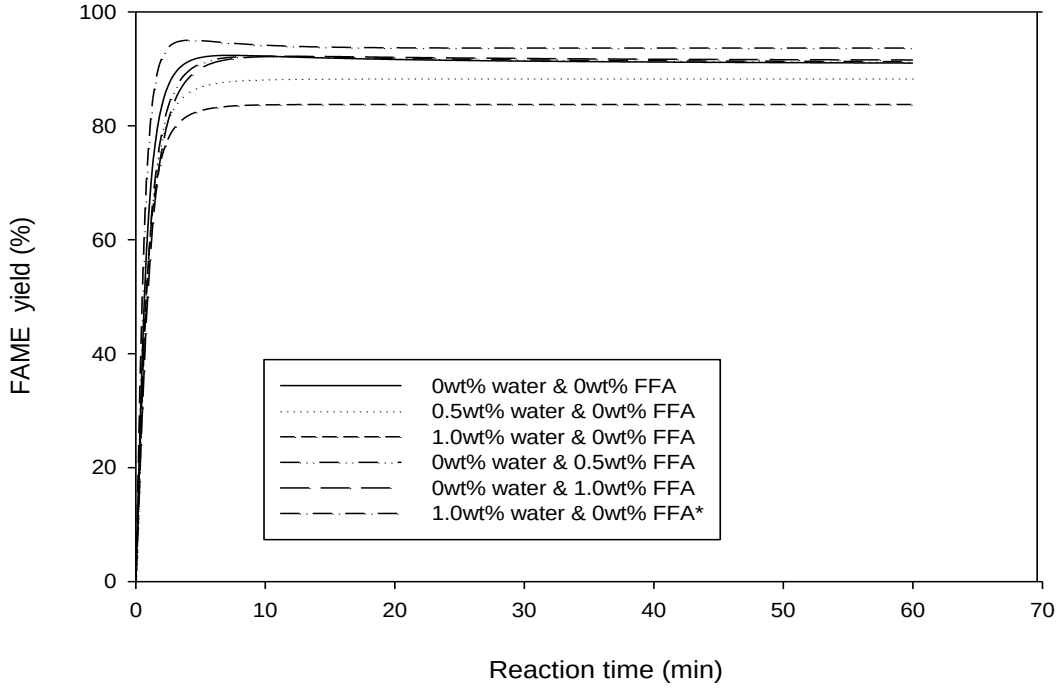

Figure 4.18: Numerical results for RSO transesterification at 60˚C, 1.0wt% KOH catalyst, 6:1 (*12:1) methanol to oil molar ratio over water content of 0 – 1.0%wt and FFA content of 0-1.0%wt.

Due to the high concentration of methoxide ions compared to the hydroxide ions in reaction mixtures for alkali-catalysed transesterification, FFA neutralisation by methoxide ions is favoured as presented below. This irreversible reaction removed catalytic species (CH_3O^-) from the alkali-catalysed transesterification process and therefore slowed down transesterification.

$$\mathrm{FFA} + \mathrm{CH_3O^-} \rightarrow \mathrm{Soap} + \mathrm{CH_3OH}$$

(FFA neutralisation)

The main problem of FFA in the alkali-catalysed transesterification is the soap produced during FFA neutralisation, leading to emulsification and gel formation, thereby inhibiting the separation of glycerol and FAME (Canakci and Van Gerpen, 2003). According to literature (Ma *et al.*, 1998; Freedman *et al.*, 1984), FFA and moisture contents must not exceed 0.5wt% and 0.3wt% respectively in alkali-catalysed

biodiesel process to avoid excessive soap formation. However, findings from this study suggest that higher moisture contents (up to 1.0wt %) can be tolerated at methanol molar ratios ≥ 12:1. Furthermore, at these conditions the reaction time required is only ~5min, significantly shorter than the reaction times usually used in industry (over 60min).

4.5.8 Summary

A more robust kinetic model for base-catalysed transesterification than the conventional model was developed. It explains various phenomena that previous models cannot by including the main saponification reactions, FFA neutralisation and the hydroxide/methoxide equilibria. Both the experimental results and model simulations showed that rapid biodiesel production (reaction times below 2min) at economically viable conversions (>96% FAME) can be achieved by increasing base catalyst and methanol concentrations, without significant problems due to excess soap formation, even in the presence of water and FFA. At a 2min residence time, the reactor in biodiesel production would be reduced to a simple plug flow reactor. This would significantly reduce the capital and running costs of the reactor. Over the whole process, the advantages would have to be weighed against the increased running costs due to increased catalyst (probably insignificant) and recycling more methanol (probably quite significant) due to the greater molar ratio used.

4.6 Transesterification of RSO with methanol using the SZB catalyst

In this section, results from the batch and continuous screening of RSO transesterification with methanol using the SZB catalyst are presented and discussed. An integral meso-OBR (volume of 10mL) was used in both continuous and batch modes to provide mixing and catalyst suspension. Table 4.10 shows the properties of the SZB catalyst. This catalyst had fewer active sites compared to the equivalent molar concentration (mmol/g) of conventional base catalysts: 25.0 mmol/g for NaOH and 17.9 mmol/g for KOH. Barrett-Joyner-Halenda (BJH) pore size of the catalyst suggested a mesoporous (2nm < BJH < 50nm) network (Hayati-Ashtiani, 2011; Gregg and Sing, 1982). The BJH pore size was determined from the N_2 desorption branch of the isotherm, relating to the amount of N_2 desorbed to the average size of pores affected by the desorption (Barrett *et al.*, 1951).

Table 4.10: Properties of the SZB catalyst

Pore volume (cm^3/g)	BET surface area (m^2/g)	BJH pore size (nm)	Active sites (mmol/g)
0.083	16.37	3.87	1.42

BJH pore size obtained for the SZB was too small to allow triglyceride and FAME molecules to access the porous network. It was reported that fatty acid molecular sizes varied linearly (R^2 = 0.995) from pentanoic to tridecanoic acids, e.g. an average molecular size of 2.8nm for pentanoic acid and 4.1nm for tridecanoic acid (Nonhebel, 2005). The average molecular size of the fatty acids in RSO, consisting mainly of oleic acid, will be considerably larger than 4.1nm. Therefore, active sites within the pores may not be accessible to RSO.

4.6.1 Effect of oscillatory mixing on FAME yield

Figure 4.19 shows the FAME yield versus reaction time for a batch transesterification at a 12:1 methanol to RSO molar ratio, 60˚C and 3.0wt% SZB catalyst over a range of Re_o of 49 – 223. The initial rate of the FAME yield increased significantly with increasing Re_o then remained constant at Re_o above 148.

The results indicated that the reaction was mass transfer limited at mixing intensities Re_o<148 and was kinetically controlled at $Re_o \geq 148$. At reaction times above 30min, there was little difference in the FAME yield at Re_o of 112, 148 and 223 as the reaction reached its equilibrium. The FAME yield was lowest at Re_o of 49 e.g. 14.0% at 5min, 37.1% at 10min, 71.5% at 30min, 75.9% at 60min, 80.4% at 90min and 84.2% at 120min reaction time. The lowest FAME yield at Re_o of 49 was due to poor mixing, leading to non-uniform suspension of catalysts. This is consistent with the findings in section 4.3.1, in that mixing inside the integral baffled reactor was insufficient in KOH-catalysed RSO transesterification even at Re_o = 71.

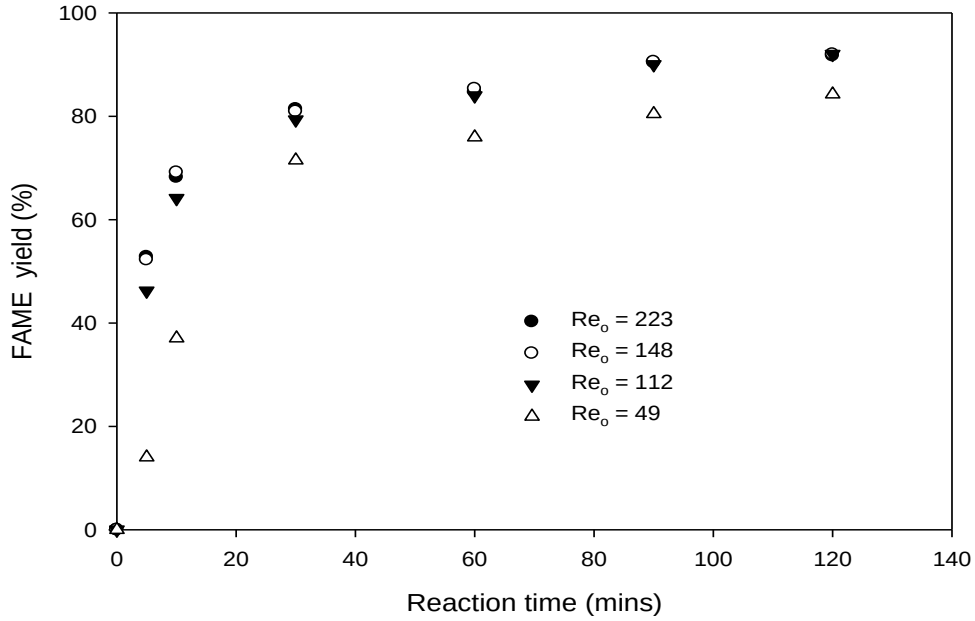

Figure 4.19: FAME yield obtained from batch transesterification at a 12:1 methanol to RSO molar ratio, 3wt% SZB catalyst, 60˚C and Re_o of 49 (2Hz, 4mm), 112 (4.5Hz, 4mm), 148 (4Hz, 6mm) and 223 (4.5Hz, 8mm), using integral baffled meso-OBR

4.6.2 Effects of the catalyst loadings and methanol molar ratio on FAME yield.

As can be observed in Figure 4.20, the FAME yield increased with the SZB catalyst loading (Figure 4.20 (a)) and the methanol to RSO molar ratio (Figure 4.20(b)). Figure 4.20(b) shows that excess methanol was required to drive the reaction towards the FAME product. The trends in the FAME yields versus methanol molar ratio at the SZB catalyst loadings in Figure 4.20(b) were similar to others, in which SrO (Liu *et al.*, 2007) and magnesia modified with strontium (Yoosuk *et al.*, 2010) were used as catalysts for transesterification of vegetable oils with methanol.

However, the FAME yield obtained in Figure 4.20(b) at 30min reaction time was 24 – 26% lower than what was achieved by others using SrO-based catalyst (Yoosuk *et al.*, 2010; Liu *et al.*, 2007). For instance, the FAME yield was 67.5% in this study compared to 95% in soybean oil transesterification with methanol at 6:1 methanol to oil molar ratio, 60˚C, 3wt% SrO loading (Liu *et al.*, 2007), and 97.3% for methanolysis of palm olein at 9:1 methanol to palm olein molar ratio, 60˚C, 5wt% SrO loading (Yoosuk *et al.*, 2010). The lower rate of the FAME yield in this study was due to the lower SZB catalyst loading and concentration of active sites as shown in Table 4.10. Due to the variation in the active site concentrations, turnover number (TON) and turnover

frequency (TOF) were used to compare the catalytic activity between the SZB and others. TON is the number of moles of the reactant (triglyceride) converting into FAME per mole of the catalytic active site while TOF is TON of the catalyst per unit time (TOF = TON/time).

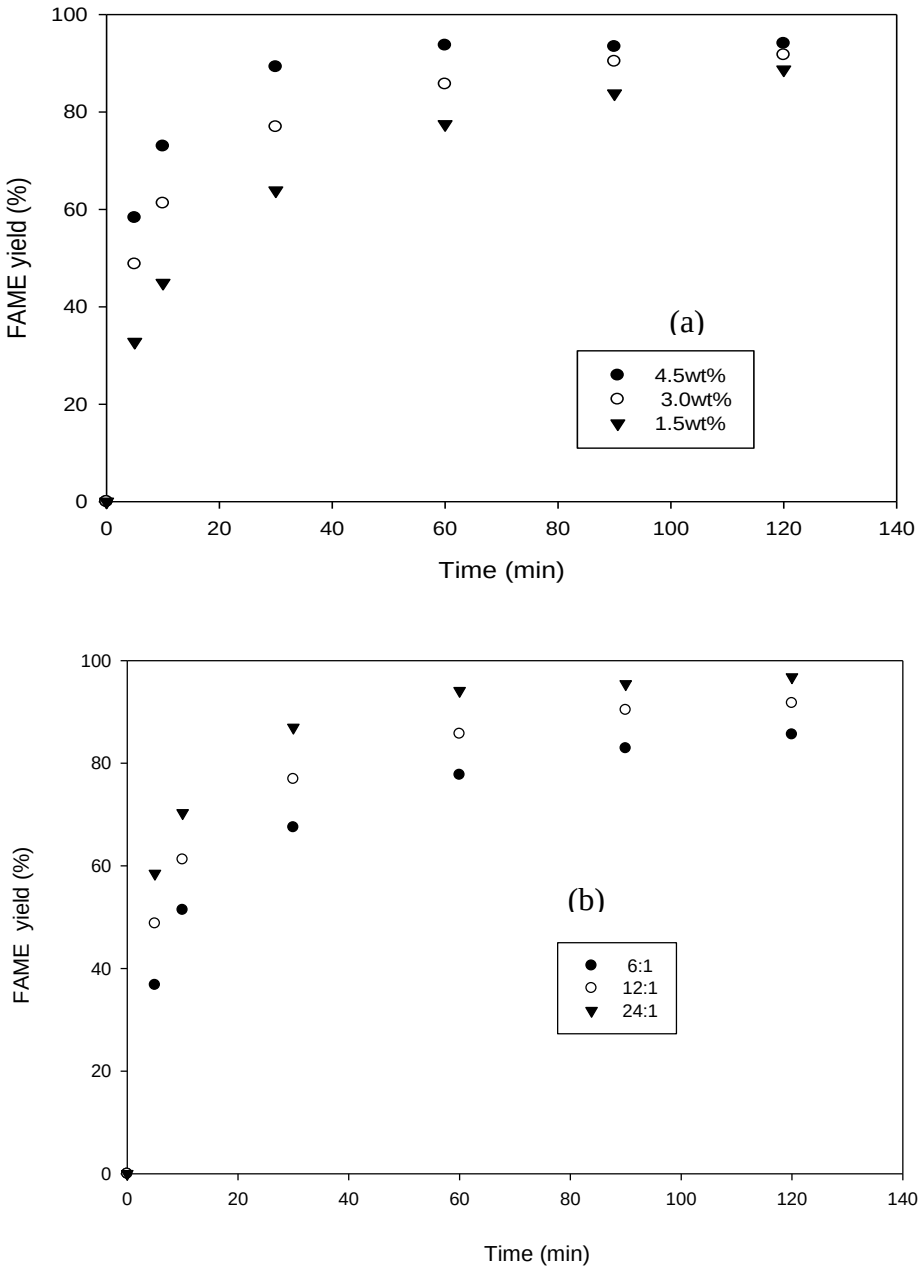

Figure 4.20: FAME yield obtained in batch transesterification of RSO at 60˚C using integral baffled meso-OBR: (a) methanol to RSO molar ratios of 12:1 and catalyst loadings of 1.5 – 4.5wt%; (b) catalyst loading of 3wt% and methanol to RSO molar ratios of 6:1, 12:1 and 24:1

The TON and TOF were obtained from a linear portion of the initial reaction rate profile for the FAME yield. The TON and TOF for the SZB were 3.91 and 46.9 h^{-1}, which were higher than the values for MgO-SrO (3.27 and 19.6 h^{-1}) and for SrO (2.0 and 4.8 h^{-1}) (Table 4.11). The differences were due to the nature of the active sites. The active site on the SZB, $Sr(OH)_2$, readily reacts with methanol to form methoxide ions, which is similar to NaOH and KOH. In contrast, methoxide ions are generated *in situ* by the interaction of methanol and the SrO or MgO-SrO in the solid matrix.

Table 4.11: Activity of catalysts in terms of TON and TOF

Catalysts[a]	Transesterification reactions	Active sites (mmol/g)	TON	TOF (h^{-1})	Reference
SZB	RSO at 6:1 molar ratio, 60°C, 5wt% catalyst	1.42	3.91	46.9	This study
MgO-SrO	Palm olein at 6:1 molar ratio, 60°C, 5wt% catalyst	5.0	3.27	19.6	(Yoosuk *et al.*, 2010)
SrO	Soybean oil at 6:1 molar ratio, 60°C, 3wt% catalyst	9.6[b]	2.0	4.8	(Liu *et al.*, 2007)
NaOH	RSO at 6:1 molar ratio, 60°C, 1wt% catalyst	25.0	4.21	50.5	(Phan *et al.*, 2012)
KOH	RSO at 6:1 molar ratio, 60°C, 1.5wt% catalyst	17.9	4.07	48.8	(Phan *et al.*, 2012)

[a]TON and TOF calculated from literature data based on the reaction conditions;

[b]100% purity assumed for the SrO.

4.6.3 Water tolerance of the SZB-catalysed RSO transesterification

As shown in Figure 4.21, water was deleterious to SZB-catalysed transesterification of RSO with methanol. The FAME yield decreased significantly with water content, e.g. the FAME yield was 52.8% at 0%vol water but was only 38.7% at 1.0vol% and only 20.6% at 2.0vol% water after 5min reaction time. At 1.0vol% and 2.0vol% water, the FAME yield exhibited a maximum at 10min reaction time, e.g. 54.5% at 1.0vol% and 22.5% at 2.0vol% water, and then decreased gradually with reaction time, e.g., 44.6% at 1.0vol% water and 12.2% at 2.0vol% after 120min reaction time. This phenomenon was similar to what was observed both from experimental and numerical modelling of base-catalysed homogeneous transesterification in section 4.5, where the FAME product was

consumed in a competitive side reaction due to the existing hydroxide ions in the hydroxide-methoxide equilibrium.

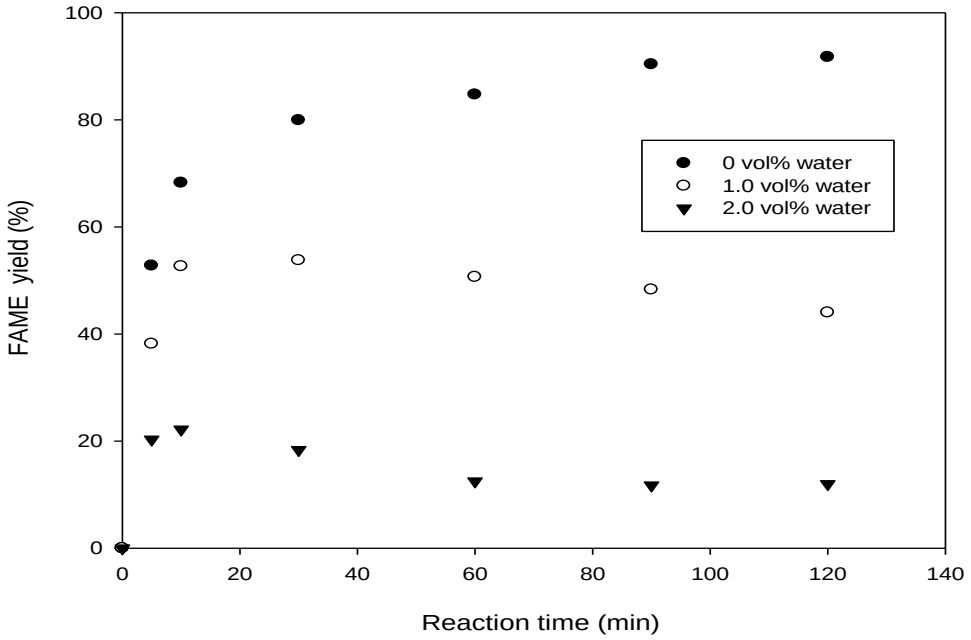

Figure 4.21: Effect of water on the FAME yield for transesterification at 12:1 methanol to RSO molar ratio, 3wt% catalyst, 60˚C and Re_o of 223, using integral baffled meso-OBR

Considering the nature of the functionality of the active sites in the SZB catalyst - $Sr(OH)_2$, a decrease in the FAME yield with water content could be explained by increased hydroxide formation. Any addition of water to the system moved the hydroxide-methoxide equilibrium reaction (Figure 4.22(a)) backwards to OH^- formation. Competitive side reactions of RSO and FAME occurred in the SZB-catalysed transesterification as shown in Figure 4.22(b). The decrease in the FAME yield after the maximum yield was due to FAME saponification. This suggests that the SZB-catalysed RSO transesterification was prone to FAME saponification, which is reminiscent of the alkali-catalysed homogeneous processes. For CaO-catalysed transesterification of soybean oil, water content over 2.8wt% was required for any significant soap formation to occur (Liu et al., 2008). At lower water contents, dissociative adsorption of water on the CaO surface to form $Ca(OH)_2$ accelerated the transesterification, resulting in an increase in the FAME yield when increased water content up to 2.03%wt. For the SZB catalyst used in this study, the basic active sites were identified as $Sr(OH)_2$ (see section

4.6.6), therefore, any further addition of water to SZB-catalysed transesterification process leads to soap formation.

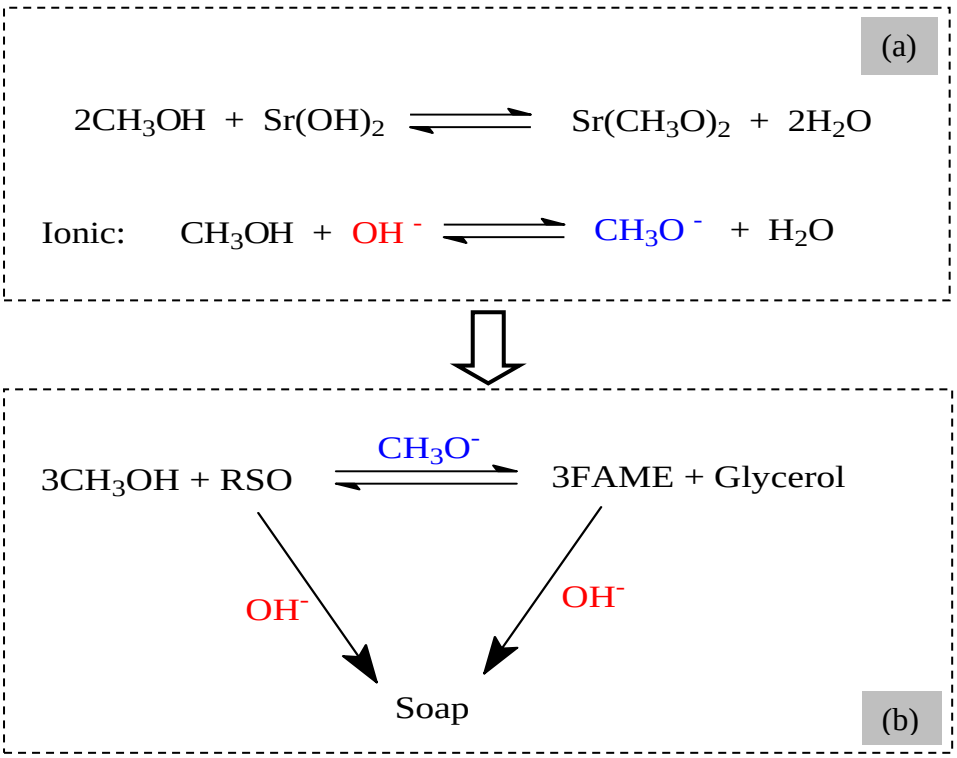

Figure 4.22: Proposed reactions (a) reaction of the strontium hydroxide functional group with methanol, (b) competitive transesterification and saponification reactions.

4.6.4 Effect of reaction temperature on SZB-catalysed transesterification.

Figure 4.23 shows the results obtained in RSO transesterification at 12:1 methanol to RSO molar ratio, 3wt% SZB catalyst over a range of temperatures of 40 - 60˚C. Over the first 60min reaction time, the FAME yield was strongly dependent on temperature, increasing 2 – 5 times/10˚C. For instance, the FAME yield was 7.1% at 40˚C but 38.8% at 50˚C and 52.8% at 60˚C after 5min reaction time. The increase in the FAME yield was due to increased rates of transesterification reactions with temperature (Bambase *et al.*, 2007; Vicente *et al.*, 2005).

The increase in the FAME yield with temperature also accelerates the transition of the reactant mixture from a three-phase (catalyst-RSO-alcohol) system to two-phase (catalyst-reaction mixture) system due to the emulsification of RSO and methanol in the presence of FAME. The maximum FAME yield was, however, almost identical for all tested temperatures as the reaction reached its equilibrium, e.g. it was 86.3% at 40˚C, 88.1% at 50˚C and 91.7% at 60˚C.

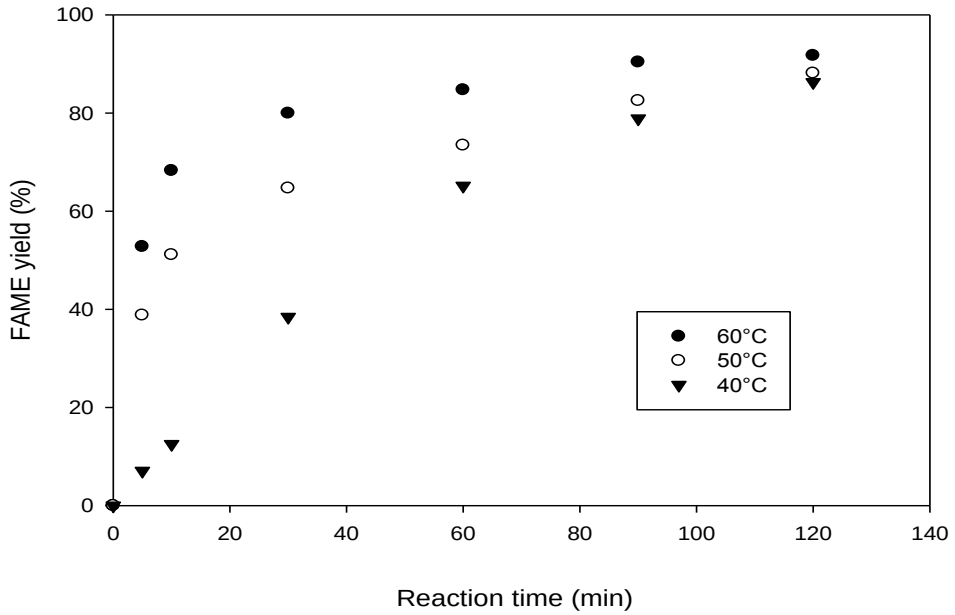

Figure 4.23: Effect of temperature on the FAME yield in batch transesterification in integral baffled meso-OBR at 12:1 methanol to RSO molar ratio and 3wt% SZB catalyst

Kinetic parameters for the SZB-catalysed transesterification were determined using the experimental data at a temperature range of 40–60˚C. As the SZB-catalysed RSO transesterification followed the homogeneous mechanisms as discussed in sections 4.6.2 and 4.6.3, the kinetics were analysed accordingly based on equation (4.13). An expression for the overall rate of formation of FAME is given in equation (4.14) below:

$$\begin{aligned} \text{TG} + \text{MA} &\underset{k_2}{\overset{k_1}{\rightleftharpoons}} \text{FAME} + \text{DG} \\ \text{DG} + \text{MA} &\underset{k_4}{\overset{k_3}{\rightleftharpoons}} \text{FAME} + \text{MG} \\ \text{MG} + \text{MA} &\underset{k_6}{\overset{k_5}{\rightleftharpoons}} \text{FAME} + \text{GL} \end{aligned} \qquad (4.13)$$

$$\frac{d[\text{FAME}]}{dt} = k_1[\text{TG}][\text{MA}] - k_2[\text{DG}][\text{FAME}] + k_3[\text{DG}][\text{MA}] - k_4[\text{MG}][\text{FAME}] \ldots + k_5[\text{MG}][\text{MA}] - k_6[\text{GL}][\text{FAME}] \qquad (4.14)$$

(k_i is a second-order reaction rate constant for i^{th} transesterification reaction, $L.mol^{-1}.s^{-1}$).

At an excess of methanol (12:1), initially the rates of the backward reactions in equation (4.13) would be negligible. Therefore, equation (4.14) was re-written as equation (4.15).

$$r_{FAME} = \frac{d[FAME]}{dt} = k_1[TG][MA] + k_3[DG][MA] + k_5[MG][MA] \quad (4.15)$$

Concentrations of the DG and MG intermediates in the equation (4.15) were solved by using a quasi-steady state approximation (QSSA) approach (Qiu *et al.*, 2012; Atkins and de Paula, 2006). This approximation assumes that the intermediates are consumed as soon as they produced, i.e., $k_1 < k_3 < k_5$. Hence, rate of change in the concentrations of the intermediates (DG and MG) is fairly small, as they rise from initial values (zero) to reach constant plateau - equations (4.16) and (4.17). Indeed, rate constants for the TG (k_1), DG (k_3) and MG (k_5) reactions increase with decreasing molecular size as reported in Bambase *et al*. (2007), where reaction rate constants of 0.0218 $mol.L^{-1}.min^{-1}$ for TG ($k_1/k_3 = 0.33$), 0.0651 $mol.L^{-1}.min^{-1}$ for DG ($k_3/k_5 = 0.29$), and 0.2280 $mol.L^{-1}.min^{-1}$ for MG were obtained for transesterification of sunflower oil with methanol at 6:1 methanol to oil molar ratio, 40˚C and 0.5wt% NaOH. The QSSA can be applied to every intermediate in chemical reactions that behaves similarly, to simplify calculations involving complex reaction kinetics.

$$\frac{d[DG]}{dt} = k_1[TG][MA] - k_2[MG][FAME] - k_3[DG][MA] + k_4[MG][FAME] \approx 0 \quad (4.16)$$

$$\frac{d[MG]}{dt} = k_3[DG][MA] - k_4[MG][FAME] - k_5[MG][MA] + k_6[GL][FAME] \approx 0 \quad (4.17)$$

Since the backward reactions are negligible at the initial rates, equations (4.16) and (4.17) were rewritten as equations (4.18) and (4.19), respectively.

$$\frac{d[DG]}{dt} = k_1[TG][MA] - k_3[DG][MA] \approx 0 \quad (4.18)$$

$$\therefore \quad [DG] = \frac{k_1}{k_3}[TG]$$

$$\frac{d[MG]}{dt} = k_3[DG][MA] - k_5[MG][MA] \approx 0 \quad (4.19)$$

$$\therefore \quad [MG] = \frac{k_3}{k_5}[DG] = \frac{k_3}{k_5}\frac{k_1}{k_3}[TG] = \frac{k_1}{k_5}[TG]$$

Combining equation (4.15) and equations (4.18) – (4.19), the rate of the formation of FAME was obtained as presented in equation (4.20).

$$r_{FAME} = k_1[TG][MA] + \frac{k_1}{k_3}k_3[TG][MA] + \frac{k_1}{k_5}k_5[TG][MA] = 3k_1[TG][MA] \quad (4.20)$$

Rate of RSO (TG) transesterification in equation (4.21) was obtained based on the stoichiometry of the reaction. The equation was simplified further and integrated to obtain equation (4.23).

$$-r_{TG} = \frac{d[TG]}{dt} = \frac{1}{3}r_{FAME} = k_1[TG][MA] \quad (4.21)$$

$$-\frac{d(1-X_{TG})}{dt} = k_1[TG]_o(1 - X_{TG})(\Phi - 3X_{TG}) \quad (4.22)$$

$$\frac{1}{(\Phi-3)[TG]_o}\ln\left[\frac{(\Phi-3X_{TG})}{\Phi(1-X_{TG})}\right] = k_1 t \quad (4.23)$$

Where:

$-r_{TG}$: rate of reaction (consumption) of the TG in RSO

X: conversions TG to FAME

$[TG]_o$: initial concentration of the TG in RSO (0.69 mol.L^{-1})

Φ: ratio of the molar concentrations of methanol (MA) to RSO =12.

Table 4.12: Kinetic parameters of the SZB-catalysed RSO transesterification.

Temperature (˚C)	k_1*10^{-3} (L.mol^{-1}. min^{-1})	Kinetic parameters
40	2.5	E_a = 65.5kJ.mol^{-1}
50	6.1	k_o = 2.2 *10^8 L.mol^{-1}.min^{-1}
60	11.3	(R^2 = 0.992)

As illustrated in Table 4.12, the rate constants for RSO transesterification increased with temperature, by a factor of approximately 2 per 10˚C rise in reaction temperature. The activation energies estimated from this study are comparable with those of base-catalysed homogeneous transesterification and 2-3 times higher than other solid catalysts reported in literature (Table 4.13). Once again, this implies that the SZB-catalysed transesterification was via homogeneous kinetic mechanism.

Table 4.13: Activation energies for vegetable oil methanolysis.

Reaction	Ea (kJ.mol^{-1})	Reference
RSO methanolysis with SZB catalyst	65.5	This study
Palm oil methanolysis with KOH catalyst	61.5[a]	(Darnoko and Cheryan, 2000b)
Sunflower oil methanolysis with NaOH catalyst	58.7[a]	(Bambase *et al.*, 2007)
Soybean oil methanolysis with NaOH catalyst	55.0[a]	(Noureddini and Zhu, 1997)
Canola oil methanolysis with SrO catalyst	19.6	(Gotch *et al.*, 2009)
Ethyl acetate methanolysis with MgO catalyst	20.1	(Dossin *et al.*, 2006)

[a]Activation energies for $TG \rightarrow DG$ reaction.

4.6.5 Continuous transesterification of RSO– a reusability test for the SZB catalyst

The results obtained from a continuous transesterification of RSO in integral baffles meso-OBR at a 12:1 methanol to RSO molar ratio, 3wt% SZB catalyst, 60˚C, Re_o of 223 and 20min residence time/reaction time (τ) are shown in Figure 4.24(a). In the experiment, the exit valve of the reactor was fitted with a 0.45μm syringe filter to prevent any loss of the charged catalyst. The FAME yield was 57.9% over the first 20 min running time (i.e. 1 residence time), and then decreased rapidly to 10.1% at 110min (5.5τ), representing 82.6% reduction in the FAME yield. The results clearly showed that the SZB catalyst was not suitable to be used for continuous heterogeneous transesterification of triglyceride with methanol in a packed bed or in the suspension form because the catalyst rapidly loses its activity.

The reduction in the FAME yield in Figure 4.24(a) was consistent with results from batch transesterification in a beaker at the same operating conditions (Yoosuk *et al.*, 2010; Gotch *et al.*, 2009). Gotch *et al.* (2009) reported that 60% reduction in the FAME yield was observed after 2 cycles for SrO catalysed methanolysis of canola oil. When magnesia modified with SrO was used (Yoosuk *et al.*, 2010), there was 28.1% reduction in the FAME yield after 5 cycles for transesterification at 6:1 methanol to palm olein

molar ratio, 60˚C, and 8wt% catalyst. These findings indicated that these catalysts were losing activity via the gradual depletion of the catalyst due to leaching. The magnesia modified with SrO was more stable than the SZB and SrO catalysts probably due to synergetic effect of the magnesia support.

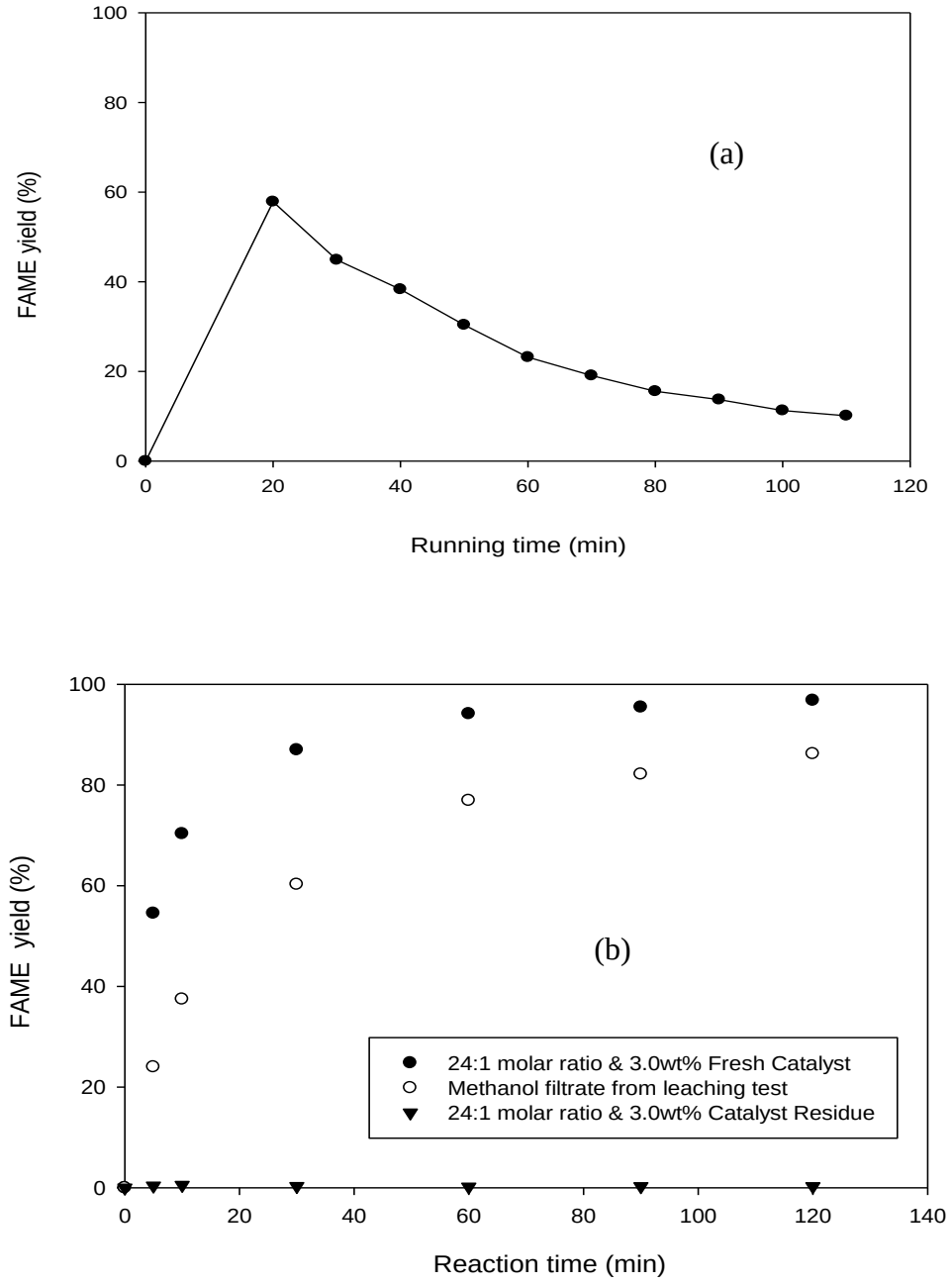

Figure 4.24: (a) continuous transesterification in integral baffles meso-OBR at a 12:1 methanol to RSO molar ratio, 3wt% SZB catalyst, 60˚C, residence time (τ) of 20min and Re_o of 223, (b) FAME yield for transesterification at a 24:1 methanol to RSO molar ratio and 60˚C, using 3wt% fresh SZB catalyst, 3wt% spent SZB catalyst (residue), methanol filtrate from leaching of 3wt% fresh SZB catalyst in batch reactions with the integral baffled meso-OBR operated at Re_o of 501

As shown in Figure 4.24(b), the FAME yield obtained from the methanol filtrate (no catalyst added) was substantial: 86.2% compared to 96.8% obtained from fresh SZB catalyst after 120min reaction time. In contrast, the FAME yield was only 0.3% for the spent SZB catalyst (residue), meaning that the residue had virtually no activity. Therefore, the SZB catalyst is extremely prone to leaching and cannot be reused. The pulse CO_2 titration of the SZB basic active sites showed that the active site concentration of the catalyst decreased from 1.42mmol/g for the fresh SZB catalyst to 0.10mmol/g for the spent catalyst (residue), corresponding to 93% loss of active sites. This implies that the SZB catalyst can be used only for batch transesterification processes, which is similar to alkali catalysts.

However, it is expected that the purification of the FAME and glycerol products would be less costly when the SZB catalyst is used. This is because Sr^{2+} ions leached into the reaction mixture can be easily removed by neutralisation using carbonic acid (H_2CO_3) to form an insoluble strontium carbonate. This neutralisation process is also recommended for transesterification reactions catalysed by other alkaline earth metal oxides and hydroxides since these metal ions form insoluble carbonates.

4.6.6 Analysis of the fresh and spent SZB catalyst

XRD analysis of the fresh and spent SZB catalysts is shown in Figure 4.25. The XRD spectra showed that the fresh SZB catalyst had 2θ peaks at 14.3°, 19.5°, 31.8°, 39.2° and 40.4°, which is in agreement with the XRD spectra of $Sr(OH)_2.H_2O$ in the JCPDS files. The absence of these peaks in the spent SZB catalyst, confirms the explanation for the reduction in the FAME yield with running time as shown in Figure 4.24(a) (section 4.6.5) for the continuous RSO transesterification. This also accounts for the high catalytic activity of the methanol filtrate in the leaching test shown in Figure 4.24(b).

The presence of $Sr(OH)_2$ in the fresh SZB was attributed to the hydration of the highly hygroscopic SrO produced during the calcinations (Bacce *et al.*, 2001). As shown in Figure 4.25, the SZB catalyst consisted mainly of strontium zirconate ($SrZrO_3$), some hydrated strontium hydroxide and traces of strontium carbonate ($SrCO_3$). These results was confirmed by the conspicuous XRD peaks of $SrZrO_3$ at 2θ angles of 30.8°, 44.1°, 54.6°, 64.2°, 72.8° and 89.1° in both fresh and spent SZB catalysts. These XRD peaks were similar to other findings (Cavalcante *et al.*, 2007). The strontium zirconate was formed from the reaction of SrO and ZrO_2 at high temperatures (e.g. 900˚C). The traces

of strontium carbonate found in the fresh and spent SZB could be due to the reaction of SrO with atmospheric CO_2 (Lima *et al.*, 2012). The most prominent XRD peaks of the $SrCO_3$ were the two close peaks at 2θ angles of 25.2° & 25.8° (Figure 4.25). An increase in the size of these peaks in the spent SZB catalyst was due to the increase in the weight fraction of the $SrCO_3$ as the $Sr(OH)_2.H_2O$ leached out from the fresh SZB catalyst matrix.

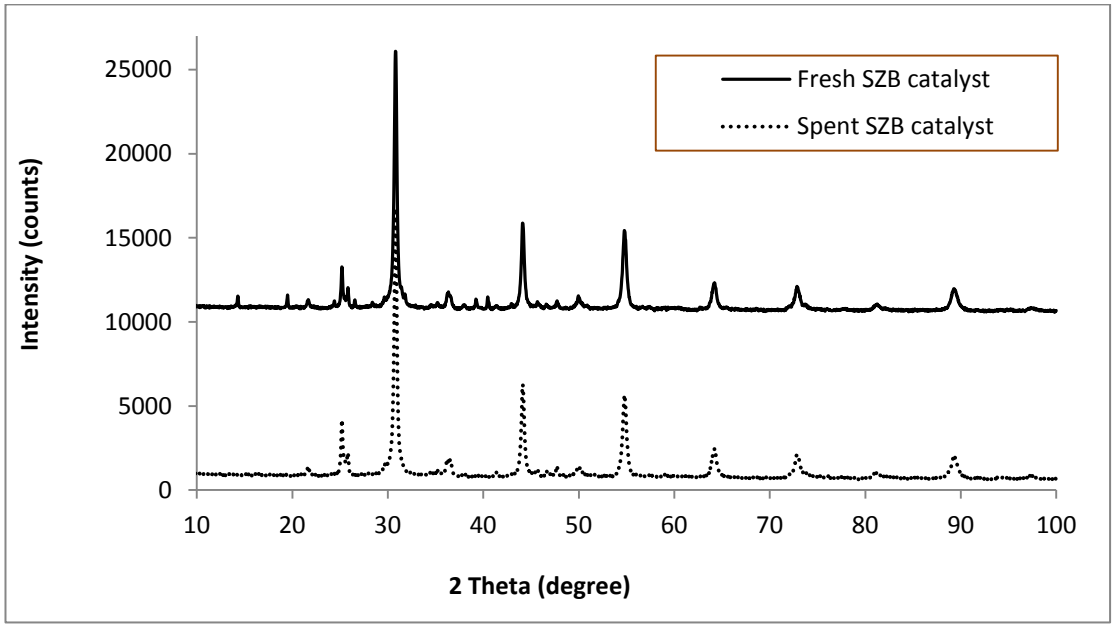

Figure 4.25: The XRD spectra of the fresh and spent (residue) SZB catalysts powder

Figure 4.26 shows the FTIR results of the fresh and spent (residue) SZB catalysts. There were increases in the peaks at 1448cm^{-1} for C = O of carbonates and 858cm^{-1} for zirconium-oxygen bond (Zr-O) stretching in the spent SZB catalyst compared to those in the fresh SZB. This indicates that the fresh catalyst has lost some soluble components, leading to an increase in the % composition of the insoluble parts –strontium zirconate ($SrZrO_3$) and strontium carbonate ($SrCO_3$). The near zero activity (0.3% FAME yield) of the spent SZB catalyst suggests that the spent catalyst (residue) contains no strontium hydroxide, which is in agreement with the findings from the XRD analysis shown in Figure 4.25.

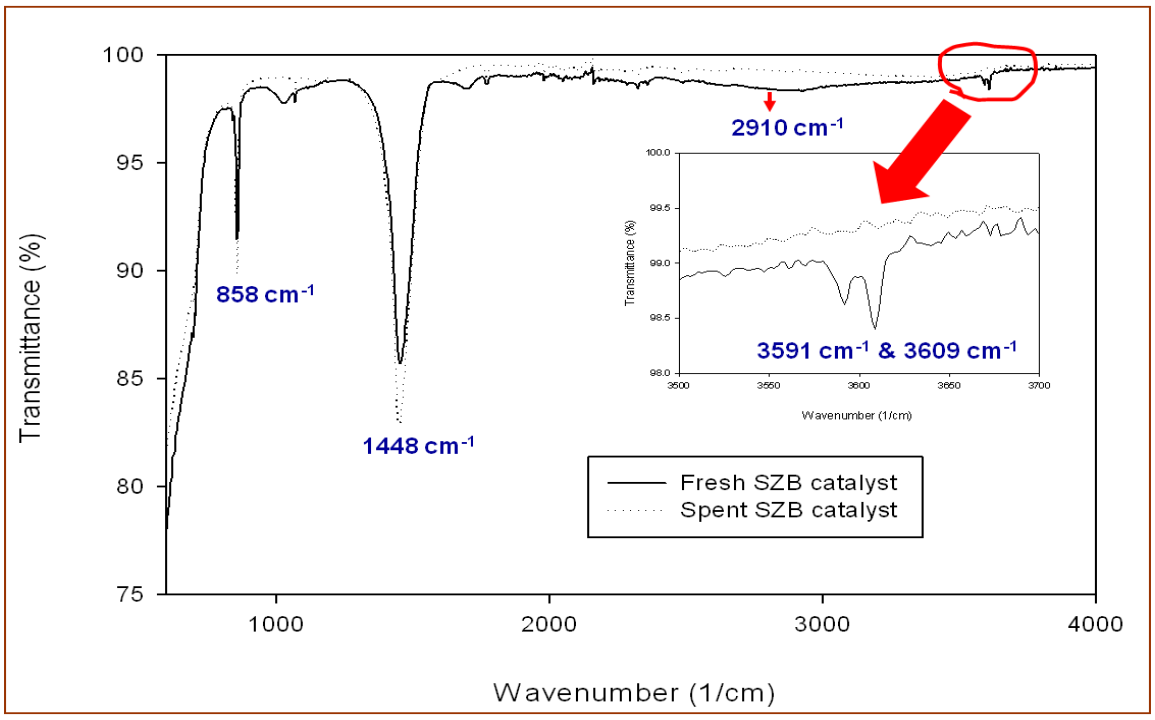

Figure 4.26: FTIR spectra of the fresh and spent SZB catalysts

As shown in Figure 4.26, the disappearance of two sharp spectra peaks at 3591cm^{-1} and 3609cm^{-1} (assigned to OH^- stretching in strontium hydroxide) in the spent SZB catalysts suggests that the dissoluble component of the fresh SZB catalyst leaching into methanol was $Sr(OH)_2$,which was also observed in the XRD results. Leaching of strontium hydroxide into the methanol explains the high FAME yield achieved using methanol filtrate (Figure 4.24(b)). The loss of $Sr(OH)_2$ leads to deactivation of the catalyst and the reduction in FAME yield in Figure 4.24(a). A broad band peak at 2910cm^{-1} in Figure 4.26 identified as the O-H deformation for the water of crystallisation, occurred in the fresh SZB catalyst, but was absent in the spent catalyst. This indicates that the water of crystallization in the fresh SZB catalyst matrix leaches into methanol.

An EDX analysis of the fresh and spent catalyst samples in Table 4.14 also confirmed the results from the XRD and FTIR analyses. The zirconium content increased from 33.8wt% in the fresh SZB catalyst to 37.0wt% in the spent SZB catalyst. The oxygen and strontium contents decreased from 22.5wt% for oxygen and 43.7wt% for strontium in the fresh SZB catalyst to 20.5wt% for oxygen and 42.5wt% for strontium in the spent SZB catalyst. No carbon associated with strontium carbonate was detected in the EDX elemental analysis.

Table 4.14: Elemental compositions of the SZB catalyst by EDX analysis

Elements	Fresh SZB (wt%)	Spent SZB (wt%)	Fresh SZB Sr: Zr : O	Spent SZB Sr : Zr : O
Oxygen	22.54	20.52	3 : 2 : 8 ($SrZrO_3$. $0.5Sr(OH)_2$)	1 : 1 : 3 Mainly: $SrZrO_3$
Strontium	43.71	42.51		
Zirconium	33.76	36.97		

The high percentage of strontium in both fresh and spent SZB catalysts in Table 4.14 indicates that most of the strontium in the sample exists in the form of strontium zirconate ($SrZrO_3$). The inactivity of the spent SZB catalyst in the RSO methanolysis showed that $SrZrO_3$ had no catalytic activity in transesterification of RSO with methanol at all tested temperatures. This is an indication that the zirconium oxide (zirconia) did not just act as a support for SrO, but underwent a chemical reaction producing catalytically inactive strontium zirconate.

4.6.7 Summary

SZB catalyst was screened for its activity, reusability and water tolerance in transesterification of RSO with methanol using an integral baffled meso-OBR in both batch and continuous modes. The SZB catalyst exhibited substantial catalytic activity. The rate of FAME production increased with both temperature and catalyst loading. The rates of FAME production decreased significantly with water content: after 2h reaction time, the FAME yield decreased from 91.7% at 0vol% water to 44.6% at 1.0vol% water and 12.2% at 2.0vol% water for RSO transesterification at a 12:1 methanol to RSO molar ratio, 60˚C and 3wt% catalyst. The catalyst lost its activity with or without the presence of water, due to leaching of the active sites, $Sr(OH)_2$, into the methanol phase. This was confirmed by the XRD, FTIR and EDX analyses. Spent SZB catalyst was found to contain only inert strontium zirconate. It can be concluded that this catalyst cannot be re-used for triglyceride transesterification.

An effective catalyst support is therefore required to minimise the leaching of the catalyst. Hence, the SZB catalyst is recommended for use only in batch transesterification processes, where it would act in a similar manner to conventional

homogeneous alkali catalysts. However, one major advantage of using the SZB catalyst is that the Sr^{2+} ions leaching into the reaction mixture can be easily removed by neutralisation using carbonic acid (H_2CO_3), as the carbonate formed is insoluble.

The integral baffled meso-OBR was successfully used to suspend and screen the SZB catalyst, thereby significantly reducing reagent required and waste generated due to the small volume of the reactor (10mL). Continuous screening of the catalyst in the integral baffled meso-OBR provides information for the reusability of the catalyst without running multiple experiments as in conventional batch reactor screening, reducing processing time and reagents required.

4.7 Heterogeneous esterification of carboxylic acids using $PrSO_3H$-SBA-15 catalyst

This section discusses the results obtained from the methyl esters production by esterification of carboxylic acids using suspended particles of $PrSO_3H$-SBA-15. The catalyst was used to catalyse the esterification of various organic acids: propanoic acid, hexanoic acid, lauric acid and palmitic acid, with methanol. The integral baffled meso-OBR (10mL) was operated in both continuous and batch modes to suspend and screen the $PrSO_3H$-SBA-15 catalyst. Table 4.15 shows the properties of the catalyst.

Table 4.15: Properties of the $PrSO_3H$-SBA-15 catalyst

Pore volume (cm^3/g)	BET surfaces area (m^2/g)	BJH pore size (nm)	Active sites (mmol/g)
0. 782	705	5.1	0.43

The BJH pore size analysis shows that the catalyst was mesoporous (2nm < BJH < 50nm) (Hayati-Ashtiani, 2011; Gregg and Sing, 1982), with pore size of about 5.1nm. Considering the molecular sizes of 2.8nm for pentanoic acid and 4.1nm for tridecanoic acid (Nonhebel, 2005), the pore size of the catalyst was higher than the expected molecular size of propanoic acid and hexanoic acid. Therefore, the acids sites inside the pores will be readily accessible to the molecules of propanoic acid and hexanoic acids. However, large steric hindrance may occur for diffusions of lauric acid and palmitic acid inside the catalyst pore network. Molecular size of lauric acid was expected to be

close to 4.1nm for tridecanoic acid, while that of palmitic acid would be considerably larger than 4.1nm.

4.7.1 Effects of $PrSO_3H$-SBA-15 catalyst loading on carboxylic acid esterification

The option to operate the integral baffled meso-OBR in batch as well as continuous flow conditions permits detailed and rapid kinetic studies. Effect of catalyst mass on reaction rate was investigated (Figure 4.27), and it revealed the first-order kinetics with respect to the catalyst. This verifies the excellent oscillatory mixing characteristics, eliminating bulk diffusion limitations for the short chain hexanoic acid. This reaction was carried out at 30:1 methanol to hexanoic acid molar ratio, Re_o = 2400 and 60˚C reaction temperature over a range of catalyst loadings (5, 7.5 and 10wt% based on hexanoic acid).

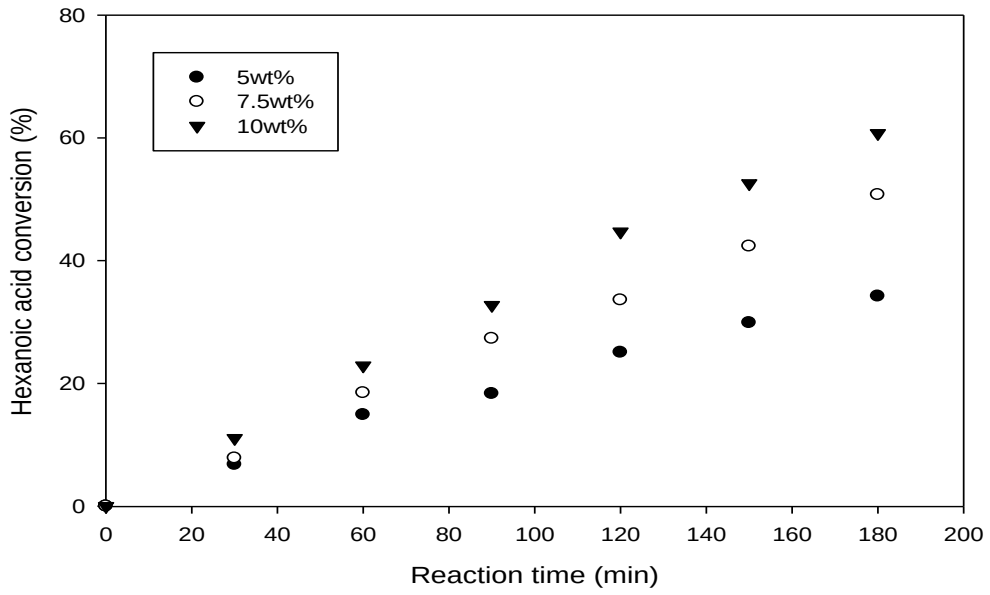

Figure 4.27: Effect of the $PrSO_3H$-SBA-15 catalyst loading on batch esterification of hexanoic acid at 30:1 methanol to hexanoic acid molar ratio, 60˚C temperature and Re_o = 2400, using integral baffles meso-OBR

The hexanoic acid conversion increased linearly with increasing catalyst concentrations. This agreed well with the other findings (Yadav and Mehta, 1994) in which the rate of esterification of acetic acid with phenethyl alcohol and cyclohexanol were directly proportional to the loading of Filtrol-24 and Amberlyst-15 catalysts, in absence of mass transfer limitations. An increase in the conversion at high catalyst loadings is because numbers of the catalyst active sites, which determine the rate of the hexanoic acid

conversion, vary linearly with the amount of catalyst used. The linear relationship between the acid conversion and the catalyst loading indicates that the active sites of the $PrSO_3H$-SBA-15 catalyst were proportionately accessible to the reactants, which is due to the uniform mixing in the integral baffled reactor.

4.7.2 Effect of methanol to acid molar ratio on carboxylic acid esterification

The effect of methanol to carboxylic acid molar ratio was investigated by $PrSO_3H$-SBA-15 catalysed hexanoic acid esterification at 60˚C and methanol to hexanoic acid molar ratios of 1:1, 2:1, 6:1 and 30:1 (Figure 4.28). As shown in Figure 4.28, hexanoic acid conversion was similar for all tested methanol:acid molar ratios up to 30:1 in the first 60 min reaction time. However after 120 min reaction, hexanoic conversion increased with methanol concentration, e.g >30% conversion for a molar ratio of methanol to acid of 30:1, but only 15% for 1:1 after 150 min reaction time.

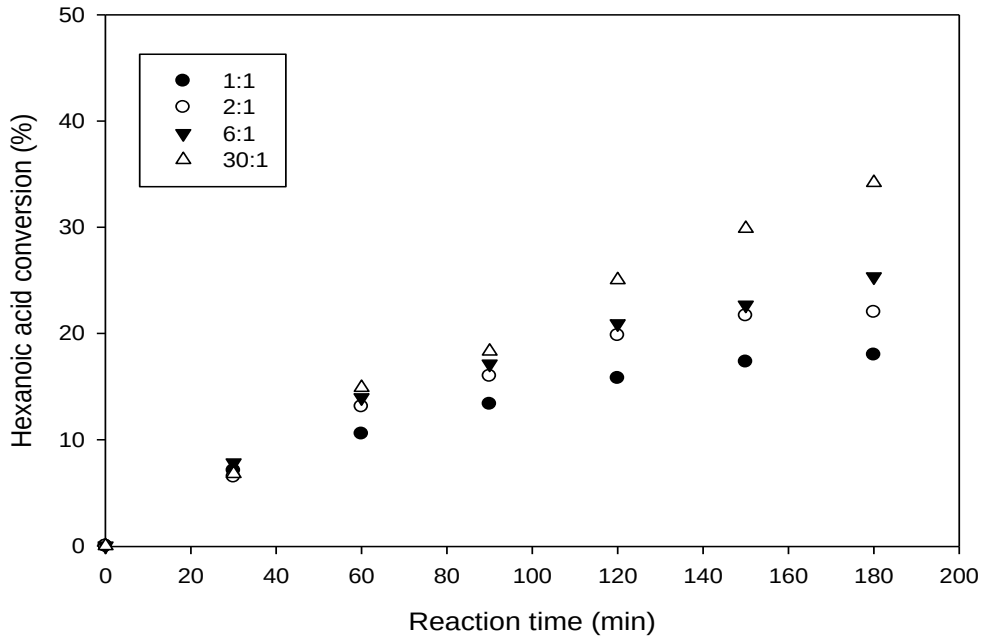

Figure 4.28: Batch esterification of hexanoic acid with methanol using integral baffles meso-OBR as a function of methanol:acid molar ratio at 60˚C, 5wt% $PrSO_3H$-SBA-15 catalyst and Re_o = 2400

The increased hexanoic acid conversion at higher methanol molar ratios was due to the reversible esterification, which requires a large excess of methanol to drive the reaction towards methyl hexanoate formation (equation 4.24).

$$CH_3(CH_2)_4COOH + CH_3OH \leftrightarrow CH_3(CH_2)_4COOCH_3 + H_2O \quad (4.24)$$

Hexanoic acid esterification reached its equilibrium of 18% after 180 min reaction time at low methanol concentrations (1:1 molar ratio). The calculated cumulative TONs at 180min for the hexanoic acid esterification using the $PrSO_3H$-SBA-15 catalyst increased with methanol to acid ratio, as shown in Table 4.16. This could be due to displacement of water from the catalytic active sites by water. Water produced by the esterification reaction may adsorb on the $–SO_3H$ sites of the PrSO3H-SBA-15 catalyst.

Table 4.16: Cumulative TON of the $PrSO_3H$-SBA-15 at various methanol molar ratios

Methanol/acid molar ratio	1:1	2:1	6:1	30:1
TON	65	81	92	137

4.7.3 Effect of water on carboxylic acid esterification

Water was found to have a strong effect on the hexanoic acid esterification as shown in Figure 4.29. The hexanoic acid conversion decreased remarkably with water levels, i.e., hexanoic acid conversion was 18% for zero water content, 10.7% for 2.5vol% water and 5.2% for 5vol% water after 180min reaction time. According to Le Chatelier's principle, as water is a product of the esterification, adding water into the reaction will drive its equilibrium back to the reactant side, reducing the methyl hexanoate yield.

Water poisoning was reported for solid acid catalysts such as $Cs_{2.5}H_{0.5}PW_{12}O_{40}$ (II), SO_4^{2-}/ZrO_2, Amberlyst-15, Nafion-H and $H_3PW_{12}O_{40}$ (Chen *et al.*, 1999). Decreased acrylic acid conversion was observed when 43.7mmol of acrylic acid was reacted with 43.7mmol of 1-butanol at 80°C and 55mmol of water in the presence of the catalysts. At equilibrium, the acrylic acid conversion was less than that obtained in the absence of water by 24% for $Cs_{2.5}H_{0.5}PW_{12}O_{40}$ (II), 99% for SO_4^{2-}/ZrO_2, 69% for Amberlyst-15, 48% for Nafion-H and 42% for $H_3PW_{12}O_{40}$. Sulphated zirconia was the most affected of all the catalysts, losing about 99% of its activity. This indicates that all these catalysts were deactivated by water. For hydrophilic solid acid catalysts, irreversible adsorption of water molecules on the active sites may deactivate the sites.

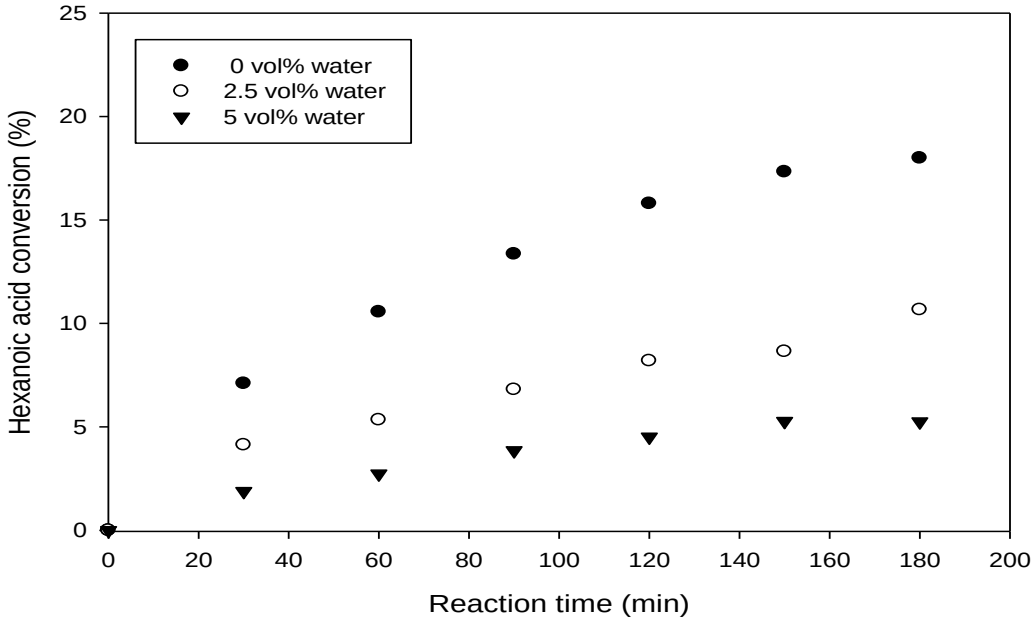

Figure 4.29: Batch esterification of hexanoic acid as a function of water levels in methanol at 1:1 methanol:acid molar ratio, Re_o = 760, 60˚C and 5wt% $PrSO_3H$-SBA-15 catalyst using integral baffles meso-OBR

4.7.4 Effects of carboxylic acid chain length on esterification

Reaction profiles for the batch esterification of a series of propanoic, hexanoic, lauric and palmitic acid (C_3-C_{16}) with methanol in integral baffles meso-OBR, at 30:1 and 60˚C reaction temperature are shown in Figure 4.30. The results clearly showed that the initial rate decreased with increasing acid chain length. This was in agreement with what was reported by Pirez *et al.* (2012) using the $PrSO_3H$-SBA-15 catalyst in a stirred tank batch reactor. The highest conversion was 56.4% for the propanoic acid while the lowest conversion of 5.4% for the palmitic acid after 180min reaction time.

TOF of the $PrSO_3H$-SBA-15 catalyst for the reactions are shown in Table 4.17. TOF of 285 h^{-1} for propanoic acid and 133 h^{-1} for hexanoic were reported for the esterification of the acids at 2:1 methanol to acid molar ratio, 60°C and 1.09g Nafion/silica composite solid acid catalyst (SAC-13) loading per 45mL of reaction mixture (Liu *et al.*, 2006b). The difference in the TOF could be due to higher amount of methanol used in the study and the acid strength of the catalysts. Acidic strength of the catalytic sites has a strong influence on the TOF, i.e., the TOF reported when H_2SO_4 was used were 727 h^{-1} for propanoic and 479 h^{-1} for hexanoic acid (Liu *et al.*, 2006b).

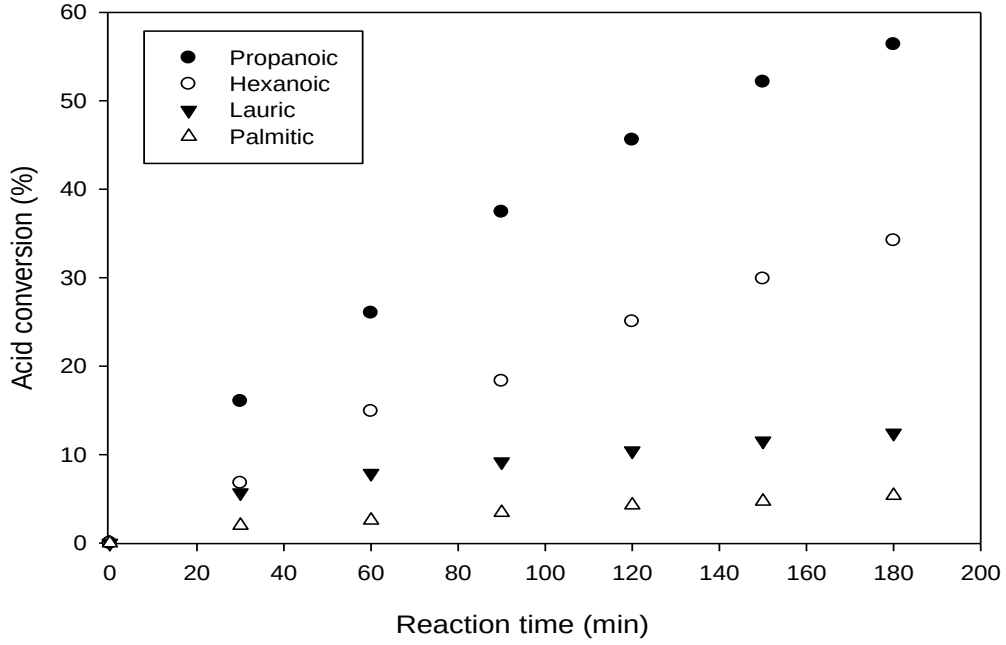

Figure 4.30: Effect of chain length on carboxylic acid conversion during batch esterification in the integral baffled meso-OBR, at a molar ratio of methanol to acid of 30:1, reaction temperature of 60˚C and 5wt% $PrSO_3H$-SBA-15 and Re_o~2400.

Table 4.17: TOF of the $PrSO_3H$-SBA-15 catalyst

Acids	Propanoic	Hexanoic	Lauric	Palmitic
TOF (h^{-1})	201.3	47.0	26.4	7.2

4.7.5 Effect of reaction temperature on carboxylic acid esterification

Reaction temperature had a strong effect on the esterification of hexanoic acid as shown in Figure 4.31. At a methanol to hexanoic acid molar ratio of 1:1 and 5wt% $PrSO_3H$-SBA-15 catalyst, the conversion increased when reaction temperature increased from 40 to 60°C. The calculated apparent activation energy for the hexanoic acid esterification using initial rates of the reaction was 46 ± 3 $kJmol^{-1}$. This was comparable with others (Berrios *et al.*, 2007), who reported activation energies of 51 $kJ.mol^{-1}$ for the esterification of sunflower oil FFA (oleic acid) with methanol at a molar ratio of methanol to acid of 60:1 and 5wt% H_2SO_4 catalyst. Good agreement was also observed with the 46.7 $kJ.mol^{-1}$ reported for oleic acid esterification with ethanol at a 120:1 ethanol/acid molar ratio and 0.1 mol% $SnCl_2$ catalyst (Cardoso *et al.*, 2008), and 46

kJ.mol^{-1} for esterification of propanoic acid with n-amyl alcohol using Amberlyst-15catalyst (Erdem and Cebe, 2006). Activation energies of 53 and 52 kJ.mol^{-1} were also reported for H_2SO_4 and SAC-13 catalysed esterification of acetic acid with methanol, respectively (Liu *et al.*, 2006a).

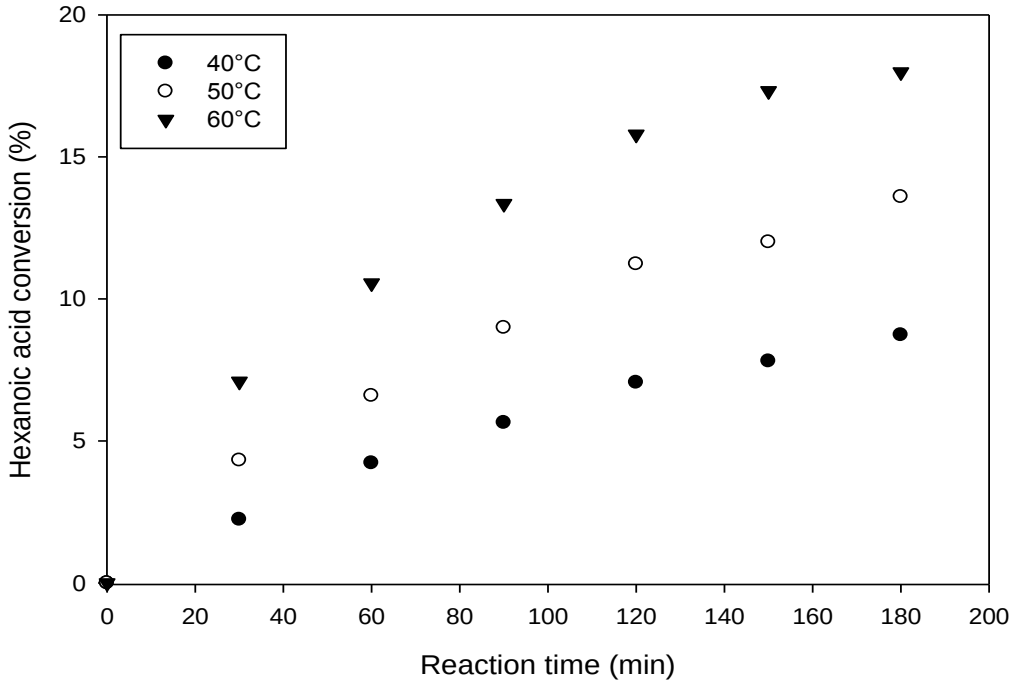

Figure 4.31: Effect of temperature on batch esterification of hexanoic acid at 1:1 methanol to acid molar ratio, 5wt% $PrSO_3H$-SBA-15 catalyst, using integral baffles meso-OBR operated at Re_o ~800

4.7.6 Reusability of the $PrSO_3H$-SBA-15 catalyst

Hexanoic acid and methanol were used as washing solvents for 10%wt $PrSO_3H$-SBA-15 catalyst to investigate the losing catalyst activity. The methanol and hexanoic acid were then collected for further reactions. Esterification was carried out at 60˚C reaction temperature and a 30:1 methanol/hexanoic acid molar without any catalyst, using: methanol leachate (filtrate) and fresh hexanoic acid, fresh methanol and acid leachate, fresh methanol and fresh hexanoic acid. As shown in Figure 4.32, the hexanoic acid conversion was 12-16% for both the methanol filtrate and hexanoic filtrate at 180min reaction time without catalyst. Fresh hexanoic acid and methanol used for the esterification in the absence of catalyst achieved only 5% hexanoic acid conversion. This indicates that the catalyst loses its activity via leaching in both hexanoic acid and methanol.

When spent catalyst was reused for esterification of hexanoic acid at a 30:1 methanol to acid molar ratio, reaction temperature of 60˚C and 5%wt spent $PrSO_3H$-SBA-15 catalyst, there was approximately 50% loss in the activity of the catalyst, i.e., only ~18% hexanoic acid conversion was achieved using spent catalyst compared to 34% obtained from the fresh catalyst after 180min reaction time. This demonstrated that the $PrSO_3H$-SBA-15 catalyst was losing activity, and may not be suitable for continuous esterification process.

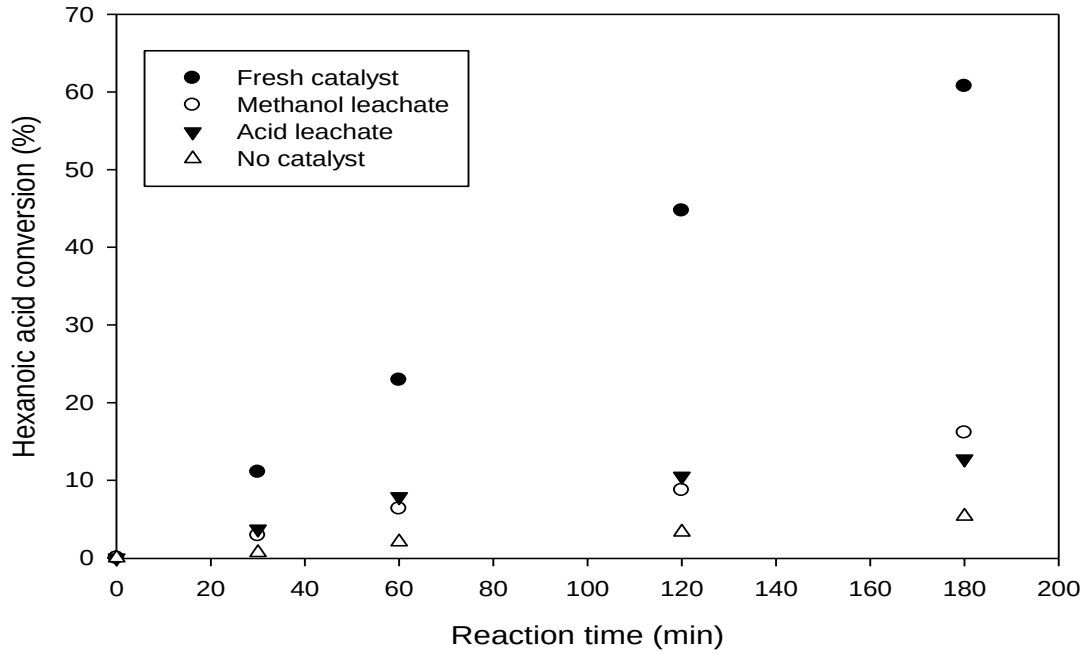

Figure 4.32: Batch esterification of hexanoic acid with methanol in integral baffles meso-OBR at a molar ratio of 30:1, 60˚C reaction temperature (hexanoic acid and methanol leachates - filtrates from leaching 10wt% $PrSO_3H$-SBA-15 catalyst, were reacted with fresh acid and methanol)

FTIR analysis of the fresh and spent $PrSO_3H$-SBA-15 in Figure 4.33 showed a decrease in intensity of O-H broad band at 3400cm^{-1}, assigned to O-H vibration in $–SO_3H$ (Shylesh *et al.*, 2004; Margolese *et al.*, 2000). The decrease in the O-H peak intensity was attributed to loss in $-SO_3H$ group to leaching, which agrees with the results in Figure 4.32. The FTIR clearly shows a strong characteristic Si-O-Si vibration bands at 800cm^{-1} and 1100cm^{-1} assigned to SBA-15 (Xie *et al.*, 2014; Shylesh *et al.*, 2004) in both fresh and spent $PrSO_3H$-SBA-15. No peaks were observed at 2950 – 2850cm^{-1} assigned to methylene stretching of the propyl attached to silica (Shylesh *et al.*, 2004). In contrast to the FTIR results, the EDX elemental analysis showed no difference in

sulphur content for the fresh and spent $PrSO_3H$-SBA-15 catalyst. This was explained by the low active site density of the catalyst (0.43mmol/g). Therefore, differences in the sulphur content of the fresh and spent catalyst could not be quantified.

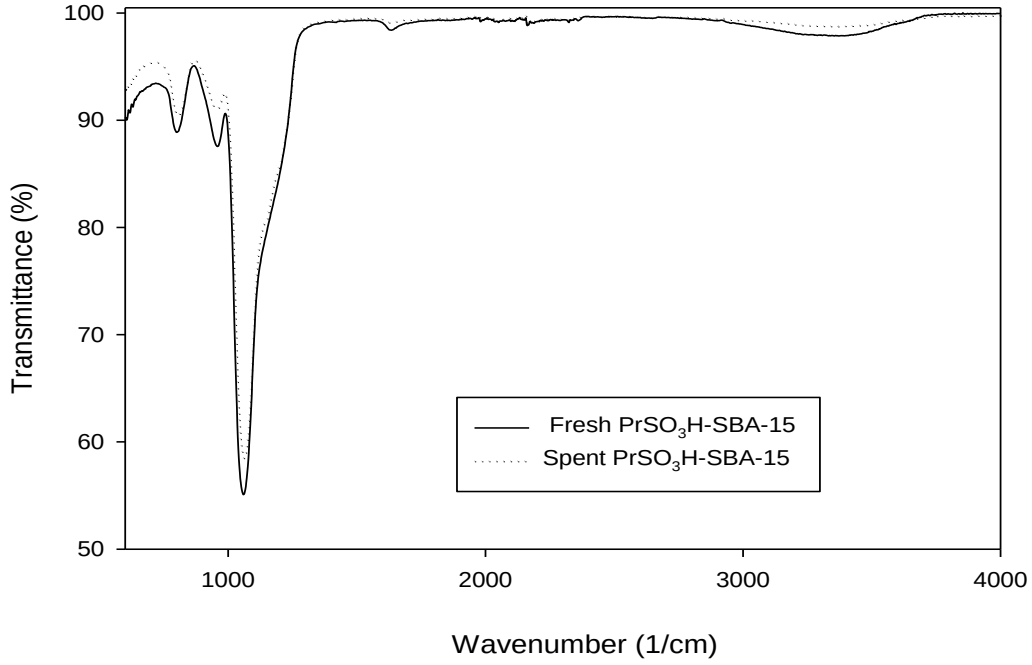

Figure 4.33: FTIR of fresh and spent $PrSO_3H$-SBA-15 catalyst

4.7.7 Continuous esterification of hexanoic acid in integral baffled meso-OBR

The feasibility of solid acid catalysed hexanoic acid esterification with methanol under continuous flow was first investigated at ramped residence times (τ) of 30min and 60min in the integral baffled reactor. As shown in Figure 4.34, the hexanoic acid esterification at 30:1 methanol to hexanoic acid molar ratio, 60˚C and 10wt% catalyst was run continuously at 30min residence time for 105min (3.5τ) and then immediately changed to 60min residence time for 150min (2.5τ) by adjusting the net flows of the reactants. The running times of 2.5 – 3.5τ were used since steady state was achieved in the integral baffles meso-OBR at about 1.5τ. Hexanoic acid conversion maintained at about 15% after ~60 min running time, with the associated TOF of 57 h^{-1} significantly higher than 31 h^{-1} reported previously under stirred batch conditions with the same catalyst (Pirez *et al.*, 2012). Higher TOF at the continuous hexanoic acid esterification in the integral baffles meso-OBR was attributed to continual removal of water produced in the reaction, which adsorb competitively on the catalytic active sites of the $PrSO_3H$-

SBA-15. Adsorption of water reduces the concentration of the catalyst active sites available for catalysing the reaction. Therefore, continuous process allows for intensification of the reaction by removal of water by-product through continuous flow of fresh methanol.

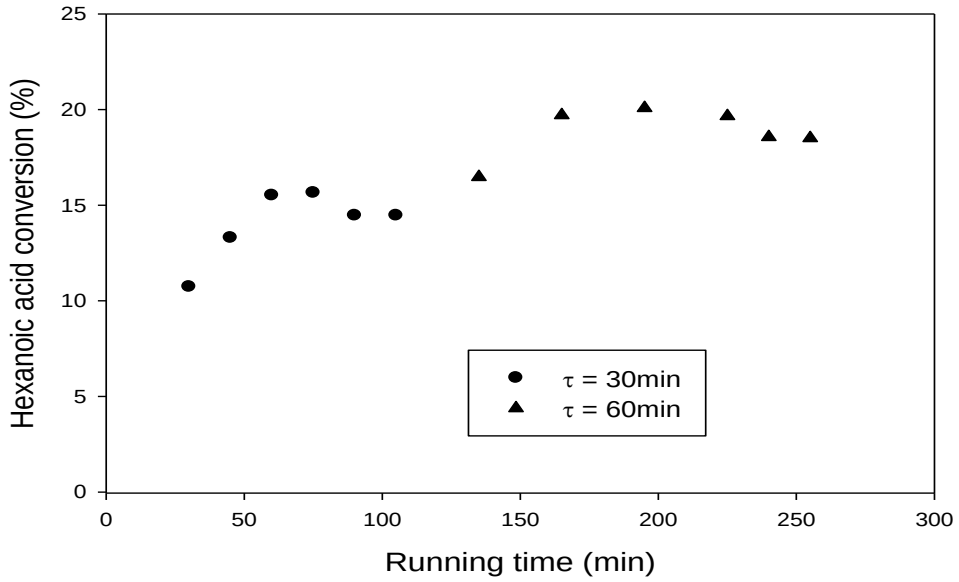

Figure 4.34: Hexanoic acid conversion for continuous esterification in the integral baffled meso-OBR at 30:1 molar ratio of methanol:acid, 60˚C, 10wt% $PrSO_3H$-SBA-15catalyst, residence times (τ) ramped from 30min (Re_n = 3.24) to 60min (Re_n = 1.62) and Re_o = 2400

Doubling the residence time (i.e. τ = 60 min) increased hexanoic acid conversion from 15% to 20%, with the cumulative TON continuing to increase linearly yielding a TOF of 38 h^{-1}. However, there was evidence of reduced hexanoic acid conversion since the conversion does not precisely double, and the conversion falls slightly with running time at this longer residence time. This was attributed to either leaching or gradual poisoning of the catalytic active sites by water, which is a by-product of the esterification reaction. As discussed in section 4.7.6, the EDX analysis of the fresh and spent $PrSO_3H$-SBA-15 catalysts showed no loss in sulphur content which suggests that leaching may be discounted. However, results in Figures 4.32 and 4.33 (section 4.7.6) suggest that the catalyst may be losing its active sites into the reaction mixture by leaching. But, there also chances that the $PrSO_3H$-SBA-15 catalyst was deactivating due to gradual accumulation of water at the acid sites. The effect of deliberately spiking reactions with a controlled amount of water was thus subsequently investigated.

4.7.8 Water tolerance of the $PrSO_3H$-SBA-15 catalyst in a continuous esterification

Water poisoning is a common problem in batch esterification as shown in Figure 4.29 and reported in literature (Liu *et al.*, 2006a; Liu *et al.*, 2006c; Chen *et al.*, 1999). This is a problem in esterification since water is the major by-product. In the case of hydrophilic solid acid catalysts, irreversible water adsorption at the active sites is widely believed to cause deactivation, driving the search for hydrophobic catalysts able to expel water from catalyst surface (Ohimain, 2013). A key advantage of the meso- OBR is to allow a wide range of experimental parameters to be explored in a single experiment in contrast to batch reactions where separate experiments must be conducted to compare initial rates under different conditions. The impact of water on esterification was therefore investigated at a 30:1 methanol:acid ratio using 10wt% catalyst, by injecting 6 mmol H_2O into the reactor after 150 min reaction time (Figure 4.35).

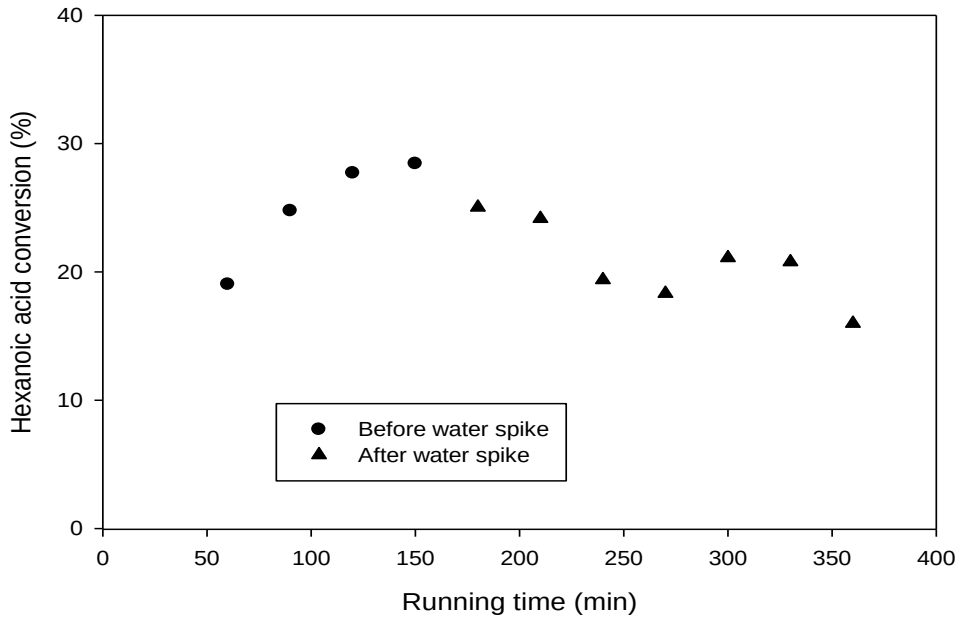

Figure 4.35: Effect of water on continuous esterification of hexanoic acid with methanol using integral baffled meso-OBR at 60˚C, a residence time (τ) of 60 min, 30:1 methanol to acid molar ratio, 10wt% $PrSO_3H$-SBA-15 catalyst, Re_n of 1.62 and Re_o of 2400

The results in Figure 4.35 showed that water addition had some effect on the hexanoic acid conversion, e.g. the conversion dropped from ~ 28% to 19% corresponding to a decrease in TOF from 52 h^{-1} to 37 h^{-1}. This finding agreed with the water spiking in batch esterification of hexanoic acid in Figure 4.29 (section 4.7.3) that presence of water causes reduction in the rate of hexanoic acid esterification. However, the parallel

spiking experiment using the same catalyst under batch conditions evidenced about 51% activity loss (Eze *et al.*, 2013). These results suggest that on-stream deactivation observed under continuous flow does not arise mainly from the accumulation of reactively formed water on the catalyst. The continuous addition of fresh hexanoic acid and methanol, accompanied by water removal, helps to drive esterification in the continuous process. Therefore, $PrSO_3H$-SBA-15 catalyst leaching contributes substantially to the catalyst deactivation in a continuous process.

4.7.9 Kinetics of carboxylic acid esterification - steric effect of chain length

Kinetic analysis was used to explain further the observed reduction in the rates of esterification as the carboxylic acid chain length increased from propanoic acid to palmitic acid. Pseudo-first order kinetics was used in the analysis due to the large excess of methanol: 30:1 methanol to acid molar ratio. The kinetic rate equations used were derived as shown in equations (4.25) – (4.27).

$$-r_A = k_{1e}[A] \tag{4.25}$$

$$-\frac{d[A]}{dt} = \frac{[A]_0 dX_A}{dt} = k_{1e}[A]_0(1 - X_A) \tag{4.26}$$

$$-\ln(1 - X_A) = k_{1e}t \tag{4.27}$$

Note that: $k_{1e} = k_{3e}[Cat][MA]_0 = k_{2e}[MA]_0$

Where:

[A]: concentration of acid ($L.mol^{-1}$); [Cat]: catalyst loading ($g.L^{-1}$)

$[MA]_0$: original concentration of the methanol ($L.mol^{-1}$)

k_{1e}: pseudo-first-order rate constant (s^{-1}); k_{2e}: second-order rate constant ($L.mol^{-1}.s^{-1}$)

k_{3e} = rate constant for esterification per catalyst loading ($L.mol^{-1}.s^{-1}.g_{(cat)}{}^{-1}L$)

Table 4.18: Rate constants for batch esterification of carboxylic acids

Acids	Catalyst loading ($g_{(cat)}L^{-1}$)	$k_{1e}*10^{-6}$ (s^{-1})	$k_{2e}*10^{-7}$ ($L.mol^{-1}.s^{-1}$)	$k_{3e}*10^{-8}$ ($L.mol^{-1}.s^{-1}.g_{(cat)}^{-1}L$)
Propanoic	2.83	75.0	34.2	121.0
Hexanoic	4.38	40.0	19.0	43.5
Lauric	6.58	8.33	4.22	6.41
Palmitic	8.55	3.33	1.78	2.08

Reactions at 30:1 MeOH:Acid molar ratio, 5wt% $PrSO_3H$-SBA-15 catalyst

The pseudo-first-order rate constants (k_{1e}) for the esterification of each acid at 30:1 methanol/acid molar ratios (Table 4.18) were obtained from plots of $-\ln(1-X_A)$ versus time, and were subsequently used to calculate the other rate constants (k_{2e} and k_{3e}). The rate constants for the reactions (k_{3e}) decreased with the carboxylic acid length acid chain.

The influence of acid chain length on the reaction rates was further investigated by the analysis of the M_T for the first-order esterification reactions and comparison with the Taft equation. M_T for the propanoic, hexanoic, lauric and palmitic acid reactions were calculated using equation (4.28). D_e of the organic acids in excess methanol was calculated using equation (4.29).

$$M_T = L\sqrt{\frac{k_{1e}}{D_e}} \qquad (4.28)$$

$$D_e = \frac{D_A \varepsilon_p}{\tau_p} \qquad (4.29)$$

Previous study have shown that mesoporous silica (SBA-15) had ordered cylindrical pore channels (Bonne *et al.*, 2011). Porosity in the range of 0.56 – 0.48 and tortuosity of 4.22 had been reported for the SBA-15 support (Armatas *et al.*, 2003). In order to calculate D_A of the carboxylic acids, Wilke-Chang equation shown in equation (4.30) was used (Wilke and Chang, 1955). M_W was 32.04 $g.mol^{-1}$ for methanol, while the Φ_A for methanol was 1.9. The parameter V_{bA} was calculated using a numerical model (Sastri *et al.*, 1997) in equation (4.31).

$$D_A = \frac{7.4*10^{-8}}{T(V_{bA})^{0.6}}(\Phi_A M_W)^{0.5} \quad (4.30)$$

$$V_{bA} = \frac{V_c}{2.68} \quad (4.31)$$

Table 4.19: Effectiveness of carboxylic acids esterification with $PrSO_3H$-SBA-15[#]

Acids	$k_{1e}*10^{-6}$ (s^{-1})	V_c ($cm^3.mol^{-1}$)	V_{bA} ($cm^3.mol^{-1}$)	D_A*10^{-6} ($cm^2.s^{-1}$)	D_e*10^{-7} ($cm^2.s^{-1}$)	M_T*10^{-4}
Propanoic	75.0	228	85.1	3.98	4.90	4.74
Hexanoic	40.0	396	147.8	2.86	3.52	4.08
Lauric	8.33	732	273.1	1.98	2.44	0.56
Palmitic	3.33	952	356.7	1.68	2.07	0.38

[#]Characteristic length of the catalyst particle = 0.6μm/2 = $6.0*10^{-5}$cm/2 = $3.0*10^{-5}$cm

As shown in Table 4.19, the M_T calculated for the $PrSO_3H$-SBA-15 catalysed esterification of propanoic, hexanoic, lauric and palmitic acids was less than 0.4 in all cases, indicating that the reactions were not limited by diffusion (Levenspiel, 1999). The effectiveness factor for the internal diffusion was nearly unity. Therefore, at the particle size (~0.6μm) used for the study, no significant difference occurred in the concentrations of the carboxylic acids at bulk liquid phase and catalyst pores based on the values of M_T in Table 4.19 (Veljkovic *et al.*, 2009; Levenspiel, 1999).

Another way of explaining the reduction in the rates of organic acids reactions with chain length was by the consideration of the bulk steric effect based on Taft equation proposed by Charton (Asif and Muneer, 2007; Powlson *et al.*, 2005). The Taft model assumes that the rates of acid-catalysed esterification are solely a function of steric effects, in which ν' is the van der Waals radii associated with a particular substituent and ψ' and *h* are constants, as shown in equation (4.32).

A modified form of the Taft equation was used to plot a linear relationship between $\log_{10}$(TOF) and ν' for C_1-C_8 acids (Liu *et al.*, 2006b). However data on ν' for acids >C_8 are not available to extend this correlation to our study for lauric (C_{12}) and palmitic (C_{16}) acids. For a straight chain organic acid, it is reasonable to assume that chain length or

molecular weight will be representative of the steric bulk, and thus may correlate with TOF. A plot of $\log_{10}$(TOF) for C_3-C_{16} organic acids measured in this study versus the chain length in Figure 4.36, confirms a linear relationship extends across the entire series. The influence of carboxylic acid chain length on the esterification rate was correlated using equation (4.33).

$$\log_{10}(\text{TOF}) = -0.09l + 2.5 \quad (4.32)$$

$$\log_{10}(-r_A) = \psi'\nu' + h \quad (4.33)$$

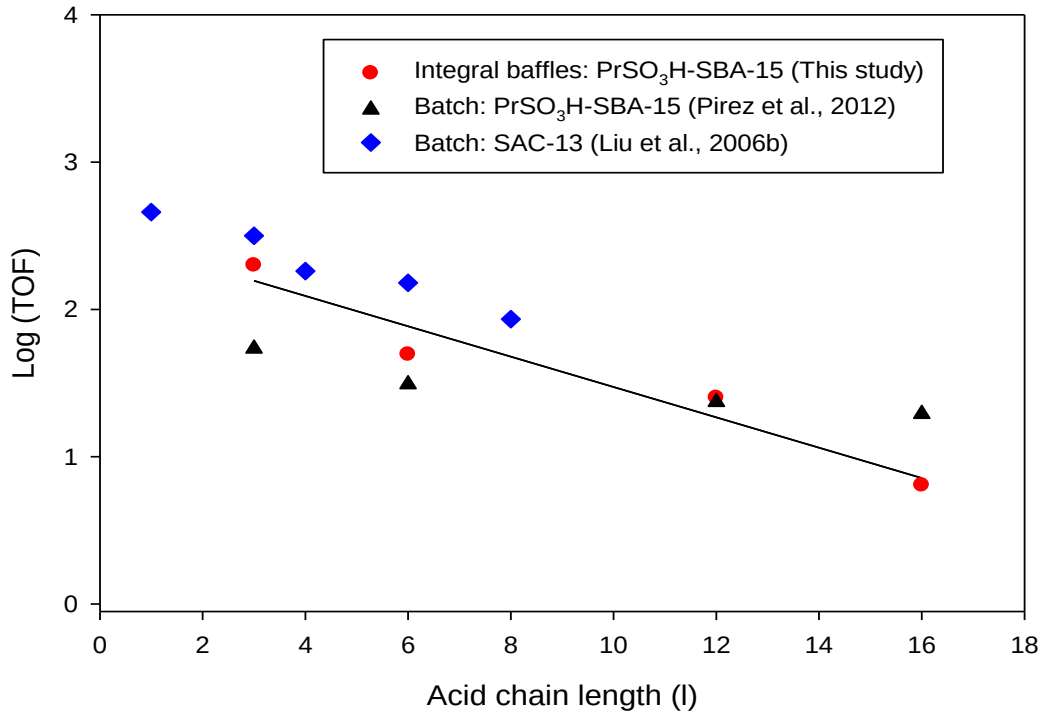

Figure 4.36: Plot of log10(TOF) versus organic acid chain length for esterification with methanol in an integral baffles meso-OBR under batch operation, and in stirred batch reactors using SAC-13 (Liu *et al.*, 2006b) and $PrSO_3H$-SBA-15catalysts (Pirez *et al.*, 2012).

Results in Figure 4.36 show that the rate of esterification of the carboxylic acids was a simple function of alkyl chain length (l). This agreed well with results from stirred tank batch reactor with silica/Nafion composite SAC-13 (Liu et al., 2006b), and stirred tank batch results with $PrSO_3H$-SBA-15 (Pirez et al., 2012). The rates of H_2SO_4 and SAC-13 catalysed esterification of C_2-C_8 organic acids deceased with the acid chain length, which was attributed to a combination of polar and steric influences of the alpha substituent on the carboxylic group (Liu et al., 2006b).

Previous studies have also shown that a linear correlation exist between Taft parameter and reaction rates for C_2-C_8 acids (Lilja *et al.*, 2002). Steric and bulk mixing effects are expected to be more significant for longer chains, wherein conformational changes are likely in order to minimise the interfacial energy between the hydrophobic alkyl chain and polar methanol solvent. For homogeneous catalysts, the impact of such a change in fatty acid 'bulkiness' may be negligible, but for a mesoporous catalyst such as $PrSO_3H$-SBA-15 (pore size ~ 5.1nm), it is likely that such conformational changes would hamper in-pore diffusion, leading to poorer performance of the $PrSO_3H$-SBA-15 compared to SAC-13. However, no diffusion limitation was observed based on the calculated T_M in Table 4.19. This could be due to the use of small $PrSO_3H$-SBA-15 catalyst particle size.

4.7.10 Summary

Heterogeneously $PrSO_3H$-SBA-15 catalysed reaction of propanoic, hexanoic, lauric and palmitic acids with methanol was investigated in batch and continuous modes using the integral baffled meso-OBR. These findings showed that the rate of carboxylic acid conversion increased with methanol molar ratio and temperature, but decreased with water content. The rates of esterification of the organic acids decreased with acid chain length due to steric hindrance. The use of meso-OBR allows for the screening of long residence times with baffled tube reactors of highly reduced length-to-diameter ratio. It also illustrates the capability of meso-OBRs to rapidly and efficiently screen solid catalysts in batch and continuous mode, permitting detailed kinetic studies and rapid optimisation of reaction conditions in a single experiment. Continuous esterification prevented water accumulation in the catalyst sites, as occurred in conventional stirred tank batch reactors.

The $PrSO_3H$-SBA-15 catalyst was found to be ineffective for RSO transesterification due to the narrow pore size. Only 0.13% FAME yield was achieved after 4hr at 60˚C and 5wt% $PrSO_3H$-SBA-15 catalyst for transesterification at 30:1 methanol to RSO molar ratio. The 5.1nm catalyst pore size probably limits the accessibility of RSO to the catalyst active sites in the mesoporous porous network. A solid acid catalyst with larger pore size would be required to catalyse RSO transesterification with methanol.

Chapter 5 Conclusions and Further Work

5.1 Conclusions

5.1.1 RTDs of the meso-OBRs

Three designs of meso-OBRs (integral baffles, wire wool packing and a sharp-edged helical baffle with a central rod) were constructed and their RTD evaluated using pulse injections of KCl tracer. The flow characteristics of the reactors were investigated at various fluid residence times of 2.5min – 60min, corresponding to net flow rates of approximately 0.42mL/min – 4mL/min (Re_n = 0.72 – 17) and oscillation conditions in the range of Re_o = 60 – 1130 (St = 0.05 – 0.4). The findings showed that N increased with Re_n for all the reactor designs, with maximum values of N = 38 for the integrally baffled design, N = 40 for the wire wool packed reactor and N = 33 for the sharp-edged helical baffle with a central rod at Re_o of 250 and 2.5min residence time (Re_n = 17).

The meso-OBRs were found to be capable of achieving a plug flow (N ≥ 10) even at very low net flow rate, Re_n = 0.72 (60min residence time). This is the first study of the RTDs of meso-OBRs at fluid net flow rate less than 0.3mL/min (60min residence time) using meso-OBRs of short length-to-diameter ratio (340mm length and 5mm internal diameter). RTD of meso-OBRs had only been reported at residence times ≤ 30min (Phan *et al.*, 2011a). This study showed that TIS model was effective in fitting the RTD data from the meso-OBRs at Re_o = 250 and Re_n = 0.72 – 17 (St = 0.1). It was observed that the meso-OBRs cannot be operated in plug flow at $Re_o \geq 565$ (St = 0.05) and $Re_n \leq$ 4.25. The mixing intensity at these conditions was very chaotic, leading to a flow pattern that resembles that of a single CSTR. At high mixing intensities ($Re_o \geq 565$) and very low net flow rates, the TIS model does not give good fitting to the experimental data due to large axial dispersion.

Optimal ψ ~11 for wire wool packed reactor and $\psi \sim 60$ for the integral baffles and the sharp-edged helix design with a central rod were obtained from the RTD study at a fixed residence time of 10min (Re_n = 4.25). These values were higher than velocity ration of $2 \leq \psi \leq 4$ reported for plug flow operation in conventional OBR at net flow conditions Re_n = 95 – 252 and St = 0.48 – 1.91 (Stonestreet and Van Der Veeken, 1999),

and $\psi \sim 4 - 8$ (St = 0.4 – 0.8) for central baffles meso-OBR at Re_n = 17.1 – 34 (Phan and Harvey, 2010). The higher values of ψ obtained in this study were due to the use of low fluid net flow rates (Re_n = 0.72 – 17), and are consistent with $\psi \sim 39 - 40$ obtained for an integral baffles meso-OBR at Re_n = 1.27 and $0.2 \leq St \leq 0.13$ (Phan *et al.*, 2011a). Finally, the RTD data from the meso-OBRs were reproducible, and not dependent on the KCl tracer concentration (density) at the experimental conditions (pulse injections using 100µL of 0.25M KCl). The delay time of the conductivity probe was found to be 2.30s, and had no effect on the RTD profiles of the meso-OBRs.

5.1.2 Steady state performance of the meso-OBRs in continuous transesterification

The meso-OBRs were evaluated for their mixing effectiveness and steady state performance in multi-phase liquid-liquid reactions, using continuous base-catalysed homogeneous transesterification of RSO at $Re_n < 2$ and $36 \leq Re_o \leq 160$, 6:1 methanol to RSO molar ratio, 10 min residence time and 60˚C reaction temperature. This study clearly showed that steady states can be easily achieved in all the meso-OBRs, which agrees well with the steady performance of a sharp-edged helix with a central rod in transesterification of RSO with methanol at 50˚C, 1wt% KOH and oscillation condition of Re_o = 316 and St = 0.1 (Phan *et al.*, 2011b). The induction times of the meso-OBRs, generally, decreased with increasing Re_o.

The approximate induction time for the reactor was 1.5τ for integral baffles, 2.0τ for wire wool and 2.5τ for sharp-edged helix with a central rod. There was a critical Re_o for minimizing the induction time for each baffle design: Re_o of 107 for integral baffles and sharp-edged helical baffles with a central rod, and 36 for wire wool. The integral baffles meso-OBR was selected for further screening of alkali-catalysed transesterification, suspension and screening of solid acid and base catalyst due to its superior steady states performance. The shortest time to steady state and highest yield of FAME (86.7 ± 1.3%) was achieved using the integral baffled design at Re_o of 160 (St = 0.05, ψ = 92), 6:1 methanol to RSO molar ratio, 60˚C, 1.5wt% KOH and 10min residence time.

5.1.3 Base-catalysed transesterification in integral baffled meso-OBR

The integrally baffled meso-OBR was selected because of its superior steady state performance – shortest induction time and highest FAME yield. The reactor was used to

screen process conditions in RSO transesterification at 6:1 methanol to RSO molar ratio, 60˚C reaction temperature and Re_o = 160, using various concentrations (0.75 – 1.5wt%) of alkali catalysts: KOH, NaOH and $NaOCH_3$ and residence times in the range of 2.5 – 20min.

The investigations showed that maximum FAME yields were rapidly achieved at relatively short reaction times when operating the reactor at a relatively high catalyst concentration (1.5wt%). The FAME yields obtained were ~97% at 5min for 1.5wt% KOH, ~96% at 10min for 1.5wt% $NaOCH_3$ and ~96% at 15min for 1wt% NaOH catalyst. Increase in the residence time beyond the optimal values caused a significant reduction in FAME content, consistent with what has been reported (Keera *et al.*, 2011; Darnoko and Cheryan, 2000a). This was only observed at higher catalyst concentrations: >1.5wt% for KOH and $NaOCH_3$ and >1wt% for NaOH at 6:1 methanol to RSO molar ratio. The decrease in FAME content was attributed to FAME saponification which was more evident when using KOH and NaOH catalysts than when using $NaOCH_3$. This was due to the higher concentration of hydroxide ions at equilibrium when using the hydroxide catalysts. No FAME saponification occurred at low catalyst concentration.

It was demonstrated in this study that biodiesel can be produced at an industrially acceptable level of conversion (> 96%) in ~ 5min residence time, by a combination of high catalyst concentration, good mixing and tight control of residence time. This represents a substantial reduction in biodiesel production time compared to the 1h typically used in industry for homogenous alkali-catalysed process. The optimal reaction time of ~ 5min using the integral baffles meso-OBR was less than 10 – 15min required to achieve >96% FAME yield in a conventional OBR at Re_o of 700 (Harvey *et al.*, 2003b). These findings showed integral baffles meso-OBR was very effective in multiphase mixing for liquid-liquid reactions, and has the capacity to achieve steady state even at low net flow rates, 2mL/min (Re_n ~1.2). This allows the use of integral baffled reactors of greatly reduced length-to-diameter ratio for screening of reactions with long residence times.

5.1.4 Kinetic model for base-catalysed homogeneous transesterification

A new kinetic model of the reaction scheme of alkali-catalysed homogeneous transesterification of RSO with methanol was developed and successfully used for

numerical investigations of the unexpected reduction in FAME content in base-catalysed transesterification reactions. The model integrated more of the reactions occurring in the base-catalysed transesterification than any other in the literature. The full set of reactions was: RSO and FAME saponification, consecutive reversible transesterification reactions, FFA neutralization and the hydroxide-methoxide equilibrium. Reaction schemes in the literature so far have not included the hydroxide-methoxide equilibrium, nor the saponification reactions. The model was implemented by numerical modelling in MATLAB using ODE45 solver (Runge-Kutta method), and validated using experimental data. The findings showed that the new kinetic model was much more robust. It explains various phenomena that the conventional reaction scheme does not, such as the peak in FAME production observed at higher catalyst concentrations (35wt%). The existence of FAME peak was due to the reaction sequence: $\mathrm{TG} \rightarrow \mathrm{FAME} \rightarrow \mathrm{Soap}$. The conventional kinetic model cannot predict the effects of RSO and FAME saponification because of the assumption that side reactions are negligible. This study embodies the first experimental investigations of the kinetics of triglyceride and FAME saponification in alkali-catalysed transesterification. Before now, no study has investigated the decrease in FAME content after maximum yield was achieved. Therefore, integration of the saponification kinetic data into the transesterification reaction scheme, which was carried out in this study, was a major contribution in understanding of the homogeneous transesterification process. The decrease in FAME content at residence times beyond the optimal values can be explained quantitatively based on the findings in the study.

The model simulation results clearly showed that rapid biodiesel production (reaction times below 2 min) at economically viable levels of conversion can be achieved by increasing base catalyst and methanol concentrations without significant problems due to excess soap formation, even in the presence of water and FFAs. Importantly, the prediction of 2min reaction time by the model was validated by experiment. The model predicts that methanol: oil molar ratios of above 9:1 are required to obtain high FAME (96.3% maximum) yield at higher catalyst concentrations (> 1.5wt% KOH). For 2wt% KOH, a methanol to oil molar ratio above 12:1 was recommended to minimise saponification reactions. The experimental and modelling results showed that RSO and FAME saponification was accelerated by water, because water reacts with methoxide ions to form hydroxide ions, which drive the saponification reactions. Methanol to oil molar ratio above 12:1 could be used for feedstocks containing 0 – 1.0wt % water to

achieve ~95% maximum FAME yield at 12:1 methanol to oil molar ratio. However, there could be an additional cost of catalyst utilisation and excess methanol recovery for commercial production of biodiesel using this protocol. Therefore, further studies are needed to optimise the process conditions.

It was observed that the kinetic rate constants of FAME saponification that fitted the model was lower in the transesterification mixture compared with what was calculated for FAME saponification in methanol-KOH. This was attributed to removal of hydroxide ions from the reaction mixture by glycerol produced during RSO transesterification. There may be need for improvement on the kinetic model developed in this study, by integration of hydroxide-glycerol reaction kinetics.

5.1.5 Transesterification of RSO using the SZB catalyst

SZB catalyst was suspended and screened for its activity, reusability and water tolerance in transesterification of RSO with methanol using the integral baffles meso-OBR in both batch and continuous modes. The catalyst exhibited substantial catalytic activity, with FAME production increasing with both temperature and catalyst loading. Reaction rate constants were $2.5*10^{-3}$ $L.mol^{-1}.min^{-1}$ at 40˚C, $6.1*10^{-3}$ $L.mol^{-1}.min^{-1}$ at 50˚C and $11.3*10^{-3}$ $L.mol^{-1}.min^{-1}$ at 60˚C, from which activation energy of 65.5kJ.mol^{-1} were calculated.

The SZB catalyst lost its activity with or without the presence of water, due to leaching of the active sites, $Sr(OH)_2$, into the methanol phase, which was confirmed by XRD, FTIR and EDX analyses. Rates of FAME production decreased significantly with water content due to RSO and FAME saponification. The SZB catalyst was prone to leaching, similar to other supported strontium oxide catalysts such as SrO-MgO (Yoosuk *et al.*, 2010) and SrO-SiO_2 (Chen *et al.*, 2012a). Findings from this study showed that the ZrO_2 support in the SZB catalyst reacted with the SrO to form catalytically inactive $SrZO_3$. Therefore, more investigations are needed to find a suitable supporting material for the SrO. A possible advantage of using the SZB catalyst over homogeneous alkaline catalyst is that the Sr^{2+} ions leaching into the reaction mixture can be easily removed by neutralisation using carbonic acid (H_2CO_3), as the carbonate formed is insoluble.

Finally, continuous screening of the SZB catalyst in the meso-OBR platform quickly provides valuable information for assessment of the activity and reusability of the

catalyst without the need for multiple experiments. In conventional batch reactor screening, multiple reactions will be required to investigate these parameters. The integrally baffled meso-OBR was successfully used to suspend and screen SZB solid catalysts, thereby significantly reducing reagent required and waste generated due to the small volume of the reactor (10mL).

5.1.6 Esterification of carboxylic acids using the $PrSO_3H$-SBA-15 catalyst.

Solid-catalysed liquid-liquid reaction in a meso-OBR was investigated using the $PrSO_3H$-SBA-15 catalysed carboxylic acid esterification. This reaction has a wide application in synthesis of fine chemicals and biofuels, such as biodiesel. The solid $PrSO_3H$-SBA-15 particles were uniformly suspended by imposing oscillatory flows, and screened for catalytic activity in esterification of propanoic, hexanoic, lauric and palmitic acids. It was found that the rates of esterification of carboxylic acids increase with reaction temperature and methanol molar ratio, but decreased with water content. Excess methanol was required to shift the reaction towards methyl ester production in accordance with Le Chatelier's principle for reversible reactions. Increasing carboxylic acid chain length led to increased steric effects, which reduced the rates of esterification.

The $PrSO_3H$-SBA-15 catalyst was found to be unsuitable for use in transesterification of RSO even at 30:1 methanol to RSO molar ratio, as only 0.13% FAME yield was achieved after 4hr at 60˚C and 5wt% catalyst. The 5.1nm catalyst pore size probably limits the accessibility of RSO to the catalyst active sites in the mesoporous porous network. Poor catalytic performance of $PrSO_3H$-SBA-15 was also reported for triolein transesterification with methanol, where only 0.1 – 0.3wt% FAME was achieved after 6h reaction at 60˚C (Dacquin *et al.*, 2012). A solid acid catalyst with larger pore size on a hydrophobic support would be an ideal catalyst for simultaneous esterification of FFA and transesterification of vegetable oils for efficient FAME production.

This study showed that the integral baffles meso-OBR has the capability for rapid and efficient continuous screening of catalysed liquid-liquid and solid-liquid-liquid reactions, permitting detailed kinetic studies and rapid optimisation of reaction conditions in a single experiment. Continuous flow operation significantly lowers the detrimental effect of water upon equilibrium-limited esterification, as less deactivation was observed in continuous esterification than in batch mode using the meso-OBR. This indicates that continuous inflow of reactants prevents an accumulation of water on the

catalyst surface which occurs in conventional stirred batch reactors and poisons the $PrSO_3H$-SBA-15 catalyst in batch esterification. Based on this study, the decrease in sulphur content and loss in activity of alkyl sulphonic acid supported mesoporous silica for triglyceride transesterification at 180˚C (Melero *et al.,* 2008) and 150˚C (Karimi *et al.,* 2012) was as a result of leaching and not thermal decomposition. At the moderate temperature (60˚C) used in this study, thermal degradation was not expected for the $PrSO_3H$-SBA-15 catalyst. Hence, the deactivation occurred due to leaching. Water poisoning was also not a factor in the catalyst deactivation reported by Melero *et al*. (2008) and Karimi *et al,* (2012) since transesterification process does not generate water.

5.2 Further work

5.2.1 The homogeneous alkali catalysts

The main objective of this research was achieved in that a meso-OBR platform was constructed and characterised for screening of homogeneous and heterogeneous catalysts for biodiesel production reactions. Homogeneous alkali-catalysed RSO transesterification using alkali metal hydroxides/methoxides remain the fastest route to biodiesel production at relatively low temperature (40 – 60˚C). This explains why these catalysts are the most commonly used type for commercial biodiesel processes. The homogeneous alkali-catalysed biodiesel process was investigated more in this study using experimental and numerical modelling. It is recommended that more investigations should be carried out to validate the model predictions on the possibility of processing vegetable oil of ~1wt% water content using alkali-catalysed transesterification at higher methanol molar ratio (>12:1). Further studies may also be required to improve the kinetic model developed in this study, by integrating the reaction kinetics of glycerol-metal hydroxide interactions in base-catalysed transesterification.

5.2.2 The solid catalysts

The solid catalysts screened in this study did not satisfy the required criteria for suitable heterogeneous biodiesel catalysts: high catalytic activity towards vegetable oil transesterification (FFA esterification) and reusability. The SZB catalyst showed substantial catalytic activity for RSO transesterification, but produces soap in the presence of water and leaches completely into the reaction mixture. Therefore, the SZB catalyst was not reusable for biodiesel production, the mode of catalysis was similar to that of homogeneous base catalysts. On the order hand, the $PrSO_3H$-SBA-15 showed no significant activity for RSO transesterification. This catalyst was active only for FFA esterification, where some sort of loss in activity due to leaching and water poisoning was observed.

In view of the shortcomings encountered in the SZB and $PrSO_3H$-SBA-15 catalysts, the following modifications are proposed:

(a) Further studies should be carried out to formulate a stable solid catalyst based on SrO. The application of ZrO_2 as SrO support in the SZB resulted in formation of $SrZrO_3$, with no catalytic activity. Therefore, a more stable catalytic support is needed for SrO.

(b) $PrSO_3H$-SBA-15 catalysed vegetable oil transesterification at moderate temperature (60˚C) should be further investigated using pore-expanded $PrSO_3H$-SBA-15. The mesoporous silica support (SBA-15) can be expanded by using porogens, such as trimethylbenzene (Chen *et al.*, 2006), triethylbenzene or triisopropylbenzene (Cao *et al.*, 2009) to swell the Pluronic P123 micelles for production of SBA-15 of mesopores with diameters 5 – 30 nm. A sulphonic acid functionalised hydrophobic support based on pore-expanded $PrSO_3H$-SBA-15 will be a suitable choice of solid acid catalyst for simultaneous transesterification of vegetable oil and FFA esterification.

5.2.3 Two-stage biodiesel process

A two-stage continuous biodiesel process using suitable and non-leaching forms of the SZB and $PrSO_3H$-SBA-15 catalysts or other appropriate heterogeneous base and acid catalysts is being proposed for investigations. Due to the low rates of acid-catalysed transesterification, a two-stage process - with FFA esterification in the first reactor and solid base-catalysed triglyceride transesterification in the second reactor would be useful in processing waste vegetable oils. This will reduce the cost of biodiesel production by using waste oils which are cheaper feedstock, and by producing biodiesel and FAME that require less downstream purifications.

5.2.4 Guide on selection of heterogeneous catalysts for biodiesel processes

Solid catalysts meant for industrial production of biodiesel must be affordable to satisfy the requirement for large-scale transesterification processes. The catalyst must also be stable and catalytically active at the operating conditions. Ideally, such catalysts would be able to catalyse FFA esterification and triglyceride transesterification simultaneously, to allow for the use of various waste oils that contain high levels of FFA. To further reduce the cost of heating and equipment, heterogeneous catalysts that operate at lower temperature and pressure would be more useful in reducing the overall operating cost of

biodiesel production. Porous catalysts designed for production of biodiesel from vegetable oil should have macroporous network to allow for effective diffusion of triglyceride into the catalytic active sites.

References

Abdullah, A. Z., Razali, N. and Lee, K. T. (2009) 'Optimization of mesoporous K/SBA-15 catalyzed transesterification of palm oil using response surface methodology', *Fuel Processing Technology,* 90, (7-8), pp. 958-964.

AOCS. (1998) *Official Test Method Cd 3b-76 for Saponification Value. In Official Methods and Recommended Practices of the American Oil Chemists Society,* 5th edition, *AOCS*: Champaign, Illinois, USA.

Armatas, G. S., Salmas, C. E., Louloudi, M., Androutsopoulos, G. P. and Pomonis, P. J. (2003) 'Relationships among pore size, connectivity, dimensionality of capillary condensation, and pore structure tortuosity of functionalized mesoporous silica', *Langmuir,* 19, (8), pp. 3128-3136.

Asif, M. and Muneer, T. (2007) 'Energy supply, its demand and security issues for developed and emerging economies', *Renewable and Sustainable Energy Reviews,* 11, (7), pp. 1388-1413.

ASTM. (2008) *Standard specification for biodiesel fuel (B100) blend stock for distillate fuels, Method D6751-08. In: Annual Book of ASTM Standards,* ASTM International: West Conshohocken, USA.

Atkins, P. and de Paula, J. (2006) *Physical Chemistry,* 8th edition, Oxford University Press: London.

Bacce, E. D., Pires, A. M., Davalos, M. R. and Jafelicci Jr, M. (2001) 'Thermal decomposition and rehydration of strontium oxalate: morphological evolution', *International Journal of Inorganic Materials,* 3, (6), pp. 443-452.

Baird, M. H. I. and Stonestreet, P. (1995) 'Energy dissipation in oscillatory flow within a baffled tube', *Chemical Engineering Research and Design,* 73, (A5), pp. 503-511.

Balat, M. and Balat, H. (2010) 'Progress in biodiesel processing', *Applied Energy,* 87, (6), pp. 1815-1835.

Bambase, M. E., Nakamura, N., Tanaka, J. and Matsumura, M. (2007) 'Kinetics of hydroxide-catalyzed methanolysis of crude sunflower oil for the production of fuel-grade methyl esters', *Journal of Chemical Technology & Biotechnology,* 82, (3), pp. 273-280.

Bannon, C., Craske, J. and Hilliker, A. (1986) 'Analysis of fatty acid methyl esters with high accuracy and reliability. V. Validation of theoretical relative response factors of unsaturated esters in the flame lonization detector', *Journal of the American Oil Chemists' Society,* 63, (1), pp. 105-110.

Barrett, E. P., Joyner, L. G. and Halenda, P. P. (1951) 'The determination of pore volume and area distributions in porous substances. I. Computations from nitrogen isotherms', *Journal of the American Chemical Society,* 73, (1), pp. 373-380.

Belfiore, L. A. (2003) *Transport phenomena for chemical reactor design.* John Wiley & Sons: New York, USA.

Berni, M. D., and Manduca, P. C. (2014) 'Bioethanol program in Brazil: Production and utilization of trade-offs for CO_2 abatement', *Journal of Clean Energy Technologies,* 2, (1), pp. 57-60.

Berrios, M., Siles, J., Martín, M. A. and Martín, A. (2007) 'A kinetic study of the esterification of free fatty acids (FFA) in sunflower oil', *Fuel,* 86, (15), pp. 2383-2388.

Boey, P. L., Maniam, G. P., Hamid, S. A. and Ali, D. M. H. (2011) 'Crab and cockle shells as catalysts for the preparation of methyl esters from low free fatty acid chicken fat', *Journal of the American Oil Chemists' Society,* 88, (2), pp. 283-288.

Bondioli, P. (2004) 'The preparation of fatty acid esters by means of catalytic reactions', *Topics in Catalysis,* 27, (1-4), pp. 77-82.

Bonne, M., Sellam, D., Dacquin, J.-P., Lee, A. F., Wilson, K., Olivi, L., Cognigni, A., Marecot, P., Royer, S. and Duprez, D. (2011) 'A general route to synthesize supported isolated oxide and mixed-oxide nanoclusters at sizes below 5 nm', *Chemical Communications,* 47, (5), pp. 1509-1511.

Boocock, D. B., Konar, S., Mao, V., Lee, C. and Buligan, S. (1998) 'Fast formation of high-purity methyl esters from vegetable oils', *Journal of the American Oil Chemists' Society,* 75, (9), pp. 1167-1172.

Bournay, L., Casanave, D., Delfort, B., Hillion, G. and Chodorge, J. A. (2005) 'New heterogeneous process for biodiesel production: A way to improve the quality and the value of the crude glycerin produced by biodiesel plants', *Catalysis Today,* 106, (1-4), pp. 190-192.

Brunauer, S., Emmett, P. H. and Teller, E. (1938) 'Adsorption of gases in multimolecular layers', *Journal of the American Chemical Society,* 60, (2), pp. 309-319.

Brunold, C. R., Hunns, J. C. B., Mackley, M. R. and Thompson, J. W. (1989) 'Experimental observations on flow patterns and energy losses for oscillatory flow in ducts containing sharp edges', *Chemical Engineering Science,* 44, (5), pp. 1227-1244.

BSI. (2003) *Fat and oil derivatives - Fatty acid methyl esters (FAME) for diesel engines - Determination of esters and linolenic acid methyl ester contents, Designation BS EN 14103,* British Standards Institution: Chiswick High Road, London.

Caldin, E. F. and Long, G. (1954) 'The equilibrium between ethoxide and hydroxide ions in ethanol and in ethanol-water mixtures', *Journal of the Chemical Society (Resumed),* pp. 3737-3742.

[References]

Canakci, M. and Van Gerpen, J. (2003) 'A Pilot plant to produce biodiesel from high free fatty acid feedstocks', *Transactions of the American Society of Agricultural Engineers,* 46, (4), pp. 945-954.

Canola Council of Canada. (2011) *The history of canola.* Available at: http://www.canolacouncil.org/oil-and-meal/what-is-canola/the-history-of-canola/ (Accessed on 12th November, 2013).

Cao, L., Man, T. and Kruk, M. (2009) 'Synthesis of ultra-large-pore SBA-15 silica with two-dimensional hexagonal structure using triisopropylbenzene as micelle expander', *Chemistry of Materials,* 21, (6), pp. 1144-1153.

Cardoso, A., Neves, S. and Da Silva, M. (2008) 'Esterification of oleic acid for biodiesel production catalyzed by $SnCl_2$: A kinetic investigation', *Energies,* 1, (2), pp. 79-92.

Cardoso, A. L., Neves, S. C. G. and Da Silva, M. J. (2009) 'Kinetic study of alcoholysis of the fatty acids catalyzed by tin chloride(II): An alternative catalyst for biodiesel production', *Energy and Fuels,* 23, (3), pp. 1718-1722.

Cavalcante, L. S., Simões, A. Z., Sczancoski, J. C., Longo, V. M., Erlo, R., Escote, M. T., Longo, E. and Varela, J. A. (2007) '$SrZrO_3$ powders obtained by chemical method: Synthesis, characterization and optical absorption behaviour', *Solid State Sciences,* 9, (11), pp. 1020-1027.

CEN. (2003) *Automotive fuels - fatty acid methyl esters (FAME) for diesel engines - requirements and tests methods, Designation EN 14214:2003,* European Committee for Standardisation: Brussels, Belgium.

Cervero, J. M., Coca, J. and Luque, S. (2008) 'Production of biodiesel from vegetable oils', *Grasas y Aceites,* 59, (1), pp. 76-83.

Chen, C. L., Huang, C. C., Tran, D. T. and Chang, J. S. (2012a) 'Biodiesel synthesis via heterogeneous catalysis using modified strontium oxides as the catalysts', *Bioresource Technology,* 113, (0), pp. 8-13.

Chen, D., Li, Z., Wan, Y., Tu, X., Shi, Y., Chen, Z., Shen, W., Yu, C., Tu, B. and Zhao, D. (2006) 'Anionic surfactant induced mesophase transformation to synthesize highly ordered large-pore mesoporous silica structures', *Journal of Materials Chemistry,* 16, (16), pp. 1511-1519.

Chen, X., Qian, W. W., Lu, X. P. and Han, P. F. (2012b) 'Preparation of biodiesel catalysed by KF/CaO with ultrasound', *Natural Product Research,* 26, (13), pp. 1249-1256.

Chen, X., Xu, Z. and Okuhara, T. (1999) 'Liquid phase esterification of acrylic acid with 1-butanol catalyzed by solid acid catalysts', *Applied Catalysis A: General,* 180, (1–2), pp. 261-269.

Colucci, J. A., Borrero, E. and Alape, F. (2005) 'Biodiesel from an alkaline transesterification reaction of soybean oil using ultrasonic mixing', *Journal of the American Oil Chemists' Society,* 82, (7), pp. 525-530.

Dacquin, J. P., Lee, A. F., Pirez, C. and Wilson, K. (2012) 'Pore-expanded SBA-15 sulfonic acid silicas for biodiesel synthesis', *Chemical Communications,* 48, (2), pp. 212-214.

Danckwerts, P. V. (1995) 'Continuous flow systems. Distribution of residence times : P. V. Danckwerts, Chem. Engng Sci. 2: 1-13, 1953', *Chemical Engineering Science,* 50, (24), pp. 3855-3855.

Darnoko, D. and Cheryan, M. (2000a) 'Continuous production of palm methyl esters', *Journal of the American Oil Chemists' Society,* 77, (12), pp. 1269-1272.

Darnoko, D. and Cheryan, M. (2000b) 'Kinetics of palm oil transesterification in a batch reactor', *Journal of the American Oil Chemists' Society,* 77, (12), pp. 1263-1267.

de Caprariis, B., Di Rita, M., Stoller, M., Verdone, N. and Chianese, A. (2012) 'Reaction-precipitation by a spinning disc reactor: Influence of hydrodynamics on nanoparticles production', *Chemical Engineering Science,* 76, pp. 73-80.

Demirbas, A. (2002) 'Diesel fuel from vegetable oil via transesterification and soap pyrolysis', *Energy Sources,* 24, (9), pp. 835-842.

Demirbas, A. (2005) 'Biodiesel production from vegetable oils via catalytic and non-catalytic supercritical methanol transesterification methods', *Progress in Energy and Combustion Science,* 31, (5-6), pp. 466-487.

Demirbas, A. (2006) 'Biodiesel production via non-catalytic SCF method and biodiesel fuel characteristics', *Energy Conversion and Management,* 47, (15-16), pp. 2271-2282.

Demirbas, A. (2009) 'Progress and recent trends in biodiesel fuels', *Energy Conversion and Management,* 50, (1), pp. 14-34.

Demirbas, M. F. and Balat, M. (2006) 'Recent advances on the production and utilization trends of bio-fuels: A global perspective', *Energy Conversion and Management,* 47, (15-16), pp. 2371-2381.

Department for Transport. (2011) *Implementation of the transport elements of the Renewable Energy Directive.* http://www.dft.gov.uk/consultations/dft-2011-05: (Accessed on 6th November, 2013).

Deshmane, V. G. and Adewuyi, Y. G. (2013a) 'Mesoporous nanocrystalline sulfated zirconia synthesis and its application for FFA esterification in oils', *Applied Catalysis A: General,* 462-463, pp. 196-206.

Deshmane, V. G. and Adewuyi, Y. G. (2013b) 'Synthesis and kinetics of biodiesel formation via calcium methoxide base catalyzed transesterification reaction in the absence and presence of ultrasound', *Fuel,* 107, pp. 474-482.

Dessimoz, A.-L., Cavin, L., Renken, A. and Kiwi-Minsker, L. (2008) 'Liquid–liquid two-phase flow patterns and mass transfer characteristics in rectangular glass microreactors', *Chemical Engineering Science,* 63, (16), pp. 4035-4044.

[References]

Dhainaut, J., Dacquin, J. P., Lee, A. F. and Wilson, K. (2010) 'Hierarchical macroporous-mesoporous SBA-15 sulfonic acid catalysts for biodiesel synthesis', *Green Chemistry*, 12, (2), pp. 296-303.

Di Serio, M., Tesser, R., Pengmei, L. and Santacesaria, E. (2008) 'Heterogeneous catalysts for biodiesel production', *Energy and Fuels*, 22, (1), pp. 207-217.

Doell, R., Konar, S. and Boocock, D. B. (2008) 'Kinetic Parameters of a Homogeneous Transmethylation of Soybean Oil', *Journal of the American Oil Chemists' Society*, 85, (3), pp. 271-276.

Dorado, M. P., Ballesteros, E., Mittelbach, M. and López, F. J. (2004) 'Kinetic Parameters Affecting the Alkali-Catalyzed Transesterification Process of Used Olive Oil', *Energy & Fuels*, 18, (5), pp. 1457-1462.

Dossin, T. F., Reyniers, M. F. and Marin, G. B. (2006) 'Kinetics of heterogeneously MgO-catalyzed transesterification', *Applied Catalysis B: Environmental*, 62, (1-2), pp. 35-45.

EBB (2013) *Statistics of the European Biodiesel Industry*, European Biodiesel Board. Available at: http://www.ebb-eu.org/stats.php (Accessed: 5th November, 2013).

Elsheikh, Y. A., Man, Z., Bustam, M. A., Akhtar, F. H., Yusup, S. and Muhammad, A. (2014) 'Preparation and characterisation of Citrulus colocynthis oil biodiesel: Optimisation of alkali-catalysed transesterification', *Canadian Journal of Chemical Engineering*, 92 (3), pp. 435-440.

Endalew, A. K., Kiros, Y. and Zanzi, R. (2011) 'Inorganic heterogeneous catalysts for biodiesel production from vegetable oils', *Biomass and Bioenergy*, 35, (9), pp. 3787-3809.

Erdem, B. and Cebe, M. (2006) 'Kinetics of esterification of propionic acid with n-amyl alcohol in the presence of cation exchange resins', *Korean Journal of Chemical Engineering*, 23, (6), pp. 896-901.

Eterigho, E. J., Lee, J. G. M. and Harvey, A. P. (2011) 'Triglyceride cracking for biofuel production using a directly synthesised sulphated zirconia catalyst', *Bioresource Technology*, 102, (10), pp. 6313-6316.

Eze, V. C., Phan, A. N., Pirez, C., Harvey, A. P., Lee, A. F. and Wilson, K. (2013) 'Heterogeneous catalysis in an oscillatory baffled flow reactor', *Catalysis Science & Technology*, 3, (9), pp. 2373-2379.

Fogler, H. S. (2005) *Elements of chemical reaction engineering*, 3rd edition, Prentice-Hall: New Delhi, India.

Fortes, I. C. P. and Baugh, P. J. (2004) 'Pyrolysis-GC/MS studies of vegetable oils from Macauba fruit', *Journal of Analytical and Applied Pyrolysis*, 72, (1), pp. 103-111.

[References]

Freedman, B., Butterfield, R. O. and Pryde, E. H. (1986) 'Transesterification kinetics of soybean oil[1]', *Journal of the American Oil Chemists' Society,* 63, (10), pp. 1375-1380.

Freedman, B., Pryde, E. H. and Mounts, T. L. (1984) 'Variables affecting the yields of fatty esters from transesterified vegetable oils', *Journal of the American Oil Chemists Society,* 61, (10), pp. 1638-1643.

Furuta, S., Matsuhashi, H. and Arata, K. (2004) 'Biodiesel fuel production with solid superacid catalysis in fixed bed reactor under atmospheric pressure', *Catalysis Communications,* 5, (12), pp. 721-723.

Furuta, S., Matsuhashi, H. and Arata, K. (2006) 'Biodiesel fuel production with solid amorphous-zirconia catalysis in fixed bed reactor', *Biomass and Bioenergy,* 30, (10), pp. 870-873.

Garcia, C. M., Teixeira, S., Marciniuk, L. L. and Schuchardt, U. (2008) 'Transesterification of soybean oil catalyzed by sulfated zirconia', *Bioresource Technology,* 99, (14), pp. 6608-6613.

Gately, C. K., Hutyra, L. R., Wing, I. S. and Brondfield, M. N. (2013) 'A bottom up approach to on-road CO_2 emissions estimates: Improved spatial accuracy and applications for regional planning', *Environmental Science & Technology,* 47, (5), pp. 2423-2430.

Glass, R. (1971) 'Alcoholysis, saponification and the preparation of fatty acid methyl esters', *Lipids,* 6, (12), pp. 919-925.

Glisic, S. and Skala, D. (2009) 'The problems in design and detailed analyses of energy consumption for biodiesel synthesis at supercritical conditions', *The Journal of Supercritical Fluids,* 49, (2), pp. 293-301.

Goff, M., Bauer, N., Lopes, S., Sutterlin, W. and Suppes, G. (2004) 'Acid-catalyzed alcoholysis of soybean oil', *Journal of the American Oil Chemists' Society,* 81, (4), pp. 415-420.

Gogate, P. R. (2008) 'Cavitational reactors for process intensification of chemical processing applications: A critical review', *Chemical Engineering and Processing: Process Intensification,* 47, (4), pp. 515-527.

Gole, V. L. and Gogate, P. R. (2012) 'A review on intensification of synthesis of biodiesel from sustainable feed stock using sonochemical reactors', *Chemical Engineering and Processing: Process Intensification,* 53, pp. 1-9.

Gotch, A. J., Reeder, A. J. and McCormick, A. (2009) 'Study of heterogeneous base catalysts for biodiesel production', *Journal of Undergraduate Chemistry Research,* 8, (1), pp. 22-26.

Gregg, S. and Sing, K. S. W. (1982) *Adsorption surface area and porosity,* 2nd edition, Academic Press: London.

[References]

Gryglewicz, S. (1999) 'Rapeseed oil methyl esters preparation using heterogeneous catalysts', *Bioresource Technology,* 70, (3), pp. 249-253.

Haas, M. J. (2005) 'Improving the economics of biodiesel production through the use of low value lipids as feedstocks: vegetable oil soapstock', *Fuel Processing Technology,* 86, (10), pp. 1087-1096.

Hammond, G. P., Kallu, S. and McManus, M. C. (2008) 'Development of biofuels for the UK automotive market', *Applied Energy,* 85, (6), pp. 506-515.

Harvey, A. P., Mackley, M. R., Reis, N., Vicente, A. A. and Teixeira, J. A. (2003a) *The 4th European Congress of Chemical Engineering.* Granada, Spain, 21st – 25th September 2003.

Harvey, A. P., Mackley, M. R. and Seliger, T. (2003b) 'Process intensification of biodiesel production using a continuous oscillatory flow reactor', *Journal of Chemical Technology and Biotechnology,* 78, (2-3), pp. 338-341.

Harvey, A. P., Mackley, M. R. and Stonestreet, P. (2001) 'Operation and optimization of an oscillatory flow continuous reactor', *Industrial and Engineering Chemistry Research,* 40, (23), pp. 5371-5377.

Hattori, H., Shima, M. and Kabashima, H. (2000) 'Alcoholysis of ester and epoxide catalyzed by solid bases', in *Studies in Surface Science and Catalysis,* 130, pp. 3507-3512.

Hayati-Ashtiani, M. (2011) 'Characterization of nano-porous bentonite (montmorillonite) particles using FTIR and BET-BJH analyses', *Particle & Particle Systems Characterization,* 28, (3-4), pp. 71-76.

Hayes, R. E. and Mmbaga, J. P. (2012) *Introduction to chemical reactor analysis,* 2nd edition, CRC Press Inc., Bosa Roca, USA.

Helwani, Z., Othman, M. R., Aziz, N., Kim, J. and Fernando, W. J. N. (2009) 'Solid heterogeneous catalysts for transesterification of triglycerides with methanol: A review', *Applied Catalysis A: General,* 363, (1-2), pp. 1-10.

Hou, X., Qi, Y., Qiao, X., Wang, G., Qin, Z. and Wang, J. (2007) 'Lewis acid-catalyzed transesterification and esterification of high free fatty acid oil in subcritical methanol', *Korean Journal of Chemical Engineering,* 24, (2), pp. 311-313.

Howes, T. and Mackley, M. R. (1990) 'Experimental axial dispersion for oscillatory flow through a baffled tube', *Chemical Engineering Science,* 45, (5), pp. 1349-1358.

Howes, T., Mackley, M. R. and Roberts, E. P. L. (1991) 'The simulation of chaotic mixing and dispersion for periodic flows in baffled channels', *Chemical Engineering Science,* 46, (7), pp. 1669-1677.

Hoydonckx, H., De Vos, D., Chavan, S. and Jacobs, P. (2004) 'Esterification and transesterification of renewable chemicals', *Topics in Catalysis,* 27, (1-4), pp. 83-96.

Huber, G. W., Iborra, S. and Corma, A. (2006) 'Synthesis of transportation fuels from biomass: Chemistry, catalysts, and engineering', *Chemical Reviews,* 106, (9), pp. 4044-4098.

IEA. (2009) *Transport, Energy and CO_2.* International Energy Agency Publications: Paris.

IEA. (2010) *World energy outlook 2010.* International Energy Agency Publications: Paris.

International Grain Council. (2008) *Grain market trends in the stockfeed and biodiesel industries.* Australian Grain 17, pp. 30-31.

Issariyakul, T. and Dalai, A. K. (2012) 'Comparative kinetics of transesterification for biodiesel production from palm oil and mustard oil', *The Canadian Journal of Chemical Engineering,* 90, (2), pp. 342-350.

Jähnisch, K., Hessel, V., Löwe, H. and Baerns, M. (2004) 'Chemistry in microstructured reactors', *Angewandte Chemie,* International Edition, 43, (4), pp. 406-446.

Jeong, G. T. and Park, D. H. (2008) 'Lipase-catalyzed transesterification of rapeseed oil for biodiesel production with tert-butanol', *Applied Biochemistry and Biotechnology,* 148, (1-3), pp. 131-139.

Jitputti, J., Kitiyanan, B., Rangsunvigit, P., Bunyakiat, K., Attanatho, L. and Jenvanitpanjakul, P. (2006) 'Transesterification of crude palm kernel oil and crude coconut oil by different solid catalysts', *Chemical Engineering Journal,* 116, (1), pp. 61-66.

Jovanović, J., Rebrov, E. V., Nijhuis, T. A., Kreutzer, M. T., Hessel, V. and Schouten, J. C. (2011) 'Liquid-liquid flow in a capillary microreactor: hydrodynamic flow patterns and extraction performance', *Industrial & Engineering Chemistry Research,* 51, (2), pp. 1015-1026.

Kalbande, S. R., More, G. R. and Nadre, R. G. (2008) 'Biodiesel production from non-edible oils of Jatropha and Karanj for utilization in electrical generator', *BioEnergy Research,* 1, (2), pp. 170-178.

Kalu, E. E., Chen, K. S. and Gedris, T. (2011) 'Continuous-flow biodiesel production using slit-channel reactors', *Bioresource Technology,* 102, (6), pp. 4456-4461.

Karimi, B., Mirzaei, H. M. and Mobaraki, A. (2012) 'Periodic mesoporous organosilica functionalized sulfonic acids as highly efficient and recyclable catalysts in biodiesel production', *Catalysis Science and Technology,* 2, (4), pp. 828-834.

Karmee, S. K., Chandna, D., Ravi, R. and Chadha, A. (2006) 'Kinetics of base-catalyzed transesterification of triglycerides from Pongamia oil', *Journal of the American Oil Chemists' Society,* 83, (10), pp. 873-877.

Keera, S. T., El Sabagh, S. M. and Taman, A. R. (2011) 'Transesterification of vegetable oil to biodiesel fuel using alkaline catalyst', *Fuel,* 90, (1), pp. 42-47.

Kim, H. J., Kang, B. S., Kim, M. J., Park, Y. M., Kim, D. K., Lee, J. S. and Lee, K. Y. (2004) 'Transesterification of vegetable oil to biodiesel using heterogeneous base catalyst', *Catalysis Today*, 93-95, pp. 315-320.

Kinney, A. J. and Clemente, T. E. (2005) 'Modifying soybean oil for enhanced performance in biodiesel blends', *Fuel Processing Technology*, 86, (10), pp. 1137-1147.

Kirumakki, S. R., Nagaraju, N. and Chary, K. V. R. (2006) 'Esterification of alcohols with acetic acid over zeolites Hβ, HY and HZSM5', *Applied Catalysis A: General*, 299, (0), pp. 185-192.

Klofutar, B., Golob, J., Likozar, B., Klofutar, C., Zagar, E. and Poljansek, I. (2010) 'The transesterification of rapeseed and waste sunflower oils: Mass-transfer and kinetics in a laboratory batch reactor and in an industrial-scale reactor/separator setup', *Bioresource Technology*, 101, (10), pp. 3333-3344.

Knothe, G. (2006) 'Analyzing biodiesel: standards and other methods', *Journal of the American Oil Chemists' Society*, 83, (10), pp. 823-833.

Knothe, G. (2008) '"Designer" biodiesel: Optimizing fatty ester composition to improve fuel properties', *Energy & Fuels*, 22, (2), pp. 1358-1364.

Kockmann, N. (2008) 'Process engineering methods and microsystem technology'. In *Micro Process Engineering: Fundamentals, devices, fabrication, and applications* (Editor), Wiley-VCH Verlag GmbH: Germany, pp. 1-45.

Kumar, D., Kumar, G., Poonam and Singh, C. P. (2010) 'Fast, easy ethanolysis of coconut oil for biodiesel production assisted by ultrasonication', *Ultrasonics Sonochemistry*, 17, (3), pp. 555-559.

Kusdiana, D. and Saka, S. (2001) 'Kinetics of transesterification in rapeseed oil to biodiesel fuel as treated in supercritical methanol', *Fuel*, 80, (5), pp. 693-698.

Lam, M. K., Lee, K. T. and Mohamed, A. R. (2010) 'Homogeneous, heterogeneous and enzymatic catalysis for transesterification of high free fatty acid oil (waste cooking oil) to biodiesel: A review', *Biotechnology Advances*, 28, (4), pp. 500-518.

Lee, D. W., Park, Y. M. and Lee, K. Y. (2009) 'Heterogeneous base catalysts for transesterification in biodiesel synthesis', *Catalysis Surveys from Asia*, pp. 1-15.

Lee, K. T. and Ofori-Boateng, C. (2013) *Sustainability of biofuel production from oil palm biomass*, Springer: Singapore.

Lee, O. K., Kim, Y. H., Na, J. G., Oh, Y. K. and Lee, E. Y. (2013) 'Highly efficient extraction and lipase-catalyzed transesterification of triglycerides from Chlorella sp. KR-1 for production of biodiesel', *Bioresource Technology*, 147, pp. 240-245.

[References]

Leung, D. Y. C. and Guo, Y. (2006) 'Transesterification of neat and used frying oil: Optimization for biodiesel production', *Fuel Processing Technology,* 87, (10), pp. 883-890.

Levenson, H. S. and Smith, H. A. (1940) 'Kinetics of the saponification of the ethyl esters of several phenyl substituted aliphatic acids[1]', *Journal of the American Chemical Society,* 62, (9), pp. 2324-2327.

Levenspiel, O. (1999) *Chemical reaction engineering,* 3rd edition. John Wiley & Sons: New York, USA.

Lilja, J., Murzin, D. Y., Salmi, T., Aumo, J., Mäki-Arvela, P. and Sundell, M. (2002) 'Esterification of different acids over heterogeneous and homogeneous catalysts and correlation with the Taft equation', *Journal of Molecular Catalysis A: Chemical,* 182–183, pp. 555-563.

Lima, D. G., Soares, V. C. D., Ribeiro, E. B., Carvalho, D. A., Cardoso, E. C. V., Rassi, F. C., Mundim, K. C., Rubim, J. C. and Suarez, P. A. Z. (2004) 'Diesel-like fuel obtained by pyrolysis of vegetable oils', *Journal of Analytical and Applied Pyrolysis,* 71, (2), pp. 987-996.

Lima, J. R. d. O., Ghani, Y. A., da Silva, R. B., Batista, F. M. C., Bini, R. A., Varanda, L. C. and de Oliveira, J. E. (2012) 'Strontium zirconate heterogeneous catalyst for biodiesel production: Synthesis, characterization and catalytic activity evaluation', *Applied Catalysis A: General,* 445–446, pp. 76-82.

Lin, L., Cunshan, Z., Vittayapadung, S., Xiangqian, S. and Mingdong, D. (2011) 'Opportunities and challenges for biodiesel fuel', *Applied Energy,* 88, (4), pp. 1020-1031.

Liu, X., He, H., Wang, Y. and Zhu, S. (2007) 'Transesterification of soybean oil to biodiesel using SrO as a solid base catalyst', *Catalysis Communications,* 8, (7), pp. 1107-1111.

Liu, X., He, H., Wang, Y., Zhu, S. and Piao, X. (2008) 'Transesterification of soybean oil to biodiesel using CaO as a solid base catalyst', *Fuel,* 87, (2), pp. 216-221.

Liu, Y., Lotero, E. and Goodwin Jr, J. G. (2006a) 'A comparison of the esterification of acetic acid with methanol using heterogeneous versus homogeneous acid catalysis', *Journal of Catalysis,* 242, (2), pp. 278-286.

Liu, Y., Lotero, E. and Goodwin Jr, J. G. (2006b) 'Effect of carbon chain length on esterification of carboxylic acids with methanol using acid catalysis', *Journal of Catalysis,* 243, (2), pp. 221-228.

Liu, Y., Lotero, E. and Goodwin Jr, J. G. (2006c) 'Effect of water on sulfuric acid catalyzed esterification', *Journal of Molecular Catalysis A: Chemical,* 245, (1–2), pp. 132-140.

López, D. E., Goodwin Jr, J. G., Bruce, D. A. and Lotero, E. (2005) 'Transesterification of triacetin with methanol on solid acid and base catalysts', *Applied Catalysis A: General,* 295, (2), pp. 97-105.

Lotero, E., Liu, Y., Lopez, D. E., Suwannakarn, K., Bruce, D. A. and Goodwin Jr, J. G. (2005) 'Synthesis of biodiesel via acid catalysis', *Industrial and Engineering Chemistry Research*, 44, (14), pp. 5353-5363.

Ma, F., Clements, L. D. and Hanna, M. A. (1998) 'The effects of catalyst, free fatty acids, and water on transesterification of beef tallow', *Transactions of the American Society of Agricultural Engineers*, 41, (5), pp. 1261-1264.

Ma, F. and Hanna, M. A. (1999) 'Biodiesel production: a review', *Bioresource Technology*, 70, (1), pp. 1-15.

Macedo, C. C. S., Abreu, F. R., Tavares, A. P., Alves, M. B., Zara, L. F., Rubim, J. C. and Suarez, P. A. Z. (2006) 'New heterogeneous metal-oxides based catalyst for vegetable oil trans-esterification', *Journal of the Brazilian Chemical Society*, 17, pp. 1291-1296.

Mackley, M. R. and Ni, X. (1991) 'Mixing and dispersion in a baffled tube for steady laminar and pulsatile flow', *Chemical Engineering Science*, 46, (12), pp. 3139-3151.

Mackley, M. R., Smith, K. B. and Wise, N. P. (1993) 'Mixing and separation of particle suspensions using oscillatory flow in baffled tubes', *Chemical Engineering Research and Design*, 71, (A6), pp. 649-656.

Mackley, M. R., Tweddle, G. M. and Wyatt, I. D. (1990) 'Experimental heat transfer measurements for pulsatile flow in baffled tubes', *Chemical Engineering Science*, 45, (5), pp. 1237-1242.

MacLeod, C. S., Harvey, A. P., Lee, A. F. and Wilson, K. (2008) 'Evaluation of the activity and stability of alkali-doped metal oxide catalysts for application to an intensified method of biodiesel production', *Chemical Engineering Journal*, 135, (1-2), pp. 63-70.

Maki-Arvela, P., Kubickova, I., Snare, M., Eranen, K. and Murzin, D. Y. (2007) 'Catalytic deoxygenation of fatty acids and their derivatives', *Energy and Fuels*, 21, (1), pp. 30-41.

Margolese, D., Melero, J. A., Christiansen, S. C., Chmelka, B. F. and Stucky, G. D. (2000) 'Direct syntheses of ordered sba-15 mesoporous silica containing sulfonic acid groups', *Chemistry of Materials*, 12, (8), pp. 2448-2459.

Matthaus, B. and Bruhl, L. (2001) 'Comparison of different methods for the determination of the oil content in oilseeds', *Journal of the American Oil Chemists' Society*, 78, (1), pp. 95-102.

Mazubert, A., Poux, M. and Aubin, J. l. (2013) 'Intensified processes for FAME production from waste cooking oil: A technological review', *Chemical Engineering Journal*, 233, pp. 201-223.

[References]

Melero, J. A., Bautista, L. F., Morales, G., Iglesias, J. and Briones, D. (2008) 'Biodiesel production with heterogeneous sulfonic acid-functionalized mesostructured catalysts', *Energy & Fuels,* 23, (1), pp. 539-547.

Mishra, S. R., Mohanty, M. K., Das, S. P. and Pattanaik, A. K. (2013) 'Optimisation of base-catalysed transesterification of Simarouba glauca oil for biodiesel production', *International Journal of Sustainable Energy*, pp. 1-8.

Mittelbach, M., and Remschmidt, C. (2006) *Biodiesel - the comprehensive handbook,* Graz: Austria.

Mittelbach, M. and Trathnigg, B. (1990) 'Kinetics of alkaline catalyzed methanolysis of sunflower oil', *Lipid / Fett,* 92, (4), pp. 145-148.

Morgunov, A. N., Perchenko, A. A. and Chernina, L. P. (1977) 'Process kinetics of neutralization of fatty acids from oxidized paraffin with aqueous sodium hydroxide solution', *Chemistry and Technology of Fuels and Oils,* 13, (1), pp. 42-44.

Moser, B. (2009) 'Biodiesel production, properties, and feedstocks', *In Vitro Cellular & Developmental Biology - Plant,* 45, (3), pp. 229-266.

Naik, M., Meher, L. C., Naik, S. N. and Das, L. M. (2008) 'Production of biodiesel from high free fatty acid Karanja (Pongamia pinnata) oil', *Biomass and Bioenergy,* 32, (4), pp. 354-357.

Nakpong, P. and Wootthikanokkhan, S. (2010) 'High free fatty acid coconut oil as a potential feedstock for biodiesel production in Thailand', *Renewable Energy,* 35, (8), pp. 1682-1687.

Ni, X., Jian, H. and Fitch, A. W. (2002) 'Computational fluid dynamic modelling of flow patterns in an oscillatory baffled column', *Chemical Engineering Science,* 57, (14), pp. 2849-2862.

Ni, X. and Pereira, N. E. (2000) 'Parameters affecting fluid dispersion in a continuous oscillatory baffled tube', *AIChE Journal,* 46, (1), pp. 37-45.

Niczke, L., Czechowski, F. and Gawel, I. (2007) 'Oxidized rapeseed oil methyl ester as a bitumen flux: Structural changes in the ester during catalytic oxidation', *Progress in Organic Coatings,* 59, (4), pp. 304-311.

Noiroj, K., Intarapong, P., Luengnaruemitchai, A. and Jai-In, S. (2009) 'A comparative study of KOH/Al_2O_3 and KOH/NaY catalysts for biodiesel production via transesterification from palm oil', *Renewable Energy,* 34, (4), pp. 1145-1150.

Nonhebel, S. (2005) 'Renewable energy and food supply: will there be enough land?', *Renewable and Sustainable Energy Reviews,* 9, (2), pp. 191-201.

Noureddini, H. and Zhu, D. (1997) 'Kinetics of transesterification of soybean oil', *Journal of the American Oil Chemists' Society*, 74, (11), pp. 1457-1463.

[References]

O'Brien, R. D. (2008) *Fats and Oils: Formulating and Processing for Applications,* 3rd edition. CRC Press Inc.: Florida, USA.

Ohimain, E. I. (2013) 'A review of the Nigerian biofuel policy and incentives (2007)', *Renewable and Sustainable Energy Reviews,* 22, pp. 246-256.

Ong, H. C., Silitonga, A. S., Masjuki, H. H., Mahlia, T. M. I., Chong, W. T. and Boosroh, M. H. (2013) 'Production and comparative fuel properties of biodiesel from non-edible oils: Jatropha curcas, Sterculia foetida and Ceiba pentandra', *Energy Conversion and Management,* 73, pp. 245-255.

Owen, N. A., Inderwildi, O. R. and King, D. A. (2010) 'The status of conventional world oil reserves-Hype or cause for concern?', *Energy Policy,* 38, (8), pp. 4743-4749.

Pask, S. D., Nuyken, O. and Cai, Z. (2012) 'The spinning disk reactor: an example of a process intensification technology for polymers and particles', *Polymer Chemistry,* 3, (10), pp. 2698-2707.

Phan, A. N. and Harvey, A. (2010) 'Development and evaluation of novel designs of continuous mesoscale oscillatory baffled reactors', *Chemical Engineering Journal,* 159, (1-3), pp. 212-219.

Phan, A. N., Harvey, A. and Lavender, J. (2011a) 'Characterisation of fluid mixing in novel designs of mesoscale oscillatory baffled reactors operating at low flow rates (0.3-0.6ml/min)', *Chemical Engineering and Processing: Process Intensification,* 50, (3), pp. 254-263.

Phan, A. N. and Harvey, A. P. (2011) 'Effect of geometrical parameters on fluid mixing in novel mesoscale oscillatory helical baffled designs', *Chemical Engineering Journal,* 169, (1-3), pp. 339-347.

Phan, A. N., Harvey, A. P. and Eze, V. (2012) 'Rapid production of biodiesel in mesoscale oscillatory baffled reactors', *Chemical Engineering & Technology,* 35, (7), pp. 1214-1220.

Phan, A. N., Harvey, A. P. and Rawcliffe, M. (2011b) 'Continuous screening of base-catalysed biodiesel production using New designs of mesoscale oscillatory baffled reactors', *Fuel Processing Technology,* 92, (8), pp. 1560-1567.

Pirez, C., Caderon, J.-M., Dacquin, J.-P., Lee, A. F. and Wilson, K. (2012) 'Tunable KIT-6 mesoporous sulfonic acid catalysts for fatty acid esterification', *ACS Catalysis,* 2, (8), pp. 1607-1614.

Powlson, D. S., Riche, A. B. and Shield, I. (2005) 'Biofuels and other approaches for decreasing fossil fuel emissions from agriculture', *Annals of Applied Biology,* 146, (2), pp. 193-201.

Prošková, A., Kučera, J., Kopicová, Z. and Škarková, L. (2013) 'Comparison of three methods for rendering plant fat transesterification', *Research in Agricultural Engineering,* 59, (2), pp. 51-55.

[References]

Qiu, Z., Petera, J. and Weatherley, L. R. (2012) 'Biodiesel synthesis in an intensified spinning disk reactor', *Chemical Engineering Journal*, 210, pp. 597-609.

Qiu, Z., Zhao, L. and Weatherley, L. (2010) 'Process intensification technologies in continuous biodiesel production', *Chemical Engineering and Processing: Process Intensification*, 49, (4), pp. 323-330.

Ramadhas, A. S., Jayaraj, S. and Muraleedharan, C. (2004) 'Use of vegetable oils as I.C. engine fuels - A review', *Renewable Energy*, 29, (5), pp. 727-742.

Rashid, U. and Anwar, F. (2008) 'Production of biodiesel through optimized alkaline-catalyzed transesterification of rapeseed oil', *Fuel*, 87, (3), pp. 265-273.

Rashid, U., Anwar, F. and Knothe, G. (2009) 'Evaluation of biodiesel obtained from cottonseed oil', *Fuel Processing Technology*, 90, (9), pp. 1157-1163.

Reddy, C., Reddy, V., Oshel, R. and Verkade, J. G. (2006) 'Room-temperature conversion of soybean oil and poultry fat to biodiesel catalyzed by nanocrystalline calcium oxides', *Energy and Fuels*, 20, (3), pp. 1310-1314.

Reeve, W., Erikson, C. M. and Aluotto, P. F. (1979) 'A new method for the determination of the relative acidities of alcohols in alcoholic solutions. The nucleophilicities and competitive reactivities of alkoxides and phenoxides', *Canadian Journal of Chemistry*, 57, (20), pp. 2747-2754.

Reis, N., Goncalves, C. N., Aguedo, M., Gomes, N., Teixeira, J. A. and Vicente, A. A. (2006a) 'Application of a novel oscillatory flow micro-bioreactor to the production of γ-decalactone in a two immiscible liquid phase medium', *Biotechnology Letters*, 28, (7), pp. 485-490.

Reis, N., Gonçalves, C. N., Vicente, A. A. and Teixeira, J. A. (2006b) 'Proof-of-concept of a novel micro-bioreactor for fast development of industrial bioprocesses', *Biotechnology and Bioengineering*, 95, (4), pp. 744-753.

Reis, N., Harvey, A. P., Mackley, M. R., Vicente, A. A. and Teixeira, J. A. (2005) 'Fluid mechanics and design aspects of a novel oscillatory flow screening mesoreactor', *Chemical Engineering Research and Design*, 83, (4 A), pp. 357-371.

Reis, N., Vicente, A. A. and Teixeira, J. A. (2010) 'Liquid backmixing in oscillatory flow through a periodically constricted meso-tube', *Chemical Engineering and Processing: Process Intensification*, 49, (7), pp. 793-803.

Reis, N., Vicente, A. A., Teixeira, J. A. and Mackley, M. R. (2004) 'Residence times and mixing of a novel continuous oscillatory flow screening reactor', *Chemical Engineering Science*, 59, (22-23), pp. 4967-4974.

Santos, J. C. O., Santos, I. M. G. and Souza, A. G. (2005) 'Effect of heating and cooling on rheological parameters of edible vegetable oils', *Journal of Food Engineering*, 67, (4), pp. 401-405.

[References]

Sastri, S. R. S., Mohanty, S. and Rao, K. K. (1997) 'A new method for predicting critical volumes of organic compounds', *Fluid Phase Equilibria,* 129, (1–2), pp. 49-59.

Schuchardt, U., Sercheli, R. and Vargas, R. M. (1998) 'Transesterification of vegetable oils: A review', *Journal of the Brazilian Chemical Society,* 9, (3), pp. 199-210.

Shylesh, S., Sharma, S., Mirajkar, S. P. and Singh, A. P. (2004) 'Silica functionalised sulphonic acid groups: synthesis, characterization and catalytic activity in acetalization and acetylation reactions', *Journal of Molecular Catalysis A: Chemical,* 212, (1-2), pp. 219-228.

Singh, D., Chopra, A., Kumar, R., Sastry, M. I. S., Patel, M. B. and Basu, B. (2013) 'Response factor correction for estimation of ester content in biodiesel', *Chromatographia*, pp. 1-5.

Smith, H. A. and Levenson, H. S. (1939) 'Kinetics of the saponification of the ethyl esters of normal aliphatic acids', *Journal of the American Chemical Society,* 61, (5), pp. 1172-1175.

Snare, M., Kubickova, I., Maki-Arvela, P., Eranen, K., Warna, J. and Murzin, D. Y. (2007) 'Production of diesel fuel from renewable feeds: Kinetics of ethyl stearate decarboxylation', *Chemical Engineering Journal,* 134, (1-3), pp. 29-34.

Srivastava, A. and Prasad, R. (2000) 'Triglycerides-based diesel fuels', *Renewable & sustainable energy reviews,* 4, (2), pp. 111-133.

Stamenković, O. S., Todorović, Z. B., Lazić, M. L., Veljković, V. B. and Skala, D. U. (2008) 'Kinetics of sunflower oil methanolysis at low temperatures', *Bioresource Technology,* 99, (5), pp. 1131-1140.

Stankiewicz, A. I. and Moulijn, J. A. (2000) 'Process intensification:transforming chemical engineering', *AIChE* 96, pp. 22-34.

Stonestreet, P. and Harvey, A. P. (2002) 'A mixing-based design methodology for continuous oscillatory flow reactors', *Chemical Engineering Research and Design,* 80, (1), pp. 31-44.

Stonestreet, P. and Van Der Veeken, P. M. J. (1999) 'The effects of oscillatory flow and bulk flow components on residence time distribution in baffled tube reactors', *Chemical Engineering Research and Design,* 77, (8), pp. 671-684.

Sun, J., Ju, J., Ji, L., Zhang, L. and Xu, N. (2008) 'Synthesis of biodiesel in capillary microreactors', *Industrial and Engineering Chemistry Research,* 47, (5), pp. 1398-1403.

Suwannakarn, K., Lotero, E., Goodwin Jr, J. G. and Lu, C. (2008) 'Stability of sulfated zirconia and the nature of the catalytically active species in the transesterification of triglycerides', *Journal of Catalysis,* 255, (2), pp. 279-286.

[References]

Thanh, L. T., Okitsu, K., Sadanaga, Y., Takenaka, N., Maeda, Y. and Bandow, H. (2010) 'Ultrasound-assisted production of biodiesel fuel from vegetable oils in a small scale circulation process', *Bioresource Technology*, 101, (2), pp. 639-645.

Uosukainen, E., Linko, Y.-Y., Lamsa, M., Tervakangas, T. and Linko, P. (1998) 'Transesterification of trimethylolpropane and rapeseed oil methyl ester to environmentally acceptable lubricants', *Journal of the American Oil Chemists' Society*, 75, (11), pp. 1557-1563.

USDA (2013) *Worldwide rapeseed oil production*, United States Department of Agriculture. Available at: http://www.fas.usda.gov/psdonline/psdQuery.aspx (Accessed: 6th November, 2013).

Veljkovic, V. B., Stamenkovic, O. S., Todorovic, Z. B., Lazic, M. L. and Skala, D. U. (2009) 'Kinetics of sunflower oil methanolysis catalyzed by calcium oxide', *Fuel*, 88, (9), pp. 1554-1562.

Vicente, G., Martínez, M. and Aracil, J. (2004) 'Integrated biodiesel production: a comparison of different homogeneous catalysts systems', *Bioresource Technology*, 92, (3), pp. 297-305.

Vicente, G., Martínez, M., Aracil, J. and Esteban, A. (2005) 'Kinetics of sunflower oil methanolysis', *Industrial and Engineering Chemistry Research*, 44, (15), pp. 5447-5454.

Vigeolas, H., Waldeck, P., Zank, T. and Geigenberger, P. (2007) 'Increasing seed oil content in oil-seed rape (Brassica napus L.) by over-expression of a yeast glycerol-3-phosphate dehydrogenase under the control of a seed-specific promoter', *Plant Biotechnology Journal*, 5, (3), pp. 431-441.

Viriya-empikul, N., Krasae, P., Nualpaeng, W., Yoosuk, B. and Faungnawakij, K. (2012) 'Biodiesel production over Ca-based solid catalysts derived from industrial wastes', *Fuel*, 92, (1), pp. 239-244.

Wang, J. J., Chang, J. and Fan, J. (2010) 'Upgrading of bio-oil by catalytic esterification and determination of acid number for evaluating esterification degree', *Energy & Fuels*, 24, (5), pp. 3251-3255.

Wang, P., Tat, M. and Gerpen, J. (2005) 'The production of fatty acid isopropyl esters and their use as a diesel engine fuel', *Journal of the American Oil Chemists' Society*, 82, (11), pp. 845-849.

Wang, Y., Ou, P. L. S. and Zhang, Z. (2007) 'Preparation of biodiesel from waste cooking oil via two-step catalyzed process', *Energy Conversion and Management*, 48, (1), pp. 184-188.

Wen, Z., Yu, X., Tu, S.-T., Yan, J. and Dahlquist, E. (2009) 'Intensification of biodiesel synthesis using zigzag micro-channel reactors', *Bioresource Technology*, 100, (12), pp. 3054-3060.

[References]

Wilke, C. R. and Chang, P. (1955) 'Correlation of diffusion coefficients in dilute solutions', *AIChE Journal*, 1, (2), pp. 264-270.

Wilson, K. and Lee, A. F. (2012) 'Rational design of heterogeneous catalysts for biodiesel synthesis', *Catalysis Science & Technology*, 2, (5), pp. 884-897.

Xiao, Y., Gao, L., Xiao, G. and Lv, J. (2010) 'Kinetics of the transesterification reaction catalyzed by solid base in a fixed-bed reactor', *Energy & Fuels*, 24, (11), pp. 5829-5833.

Xie, W., Peng, H. and Chen, L. (2006) 'Transesterification of soybean oil catalyzed by potassium loaded on alumina as a solid-base catalyst', *Applied Catalysis A: General*, 300, (1), pp. 67-74.

Xie, W., Qi, C., Wang, H. and Liu, Y. (2014) 'Phenylsulfonic acid functionalized mesoporous SBA-15 silica: A heterogeneous catalyst for removal of free fatty acids in vegetable oil', *Fuel Processing Technology*, 119, pp. 98-104.

Xie, W. and Yang, Z. (2007) 'Ba-ZnO catalysts for soybean oil transesterification', *Catalysis Letters*, 117, (3-4), pp. 159-165.

Yadav, G. D. and Mehta, P. H. (1994) 'Heterogeneous Catalysis in Esterification Reactions: Preparation of Phenethyl Acetate and Cyclohexyl Acetate by Using a Variety of Solid Acidic Catalysts', *Industrial & Engineering Chemistry Research*, 33, (9), pp. 2198-2208.

Yan, S., DiMaggio, C., Mohan, S., Kim, M., Salley, S.O., and Simon Ng, K.Y. . (2010) 'Advancements in heterogeneous catalysis for biodiesel synthesis', *Topics in Catalysis*, 53, pp. 721–736.

Yoosuk, B., Krasae, P., Puttasawat, B., Udomsap, P., Viriya-empikul, N. and Faungnawakij, K. (2010) 'Magnesia modified with strontium as a solid base catalyst for transesterification of palm olein', *Chemical Engineering Journal*, 162, (1), pp. 58-66.

Yussof, H. W. (2012) *An evaluation of heterogeneous quaternary ammonium catalysts for transesterification of triglycerides.* PhD thesis, Newcastle University.

Zabeti, M., Wan Daud, W. M. A. and Aroua, M. K. (2009) 'Activity of solid catalysts for biodiesel production: a review', *Fuel Processing Technology*, 90, pp. 770–777.

Zhao, L., Qiu, Z. and Stagg-Williams, S. M. (2013) 'Transesterification of canola oil catalyzed by nanopowder calcium oxide', *Fuel Processing Technology*, 114, pp. 154-162.

Zheng, M., Skelton, R. L. and Mackley, M. R. (2007) 'Biodiesel reaction screening using oscillatory flow meso reactors', *Process Safety and Environmental Protection*, 85, (5 B), pp. 365-371.

Appendices

Appendix A: Catalysts adsorption isotherms, surface area and pore size

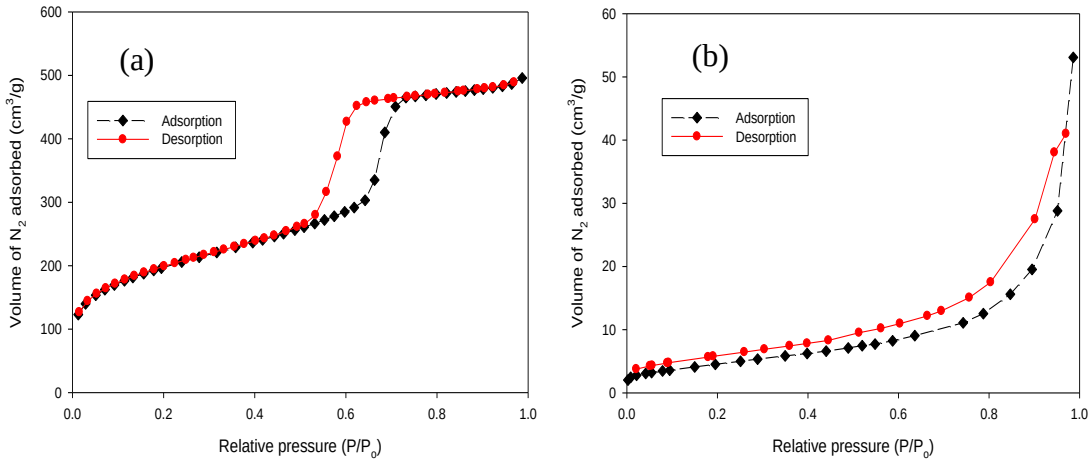

Figure A.1: Adsorption-desorption isotherms for: (a) $PrSO_3H$-SBA-15 and (b) SZB catalysts.

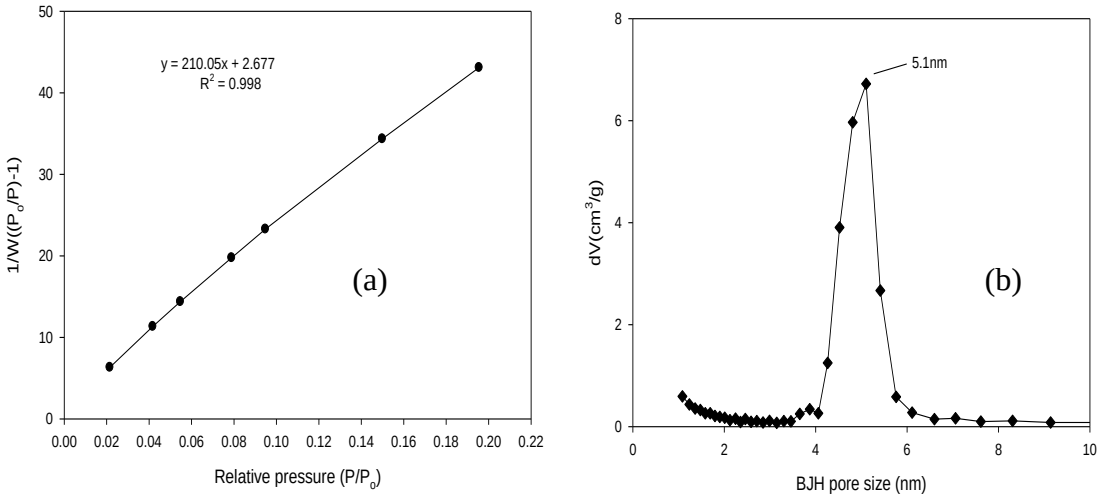

Figure A.2: A typical (a) BET plot for the calculations of the catalyst surface area (SZB) (b) BJH plot calculation of pore size ($PrSO_3H$-SBA-15)

[Appendices]

BET surface area of the catalysts can be calculated from the BET plot using equation (A.1).

$$S_{BET} = \frac{1}{(S+I)} . \frac{N_A . A_c}{M_w} \qquad \text{(A.1)}$$

Where:

N_A: Avogadro's number, 6.022 x 10^{23} per mole

S_{BET}: Brunauer–Emmett–Teller surface area;

S: slope of the BET plot; I: intercept of the BET plot (refer to Figure A.2 (a))

A_c: cross-sectional area of N_2 (0.162 nm^2); Mw: molecular mass of N_2 (28.01g.mol^{-1})

For example, BET surface area of SZB from Figure A.2(a) is

$$S_{BET} = \frac{1}{(210.05+2.677)} . \frac{(6.022\ x\ 10^{23})(0.162)(10^{-9})^2}{28.01} m^2/g = 16.371\ m^2/g$$

The catalyst pore size distribution in Figure A.2 (b) was a plot of $\frac{d(V_{ad})}{d(D_p)}$ against D_p. The volume of the N_2 adsorbate (V_{ad}) was from the desorption branch of the isotherm. The pore diameter, D_p, can be calculated as follows:

$$D_p = 2(R_k + t_H) \qquad \text{(A.2)}$$

$$R_k(nm) = \frac{0.414}{log(P/P_o)} \qquad \text{(A.3)}$$

$$t_H(nm) = 0.354 \left[\frac{5}{2.303\ log(P_o/P)}\right]^{1/3} \qquad \text{(A.4)}$$

Where: P/P_o is the relative pressure; R_k is Kelvin radius; t_H = thickness of the N_2 film adsorbed on the walls of the pore at the relative pressure. The Quantachrome surface area and pore size analyser (NOVA 2000e) used in the study was automated. Hence, the instrument performed the above calculations.

Appendix B: Viscosity and density data for the RSO-methanol system.

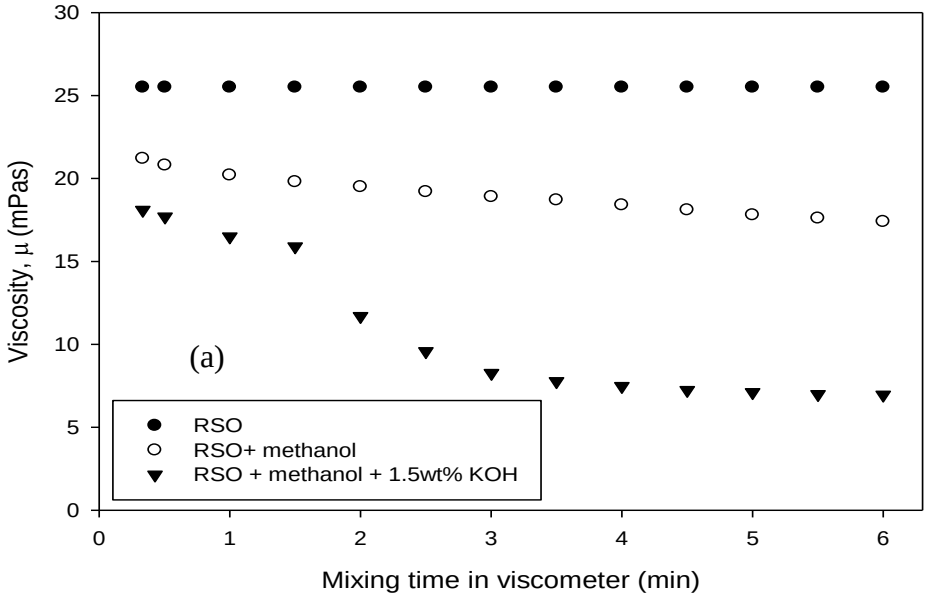

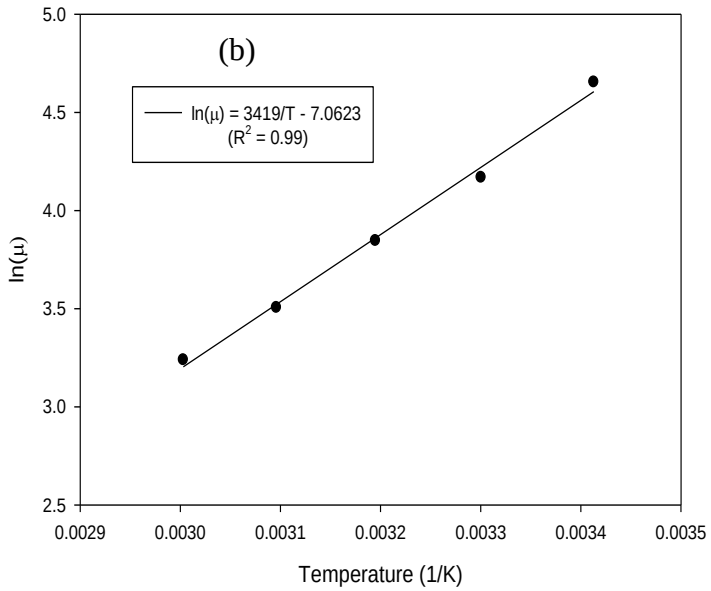

Table A.1: Densities of RSO at various temperatures

Temperature (K)	Density (kg.m-3)
295	911
304	905
313	900
324	894
333	891

Figure A.3: (a) Viscosity profiles at 60˚C for RSO, RSO-methanol and RSO-methanol with 1.5wt% KOH using methanol to RSO molar ratio of 6:1, (b) correlation between the viscosity of RSO and temperature.

Average viscosities of the systems were calculated at the plateau as indicated in the Figure A.3 (a). The viscosities were 25.5 mPas for RSO, 18.9 mPas for RSO-methanol and 7.2 mPas for RSO-methanol with 1.5wt% KOH. A correlation between the viscosity of the RSO and temperature was obtained as shown in Figure A.3 (b).

Appendix C: Confluent PVM pump commands

The Confluent pumps were operated through commands inputs in the Sapphire Commander software. Some of the basic Sapphire pump commands used were:

/**N**S1L20v1000V**N$_f$**c2700gOA**N$_a$**AOGR (for continuous oscillations)
/**N**IV5800A3000OV**N$_o$**AOGR (for continuous pumping)
/**N**IV5800A3000OAOGR (single pump action required for filling the system)
/**N**T (to stop pump)
/**N**ZR (to initialise pump)

Where:
N = pump serial number (**N** = 1, 2, 3, 5 ...)
N$_f$ = frequency factor which depends on the selected amplitude and size of syringe.
N$_a$ = amplitude factor which depends on the size of pump syringe used.
N$_o$ = flow output factor which is calculated based on the desired fluid flow rate.

The parameters **N$_f$** and **N$_a$** are chosen from the pump chart based on the desired oscillatory conditions. Input flow rates of the reactants are necessary in estimation of the **N$_o$** parameter for the pumps. This is function of the size of the pump syringe. For example, when 1ml (1000µl) pump syringe is used to pump fluid at volumetric rate Q (µl.s^{-1}) into the reactor, the flow output parameters (N_o) is calculated from the expression:

$$N_o = \frac{(2)(3000)Q}{1000} = 6Q \qquad \text{(A.5)}$$

For instance, at RSO flow rate of 2.3253mL/min, the value of

$the\ N_o = \frac{6(2.3253\ x10^3)}{60} = 232.53 \approx 233$ (Q = 2.3253 mL.min^{-1}).

The frequency factor (N_f) and amplitude factor (N_a) were selected using a chart for the PVM syringe pump (Table A.2). Values of N_f and N_a were dependent on the volume of the syringe used as indicated in the chart.

Table A.2: Chart for selection of oscillations in PVM syringe pumps

	amplitude, xo (mm)						
frequency f(Hz)	0.25	0.5	1	1.5	2	3	4
0.5			140	202	266	390	520
1	161	292 /170	290	430	570	830	232
2	363	672/370	670	1000	1315	365 / 2030	467
3	642	1192/650	1300	1850	410 / 3000	563	723
4	1033	2845/1100	2800	450	565	785	1017
5	950	530/2300	325	586	738	1050	1373
6		860	450	750	950	1350	1902
7		239	870	934	1170	1820	
8	230	328	999	1121	1500		
9	242	410	747			key	syringe
10	334	520	950				0.5ml
11	420	671					1ml
12	550	870					5ml
13	700						5ml (alternative
14	915						

computer command (A)	Syringe volume		
amplitude (xo)	0.5ml	1ml	5ml
0.25	A30A	A15A	A3A
0.5	A60A	A30A	A6A
1	A120A	A60A	A12A
1.5	A180A	A90A	A18A
2	A240A	A120A	A24A
3	A360A	A180A	A36A
4	A480A	A240A	A48A

Example:

For oscillations at 2Hz frequency and 4mm amplitude using a 5mL syringe, the values of N_f and N_a are used in the pump commands for oscillation were N_f = 467 and N_a = 48.

Appendix D: MATLAB mathematical program used in the modelling

```
function cp=firstequ3(t,c)
global k1 k2 k3 k4 k5 k6 m n k9 k7 k8 k8a k8b


%odes (approximate mass balances)
cp=zeros(11,1);


c1=(c(8)*((-k1*(c(1)^m)*(c(2)^n))+(k2*(c(3)^m)*(c(5)^n)))...
    -(k7*(c(9))*(c(1)^m))); %TG

c2=(c(8)*((k2*(c(3)^m)*(c(5)^n))+(k4*(c(4)^m)*(c(5)^n))... %METHANOL
    +(k6*(c(6)^m)*(c(5)^n)))+(c(8)*((-k1*(c(1)^m)*(c(2)^n))...
    +(-k3*(c(3)^m)*(c(2)^n))+(-k5*(c(4)^m)*(c(2)^n)))+...
    (k8*(c(9))*(c(5)^m))+(-k8a*c(2)*c(9))+(k8b*c(8)*c(10))));

c3=((c(8)*((k1*(c(1)^m)*(c(2)^n))+(-k3*(c(3)^m)*(c(2)^n))…
   +(k4*(c(4)^m)*(c(5)^n))+(-k2*(c(3)^m)*(c(5)^n))))); %DG

c4= ((c(8)*((k3*(c(3)^m)*(c(2)^n))+(-k5*(c(4)^m)*(c(2)^n))...
    +(k6*(c(6)^m)*(c(5)^n))+(-k4*(c(4)^m)*(c(5)^n))))); %MG

c5= ((c(8)*((-k2*(c(3)^m)*(c(5)^n))-(k4*(c(4)^m)*(c(5)^n))...
    -(k6*(c(6)^m)*(c(5)^n))+(k1*(c(1)^m)*(c(2)^n))+...
     +(k3*(c(3)^m)*(c(2)^n))+(k5*(c(4)^m)*(c(2)^n))))...
     -(k8*(c(9))*(c(5)^m))); %FAME


c6=((c(8)*((k5*(c(4)^m)*(c(2)^n))-(k6*(c(6)^m)*(c(5)^n))))...
    +(k7*(c(9))*(c(1)^m))); %GL

c7=((-k9*(c(7)^m)*(c(9)))-(k9*(c(7)^m)*(c(8))));%FFA

c8=((-k9*(c(8)^n)*(c(7)^m))+(k8a* c(2)*c(9))-(k8b*c(8)*c(10)));
                                                    %alkoxide

c9=((c(9)*((-k7*(c(1)^m))+(-k8*(c(5)^m))+(-k9*(c(7)^m))...
   +(-k8a*c(2)))+(k8b*c(8)*c(10))));%OH

c10=(k8a* c(2)*c(9) -k8b*c(8)*c(10)+(k9*(c(7)^m)*(c(9)))); %WATER

c11=((c(9)*((k7*(c(1)^m))+(k8*(c(5)^m))+(k9*(c(7)^m))))...
    +(k9*(c(7)^m)*(c(8))));%soap


cp=[c1;c2;c3;c4;c5;c6;c7;c8;c9;c10;c11];
```

[Appendices]

```
global k1 k2 k3 k8 m n k4 k5 k6 k7 k9 RO T ke Co Cw k8a k8b

%parameters
m=1;
n=1;
T=333;
Ke=3.2;
TG=1;
MWtg=881;
MA=6;
MWma=32;
Wcat=35;
MWcat=56;
W=0;
Wma=32;
FFA=0.03;
MWffa=281;
k1=4.26*10^9*exp(-58740/(8.314*T));
k2=4.304*10^6*exp(-44930/(8.314*T));
k3=2.176*10^11*exp(-67146/(8.314*T));
k4=6.559*10^9*exp(-58184/(8.314*T));
k5=8.679*10^5*exp(-30010/(8.314*T));
k6=1.975*10^7*exp(-46009/(8.314*T));
k7=1.269*10^11*exp(-69104/(8.314*T));
k8=1.962*10^10*exp(-61160/(8.314*T));
k9=6.136*10^5*exp(-31394/(8.314*T));
Vtg=TG*MWtg/918;
Vma=MA*MWma/792;
Vt=Vtg+Vma;
Ctg=(TG/Vt);
Cma=MA/Vt;
%ke=Ke*Cma;
k8b=1;
k8a=k8b*Ke;
Cffa=((((FFA*TG*MWtg)/(100*MWffa)))/Vt);
Cw=((((W*TG*MWtg)/(100*18))+((W*MA*MWma)/(100*18)))/Vt);
Co=((((Wcat*TG*MWtg)/(100*MWcat)))/Vma);
X=(-((Ke*Cma)+Cw)+sqrt((((Ke*Cma)+Cw)^2)+(4*Ke*Cma*Co)/2));
OH=Co*X;
RO=Co-OH;

[T,C]=ode45(@firstequ3,[0:10:600],[Ctg Cma 0 0 0 0 Cffa RO OH Cw 0]);
%plotting a graph
plot (T,C),axis([0 600 0 1.0]), grid on, xlabel('Time (s)'),ylabel...
('Concentration (mol/L)'), legend
('TG','methanol','DG','MG','FAME','GL')
```

[Appendices]

Appendix E: European biodiesel specifications

Table A.3 : European Biodiesel Standards EN 14214 and EN 14213 (Knothe, 2006)

Property	Test method	Limits		Unit
		EN 14214	EN 14213	
Ester content	EN 14103	96.5 min	96.5 min	% (mol/mol)
Density; 15°C	EN ISO 3675, EN ISO 12185	860–900	860–900	kg/m^3
Viscosity; 40°C	EN ISO 3104, ISO 3105	3.5–5.0	3.5–5.0	mm^2/s
Flash point	EN ISO 3679	120 min	120 min	°C
Sulfur content	EN ISO 20846; EN ISO 20884	10.0 max	10.0 max	mg/kg
Carbon residue (10% distillation residue)	EN ISO 10370	0.30 max	0.30 max	% (mol/mol)
Cetane number	EN ISO 5165	51 min	—	
Sulfated ash	ISO 3987	0.02 max	0.02 max	% (mol/mol)
Water content	EN ISO 12937	500 max	500 max	mg/kg
Total contamination	EN 12662	24 max	24 max	mg/kg
Copper strip corrosion (3h, 50°C)	EN ISO 2160	1	—	degree of corrosion
Oxidative stability, 110°C	EN 14112	6.0 min	4.0 h	h
Acid value	EN 14104	0.50 max	0.50 max	mg KOH/g
Iodine value	EN 14111	120 max	130 max	g I_2/100 g
Linolenic acid content	EN 14103	12.0 max	—	% (mol/mol)
Content of FAME with ≥4 double bonds		1 max	1 max	% (mol/mol)
Methanol content	EN 14110	0.20 max	—	% (mol/mol)
MAG content	EN 14105	0.80 max	0.80 max	% (mol/mol)
DAG content	EN 14105	0.20 max	0.20 max	% (mol/mol)
TAG content	EN 14105	0.20 max	0.20 max	% (mol/mol)
Free glycerine	EN 14105, EN 14106	0.020 max	0.02 max	% (mol/mol)
Total glycerine	EN 14105	0.25 max	—	% (mol/mol)
Group I metals (Na + K)	EN 14108, EN 14109	5.0 max	—	mg/kg
Group II (Ca + Mg)	prEN 14538	5.0 max	—	mg/kg
Phosphorus content	EN 14107	10.0 max	—	mg/kg
Cold filter plugging point	EN 116	—		°C
Pour point	ISO 3016	—	0 max	°C
Heating value	DIN 51900-1			
	DIN 51900-2			
	DIN 51900-2	—	35 min	MJ/kg

Appendix F: SEM of the SZB and $PrSO_3H$-SBA-15 catalysts

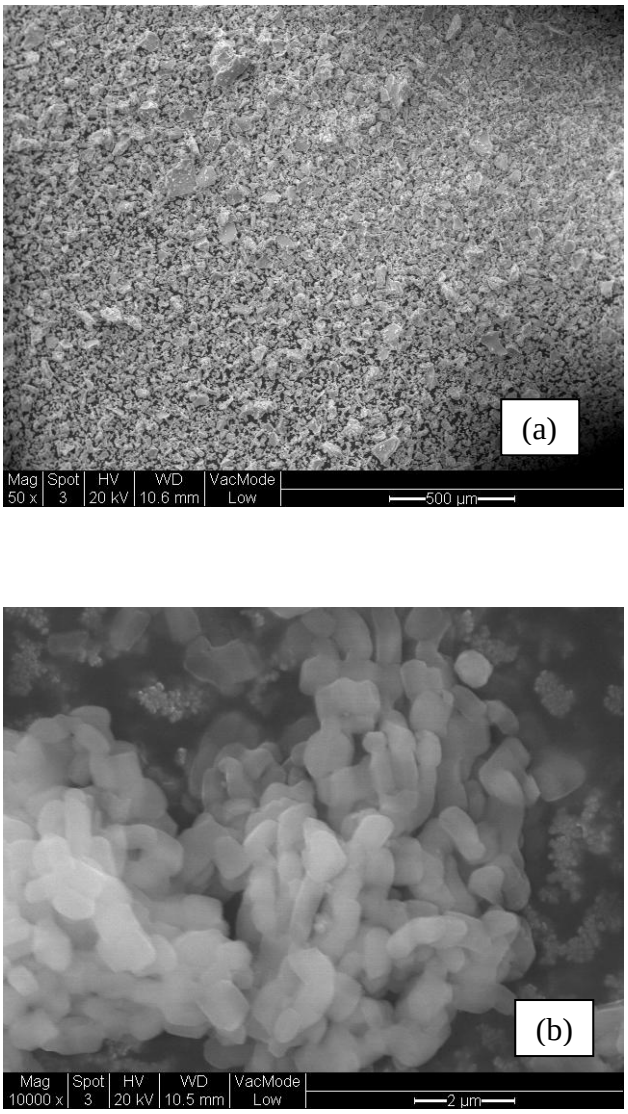

Figure A.4: SEM of the catalysts (a) SZB, (b) $PrSO_3H$-SBA-15